HYDROSTATIC EXTRUSION OF BIMETALLIC COMPOSITES

By

Horacio Helman, Ing. Mec. y Elect.

January, 1976.

A thesis submitted for the degree of
Doctor of Philosophy of the University
of London and for the Diploma of
Imperial College.

Mechanical Engineering Department
Imperial College
London, S.W.7.

SUMMARY

HYDROSTATIC EXTRUSION OF BIMETALLIC COMPOSITES

An experimental procedure capable of producing a copper-stainless steel composite wire by hydrostatic extrusion-drawing is described. It includes the production of wires with different internal geometries.

For the case of a copper sleeve and a single stainless steel core (or vice versa), theoretical models predicting the stress distribution in the deforming zone are presented. In particular, a form of the Method of Weighted Residuals is adapted for the integration of the Prandtl-Reuss equation and an approximate polynomial solution for the stress distribution associated with Avitzur's velocity field is obtained.

All solutions show reasonable agreement with the experimental values.

In addition, the temperature distribution produced by the deformation process is obtained.

Since polynomial solutions may involve the calculation of a large number of terms in an usually fine net, the computation time required by the process and the rounding errors produced may be important. In order to reduce the weight of these factors, a procedure for the economization of polynomial solutions is obtained, as a generalization of Lanczo's method for the case of a single variable.

CONTENTS

LIST OF FIGURES

NOTATIONS

A	Coefficient matrix of a polynomial expansion.
A_{ij}	Free parameters in the stress function.
α	Semi-angle of the die.
A_c, A_t	Cross-sectional areas of core and tube respectively.
B_{ij}	Free parameters in the stress function.
β	Semi-angle of the core/tube interface.
c	Specific heat.
C_k	Constant of hardening.
δ	Kronecker "delta" function.
D	Dragging function.
D_i^t, D_f^t	Initial and final external diameters of the tube.
D_i^c, D_f^c	Initial and final diameters of the core.
ε_{ij}	Strain tensor component.
$\dot{\varepsilon}_{ij}$	Strain rate tensor component.
$\bar{\varepsilon}$	Equivalent strain.
ε	Permissible error bound.
ϕ_1, ϕ_2	Stress functions.
f	Yield function.
$F(\alpha)$	Avitzur function.
g_i	Weighting factors.
g	Coefficient of friction.
γ_c, γ_t	Fraction of volume of core and tube respectively.
$\Gamma_1, \Gamma_2, \Gamma_3, \Gamma_4$	Boundary surfaces of the deforming zone.
$\dot{h}_v$	Heat generated during the deformation per unit volume and time.
$\dot{h}_s$	Heat generated at the tube/die interface.
H	Slope of the stress-strain curve.
h_i^t, h_f^t	Initial and final thickness of the tube.
I_2	Second strain rate deviatoric invariant.
J^*	Power of deformation.
k	Generical shear yield stress.
k^c, k^t	Shear stresses of core and tube.
k_o^c, k_o^t	Initial shear stresses of core and tube.
K	Thermal conductivity.
μ	Coefficient of friction.
ω	Y_{soft}/Y_{hard}.
p_n	Hydrostatic pressure.
p	Normal stress or pressure.
$P(x)$	Polynomial expression.
$P_\varepsilon(x)$	Economized form of the polynomial expression.
P^{ch}	Chebyshev expansion of a polynomial expression.

q	Dragging factor.
R	Extrusion ratio.
R_I, R_F	Initial and final radii of the spherical surfaces.
r_i^t, r_f^t	Initial and final external radii of the tube.
r_i^c, r_t^c	Extrusion ratios of core and tube respectively.
$R_{1n}, R_{2n}, R_{3n}, R_{4n}$	Error functions.
R_n	Total error function.
ρ	Density of the metal.
σ_{ij}	Stress tensor component.
$\bar{\sigma}$	Equivalent stress.
σ'_{ij}	Deviatoric stress tensor component.
σ_m	Hydrostatic stress component.
T'	Deviatoric stress tensor.
t	Time.
T	Temperature (^oC).
$T^*(x)$	Shifted Chebyshev polynomials of first kind.
τ	Shear stresses.
T_j	Generical stress.
V	Velocity field.
v_r, v_z	Velocity field components.
$W(x)$	Weighting functions.
$\dot{W}$	Power.
ψ	Stream or flow function.
Y	Generical yield stress.
Y^c, Y^t	Yield stresses of core and tube respectively.
Y_o^c, Y_o^t	Initial values of the yield stress of core and tube.

ACKNOWLEDGEMENTS

I wish to express my sincere thanks and gratitude to Dr. Bela Lengyel for suggesting this project and for his help and guidance throughout this work.

I gratefully acknowledge Dr. E.L. Ortiz, Mathematics Department, for his valuable help and advice on the mathematical aspects of this project.

Thanks are due to Professor J.M. Alexander for his kind permission to use the facilities of the Metalworking Laboratory.

The assistance given by all members of the staff, in particular Messrs. P.G. Ashford, M.G. Gutteridge, J. Pooley, R. Baxter, J. Plumb and N. Keith is duly acknowledged.

My thanks are also due to my colleagues, in particular T. Ravindranath, for their help and stimulating discussions.

Finally my thanks are due to Mrs. Shelagh Murdock for typing the manuscript.

H. Helman

January 1976

I. INTRODUCTION

I.1 The hydrostatic extrusion-drawing process

Hydrostatic extrusion is a relatively new forming process possessing many advantages over conventional extrusion methods. The development of the hydrostatic extrusion and the application of hydrostatic pressure to the forming of metals represents new approaches to the field of cold forming [1].

The first scientific attempts in the use of these methods correspond to Bridgman [2], although the first known description of the hydrostatic extrusion process appears to have been presented by James Robertson in 1893 [3], in patents taken out in Britain and the U.S.A. However, there is no record of any practical work done with this equipment.

A detailed and comprehensive description of the features of the process we are dealing with, can be seen in [1], [4] and [5]. Some of the outstanding aspects of the process can be inferred from Fig. 1.

An interesting resumé of these characteristics is presented in [5] as follows:

(i) Friction between billet and container is absent; long billets can be extruded without a corresponding increase in the extrusion pressure.

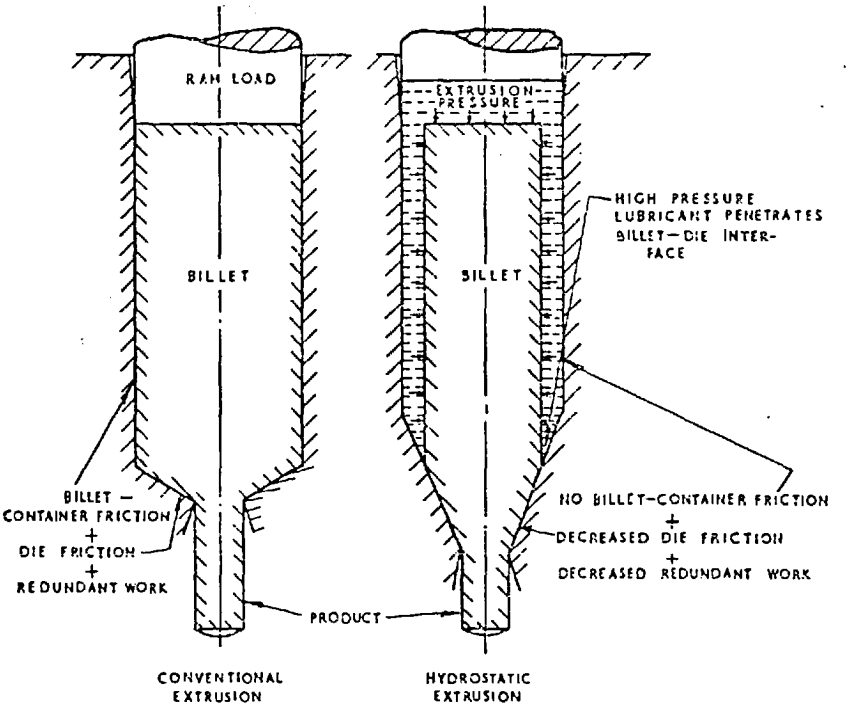

Figure 1 Comparison of conventional and hydrostatic extrusion.

(ii) Since friction between die and billet is low, dies of small angle may be used to reduce redundant deformation and extrusion pressure. Harder materials can be cold extruded because shearing of the billet along the die face which could lead to fracture in conventional extrusion is reduced.

(iii) Within limits, it is not necessary to use cylindrical billets of closely controlled dimensions. Non-straight billets, or coils of wire with free or clamped-back end, can be extruded into straight products. The cladding of long lengths of wire is also possible.

(iv) Support can be given to the die by surrounding it with the high pressure fluid. Products of complex sections can be

extruded through thin-walled dies.

(v) The process is versatile. Simple die replacement enables billets of various sizes and sections to be extruded. Stepped products can be produced.

(vi) The strength of the extruded wire is more often higher than in conventional wire drawing owing to the absence of internal voids and pores in extrusion under large compressive stresses.

Possible disadvantages:

(i) Considerable compression of the fluid has to occur (typically up to one-third of the volume) to generate sufficiently high pressures (e.g. 30 Kbar). This results in large amounts of stored energy, which reduces efficiency and may be dangerous.

(ii) The billet must be tapered at its front end and held against the die to produce initial sealing.

(iii) Once the billet has begun to extrude it is difficult to control the rate of extrusion. Consequently, extrusion speed is often too high; undesirable heating and softening of the billet may occur. In such cases the billet and fluid are ejected violently from the container, unless some means of control is provided. Lack of control of the extrusion speed

often leads to instability, which is featured by "stick-slip" movement on the extrudate and by its fluctuating pressure-time characteristics.

(iv) In production, containment of fluid requires ancillary equipment if a horizontal arrangement is used. A large number of repeated cycles of operation may require frequent changes of the seal between the moving punch and static container, or the development of special sealing arrangements. This may cause fatigue in container, punches and other items.

The enormous pressures required in hydraulic extrusion may be reduced, and the extrusion speed controlled, by additionally pushing or pulling the billet into the die. These techniques are often called billet and product augmentation respectively. The latter is the procedure adopted in the experiments carried out in the present work. This technique has received extensive development at Imperial College by B. Lengyel et al. [74], [75], [76], where a special rig was designed for this purpose.

I.2 Theoretical models for the extrusion process

The extrusion of a solid billet through conical dies is a very well studied process and several theoretical solutions for the extrusion pressure have been obtained through different approaches.

The Siebel's analysis [6] based on uniform deformation and the slab method first proposed by Sachs [7] and later presented by Hoffman and Sachs [8] are, perhaps, the oldest theoretical analyses of the extrusion problem. Their solutions involve the use of a constant coefficient of friction and the assumption that stresses are constant on a cross section. Tresca's yield criterion is used for the determination of plastic state, and, since the direction normal to the die surface is assumed as principal, the approach holds good for relatively small die angles.

Solutions have also been obtained by means of the slip-line approach. A detailed and comprehensive mathematical treatment for the plane strain extrusion, based on Hencky's slip-lines field method, was done by R. Hill [9]. In this work both the boundaries between the die and the deforming metal and the metal itself outside the plastic zone are treated as rigid. It is also assumed that this rigid material does not account for the elastically loaded material that surrounds the plastic zone.

W. Johnson obtained a slip-line solution for the extrusion through wedge-shaped dies [10]. He obtained the corresponding solutions for several angles of dies and coefficients of friction and also took into account different possible

geometries of the dead metal zone. In this paper, due to the particular geometry adopted, only small reductions have been considered. However, this work was extended to the extrusion through square dies of large reductions [11] where solutions were given for different geometries, coefficients of friction and position of the dead metal zone. He also gives some empirical expressions to calculate the average extrusion pressures for the different cases. These cases correspond to steady state conditions, where the slug remaining to be extruded is required to be longer than the depth of the associate slip-line field. In [12] Johnson also considered the modification to the slip-line solutions to accommodate shorter slug lengths and the form of doing so is described for the case of square dies.

The slip-line method is strictly applicable only to plane-strain problems. However, experimental evidence presented by Thomsen, E.G. et al. [13], [14] seems to indicate that a plane strain analysis can be used with axisymmetric extrusion problems. In these works plane-strain and axially symmetric approximate solutions for a perfect plastic material are compared with experimental results obtained from the extrusion of pure aluminium. It was found that the axially symmetric solution shows little advantage over the simpler plane strain solution and that the plane strain yield mean

stress and axial stresses are in good agreement with the experimental results. However, since the treatment has been limited to rigid-perfectly plastic isotropic solids it cannot deal properly with materials that exhibit strain hardening.

The visioplasticity method [15] has also allowed to obtain solutions for axisymmetrical extrusion problems, such as extrusion of solid rods and tubes of lead [16], [17], [18], [19]. By analysing the grid-line pattern on a meridian plane of the deforming zone the strain rate, strain and stress distributions were obtained by solving the equilibrium equations, the stress-strain relationship and the yield criterion. All these works involve a great deal of time-consuming operations, including graphical differentiations and integrations. An attempt was made to reduce the complexity of the method by Kobayashi, S. et al. [20]. Using a digital computer, velocity, strain rate, strain and stress distribution were obtained for the extrusion of a specimen of aluminium. The flow pattern for steady state conditions was obtained in direct extrusion through a conical die of 60° included angle and an extrusion ratio of 2, at a slow speed. They obtained a full description of the stress field in the deforming zone. As was pointed out in [14], there is a good agreement between the solutions obtained by these last two methods in most cases.

Another source of solutions for the extrusion problems is the Upper Bound theorem. B. Avitzur produced upper bound solutions for wire drawing and extrusion through conical dies of small and large cone angle [21], [22], by means of a radial velocity field and spherical boundaries. On the assumption that the maximum front tension cannot exceed the yield limit of the material under uniaxial tension, a solution is obtained for the maximum possible reduction in wire drawing. An analogous assumption, i.e. that the absolute value of the pushing stress cannot exceed the yield value, gives a criterion for the maximum possible reduction in extrusion. The effect of each of the process variables on the drawing stress in wire drawing and the pushing stress in extrusion is presented graphically. Since Avitzur's solution is widely used in the present work, a detailed analysis of the process variables and the velocity field are included in further chapters. Avitzur et al. generalize his velocity field by introducing generalized boundaries for the plastic zone [23].

E.R. Lambert and S. Kobayashi produced a theory on the mechanics of axisymmetric extrusion through conical dies [24]. Their upper bound approach is based on the development of an admissible velocity field without discontinuities, obtained by superposition of basic flow patterns. This velocity field, as is shown in the diagram, is described by

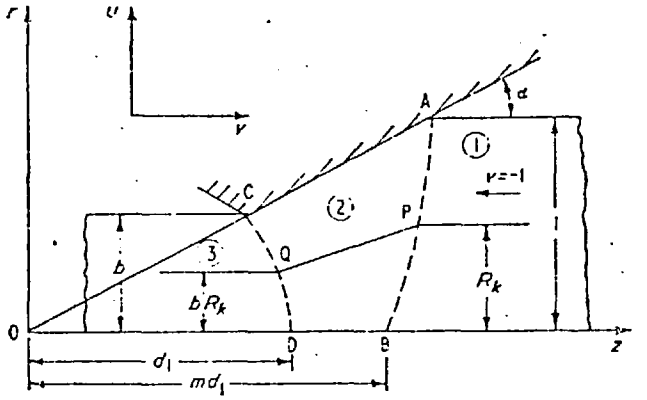

Admissible velocity field for axisymmetric extrusion

the following flow functions: in regions 1 and 3

$$\psi_1 = \frac{r^2}{2} \quad \text{and} \quad \psi_3 = \frac{r^2}{2b^2}$$

while in region 2 the flow lines are

$$z = cr + d$$

where c and d are determined for each flow line, for the given velocity discontinuity curves. Based on this velocity field, an upper bound to the average forming pressure was calculated for the extrusion of a rod with a semi-cone angle of 45^o and a reduction of 75% in area. Three different friction conditions were considered and the influence of the coefficient of friction on the deforming characteristics discussed. Most of the mechanical variables involved in the process were analyzed and plotted. This solution constitutes a lower and consequently more realistic upper bound. Values for the variables have to be determined numerically and the shape of the entry and exit boundaries of the plastic zone were determined by

minimising the energy of deformation. All these results show good agreement with those obtained by the visioplasticity approach.

As an extension of his previous work [22], Avitzur studied the hydrostatic extrusion of solid billets [25]. Based on the velocity field discussed earlier, expressions are provided giving the required extrusion pressure as a function of the other process variables and also the cone angle which minimizes the required pressure. He found that for any combination of extrusion ratio and friction condition there exists an optimum cone angle for which the required pressure is minimum.

H.Ll.D. Pugh carried out a study in the mechanics of the process of hydrostatic extrusion [26] through an upper bound approach. Solutions were obtained for the redundant work and friction which together with the work for homogeneous deformation lead to an expression for the extrusion pressure in terms of the constitutive equation of the metals. He tried several velocity fields with different limit surfaces for the deforming zone: (i) plane boundaries perpendicular to the axis, (ii) conical boundaries, and (iii) spherical boundaries with centre at the apex of the conical die, as can be seen in the following diagrams.

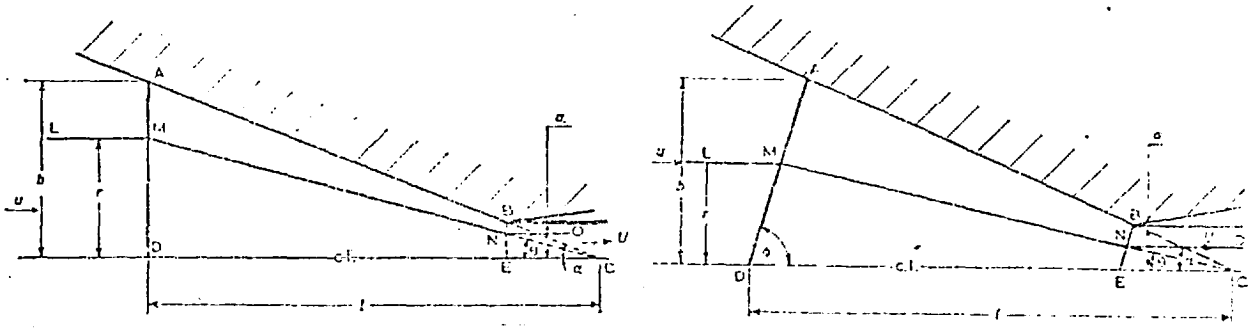

He found that of the three types of boundaries considered, the estimate for the redundant work obtained with the plane transverse boundary is much higher than the conical and spherical ones which produce fairly similar results. Consequently he adopted spherical surface limits for the deforming zone and for such field the required extrusion pressure for various die angles and extrusion ratios were calculated and plotted. They are as shown on the following page.

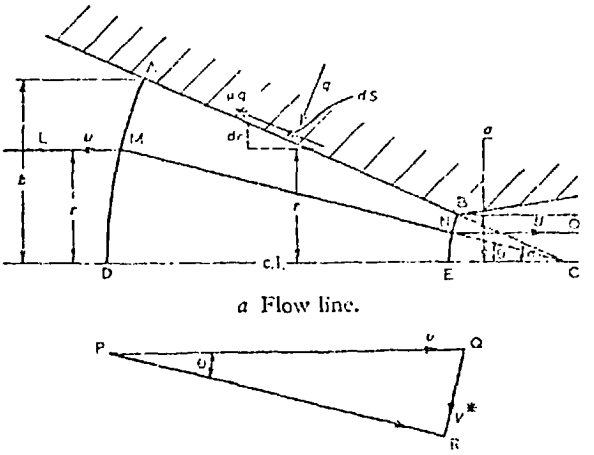

a Flow line.

b Velocity components along flow line immediately to the right of M.

Flow through a conical die with spherical entry and exit boundaries

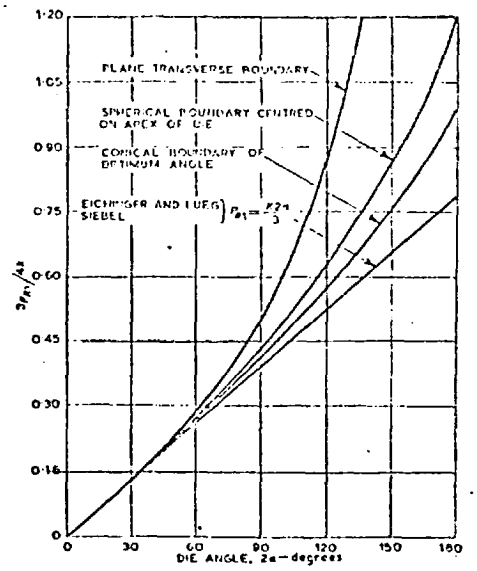

The material used was 99.5% pure aluminium and aluminium alloy HD 44 and these results were in good agreement with the experimental ones. The model allows for an estimation of the coefficient of friction to be made, which seems to be in the order of what is expected in a hydrostatic extrusion process.

I.3 The coextrusion process

A relatively less analyzed process, the coextrusion of dissimilar metals, is a subject of great technological interest. There are many requirements in industry which cannot be met satisfactorily by one material and involve the use of combinations of metals. Thus one material is a better conductor of heat or electricity, or offers greater resistance to, for example, corrosion or irradiation damage. Often such requirements can be met by cladding and a number of bi-metal rods and wire combinations are actually in use, obtained by several techniques such as rolling, extrusion and drawing. The hydro-

static extrusion process offers considerable versatility in the production of bi-metallic and multi-metallic products.

The cladding operation, where a tube of one metal is mounted over a rod or core of another metal to provide a composite with a good mechanical bond on the interface, precedes the subsequent drawing or extrusion operation. In rod cladding no contact is forced on the sleeve and core until they enter the die. Thus at the entrance core and sleeve are free to move, each at its own velocity. Passing through the die, a rigid bond of the core-sleeve composite is produced and the exit velocities of both components are identical. Even if no metallurgical bonding is produced at the interface, the mechanical packing of the two metals may form a sufficient bond. The contact surface of core and sleeve are not perfectly cylindrical (they are undulant surfaces); the crests on each surface, nevertheless, fit tightly the valleys on the other surfaces to form an inseparable mechanical lock [27].

A preliminary investigation on the experimental bases which govern the extrusion of rod, tube and can from combinations of dissimilar metals has been made by E. Whitfield [28] at the National Engineering Laboratory. The results obtained showed that flow of metals during the coextrusion process is dependent on their relative mechanical properties, dimensions

and geometrical disposition of the dissimilar metals in the original billet as well as the die geometry. Whitfield also measured the influence on the required hydrostatic pressure of the different combinations of metals and proportions. No metallurgical bonding was achieved under the conditions of the experiment at room temperature.

Whitfield also carried out experiments in order to approximately determine the minimum value of the initial plating thickness required for the successful extrusion of copper-plated billets of mild steel into rods, tubes and cans [29]. He found that this value is dependent on the extrusion ratio of the particular experiment and that the ratio of the initial plating thickness/extrusion ratio is approximately constant. The extrusion pressure-characteristics obtained during the extrusion of plated billets are similar to those for unplated ones. The adhesion of copper on the extruded products was said to be satisfactory; no metallurgical analysis of the interface was reported.

J.M. Alexander and B.C. Whitlock carried out research into the production of bimetallic strips by extruding two dissimilar metals from separate containers through a single die [30]. Experiments involve the extrusion of tin and lead at room temperature and copper and silver at 750°C. They have

achieved bond strengths at least equal to the strength of the weaker metal. Upper bound and slip-line solutions were used in order to estimate extrusion pressure and interfacial stresses. The comparisons between the actual extrusion pressure required in the tests and their calculated upper bounds are shown in the following graph:

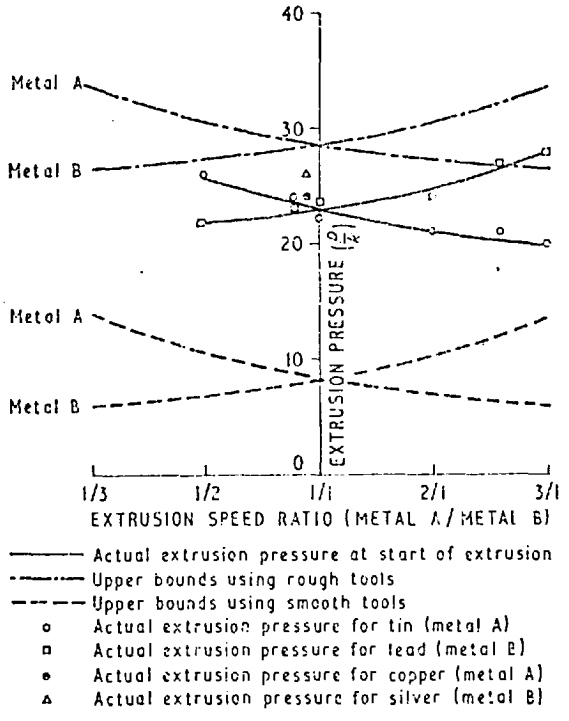

The results of metallographic examinations of the bimetallic strips showed that at the interface, intimate contact had been achieved between the dissimilar metals.

B. Avitzur [31] made a very comprehensive analysis of the mechanical conditions of the coextrusion process and

the corresponding governing variables. These variables are:

(i) Percent reduction in area.

(ii) Semi-cone angle of the die.

(iii) Die land length.

(iv) Friction.

(v) Relative size of the core, related to tube.

(vi) Ratio of the flow stress of the core to the flow stress of the tube.

(vii) Prescribed body tractions (front tension in extrusion and back tension in drawing.

He aimed at producing a criterion for the analysis of failure of composites obtained by drawing or extrusion.

A successful drawing or extrusion results from homogeneous deformation and thus identical elongation in both tube and core. If the core, being harder to an excessive degree, resists deformation so that it elongates less than the sleeve, failure by core fracture is imminent. If the sleeve is harder than the core to an excessive degree, the sleeve resists deformation and elongates less than the core, and failure by sleeve fracture is imminent.

The combination of variables causing failure are presented in graphs, for different values of the core/sleeve

radius ratio, core/sleeve yield stress ratio and die angle. In the following graph the criterion for sound flow in extrusion is illustrated:

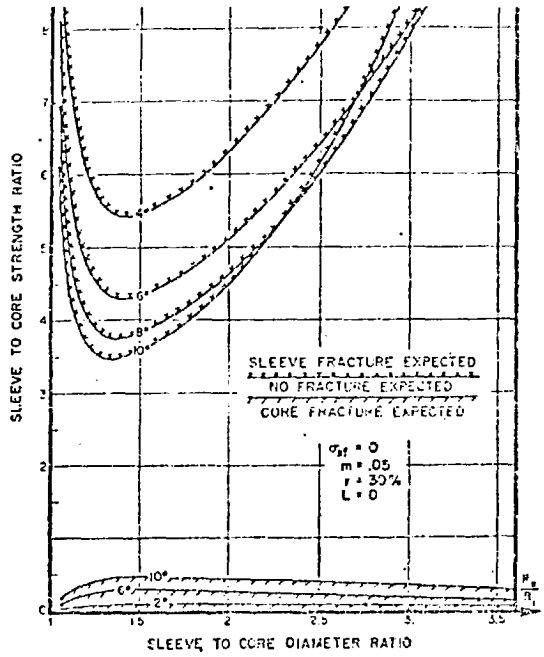

The comparison of the criteria for sound flow in drawing and extrusion follows next:

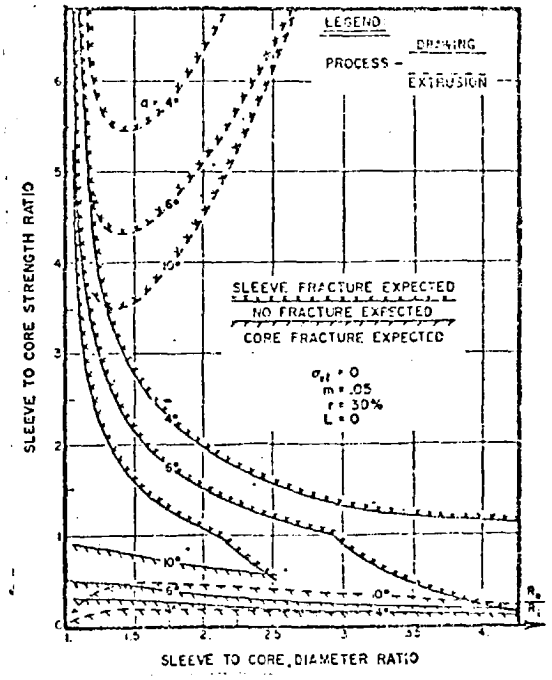

While no attempt is made to fully characterize the behaviour expressed in the various cases presented in the paper, he pointed out some general trends to apply as failure criteria,

even if these tendencies may be violated occasionally:

(i) The harder the sleeve, for $Y^c/Y^t < 1$, the more likely it is that fracture will occur.

(ii) The harder the core, for $Y^c/Y^t > 1$, the more likely it is that core fracture will occur.

(iii) The greater the departure of the strength ratio unity, the more likely it is that fracture will occur and the narrower becomes the range of process variables within which sound flow is likely to occur.

(iv) The higher the mean pressure (higher back pressure, lower front tension), the wider the range of variables for which sound flow is expected. Thus in extrusion, the range of sound flow is wider than in drawing.

(v) Normally, the higher the friction, the narrower the range for sound flow, except that core fracture in extrusion is deterred by higher friction.

The experimental results presented verify the validity of the fracture criteria.

B. Avitzur et al. [32] also studied the hydrostatic extrusion of hard core clad rods considering specifically the influence on the mechanics of the process of the bond between core and sleeve. In order to cover a range of bond strengths,

two pairs of materials were used. These were copper clad with solder and a Nb-Ti alloy clad with commercially pure aluminium. They also studied the combinations of mechanical conditions leading to failure and they present the results in the graph that follows:

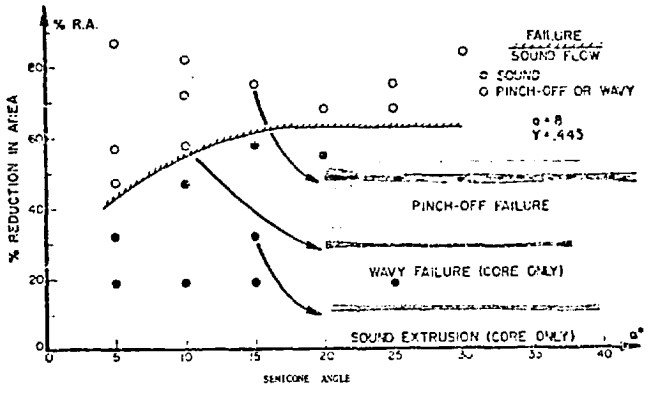

Sound and failure zones for solder clad copper (metallurgical bond)

The experimental results show that fracture in hard core clad rod is not controlled by an inherent brittleness of either core or sleeve materials but controlled by process variables.

An attempt has been made by J.M. Story, B. Avitzur and W.C. Hahn Jr. [33] to consider the influence that the combination of variables leading to failure has on the extrusion into receiver pressure. The experiments showed that increasing the receiver pressure increases the range of acceptable process

variables to produce a sound flow. The results are presented graphically, pointing out the sound and failure zones for single and three core, pure aluminium clad Nb-44% Ti. Some important conclusions of their work are:

(i) There seems to be an optimum diameter ratio above and below which the size of the successful region will be significantly smaller.

(ii) The range of acceptable reductions in area will tend to decrease with increasing die semi-cone angle.

(iii) The strength ratio is very critical. An increase in strength ratio (25-50%) will significantly reduce the size of the safe or successful zone.

(iv) Increasing receiver pressure will increase the size of the safe zone.

Based on Avitzur's velocity field, P.B. Mellor et al. [34] produced an upper bound solution to predict failure conditions in the hydrostatic extrusion of composite rods. A detailed analysis of the theoretical basis of this approach is discussed in Chapter V.

C.S. Hartley [35] produced an upper bound analysis for the tube extrusion. A kinematically admissible velocity field has been proposed based on the superposition of three velocity fields corresponding to the three zones in which the

workpiece is divided. Analysis of tube extrusion shows that the linear relation between extrusion pressure and the logarithm of the extrusion ratio is varied by fixing the mandrel size and die-cone angle and varying product diameter.

In [36], J.M. Alexander and C.S. Hartley carried out a comparative study of experimental results obtained from the hydrostatic extrusion of copper-cover red aluminium rods with theoretical results derived from Hartley's upper bound solution [35]. The study compares the experimental values obtained for the extrusion constant K and the required extrusion pressure for different extrusion ratios and die angles, showing a good agreement between them. They also compared a finite elements solution for the flow lines corresponding to the coextrusion of two dissimilar metals with the experimental ones obtained from observation of billets which have been split on a meridional plane, these being remarkably similar.

I.4 Temperature distribution during deformation

The temperature rise during the process of deformation is a very important parameter to be considered in predicting mechanical properties of metallic products. During the extrusion process the temperature rise may be significantly high (for high speed or large extrusion ratios), and therefore become relevant not only the knowledge of the temperature of

the product but also the temperature distribution in the deforming zone to predict the local heating and its mechanical and metallurgical consequences. In particular this information is necessary in the study of pressure welding conditions in the extrusion of composites.

Several attempts have previously been made to estimate the temperature rise in conventional extrusion and in the drawing process. Possibly the first work on the subject was done by Siebel and Kobitzsch [39] for wire drawing, assuming uniform deformation and a constant coefficient of friction. More recently, Singer and Coakham [40] and Singer and Al-Samarrai [41] measured the emergent temperature of the product in extruded billets, for several materials and ram speeds. In [41] an attempt is also made to predict the temperature rise of the emerging product by assuming a simple model in which all deformation takes place as the metal crosses the die-exit plane. They considered only axial heat flow and neglect the container friction.

Johnson and Kudo [42] obtained a temperature field for the extrusion process by an upper-bound approach. In their assumptions they consider a rigid-perfect plastic material, neglect the die friction and assumed the deforming process as being adiabatic.

Based on a visioplasticity approach, W. Fister [43] obtained the strain rate and stress distribution corresponding to the deforming zone for the hot extrusion of aluminium. From these fields he derived the temperature rise taking place in the metal. In this work the influence of temperature rise on the yield stress of the metal was taken into account.

By using a numerical approach, J.F.W. Bishop [44] estimates the temperature field in the deforming zone of a rigid-plastic plane-strain extruded material. He evaluates velocities and strain rates by means of a slip-lines solution, assuming no friction at the material-die interface. In this paper the deformation, thus heat generation, is regarded as taking place instantaneously, followed by a static heat conduction during a small interval of time. With these assumptions Bishop obtained the numerical solution by means of the finite difference method.

T. Altan and S. Kobayashi [45] also studied the extrusion process, by means of a visioplasticity approach obtaining the corresponding stress and strain fields. They adopted Bishop's sequence of heat generation and metal transportation followed by a static conduction process. In their development they considered temperature-dependent heat parameters for the conduction process, a constant value for the

coefficient of friction and estimate the normal stress on the die and container by means of an empirical formula. The temperature field was finally obtained by means of the Dusinberre's [46] finite difference approach.

Lengyel, B. and R.M. Guha [47] estimate the temperature distribution in the deforming zone for the process of hydrostatic extrusion. They developed a time based simulation computing model to follow up the extrusion process, where instantaneous heat generation was followed by static conduction, convection and radiation during a small period of time, by means of the finite difference method. Temperature was estimated at various extrusion speeds and coefficients of friction, taking into account the temperature and strain rate dependence of the yield stress and heat parameters of the deforming metal and tools.

Despite the fact that there are models capable of describing the temperature distribution arising from the deformation of a single metal wire, no attempt has yet been made to estimate the temperature distribution in the deforming zone of composite billets.

I.5 The Method of Weighted Residuals

Crandall has used the term "Method of Weighted Residuals" to denote a general approximation procedure for

solving various types of differential equations and boundary-value problems. The procedure is to assume an approximate solution in the form of a linear combination of known trial functions with adjustable constants. By substituting the form into the governing equation, a residual function is obtained, which is then required to be orthogonal to a selected set of weighting functions.

The application of the method of weighted residuals to solve a single scalar differential equation is discussed by Crandall [48] and Kantorovich and Krylov [49]. A generalization of this procedure to the integration of vector differential equations and systems of differential equations is considered by Finlayson and Scriven in [50] and by Finlayson in [51]. This generalization applies to the study of deformation phenomena where it is necessary to use the method of weighted residuals to tensor differential equations, including realistic boundary conditions. Details of the mathematical aspects of this method are given in Chapter VI.

E. Steck considered the application of the method of weighted residuals to obtain the stress and strain fields in the process of extrusion of solid billets through conical dies and compression (upsetting) of right cylindrical specimens between parallel platens [52], [53], [54].

Solutions for the stress and strain field were obtained by means of a direct integration of the Prandtl-Reuss non-linear tensorial equations describing the plastic state. This procedure has been used in this work and is considered in detail in following chapters.

I.6 Scope of the work

In the present work we aim to obtain a numerical description of the stress and temperature field in the deforming zone corresponding to the coextrusion of two dissimilar metals. Our immediate concern is to analyze the conditions of pressure and temperature existing at the tube-core interface leading to the formation of a metallurgical bonding.

The solid state bonding of metals by rolling and indentation have been extensively analyzed and there is in the literature relevant information for obtaining a successful metallurgical bonding. The process of coextrusion, as far as the relevant parameters of the joint formation is concerned (pressure, temperature, extrusion ratio, superficial contamination, etc.) has not yet so far been extensively considered. There exists little information on the threshold extrusion ratios to obtain bonding and the variables defining this ratio for different metals and working conditions. Hence, it is

considered that the study of these conditions would be of practical interest. Therefore it is proposed to examine numerically the stress and temperature fields in the deforming zone, particularly at the interface. It is hoped that this information will eventually lead to a better understanding of the mechanisms for the joint formation during hydrostatic extrusion at room temperature.

It also appears that the method of weighted residuals offers a relatively easy, concise and satisfactory solution and less demanding in terms of computing resources.

II. ELEMENTS OF CONTINUUM MECHANICS

II.1 Introduction

The theories of elasticity and plasticity describe the deformation process of most of the materials commonly used in engineering. These theories are based on experimental studies of the relationships between stresses and strains of polycrystalline aggregates and hence their development was, to some extent, independent of the knowledge of the structure of matter. Their macroscopic conclusions hold for an idealized material model named "continuous".

Among other principal applications of the Continuum Mechanics is the determination of stresses, strains and displacement of a solid subjected to external forces. The equations representing physical and geometrical restrictions to possible mathematical solutions for this problem are well known [55], [56]. In a general case these conditions are expressed in terms of partial differential equations, linear or non-linear, depending on the constitutive equation corresponding to the solid being considered.

In most cases exact solutions to such equations are impossible to obtain, and often not even an approximate form. Difficulties arise from the fact that boundary conditions involve restrictions arbitrarily imposed, not always easy to introduce in the governing equations of the process. Constitutive

equations in the Theory of Plasticity add a non-linear behaviour to the governing equations that, in general, make it impossible to obtain theoretical solutions for most of the problems.

Needless to say that even in cases where the difficulties can be overcome and solutions obtained, such solutions do not necessarily represent the true stresses and strains. The degree of accuracy depends upon how well the constitutive equations describe the mechanical behaviour of the material being deformed, under the particular set of circumstances in which the deformation process takes place. Consequently in order to understand the limitations of such solutions, it is often necessary, while dealing with real problems, to resort to the available knowledge of the structure of matter and the mechanisms developed by Solid State Physics. As long as the microscopic and macroscopic points of view are not completely related, it is necessary to take into account both of them, as they provide complementary information. The present trend is not to make unilateral approaches, either mechanical or physical, but to widen constantly the field of observation [57], [58], [59], [60].

It would be desirable to take from Solid State Physics the essential assumptions for the Theory of Plasticity, based on the analysis of elementary physical processes. The immediate requirements of solutions to technical problems and the fact

that Physics cannot yet meet them, makes it unavoidable that these assumptions are based on phenomenological hypothesis or on experimental investigation. Consequently such conclusions are not general and constitute a reasonable approximation to a limited number of real processes.

II.2 Stress field

The stress distribution will be analysed by means of Cauchy's stress tensor σ_{ij}, [55], [56], [61], [62], [72]; its representative matrix in a Cartesian system of coordinates x_i ($i = 1,2,3$) being:

$$\sigma_{ij} = \begin{bmatrix} \sigma_{11} & \sigma_{12} & \sigma_{13} \\ \sigma_{21} & \sigma_{22} & \sigma_{23} \\ \sigma_{31} & \sigma_{32} & \sigma_{33} \end{bmatrix} \qquad (1)$$

with the condition $\sigma_{ij} = \sigma_{ji}$

Tensor σ_{ij} can be split into the deviatoric and hydrostatic or spherical components:

$$\sigma_{ij} = \sigma'_{ij} + \sigma_m \delta_{ij} \qquad (2)$$

where $\sigma_m = \frac{1}{3}\sigma_{ii}$ and δ_{ij} is the Kronecker delta.

Consequently, the deviatoric stress tensor is

$$\sigma'_{ij} = \sigma_{ij} - \sigma_m \delta_{ij} \qquad (3)$$

The principal invariants of σ'_{ij} are given by the expressions

$$J_1' = \sigma_{ii}' = 0$$
$$J_2' = \tfrac{1}{2}\sigma_{ij}'\sigma_{ij}' \qquad (4)$$
$$J_3' = \det[\sigma_{ij}']$$

In a cylindrical coordinate system (r, θ, z) the matrix components of σ_{ij} are:

$$\sigma_{ij} = \begin{bmatrix} \sigma_r & \tau_{r\theta} & \tau_{rz} \\ \tau_{\theta r} & \sigma_\theta & \tau_{\theta z} \\ \tau_{zr} & \tau_{z\theta} & \sigma_z \end{bmatrix} \qquad (5)$$

and they are shown in the following diagram:

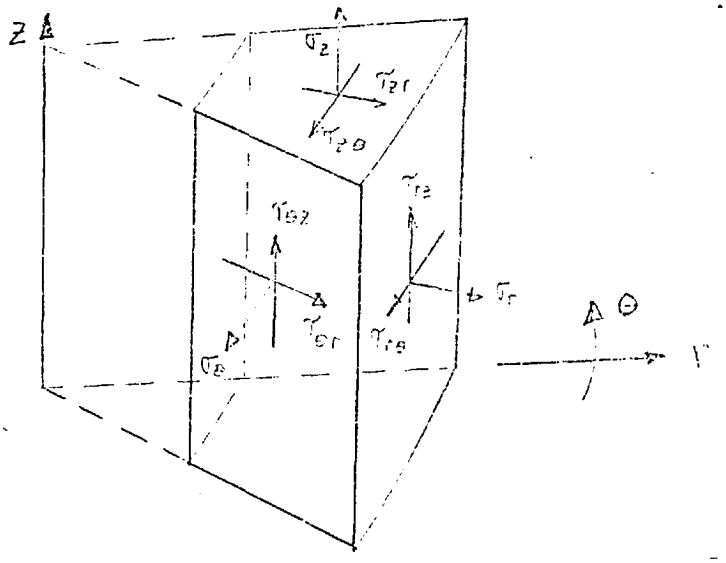

Due to axial symmetry

$$\tau_{\theta r} = \tau_{\theta z} = \tau_{r\theta} = \tau_{z\theta} = 0$$

and the remaining functions are independent of the variable θ. Under these conditions the second principal invariant has the form:

$$J_2' = (\ \sigma_r' \sigma_\theta' + \sigma_\theta' \sigma_z' + \sigma_z' \sigma_r') + \tau_{rz}^2 \qquad (6)$$

II.2.1 Equivalent stress

The equivalent stress $\bar{\sigma}$ is defined by the expression [72]:

$$\bar{\sigma} = \sqrt{3J_2'} = \sqrt{\frac{3}{2}\sigma_{ij}' \sigma_{ij}'} \qquad (7)$$

In axial symmetry, equation (7) has the form:

$$\bar{\sigma} = \left[3(-\sigma_r' \sigma_\theta' - \sigma_\theta' \sigma_z' - \sigma_z' \sigma_r' + \tau_{rz}^2)\right]^{\frac{1}{2}} \qquad (8)$$

II.2.2 Stress functions

The equilibrium condition in terms of stresses is given by

$$\frac{\partial \sigma_{ij}}{\partial x_j} = 0 \qquad \begin{cases} i = 1,2,3 \\ j = 1,2,3 \end{cases} \qquad (9)$$

body forces being neglected, where x_j is a generical coordinate. In the case of cylindrical coordinates and axisymmetric conditions, equation (9) can be expressed in scalar form as:

$$\begin{aligned} &\frac{\partial \sigma_r}{\partial r} + \frac{\partial \tau_{rz}}{\partial z} + \frac{\sigma_r - \sigma_\theta}{r} = 0 \\ &\frac{\partial \sigma_\theta}{\partial \theta} = 0 \\ &\frac{\partial \tau_{rz}}{\partial r} + \frac{\partial \sigma_z}{\partial z} + \frac{\tau_{zr}}{r} = 0 \end{aligned} \qquad (10)$$

It can be shown that selecting two functions ϕ_1 and ϕ_2 such that:

$$\sigma_r = \frac{1}{r}\frac{\partial^2\phi_1}{\partial z^2} + \frac{\phi_2}{r}$$

$$\sigma_\theta = \frac{\partial\phi_2}{\partial r} \qquad (11)$$

$$\sigma_z = \frac{1}{r}\frac{\partial^2\phi_1}{\partial r^2}$$

$$\tau_{rz} = -\frac{1}{r}\frac{\partial^2\phi_1}{\partial r\partial z}$$

where $\phi_1 = \phi_1(r,z)$ and $\phi_2 = \phi_2(r,z)$ are scalar stress functions, equations (1) are automatically satisfied [61].

II.3 Strains and strain rates [61], [62]

As in the case of stresses, strains are obtained in terms of Cauchy's strain tensor given by

$$\varepsilon_{ij} = \tfrac{1}{2}\left(\frac{\partial u_i}{\partial x_j} + \frac{\partial u_j}{\partial x_i}\right) \qquad (12)$$

where u_i are functions describing the displacement field.

Its representative matrix in a Cartesian system of coordinates x_i $(i = 1,2,3)$ is:

$$\varepsilon_{ij} = \begin{bmatrix} \varepsilon_{11} & \varepsilon_{12} & \varepsilon_{13} \\ \varepsilon_{21} & \varepsilon_{22} & \varepsilon_{23} \\ \varepsilon_{31} & \varepsilon_{32} & \varepsilon_{33} \end{bmatrix} \qquad (13)$$

Expressed in terms of a cylindrical system of coordinates (r, θ, z) and in a case of axial symmetry:

$$\varepsilon_{ij} = \begin{bmatrix} \varepsilon_r & 0 & \varepsilon_{rz} \\ 0 & \varepsilon_\theta & 0 \\ \varepsilon_{rz} & 0 & \varepsilon_z \end{bmatrix} \tag{13}$$

The strain rate tensor is defined as

$$\dot{\varepsilon}_{ij} = \frac{\partial \varepsilon_{ij}}{\partial t}$$

and in terms of velocities of displacements v_i as

$$\dot{\varepsilon}_{ij} = \tfrac{1}{2}\left(\frac{\partial v_i}{\partial x_j} + \frac{\partial v_j}{\partial x_i}\right) \tag{14}$$

The three principal invariants of ε_{ij} are:

$$\begin{aligned} J_1 &= \dot{\varepsilon}_{ii} \\ J_2 &= \tfrac{1}{2}\,\dot{\varepsilon}_{ii}\,\dot{\varepsilon}_{jj} - \tfrac{1}{2}\,\dot{\varepsilon}_{ij}\,\dot{\varepsilon}_{ij} \\ J_3 &= \det\left[\dot{\varepsilon}_{ij}\right] \end{aligned} \tag{15}$$

The incompressibility condition leads to:

$$\dot{\varepsilon}_{ii} = 0 \tag{16}$$

The strain rate tensor can also be expressed in terms of a deviatoric component $\dot{\varepsilon}'_{ij}$ and a hydrostatic or spherical one $\dot{\varepsilon}_m \delta_{ij}$ as:

$$\dot{\varepsilon}_{ij} = \dot{\varepsilon}'_{ij} + \dot{\varepsilon}_m \delta_{ij}$$

where $\dot{\varepsilon}_m = \frac{1}{3}\dot{\varepsilon}_{ii}$. Consequently, the deviatoric strain rate tensor is given by:

$$\dot{\varepsilon}'_{ij} = \dot{\varepsilon}_{ij} - \dot{\varepsilon}_m \delta_{ij} \tag{17}$$

with its three invariants:

$$\begin{aligned} I_1 &= \dot{\varepsilon}'_{ii} = 0 \\ I_2 &= \tfrac{1}{2}\dot{\varepsilon}'_{ij}\dot{\varepsilon}'_{ij} \\ I_3 &= \det\left[\dot{\varepsilon}'_{ij}\right] \end{aligned} \tag{18}$$

The form of I_2 under axisymmetric conditions is:

$$I_2 = -(\dot{\varepsilon}'_r\dot{\varepsilon}'_\theta + \dot{\varepsilon}_\theta\dot{\varepsilon}'_z + \dot{\varepsilon}'_z\dot{\varepsilon}'_r) + \dot{\varepsilon}^2_{rz} \tag{19}$$

A basic assumption of the infinitesimal elasto-plastic theory is that strain ε_{ij} (or strain rate $\dot{\varepsilon}_{ij}$) components can be expressed in terms of its elastic and plastic components as

$$\varepsilon_{ij} = \varepsilon^E_{ij} + \varepsilon^P_{ij} \quad \text{or} \quad \dot{\varepsilon}_{ij} = \dot{\varepsilon}^E_{ij} + \dot{\varepsilon}^P_{ij}$$

Frequently it is possible to neglect the elastic component in relation to the plastic component. In this case, the plastic component is assumed as being the total strain. This assumption also holds for strain rates:

$$\varepsilon_{ij} = \varepsilon^P_{ij} \quad \text{or} \quad \dot{\varepsilon}_{ij} = \dot{\varepsilon}^P_{ij} \tag{20}$$

II.3.1 Stream function

Equation (16), $\dot{\varepsilon}_{ii} = 0$, is the form adopted by the continuity equation for a fluid of constant density. This condition must be satisfied for any strain rate field $\dot{\varepsilon}_{ij}$ in order to be considered as kinematically admissible.

In the case of cylindrical coordinates (r, θ, z), equation (16) has the form:

$$\frac{\partial v_r}{\partial r} + \frac{1}{r}\frac{\partial v_\theta}{\partial \theta} + \frac{v_r}{r} + \frac{\partial v_z}{\partial z} = 0 \qquad (21)$$

or, under axisymmetric conditions:

$$\frac{\partial v_r}{\partial r} + \frac{v_r}{r} + \frac{\partial v_z}{\partial z} = 0 \qquad (22)$$

It is easy to show that if a scalar stream function $\psi = \psi(r,z)$ is selected, such that

$$\begin{aligned} v_r &= \frac{1}{r}\frac{\partial \psi}{\partial z} \\ v_z &= -\frac{1}{r}\frac{\partial \psi}{\partial r} \end{aligned} \qquad (23)$$

the continuity equation (22) is automatically satisfied.

Developing equation (14) for the case of cylindrical coordinates one obtains:

$$\begin{aligned} \dot{\varepsilon}_r &= \frac{\partial v_r}{\partial r} & \dot{\varepsilon}_{r\theta} &= \frac{\partial v_\theta}{\partial r} - \frac{v_\theta}{r} + \frac{1}{r}\frac{\partial v_r}{\partial \theta} \\ \dot{\varepsilon}_\theta &= \frac{1}{r}\frac{\partial v_\theta}{\partial \theta} + \frac{v_r}{r} & \dot{\varepsilon}_{rz} &= \frac{\partial v_r}{\partial z} + \frac{\partial v_z}{\partial r} \\ \dot{\varepsilon}_z &= \frac{\partial v_z}{\partial z} & \dot{\varepsilon}_{\theta z} &= \frac{\partial v_\theta}{\partial z} + \frac{1}{r}\frac{\partial v_z}{\partial \theta} \end{aligned} \qquad (24)$$

Under conditions of axisymmetry $v_\theta = 0$, $v_r = v_r(r,z)$ and $v_z = v_z(r,z)$, equations (24) are reduced to:

$$\begin{aligned} \dot{\varepsilon}_r &= \frac{\partial v_r}{\partial r} & \dot{\varepsilon}_{r\theta} &= 0 \\ \dot{\varepsilon}_\theta &= \frac{v_r}{r} & \dot{\varepsilon}_{\theta z} &= 0 \\ \dot{\varepsilon}_z &= \frac{\partial v_z}{\partial z} & \dot{\varepsilon}_{rz} &= \frac{\partial v_r}{\partial z} + \frac{\partial v_z}{\partial r} \end{aligned} \qquad (25.a)$$

In the case of a spherical coordinate system (R, φ, θ) the velocity components become:

$$\bar{v} = (v_R, v_\varphi, v_\theta)$$

and the corresponding strain rate field is described by:

$$\begin{aligned} \dot{\varepsilon}_{RR} &= \frac{\partial v_R}{\partial R} & \dot{\varepsilon}_{R\theta} &= \frac{1}{2R}\frac{\partial v}{\partial \theta} \\ \dot{\varepsilon}_{\varphi\varphi} &= \frac{v_R}{R} & \dot{\varepsilon}_{\theta\varphi} &= \dot{\varepsilon}_{R\varphi} = 0 \\ \dot{\varepsilon}_{\theta\theta} &= \frac{v_R}{R} = -(\dot{\varepsilon}_{RR} + \dot{\varepsilon}_{\varphi\varphi}) \end{aligned} \qquad (25.b)$$

Finally, referred to a cylindrical coordinate system, the strain rate field can be expressed in terms of the stream function as:

$$\begin{aligned} \dot{\varepsilon}_r &= \frac{\partial}{\partial r}\left(\frac{1}{r}\frac{\partial \psi}{\partial z}\right) \\ \dot{\varepsilon}_\theta &= \frac{1}{r^2}\frac{\partial \psi}{\partial z} \\ \dot{\varepsilon}_z &= -\frac{\partial}{\partial z}\left(\frac{1}{r}\frac{\partial \psi}{\partial r}\right) \end{aligned} \qquad (26)$$

$$\dot{\varepsilon}_{rz} = \frac{\partial}{\partial z}\left(\frac{1}{r}\frac{\partial \psi}{\partial z}\right) - \frac{\partial}{\partial r}\left(\frac{1}{r}\frac{\partial \psi}{\partial r}\right)$$

(26, continued)

$$\dot{\varepsilon}_{r\theta} = \dot{\varepsilon}_{\theta z} = 0$$

II.4 Elements of the Mathematical Theory of Plasticity [67], [68], [69]

II.4.1 Yield function

Assuming a homogeneous material with an isotropic rule of hardening, the yield function may be written as

$$f(\sigma_{ij}) = C(L) \qquad (27)$$

In general, L is a functional depending on the plastic strain history of the material:

$$L = L\left[\varepsilon^{t}_{\tau=-\infty}(\tau)\right]$$

and C is a scalar function. In a 9^{th}-dimensional space of stresses, function C measures the instantaneous "size" of the yield surface.

Assuming an isotropic behaviour of the material before and during the deformation, and since $f(\sigma_{ij})$ is a scalar function, it is possible to express f in terms of the eigenvalues of σ_{ij} or in terms of the principal invariants:

$$f(\sigma_{ij}) = f(J_1, J_2, J_3) \qquad (28)$$

By assuming constancy of volume, equation (28) can be expressed in terms of the principal invariants of the deviatoric stress tensor σ'_{ij}, that is

$$f(\sigma'_{ij}) = f(J'_2, J'_3) \tag{29}$$

The most common expressions for equation (29) are those given by von Mises and Tresca.

(i) Von Mises yield criterion:

This is the simplest possible form of equation (29) and is given by:

$$f = J'_2 - k^2 = 0$$

or

$$f = \tfrac{1}{2}\sigma'_{ij}\sigma'_{ij} - k^2 = 0 \tag{30}$$

where k is a scalar function depending on plastic strain history.

Despite the fact that physical interpretations have been suggested for this criterion, based on the shear strain energy, they should be merely considered as formals [61].

(ii) Tresca yield criterion:

In terms of the principal stresses σ_1, σ_2 and σ_3, where $\sigma_1 > \sigma_2 > \sigma_3$, the Tresca criterion is expressed by:

$$f = \sigma_1 - \sigma_3 - 2k^* = 0 \qquad (31)$$

Experiments give, in general, little backing to the hypothesis of isotropic hardening, necessary to the validity of these criteria [63], [64], [65], [66]. The permanent preference for this hypothesis is due to its mathematical simplicity and to the fact that if unloading is not performed during the process of deformation, the results produced are in reasonable agreement with the experiments.

II.4.2 Equivalent strain

From the expression of plastic work and assuming $f = J_2'$, the equivalent strain is:

$$d\bar{\varepsilon} = \sqrt{\frac{2}{3} d\varepsilon^P_{ij} \, d\varepsilon^P_{ij}} \qquad (32)$$

Drucker [71], [73], has proved that expression (32) is reasonably correct for any yield function of the form $f(J_2', J_3') = 0$.

II.4.3 Plastic stress-strain relationships

For a material that behaves according to Drucker's postulate [70], [71], [73], the general expression for the plastic stress-strain relationship is

$$d\varepsilon^P_{ij} = G \frac{\partial f}{\partial \sigma_{ij}} \frac{\partial f}{\partial \sigma_{RR}} d\sigma_k \qquad (33)$$

where G is a scalar function depending on stresses, strain and loading history. For a material that hardens isotropically, equation (33) can be written as

$$d\varepsilon^{P}_{ij} = G \frac{\partial f}{\partial \sigma_{ij}} df$$

or, in another form:

$$d\varepsilon^{P}_{ij} = \frac{\partial f}{\partial \sigma_{ij}} d\lambda \qquad (34)$$

where $d\lambda = Gdf$.

If equation (30) is used as a yield function, equation (34) becomes:

$$d\varepsilon^{P}_{ij} = \sigma'_{ij} d\lambda \qquad (35)$$

or, in terms of strain rates:

$$\dot{\varepsilon}^{P}_{ij} = \Delta\sigma'_{ij} \qquad (36)$$

where $\Delta = \frac{d\lambda}{dt}$.

Equations (35) or (36) are known as the Prandtl-Reuss relationship. The value of Δ can be calculated by substituting equation (36) in the von Mises yield criterion (30); then the following expression is obtained:

$$\frac{1}{2\Delta^2} \varepsilon^{P}_{ij} \varepsilon^{P}_{ij} = k^2 \qquad (37)$$

In another form:

$$I_2 = k^2 \Delta^2$$

where I_2 is the second principal invariant of the strain rate tensor. Finally

$$\Delta = \frac{\sqrt{I_2}}{k}$$

and replacing this value in equation (36):

$$\sigma'_{ij} = \frac{k}{\sqrt{I_2}} \dot{\varepsilon}^P_{ij} = \frac{k}{\sqrt{\frac{1}{2} \dot{\varepsilon}^P_{ij} \dot{\varepsilon}^P_{ij}}} \dot{\varepsilon}^P_{ij} \qquad (38)$$

which is the form to be used throughout this work.

II.4.4 Power of plastic deformation

The power involved in the plastic deformation of a material volume V according to a strain rate field $\dot{\varepsilon}^P_{ij}$ and under a deviatoric state of stress σ'_{ij} is:

$$\dot{w} = \int_V \sigma'_{ij} \dot{\varepsilon}^P_{ij} \, dV \qquad (39)$$

For a material obeying the Prandtl-Reuss relationship, equation (38) is then valid and consequently:

$$\dot{w} = \int_V \frac{k}{\sqrt{I_2}} \dot{\varepsilon}^P_{ij} \dot{\varepsilon}^P_{ij} \, dV$$

or

$$\dot{w} = \int_V 2k\sqrt{I_2} \, dV \qquad (40)$$

If k has a constant value all over V and the material does not exhibit strain hardening, equation (40) can be written as:

$$\dot{w} = 2k \int_V \sqrt{I_2} \, dV$$

or

$$\dot{w} = \frac{2}{\sqrt{3}} Y \int_V \left[\frac{1}{2} \dot{\varepsilon}^P_{ij} \dot{\varepsilon}^P_{ij} \right]^{\frac{1}{2}} dV \qquad (41)$$

III. EXPERIMENTAL WORK

III.1 Introduction

The general aim of this experimental work is to obtain a composite wire of copper and stainless steel, by means of an existing rig for hydrostatic extrusion-drawing processes. Most of the experiments have been carried out with copper as sleeve and stainless steel as core, but the inverse combination was also tried.

The main purpose of these experiments is to produce an adequate composite specimen, suitable for being extruded in our equipment and to gather relevant information to fit in theoretical models describing the stress and temperature fields developed during the extrusion process.

III.2 Experimental equipment

III.2.1 The hydrostatic extrusion-drawing rig

The complete and detailed description of the rig can be seen in [74], [75]. We here merely list some characteristics of the equipment relevant to our work. A general view of the total apparatus can be seen in Fig. 2, and a schematic view of it in Fig. 3.

III.2.2 Pressure vessel

The pressure vessel consists in a maraging steel liner, 25.4 mm dia. bore and 660 mm long. It is designed on the basis of a plastic liner with elastic support cylinders [5]. There are two outer cylinders: one in the form of sleeves and the other in rings assembled with an interference, giving a total external diameter of 381 mm. The maximum designed working pressure is 30 k.

Since at high extrusion pressures the fluid reduces significantly its volume, a large amount of elastic energy is stored in it. In order to lessen the risk involved in this situation, filler cylinders are used to reduce the volume of fluid in the bore.

II.2.3 Intensifier cylinder and oil pump

At one end of the pressure vessel is located an intensifier cylinder used to pressurise the vessel by acting on the plunger. The intensification ratio is 31.7.

The pressure existing on the low pressure side of the intensifier is supplied by an electrohydraulic pump "Stansted", model TC/10 612PF, manufactured by Standted Filtration Ltd. The pump operates with Shell Tellus 27 hydraulic oil, at a maximum working pressure of 1034 MN/m^2., with a rate delivery of 3.8 cm^3/s.

The pump has a special device to hold automatically a preset pressure indefinitely by supplying any flow demand within its capacity. Nevertheless, this control operation was done manually since this device was not sensitive enough to our requirements.

III.2.4 Dies and die holder

III.2.4.1 Dies

A set of dies was designed to be used with the composite specimen and different extrusion ratios. A drawing corresponding to one of them can be seen in Fig. 4. Dies were made of KE 180 steel, hardened to HRC 62 min. and 30^{o} included is the angle used throughout the experiments.

III.2.4.2 Die holder

The general structure of the die holder was maintained as in [75]. Only some minor design modifications to reduce stress concentration were made. The new shape can be seen in Fig. 5. This change has been made since several die holders cracked at hydrostatic pressures about 15.5 kb. The new design supported 20 kb satisfactorily.

III.2.5 High pressure plunger

The main characteristics of the plunger operating in the bore of the vessel were kept as in [76], except for a

design modification aiming to reduce stress concentration.

This was done after the original plunger was broken into pieces at a pressure of 20 kb. The new design is shown in Fig. 6.

III.2.6 Extrusion fluid

The main characteristics of an appropriate extrusion fluid must be: (i) a good lubricant, and (ii) not to "freeze" at the high pressures used in the process. It is important to remark that at the usual pressures developed during the extrusion process, fluids reduce their volumes in a 30-50% range.

Due to the important increase in the viscosity of fluids at high pressures, not all lubricants are suitable for being used in this process. A comparative analysis of the ones more commonly used is presented in [1] and [77]. An illustrative plot relevant to fluid behaviour is presented in Fig. 7 [1].

One of the more adequate fluids for transmitting the load acting on the plunger to the whole fluid volume and to convert it into hydrostatic pressure, at the highest working pressures, is castor oil. However, the addition of 20% methanol was necessary to avoid freezing.

III.2.7 Drawing bench

As drawing bench, a 50 kN drawing jack manufactured

by M/s Duff-Norton & Co. was used. It has a continuous variation speed through a gear box, from 1.6 to 14 mm/s. Modifications made in the supporting structure enlarged its drawing capacity in length up to 560 mm.

The drawing head is a standard Instron jaw, capable of gripping any wire diameter. A load cell is located between the jaw and the jack screw, in order to measure the drawing force. The load cell works with an ordinary four arms strain gauges bridge connection and it has a load capacity of 9 kN. The measurement instrument is a U.V. recorder, properly calibrated.

The rig allows operating under the entire range of driving stress ratios (D.S.R.);

(D.S.R.) = Extrusion pressure/drawing stress.

It is possible to obtain conditions going from pure drawing (D.S.R. = 0) up to pure hydrostatic extrusion (D.S.R. = ∞).

III.2.8 Pressure measurement [78]

III.2.8.1 The coil

The pressure in the high pressure vessel is measured by the change in electrical resistance of a 100 Ω manganin coil, of 42 S.W.G. wire (0.1016 mm dia.).

The wire is kept for approximately 10 hours at a temperature of 140°C, aiming to stabilize the electrical resistance and to relax residual stresses. This procedure is suggested by Johnson-Matthey, the manufacturer of the wire.

The coils are prepared according to the following geometry:

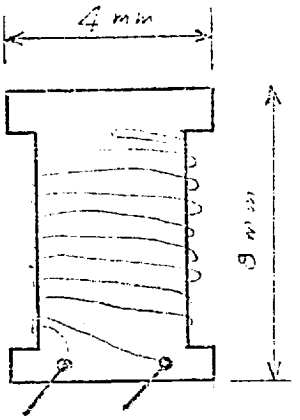

The wire is tightly coiled in a non-inductive way and the ends soldered to two copper terminals riveted to a piece of insulating material. These points are then connected to the plunger terminals by means of two stronger leads. Originally the ends of the coil were directly connected to the plunger terminals. In this condition, the wire breaks every time a violent drop in the pressure takes place, as happens when the billet is acidentally expelled through the die during a free extrusion experiment.

The present form of connection proved to support satisfactorily these events saving the long time usually required to replace a broken coil [76].

Coils are calibrated in a dead weight machine, checking the resistance with a Wheatstone bridge. The more representative value obtained for the change in resistance with pressure is $1.65 \times 10^{-7}\ \Omega/\Omega/\text{psi}$. and the law of variation linear within the observed range. The calibration line is shown in Fig. 8.

III.2.8.2 Measurement circuit

The manganin coil is an arm of the Wheatstone bridge connection, as follows:

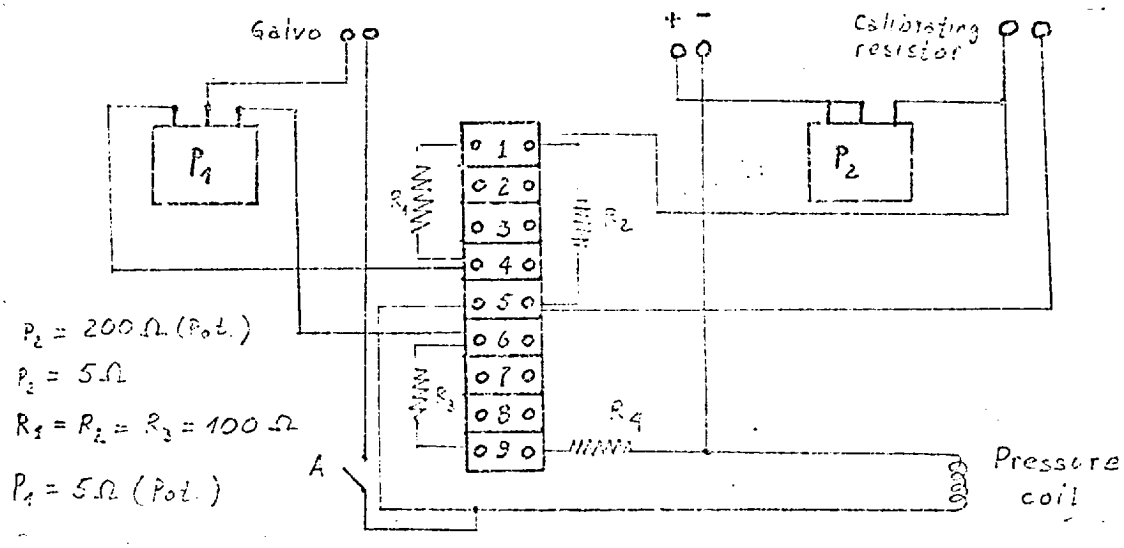

The measurement instrument used is an Ultraviolet Recorder S.E. Type 3006, with a galvanometer Type A-100 (0.130 mV/cm sensitivity). For the calibration of the recorder, a calibrating resistor is used that when connected to the bridge produces a displacement from equilibrium equivalent to the effect of a 7.72 kb pressure acting on the manganin coil.

III.3 Metals and billet characteristics

The copper tube used throughout the experiments is a commercial type, 24 gauge (3.64 mm bore) in "hard" condition.

The stainless steel core was provided by:

M/s Bekaert S.A.

B - 8550 Swevegum

Belgium.

with a chemical composition as follows:

17.7 Cr: 9% Ni: 1.66% Mn: 0.192% Si:
0.07% C: 0.026% P: 0.02% S: Fe up to complete balance.

The stainless steel wire is annealed according to the following procedure: maintained at 1100°C in vacuum furnace and then air-cooled at room temperature.

Experiments with composite specimens have shown that the best results are obtained when the plastic deformation characteristics of both components are similar [112]. This situation is reasonably achieved with fully annealed stainless steel and copper in "hard" state.

After several trials, the following is the final design adopted for the composite billet:

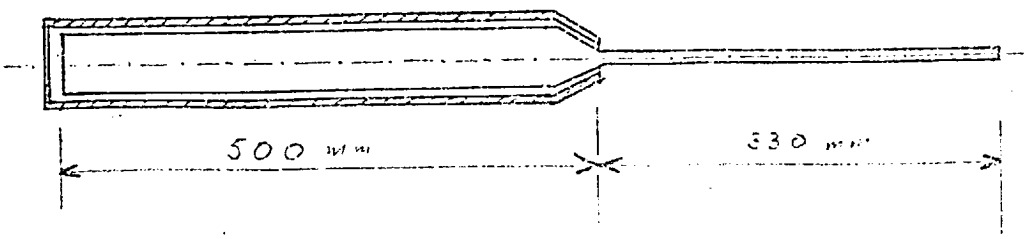

It is important to keep the tube-bore clearance as small as possible to avoid geometrical distortions in the product.

Once the core is inside the tube, the back of the tube is closed with soft soldering while the other end is tapered by pushing it manually through a 40^{o} included conical die.

III.4 Experimental techniques

The conical end of the described specimen is then lapped against the die until a definite contact surface appears on the tube cone, as to assure a proper sealing of the high pressure, at the beginning of the process.

Once this condition is attained, the specimen is located into the bore of the pressure vessel, full of fluid, and the whole equipment is assembled. The tag passing through the die allows the application of a small load by means of the jack. This operation will keep the core against the tube and the tube against the die, as to permit to build up some pressure.

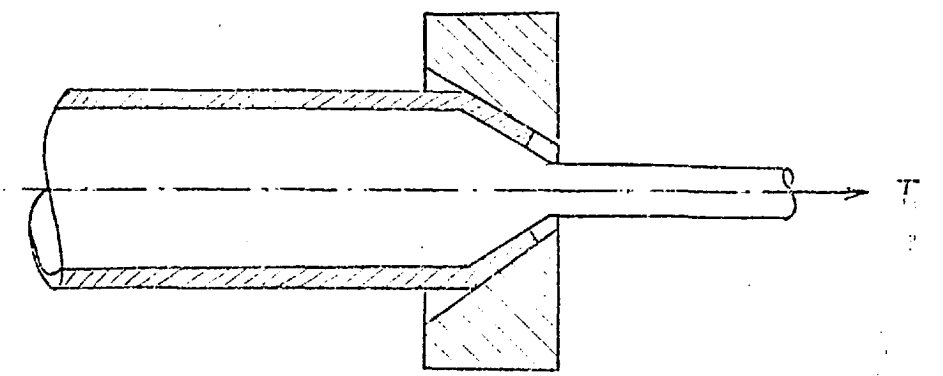

The pressure makes the tube collapse over the core, producing a very strong grip. As a consequence, the composite billet can be pulled as a solid wire from the core tag.

Pressure is raised in the container by pumping oil into the low pressure side of the intensifier cylinder. The high pressure induced in the vessel is measured by means of the manganin coil and recorded in the U.V. recorder.

Since the drawing jack is of the screw type, motor driven, a start-stop push button is used to control the extrusion process, by means of the product augmenting pull the jack exerts.

The process begins by pumping up to the desired pressure and then the pulling jack is started. The drawing jack pull needed to start and maintain the extrusion process at a chosen hydrostatic pressure is recorded on the same U.V. recorder as the pressure, from the load cell.

The simultaneous measurement of the pressure and the drawing pull allows the construction of graphs with the "pulling stress-hydrostatic pressure" relationship, corresponding to the extrusion ratio to be considered.

III.5 Results

Composite specimens with extrusion ratios 2.7, 4.3

and 5.6 have been processed with the minimum speed, aiming to obtain the "pulling stress-hydrostatic pressure" relationships.

The plots are shown in Fig. 9. Each point in the graphs is the average of three experiments carried out under similar conditions. The determination of these points is reasonably free from scatter in all the extrusion ratios tested. A photograph of the cross sections of these wires together with the original one is shown in Fig. 10.

In Fig. 11, the "pulling stress-hydrostatic pressure" relationship corresponding to the stainless steel wire is presented.

From examination of the composite specimen graphs it can be seen that they follow the pattern predicted by the theory existing in the literature for solid wires, referring to their linear trend. A theoretical interpretation of these results is considered in the following chapters.

The same relationship, corresponding to the process of a stainless steel sleeve-copper core specimen with an extrusion ratio of 2.7, is shown in Fig. 12.

III.6 Multicore specimens

As a complement to these experiments, a multicore specimen has been tried, as a first step in the line of

production of superconductor wires.

The cross-section designed is shown below:

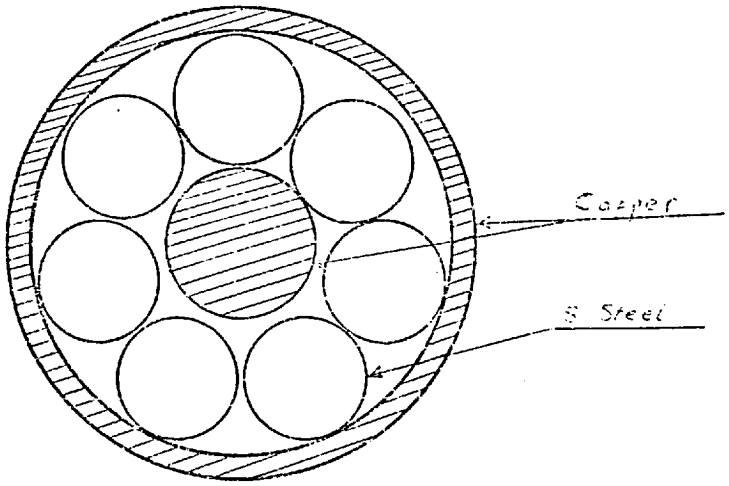

Materials used are of the same characteristics as the previous specimens. The assembly of the billet follows a similar procedure as described before. A photograph with a cross-section of the original billet and that corresponding to a product obtained with an extrusion ratio 2.7 is shown in Fig. 13.

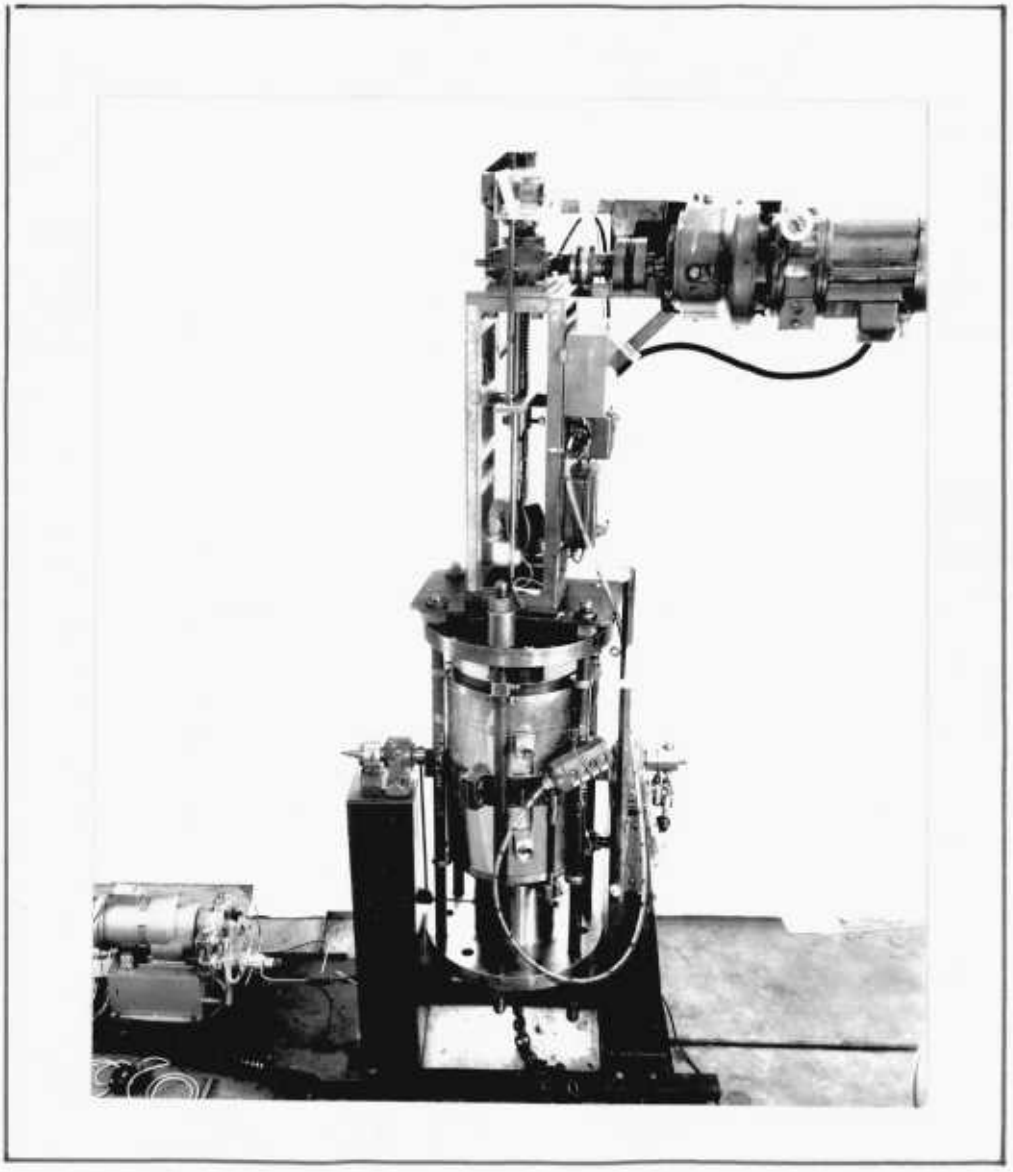

FIGURE 2 . General view of the hydrostatic extrusion-drawing rig.

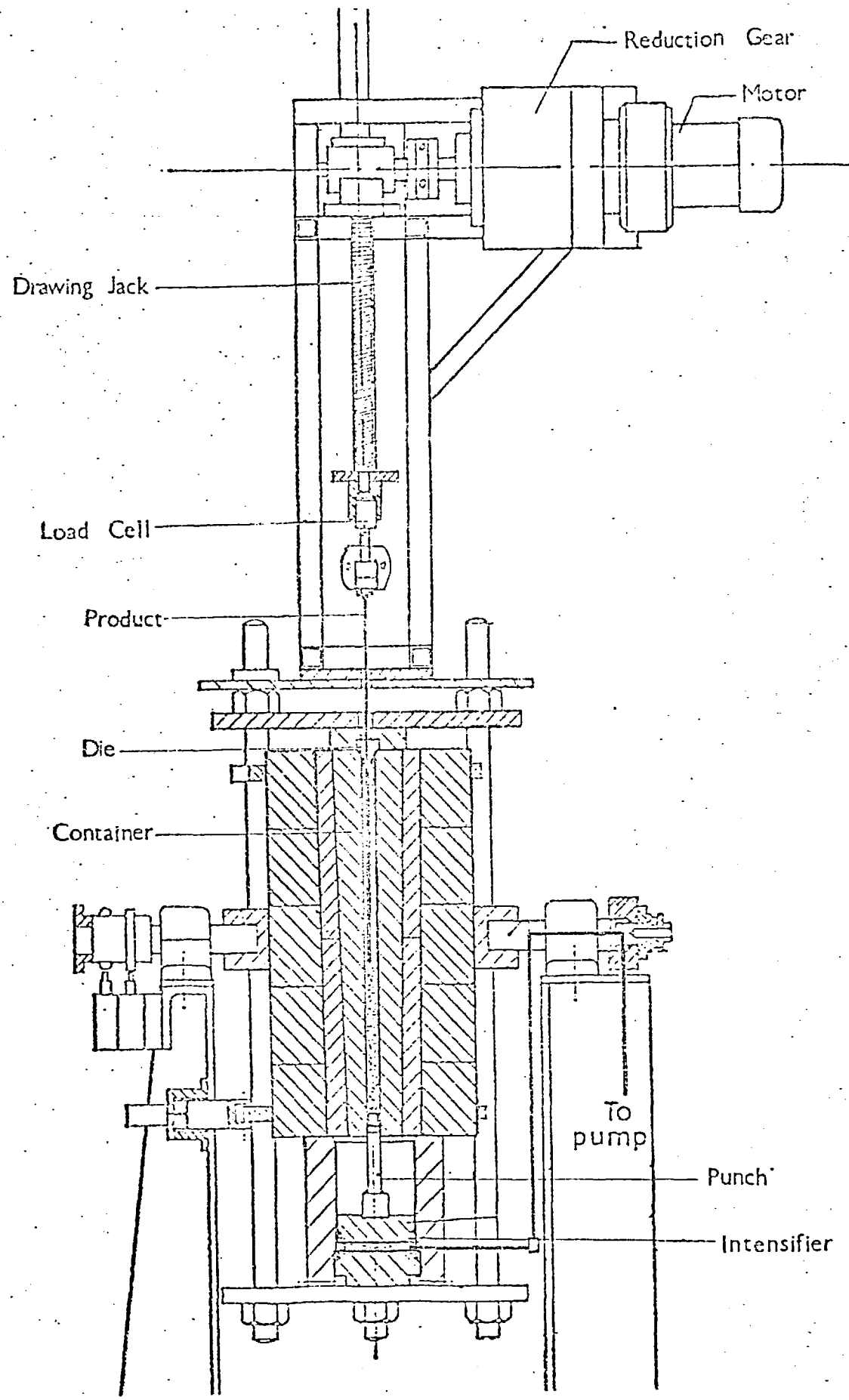

FIGURE 3 . Schematic view of the hydrostatic extrusion-drawing rig.

Scale 2:1

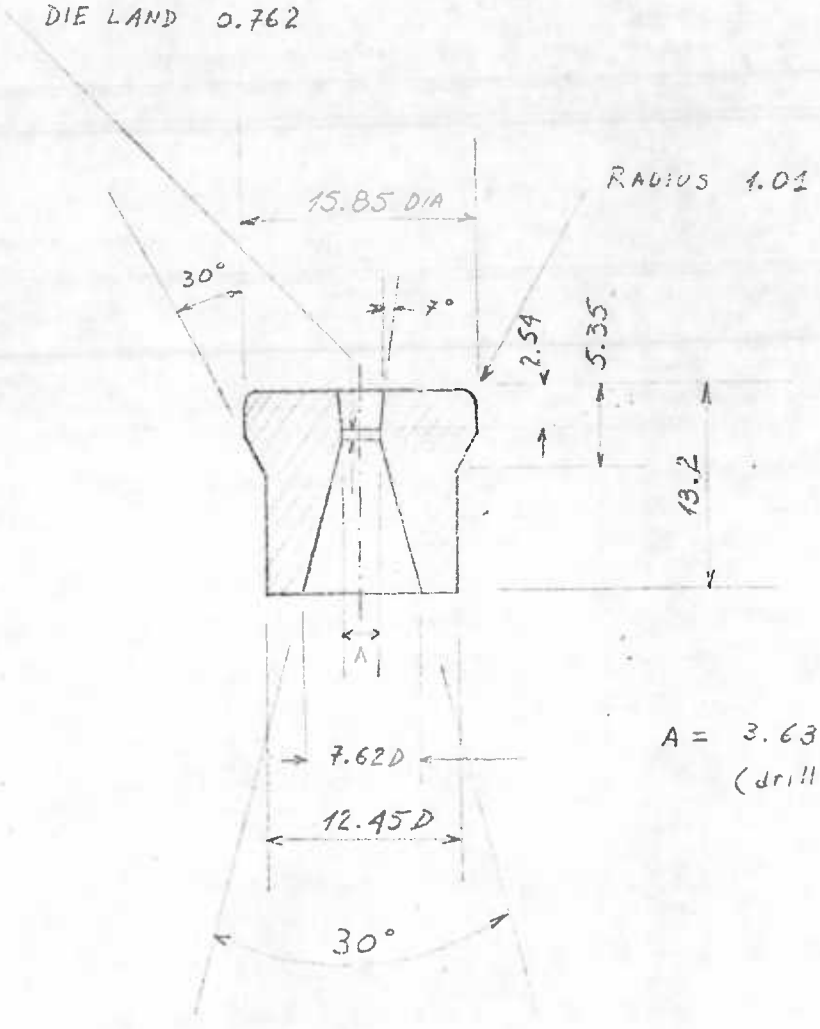

A = 3.632 mm
(drill Nº 27)

DIE - MAT KEA 180
HARDEN TO HRC 62 MIN
ALL DIMENSIONS IN mm

Figure 4

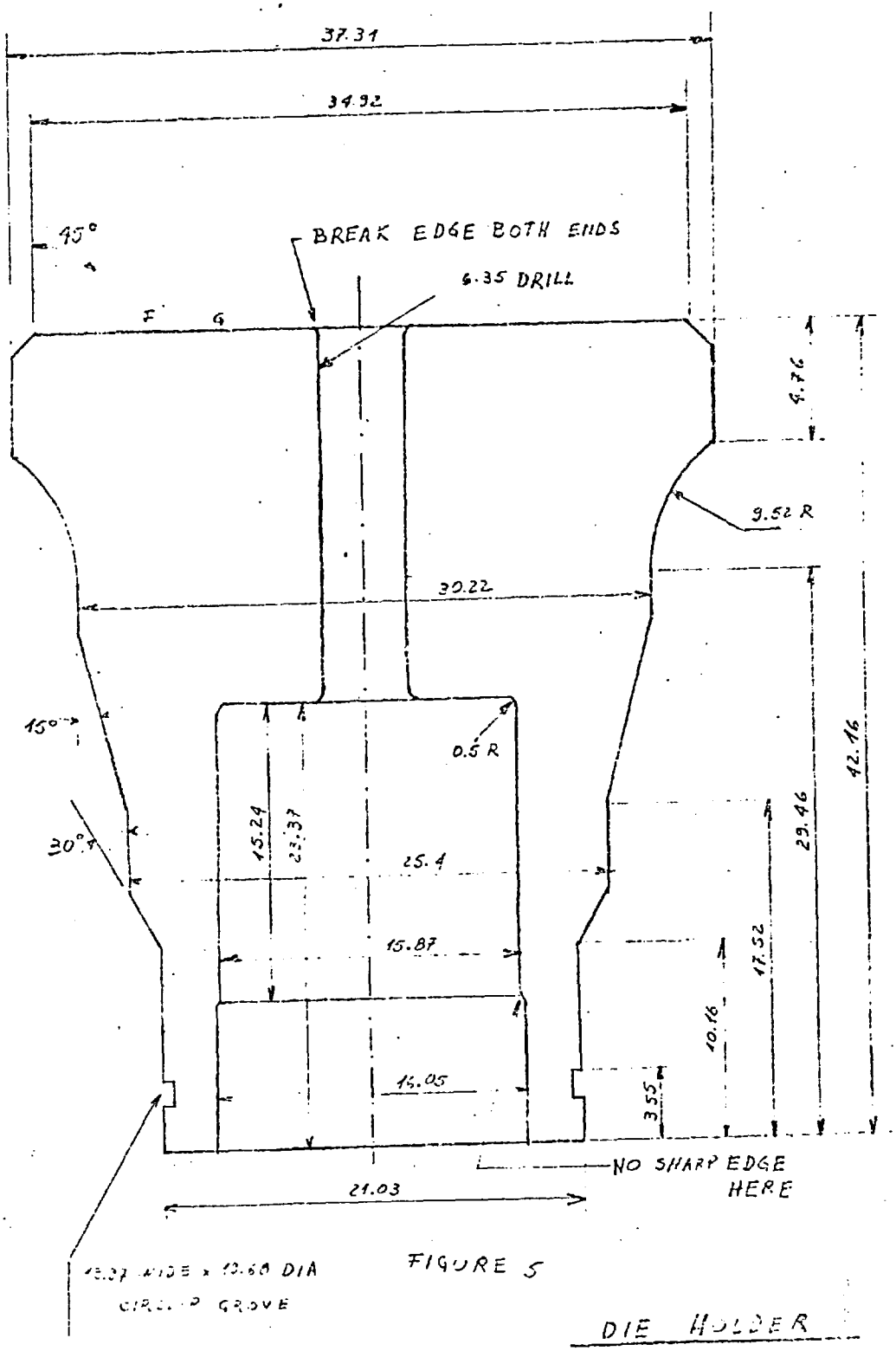

FIGURE 5

DIE HOLDER

MAT. A 180 - TEMPER TO 300°C

LAP FACE "F" FLAT

ALL DIMENSIONS IN mm

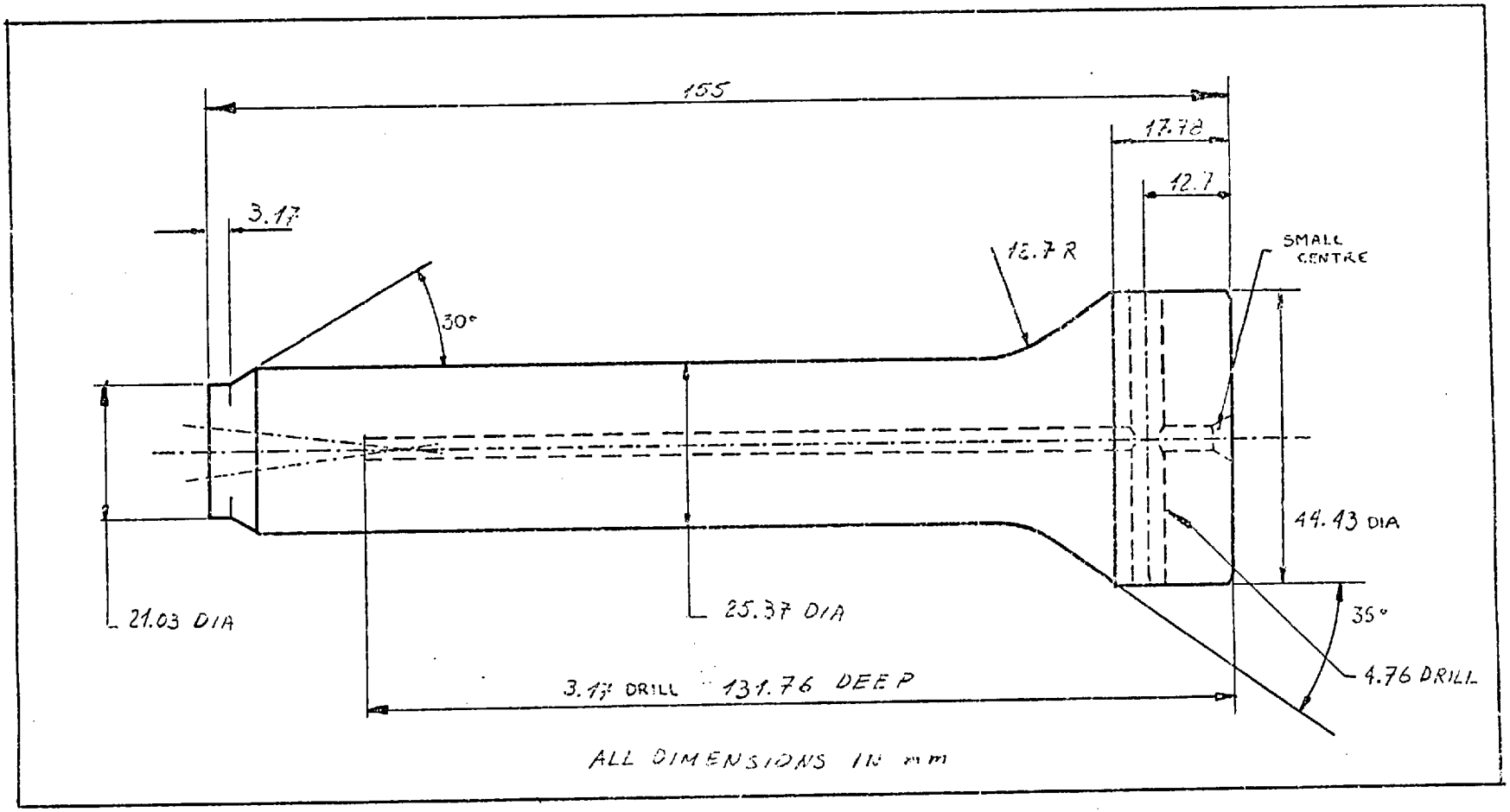
155
17.72
12.7
3.17
12.7 R
SMALL CENTRE
30°
44.43 DIA
21.03 DIA
25.37 DIA
35°
4.76 DRILL
3.17 DRILL
131.76 DEEP
ALL DIMENSIONS IN mm

FIGURE 6

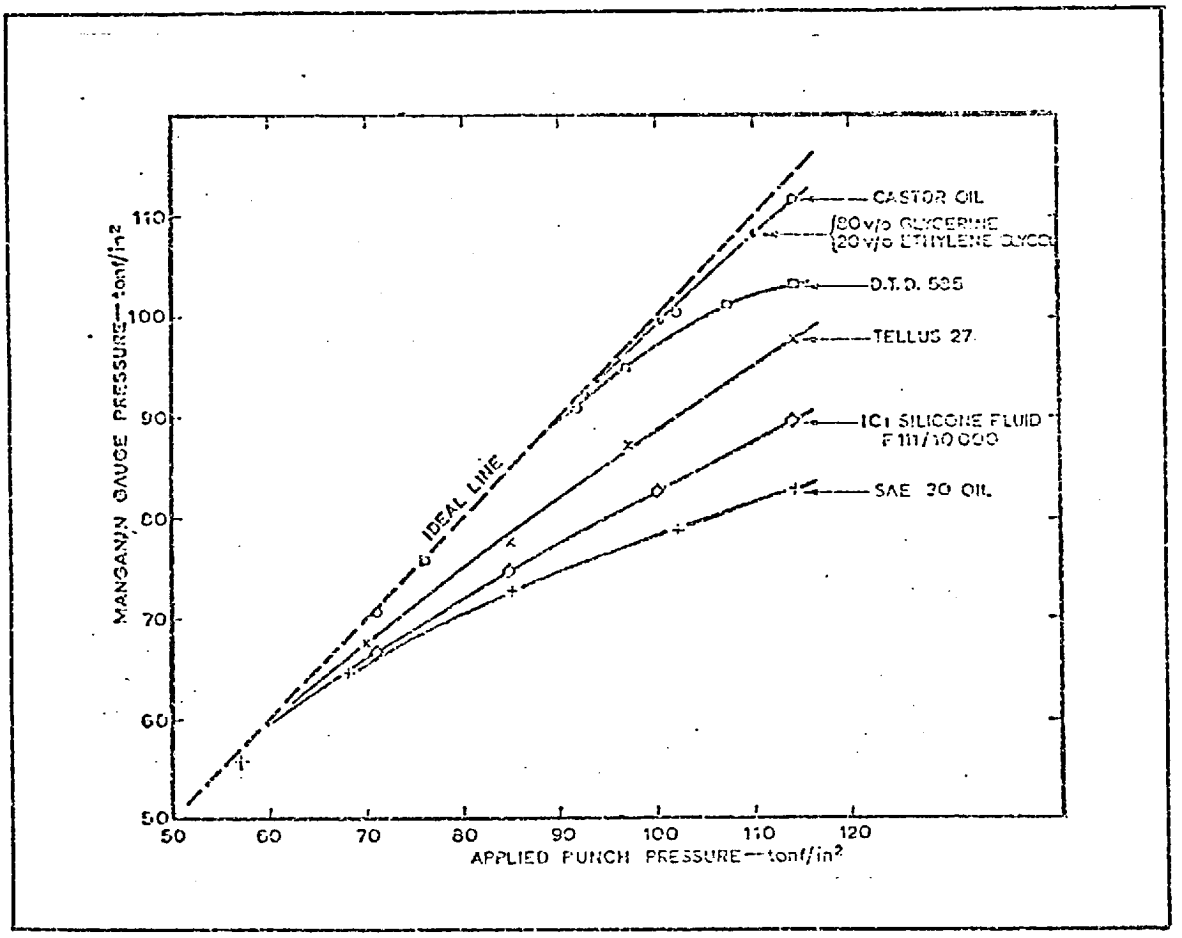

FIGURE 7 . Behaviour of different fluids under high pressure.

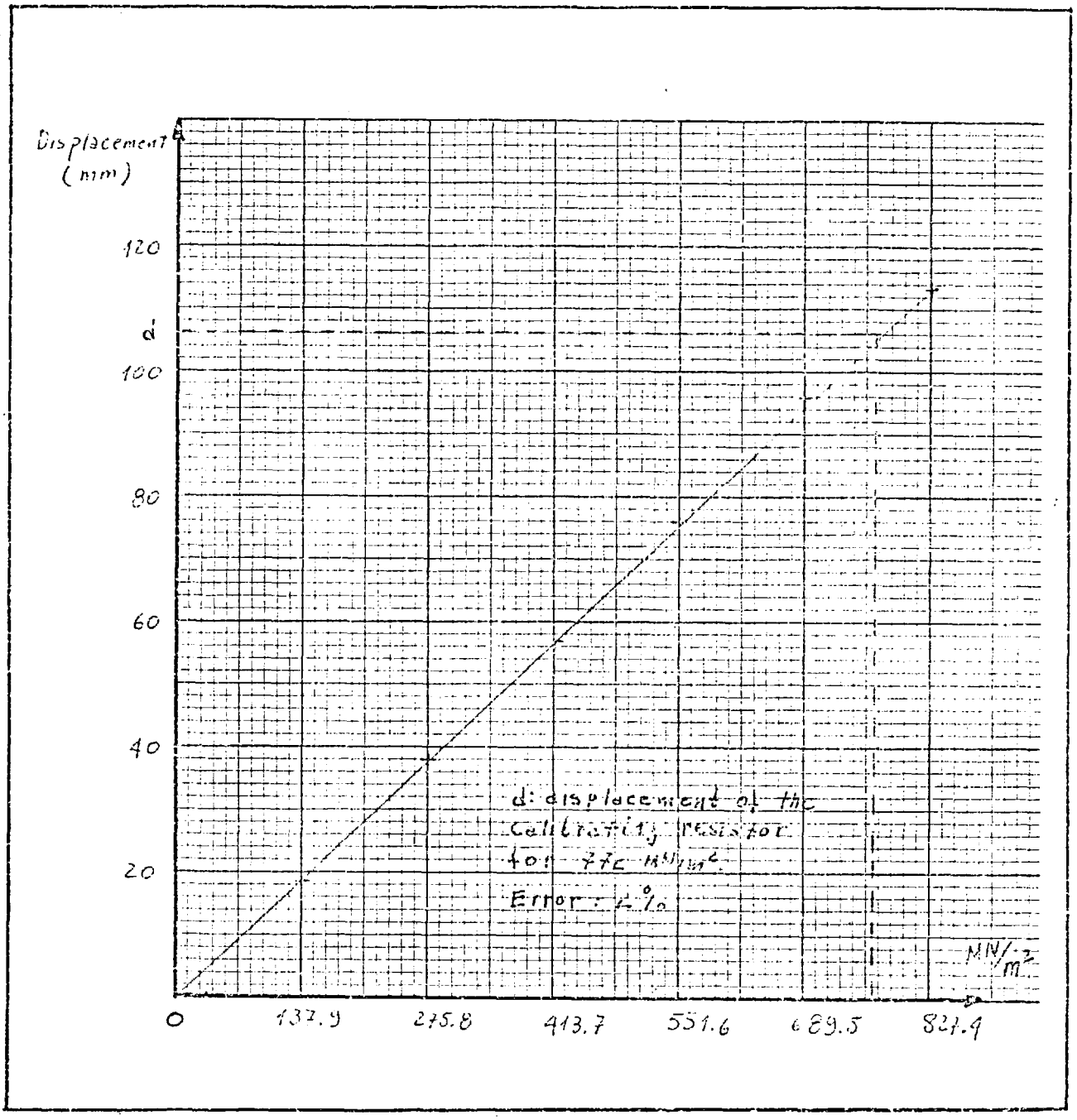

FIGURE 8 . Calibration
of the manganin coil.

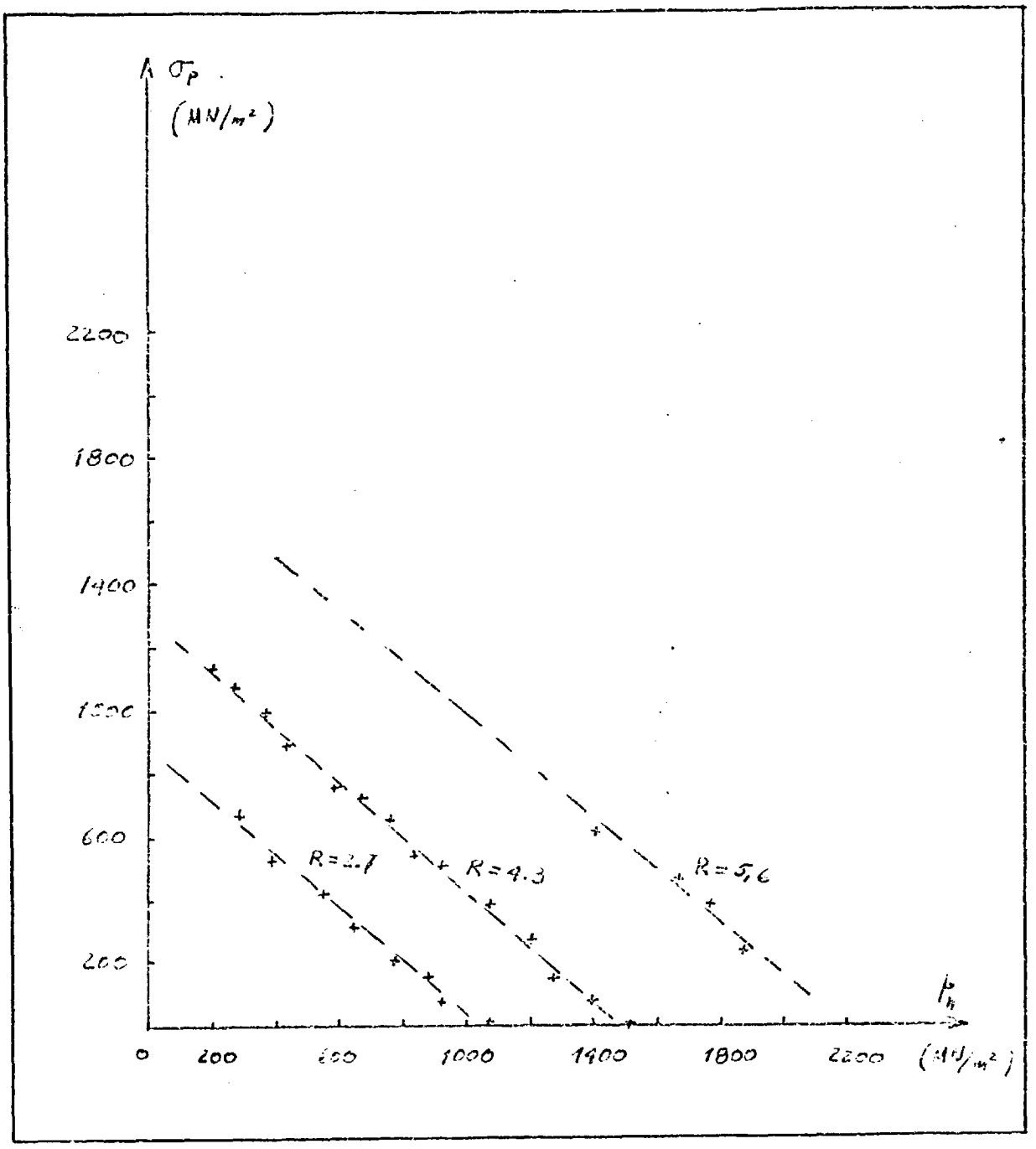

FIGURE 9 . Pulling stress-hydrostatic pressure charcteristics of composites specimens under different extrusion ratios.

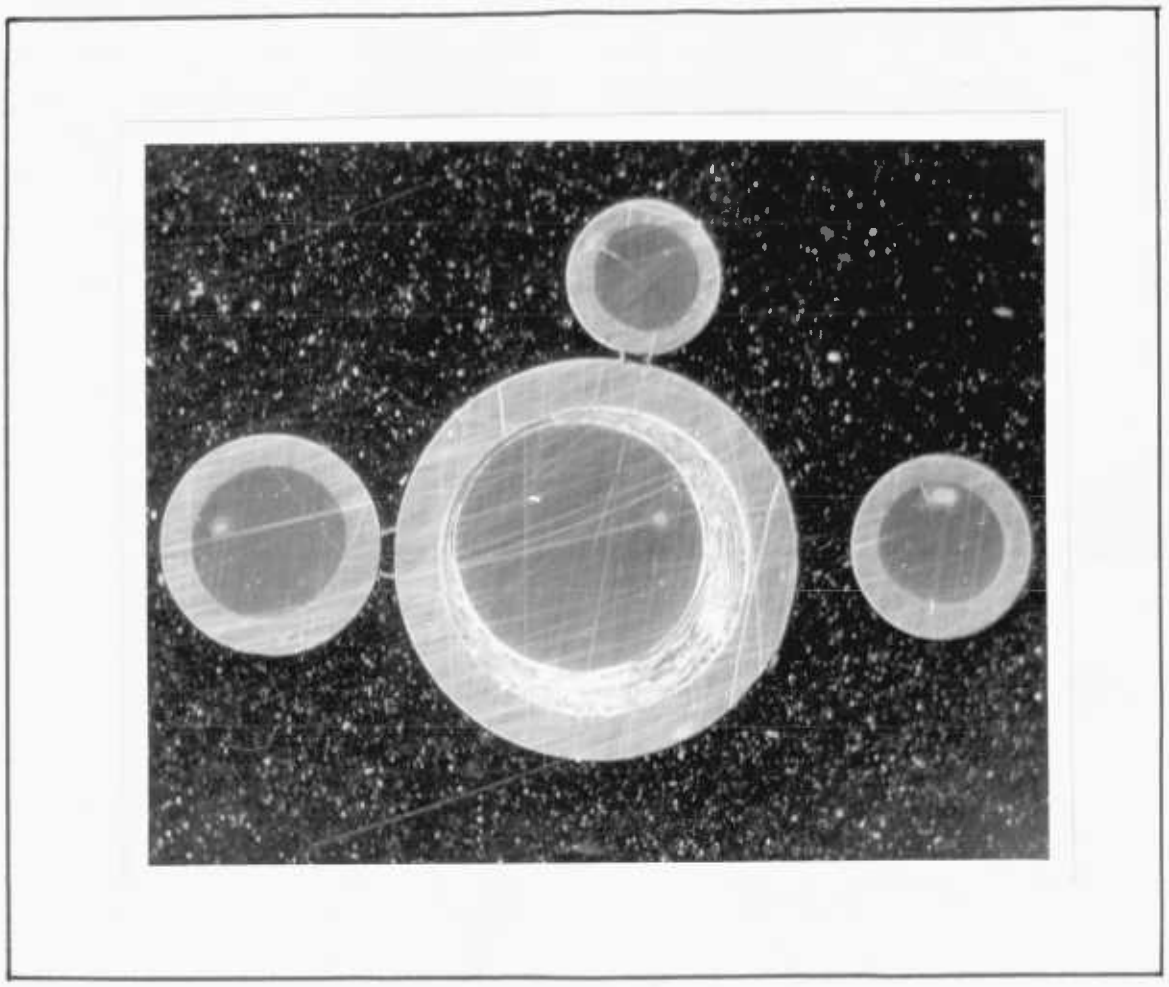

FIGURE 10 . Cross-sections of a composite billet and products of various reductions.

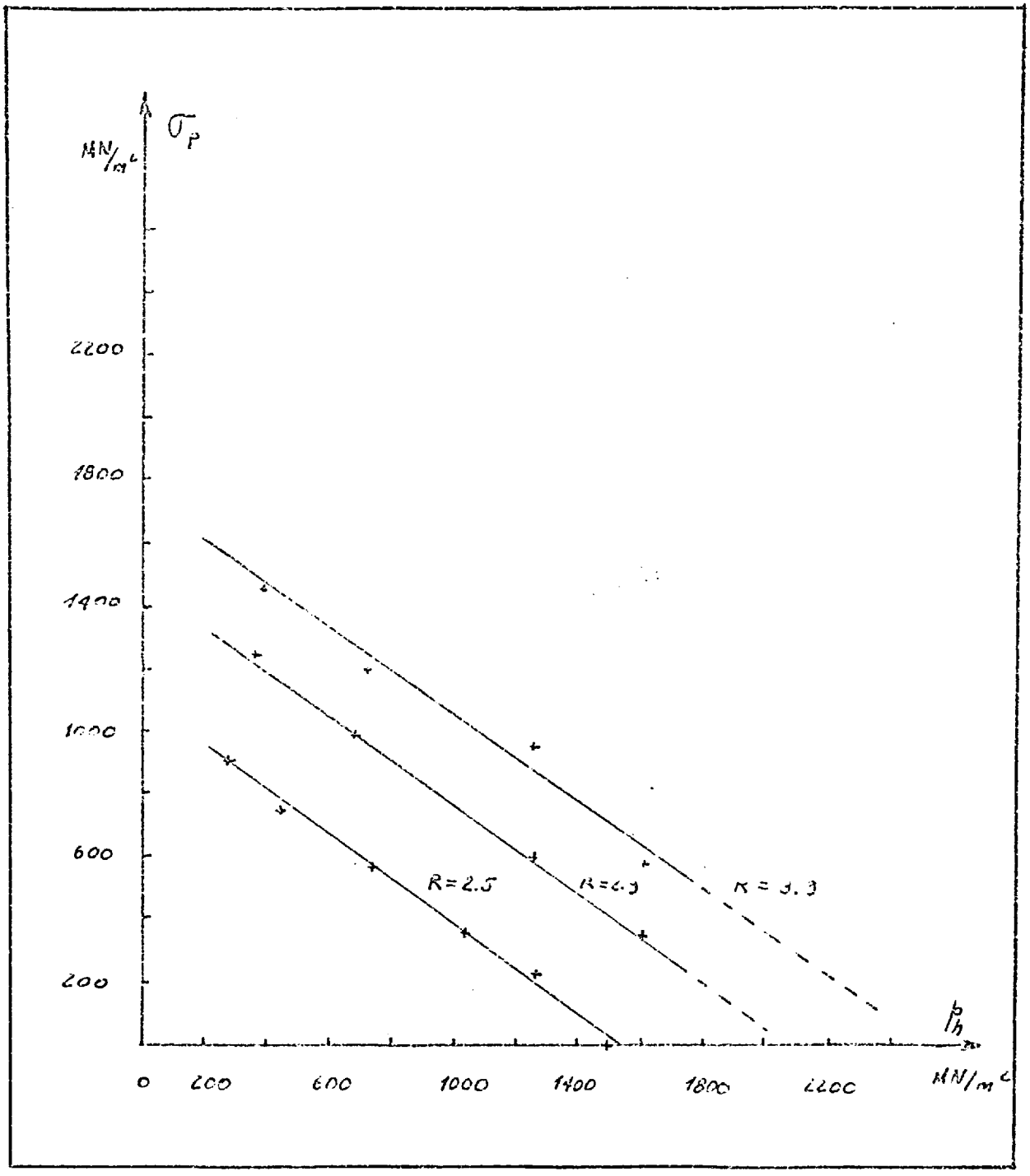

FIGURE 11 . Pulling stress-hydrostatic pressure characteristics of stainless steel specimens under different extrusion ratios.

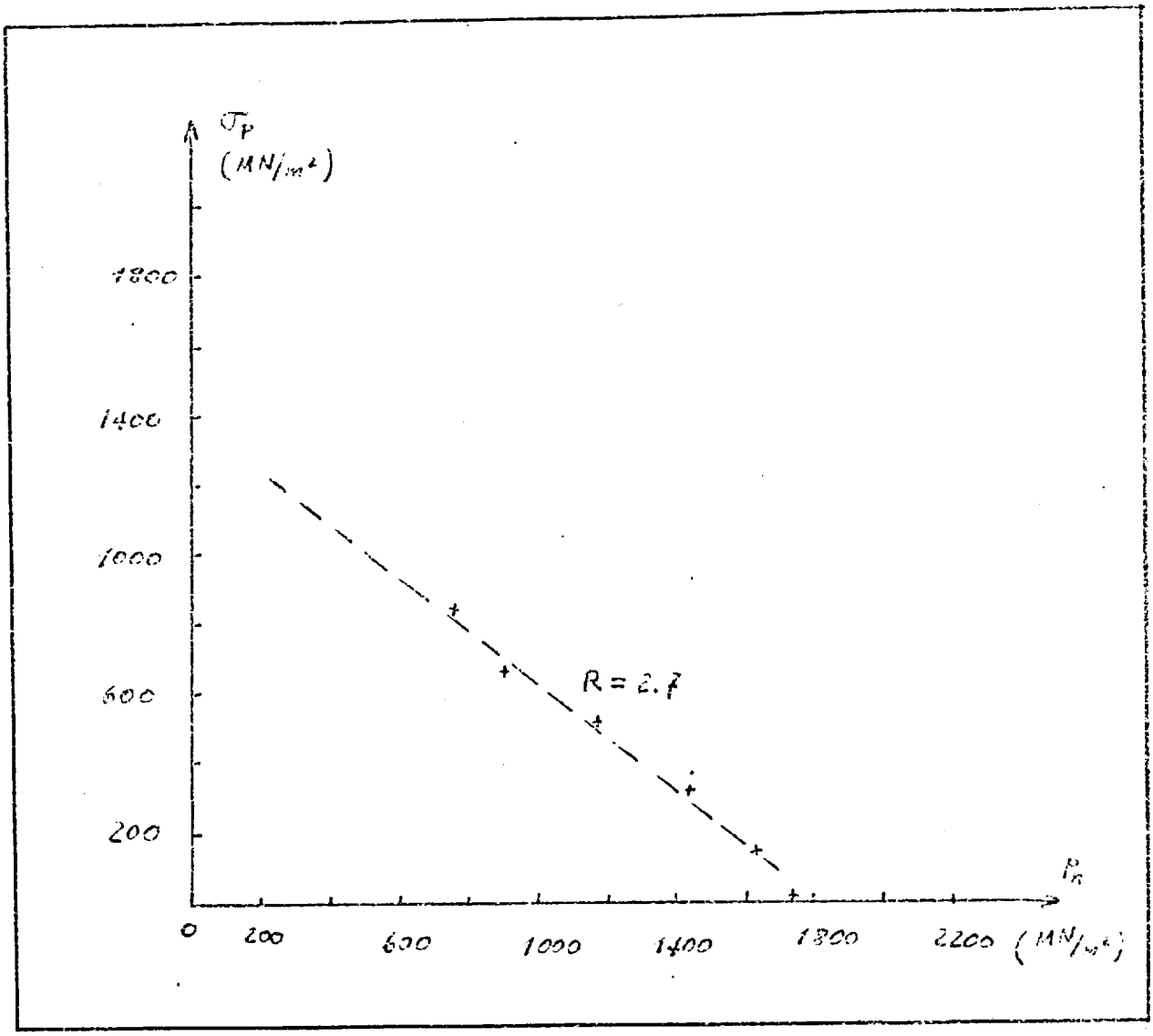

FIGURE 12 . Pulling stress-hydrostatic pressure characteristic for a stainless steel sleeve-copper core specimen.

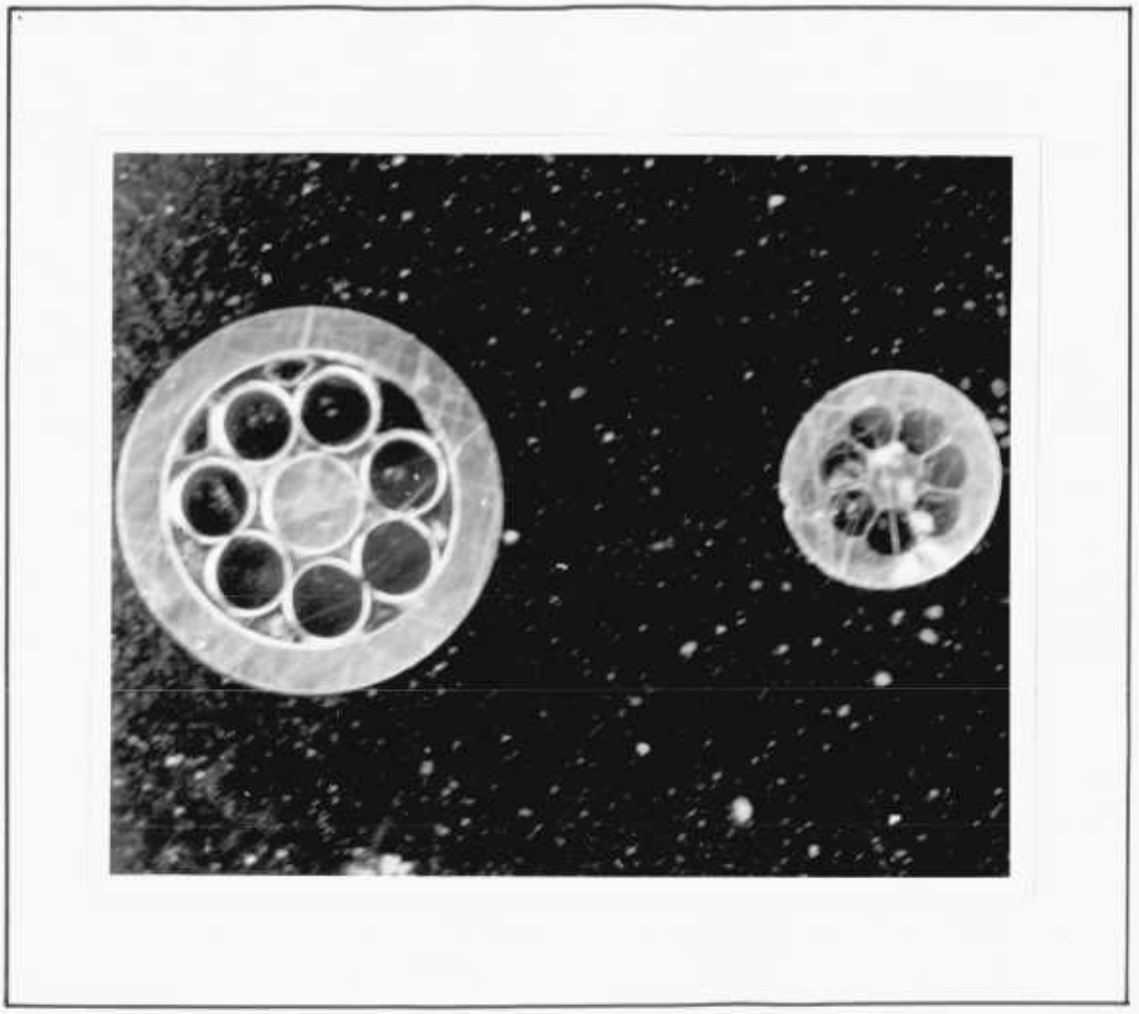

FIGURE 13 . Cross-sections of a multicore billet and product.

IV. SLAB METHOD APPROACH TO THE COEXTRUSION OF TWO DIFFERENT METALS [79]

IV.1 Introduction

In the present section, the coextrusion of two metals by the process of hydrostatic extrusion-drawing will be considered from the "slab method" point of view. Such analysis is based on the assumption of a uniform state of stress at all points of a plane normal to the die axis.

This approach was first proposed by Sachs [7] and later presented by Hoffman and Sachs [8], for the extrusion of a single metal.

In a composite specimen where the yield stress of the tube is lower than that of the core, one might expect the tube to flow more easily through the die. However, the friction between the core and the tube tends to partially restrain the flow of the tube and, at the same time, drag the core along with it. If, on the contrary, the tube is harder than the core, the opposite situation will take place. This interaction will be referred to as the dragging effect.

A section of the composite specimen and the notation used are illustrated in Fig. 14.

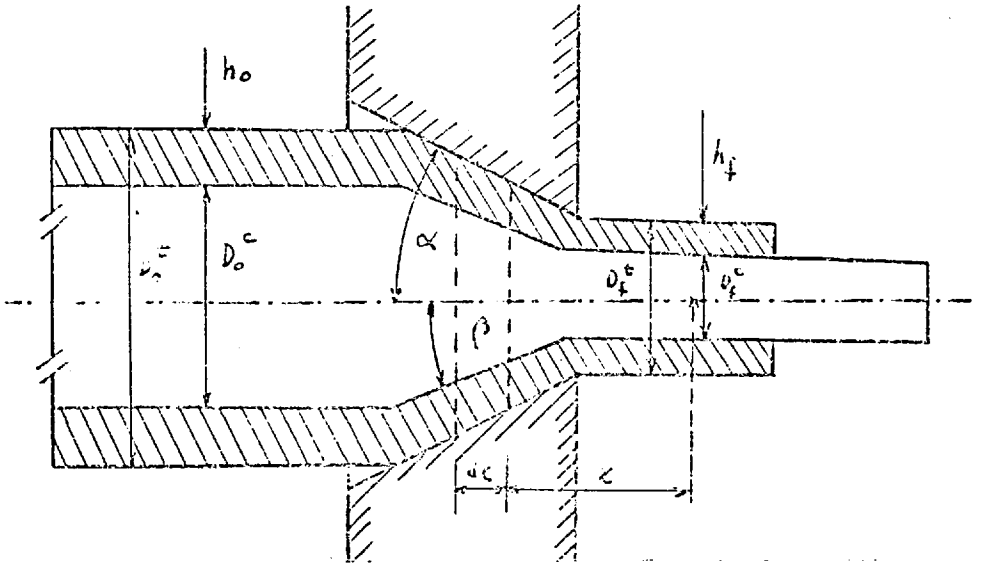

FIGURE 14

In the present analysis a rigid perfectly plastic material model will be assumed throughout the calculations. It will also be assumed that the metals are isotropic before the deformation starts and no anisotropy is developed during the process of deformation.

IV.2 Dragging effect

Due to the tendency of the soft metal to flow faster than the hard one through the die and owing to this differential velocity being resisted by stresses developed at the interface, a compressive state of stress is set up in the soft metal and a tensile state of stress in the hard metal. As a result of this, the soft metal behaves as a harder one and the hard metal presents an apparently lower yield stress.

This phenomenon had also been observed and analyzed in the sandwich rolling and drawing of hard metals [80], [81], [82], [83].

It will be assumed that the state of stress developed at the interface can be represented by a cylindrical state of tangential stress, of a constant value along the interface.

It is apparent that the tangential stress τ will depend on the relationship ω of the yield stresses of both materials, ω being defined as

$$\omega = \frac{Y_{soft}}{Y_{hard}}$$

Since τ is generated by a differential mechanical behaviour, it must vanish when both metals are mechanically equivalent ($\omega = 1$) or if $Y_{soft} = 0$ ($\omega = 0$, behaviour comparable to the corresponding to an ideal fluid).

One of the simplest forms of representing this characteristic of τ is by means of a quadratic function ϑ, which will be referred to as function of dragging, that is

$$\vartheta = -\omega^2 + \omega \qquad 0 \leqslant \omega \leqslant 1$$

which plots as

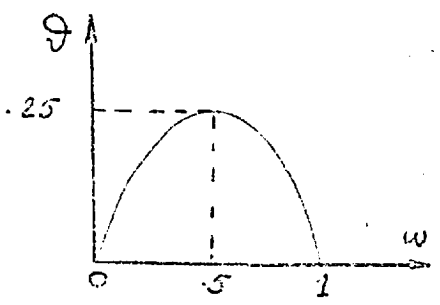

Hence, τ can be expressed in terms of ϑ as

$$\tau = q\vartheta$$

q being a constant. The sign of q will define the positive or negative concavity of ϑ which will point out the sense of τ. This sense will depend upon which material (core or tube) is softer and that is merely a metter of convention. In our analysis $q > 0$ if the tube is softer than the core.

The maximum value that τ can reach is the shear yield stress of the softer metal, that is

$$\tau = q\vartheta = k_{soft}$$

As the maximum possible value for $\vartheta = 0.25$, the upper bound for $q = 4 \times k_{soft}$.

IV.3 State of stress on the core

Stresses acting on an element of the core are shown in Fig. 15.

FIGURE 15

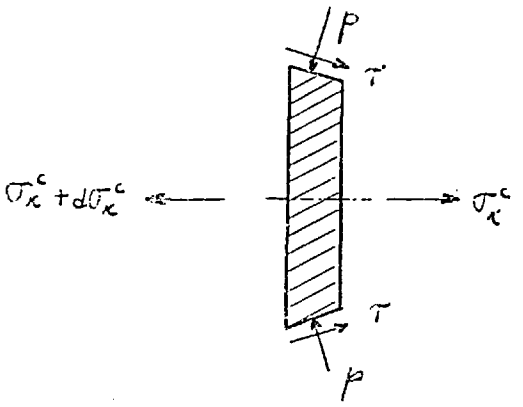

The assumed state of stress is such that the axial and radial directions are both principal directions, corresponding to principal stresses of σ_x and -p respectively.

Let us consider the equilibrium of an element of volume limited by two planes perpendicular to the axis, at distances x and x + dx from the apex of the conical die. The forces involved are axisymmetrically distributed and, consequently, the resultants act along the x-axis. These forces are as follows:

(i) Due to axial stress: Neglecting infinitesimals of second order, the expression

$$(\sigma_x + d\sigma_x)\frac{\pi}{4}(D + dD)^2 - \sigma_x \frac{\pi}{4} D^2 = \frac{\pi D}{4}(\sigma_x d\sigma_x + 2\sigma_x dD) \quad (42)$$

is obtained.

(ii) Due to normal pressure: The resultant of the normal pressure generated on the surface in contact with the die and transmitted to the core is

$$p\frac{\pi}{2} D dD \quad (43)$$

(iii) Due to dragging effect: Integrating over the conical surface of the volume element, the expression

$$-\frac{\vartheta \pi D}{2 \tan\beta} dD \quad (44)$$

is obtained.

Applying the equilibrium condition for the x-direction, the equation

$$D d\sigma_x + 2\sigma_x dD + 2p\,d\,D - \frac{2q\vartheta}{\tan\beta} dD = 0 \qquad (45)$$

is obtained.

For the particular state of stress assumed, both Tresca and von Mises yield criteria lead to the expression:

$$\sigma_1 - \sigma_3 = Y^c$$

In this case $\sigma_1 = \sigma_x$ and $\sigma_3 = -p$, hence

$$p = Y^c - \sigma_x \qquad (46)$$

Substituting (46) in equation (45), the differential equation

$$d\sigma_x = 2\left(\frac{q\vartheta}{\tan\beta} - Y^c\right)\frac{dD}{D} \qquad (47)$$

is obtained.

The boundary conditions are

$$D = D_i^c \qquad \sigma_x = \sigma_i^c$$
$$D = D_f^c \qquad \sigma_x = \sigma_f^c$$

Integrating (47) with these conditions and q, β and Y^c being constant, the expression

$$\sigma_f^c = \sigma_i^c + (Y^c - \frac{q\vartheta}{\tan\beta}) \ln R_c \qquad (48)$$

is obtained. By setting $\sigma_i^c = -p_h$ (hydrostatic pressure), expression (48) becomes

$$\sigma_f^c = - p_h + Y^c (1 - \frac{q\vartheta}{Y^c \tan\beta}) \ln R_c \qquad (49)$$

The relationship

$$m = \frac{q\vartheta}{Y^c}$$

evaluates the dragging stress related to the yield stress of the core. Calling

$$n = 1 - \frac{m}{\tan\beta}$$

expression (49) can be written as

$$\sigma_f^c = - p_h + n Y^c \ln R_c \qquad (50)$$

Being the value of $n < 1$, expression (50) shows that the material is behaving with an apparent yield stress $\bar{Y}^c$, lower than the actual one, that is

$$Y^{-c} = n Y^c < Y^c$$

From the expression of n it is deduced that if

$$\tan\beta = \frac{q\vartheta}{Y^c}$$

the dragging stress would be equal to the stress required for deformation. In that case, the apparent yield stress would be zero.

Equation (49) may be written as

$$\sigma_f^c = - p_h + Y^c \ln R_c - \frac{q\vartheta}{\tan\beta} \ln R_c \qquad (51)$$

or, in another form

$$\sigma_f^c + \frac{q\vartheta}{\tan\beta} \ln R_c = - p_h + Y^c \ln R_c \qquad (52)$$

Considering equations (50) and (52) it follows that the advantages of the extrusion of hard cores with soft sleeves is thus to apparently reduce the yield stress of the core by the tensile stress imposed by the interlayer friction and it is directly comparable to the addition of a pulling stress of

$$\frac{q\vartheta}{\tan\beta} \ln R_c \qquad (53)$$

If for some combination of values in expression (53) it happens that

$$\frac{q\vartheta}{\tan\beta} \ln R_c > Y^c$$

the core will fail by tensile stress. As was pointed out, this is often the case in processes with similar situations [31], [34].

IV.4 State of stress on the tube

Stresses acting on an element of tube are illustrated in Fig. 16.

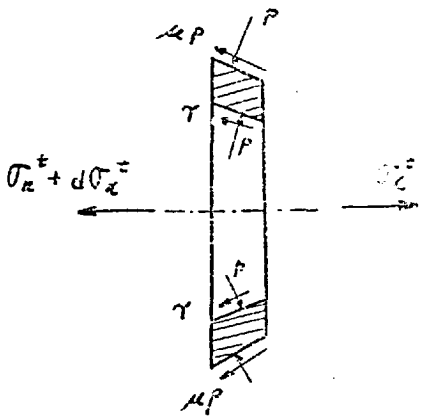

FIGURE 16

Again, the axial and radial directions are both principal and the corresponding principal stresses σ_x and -p respectively.

As before, it will be considered the equilibrium of an element of tube limited by the same planes as used for the element of core located at distances x and x + dx from the apex of the conical die. All forces are axisymmetrically distributed and thus the resultants act along the x-axis. These forces are as follows:

(i) Due to axial stress: Neglecting infinitesimals of the second order, the expression

$$(\sigma_x + d\sigma_x)(h + dh)\pi D - \sigma_x h\pi D = (\sigma_x dh + h d\sigma_x)\pi D \quad (54)$$

is obtained.

(ii) Due to normal pressure exerted on the tube at the

tube-die interface

$$p\pi D \tan\alpha dx \tag{55}$$

(iii) Due to normal pressure at the tube-core interface

$$-p\pi D \tan\beta dx \tag{56}$$

that is, opposite to expression (43). Considerations of radial equilibrium suggest that the frictional contribution to the die pressure is small and, consequently, die and core pressures are equal [84].

(iv) Due to friction with the die: By assuming Coulomb friction with a constant coefficient at the tube-die interface, one gets:

$$\mu p\pi D\, dx \tag{57}$$

(v) Due to dragging effect: With similar assumptions as before, the dragging force on the element of tube is:

$$q\vartheta \pi D\, dx \tag{58}$$

Expression (58) is equal to expression (44) but is being considered with opposite sense.

Applying the equilibrium condition, the equation

$$(\sigma_x dh + h d\sigma_x)\pi D + p\pi D(\tan\alpha - \tan\beta)dx + \pi D(q\vartheta + p\mu)dx = 0$$

is obtained.

Introducing the value

$$dh = dx(\tan\alpha - \tan\beta)$$

the equilibrium equation becomes

$$(\sigma_x dh + h d\sigma_x) + p dh + \frac{q\vartheta + p\mu}{\tan\alpha - \tan\beta} dh = 0 \qquad (59)$$

or, by calling

$$a = \tan\alpha - \tan\beta$$

$$b = 1 + \frac{\mu}{a}$$

expression (59) can be written as:

$$h d\sigma_x + (\sigma_x + pb + \frac{q}{a}\vartheta) dh = 0 \qquad (60)$$

Assuming that the same plastic conditions described in (46) are valid, hence

$$p = Y^t - \sigma_x \qquad (61)$$

Substituting (61) in (60), the differential equation

$$h d\sigma_x + \left[\sigma_x(1-b) + bY^t + \frac{q}{a}\vartheta \right] dh = 0 \qquad (62)$$

is obtained. Integrating (62) with the following boundary conditions

$$h = h_o \qquad \sigma_x = -p_h$$

$$h = h_f \qquad \sigma_x = \sigma_f^t$$

and μ, q, β, α and Y^t constant, one gets:

$$\sigma_f^t = - p_h r^{\frac{\mu}{a}} + \frac{a}{\mu}\left[bY^t + \frac{q\vartheta}{a}\right](1 - r^{\frac{\mu}{d}}) \qquad (63)$$

where

$$r = \frac{h_f}{h_o}$$

In another form:

$$\sigma_f^t = - p_h r^{\frac{\mu}{a}} + (1 + \frac{a}{\mu})Y^t(1 - r^{\frac{\mu}{a}}) + \frac{q\vartheta}{\mu}(1 - r^{\frac{\mu}{a}}) \qquad (64)$$

Consequently, the compressive stress created on the tube as a result of restraining its flow speed, is

$$\frac{q\vartheta}{\mu}(1 - r^{\frac{\mu}{a}}) \qquad (65)$$

In a case in which the core is the softer metal, the whole situation would be reversed. By this we mean that the core would be supporting compressive stresses while the tube would be subjected to a tensile stress. In such a case, if it happens to be

$$\frac{q\vartheta}{\mu}(1 - r^{\frac{\mu}{a}}) > Y^t \qquad (66)$$

the tube will fail by tensile stress. Failures of this type have been observed in experiments being carried out with copper tube and aluminium as a core [85]. It is interesting to point out that from expression (65) it follows that an increment in

the coefficient of friction would tend to relax the tensile force acting on the tube and could prevent failure. This fact applies more accurately to real situations when the tube wall is very thin.

IV.5 Mean pulling stress

The total pulling stress acting on the composite specimen can be calculated through the expression

$$T = \sigma_f^c A_c + \sigma_f^t A_t$$

where σ_f^c and σ_f^t are given by expressions (51) and (64) respectively.

Therefore, the mean pulling stress will be given by

$$\sigma_p = \frac{T}{A_c + A_t} = \sigma_f^c \gamma_c + \sigma_f^t \gamma_t \qquad (67)$$

Substituting expressions (51) and (64) in equation (67), the equation

$$\sigma_p = -p_n(\gamma_c + \gamma_t r^{\frac{\mu}{a}}) + \gamma_c Y^c \ln R_c + \gamma_t (1 + \frac{a}{\mu})(1 - r^{\frac{\mu}{a}}) + q\vartheta\left[\frac{\gamma_t}{\mu}(1 - r^{\frac{\mu}{a}}) - \frac{\gamma_c}{\tan\beta} \ln R_c\right] \qquad (68)$$

is obtained.

Conditions of uniform deformation require that both metals, core and tube, must deform under the same extrusion

ratio. This condition implies that the apex of the conical surface of the core must coincide with the apex of the conical surface of the die (see Appendix A). This fact has been confirmed by specimens subjected to different extrusion ratios, as described in Appendix A.

Under the above circumstances it is possible to express

$$r = R^{-\frac{1}{2}}$$

and also $a = (1 - \sqrt{\gamma_c})\tan\alpha$

Finally, equation (68) can be written as

$$\sigma_p = -p_h(\gamma_c + \gamma_t R^{-\frac{\mu}{2a}}) + \gamma_c Y^c \ln R + \gamma_t(1 + \frac{a}{\mu})Y^t(1 - R^{-\frac{\mu}{2a}}) + q\vartheta\left[\frac{\gamma_c}{\mu}(1 - R^{-\frac{\mu}{2a}}) - \frac{\sqrt{\gamma_c}}{\tan\alpha}\ln R\right] \qquad (69)$$

IV.6 Normal pressure at the interface

The normal pressure acting on the core can be calculated from equation (69). That is

$$p = Y^c - \sigma_x$$

From (47) we get

$$\sigma_x = -p_h + nY_c \ln\left(\frac{D_i^c}{D^c}\right)^2 \qquad (70)$$

D^c being a generical value for the diameter of the core. Substituting equation (70) into (46), expression

$$p = p_h + Y^c \left[1 - n \ln \left(\frac{D_i^2}{D^c} \right)^2 \right] \quad D_f^c \leqslant D^c \leqslant D_i^c \qquad (71)$$

is obtained. This expression describes the distribution of normal pressure along the tube-core interface in terms of the diameter of the core.

IV.7 Conclusions

Once materials, conditions of lubrication and extrusion ratio are given, equation (69) can be written as

$$\sigma_p = - M p_h + N \qquad (72)$$

where

$$M = \gamma_c + \gamma_t R^{-\frac{\mu}{2a}} \qquad (73.a)$$

$$N = \gamma_c Y^c \ln R + \gamma_t \left(1 + \frac{a}{\mu}\right) Y^t \left(1 - R^{-\frac{\mu}{2a}}\right) + q\vartheta \left[\frac{\gamma_t}{\mu} \left(1 - R^{-\frac{\mu}{2a}}\right) - \frac{\sqrt{\gamma_c}}{\tan\alpha} \ln R \right] \qquad (73.b)$$

The graphical representation of equation (72) in a $\sigma_p - p_h$ plot is a straight line, where M is the slope and N represents the calculated value for the free extrusion pressure.

From the experimental lines it is possible to determine the values of μ and q.

If S is the slope of the experimental line, from equation (73.a) the expression for

$$\mu = -2a \frac{\ln\left(\frac{s - \gamma_c}{\gamma_t}\right)}{\ln R} \qquad (74)$$

is obtained.

From equation (73.b) and by using the experimental value of the free extrusion pressure N_{exp}, the value of q is obtained:

$$q = \frac{N_{exp} - \gamma_c Y^c \ln R - \gamma_t (1 + \frac{a}{\mu}) v^t (1 - R^{-\frac{\mu}{2a}})}{\vartheta(\frac{\gamma_t}{\mu}(1 - R^{-\frac{\mu}{2a}}) - \frac{\sqrt{\gamma_c}}{\tan\alpha} \ln R)} \qquad (75)$$

Experiments were conducted with copper tube and stainless steel core and with stainless steel tube and copper core. In all cases the resultant drawing force and the hydrostatic pressure were measured.

Fig. 17 shows the values corresponding to experiments carried out with copper tube and stainless steel core. It contains the drawing stress-hydrostatic pressure plot for different extrusion ratios. The experimental lines are shown together with the theoretical ones. Fig. 18 shows the theoretical and experimental lines corresponding to the stainless steel tube-copper core experiments. Figs. 19 and 20 show lines corresponding to the extrusion of copper and stainless steel as single metals.

The values used throughout the calculations of equation (69) corresponding to Fig. 18 lines are:

$$Y^c = 460 \text{ MN/m}^2$$

$$Y^t = 1150 \text{ MN/m}^2$$

$$\gamma_c = \gamma_t = 0.5$$

Values for μ were also deduced from experimental lines.

It follows from the analysis of Figs. 17 and 18 and other reported information [31], [34] that the model predicts qualitatively the distinctive characteristics of the process of coextrusion.

Figs. 17 and 18 also show that values for the lines $\sigma_p - p_h$ calculated by means of equation (69) are lower than the experimental ones. This can be due, among other simplificative factors, to the hypothesis of homogeneous deformation, the inattention paid to the tendency in the materials of work hardening and to redundant work of deformation.

These assumptions constitute an oversimplification of the process and could lead to the low values predicted. Some of these hypotheses will be improved in further sections.

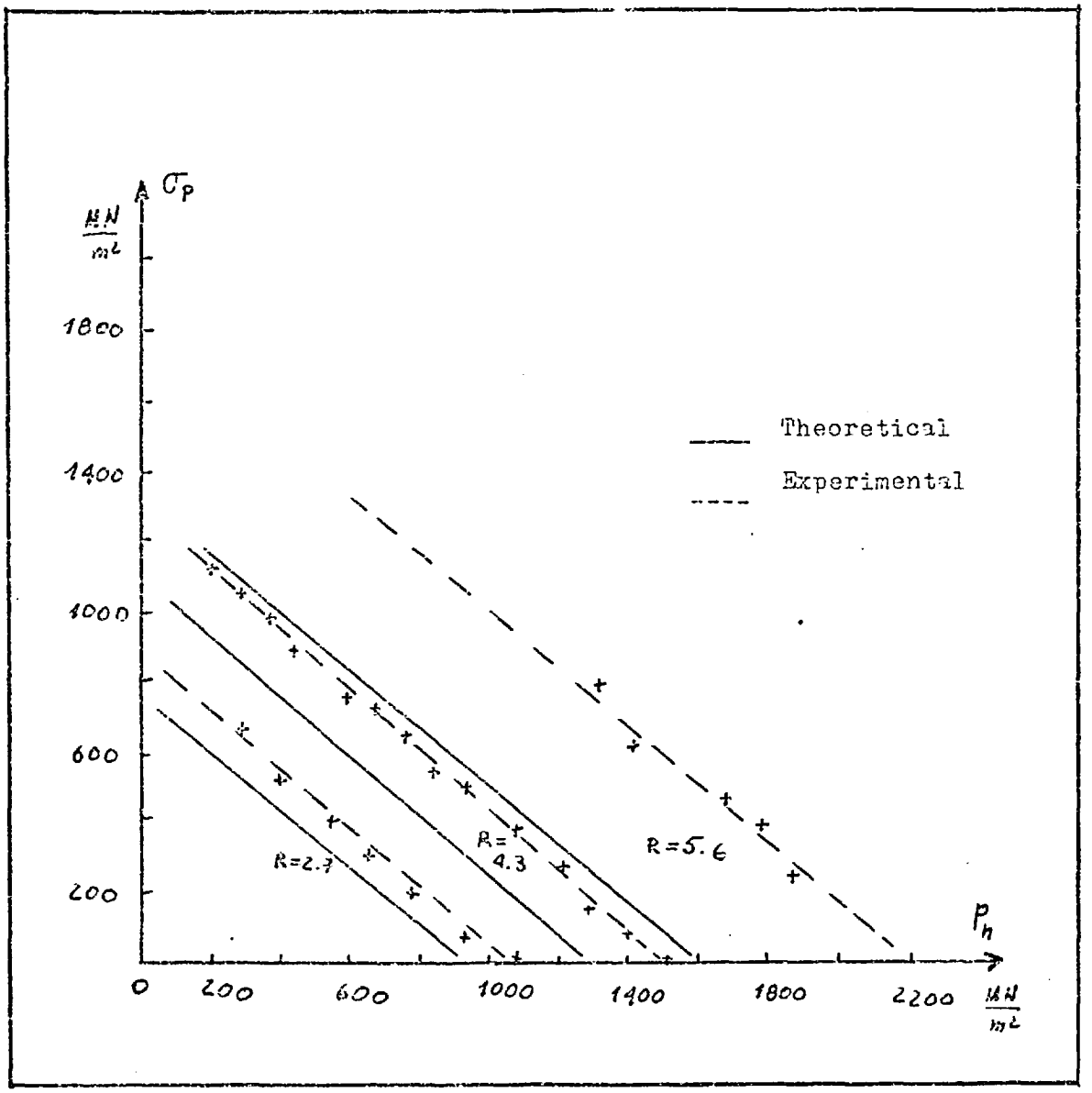

FIGURE 17 . Theoretical and experimental results for copper tube-s.steel core specimens.

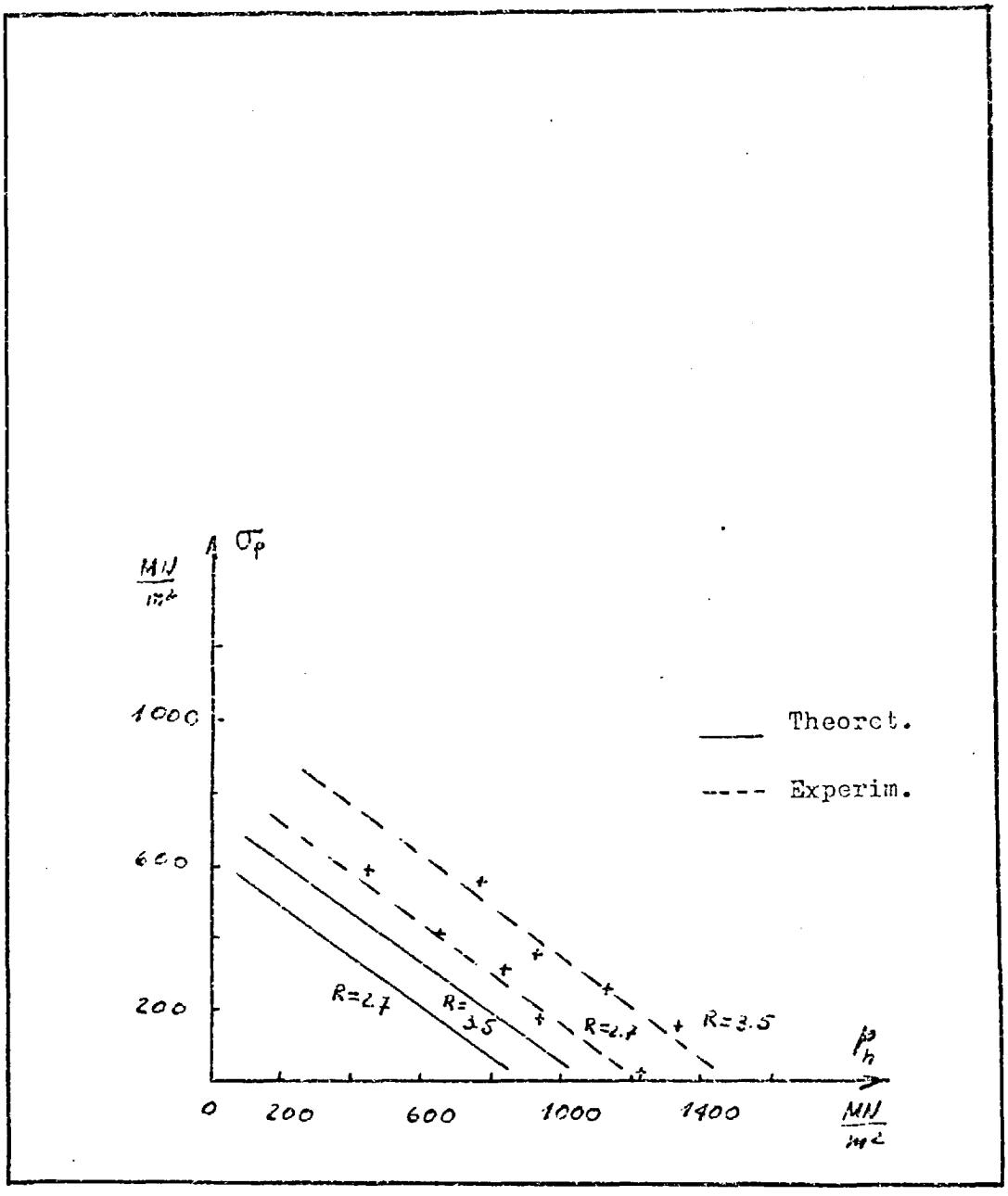

FIGURE 18 . Theoretical and experimental results for s.steel tube-copper core specimens.

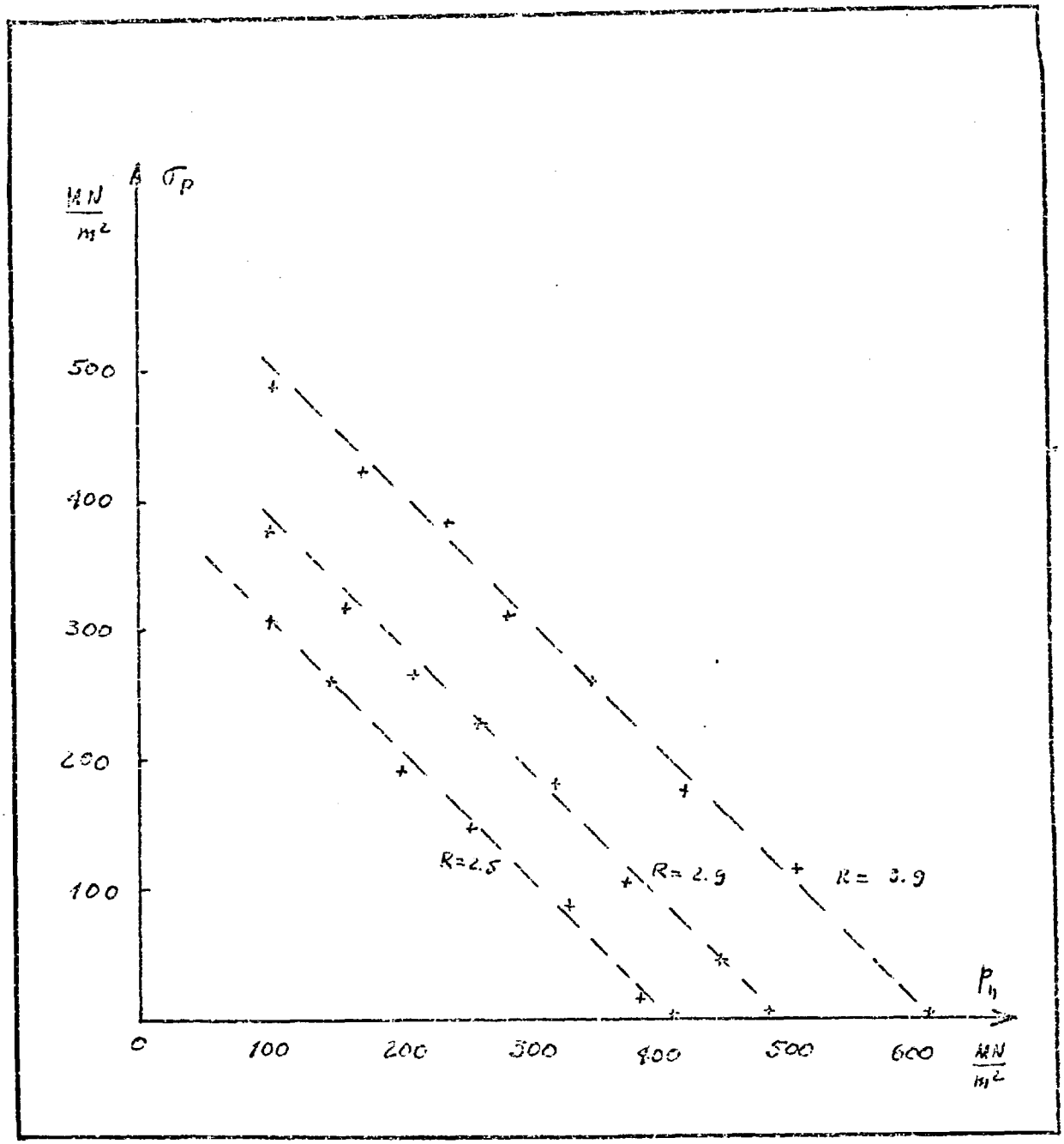

FIGURE 19 . Pulling stress-hydrostatic pressure charcteristics for copper wire.

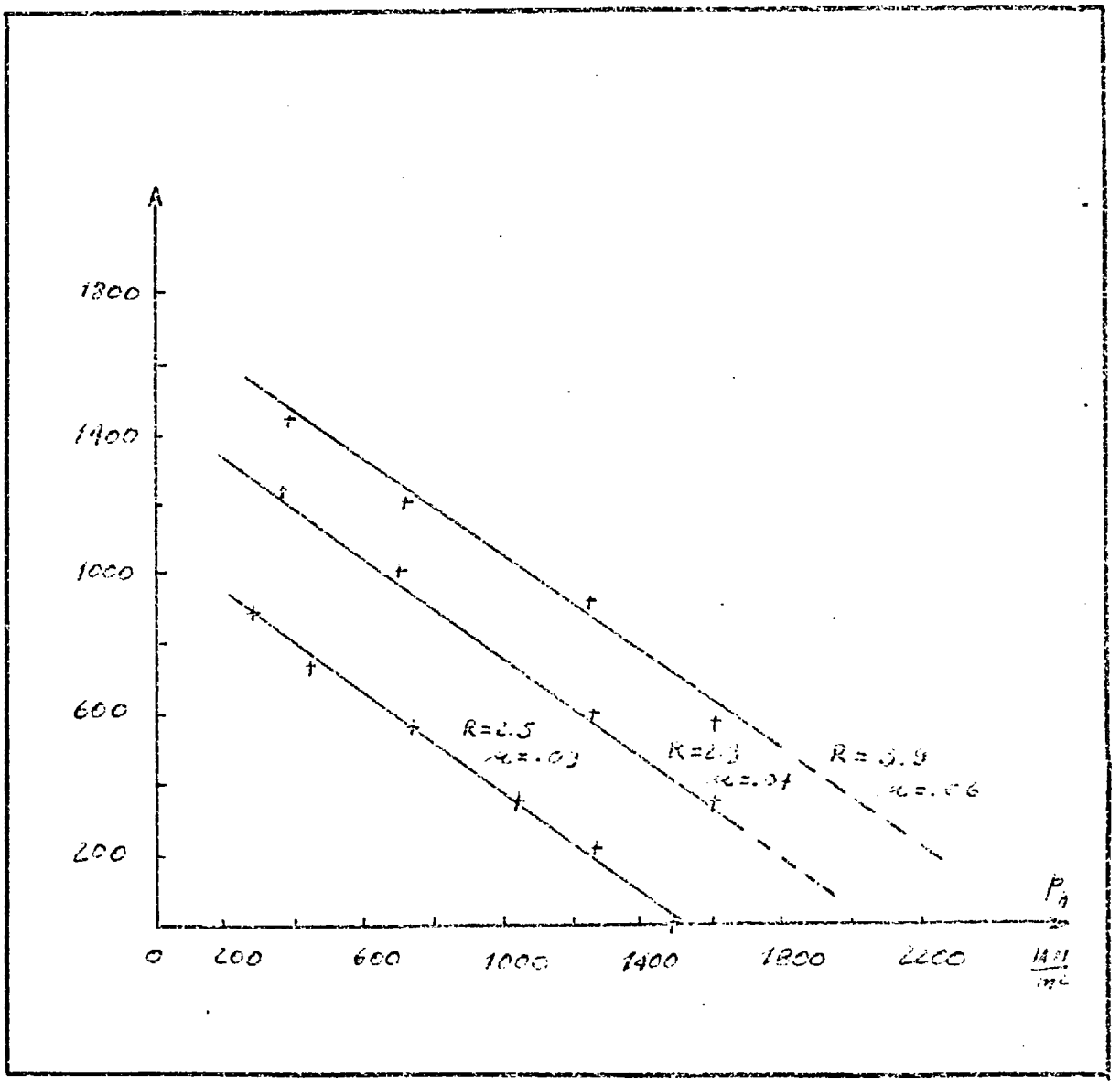

FIGURE 20 . Pulling stress-hydrostatic pressure charcteristics for stainless steel wire.

V. UPPER BOUND SOLUTION FOR THE COEXTRUSION OF TWO DIFFERENT METALS [79]

V.1 Introduction

The limit theorems provide a mathematical formulation for obtaining bounds to the load required to deform a continuum solid body. These theorems can be deduced from general extremum principles based on energy considerations. A rigorous analysis of this theory can be seen in several books [86], [87] basically concerning a rigid plastic material model.

The upper bound theorem is one of these theorems and constitutes a powerful mathematical tool to establish upper limits for the state of stress necessary to make a solid deform according to some prescribed kinematically admissible velocity pattern.

In this approach, equilibrium conditions are allowed to go unsatisfied and the main concern is to find a kinematically admissible velocity field. The assumptions for such a field require satisfying the incompressibility condition (equation 16) throughout the volume and boundary conditions that allow velocity discontinuities tangential to the boundary but no discontinuities normal to it.

The upper bound theorem states [88]:

"If a kinematically admissible velocity field exists, the load

required to be applied to cause the velocity field to operate, constitutes an upper bound solution".

The analytical expression of the theorem for a solid obeying von Mises yield criterion and characterised as an isotropic rigid-perfectly plastic material is [62]:

$$J^* = \frac{2}{\sqrt{3}} Y \int_V \left[\frac{1}{2}\dot{\varepsilon}^p_{ij}\,\dot{\varepsilon}^p_{ij}\right]^{\frac{1}{2}} dV + \int_{S_\Gamma} \tau^* |\Delta v|\, dS_\Gamma - \int_{S_t} T_j v_j dS_t \tag{76}$$

where V is the deformed volume, S_Γ represents surfaces of discontinuities within V, and S_t is the portion of the outer surface where external stresses T_j are applied. According to the sign convention, in equation (76) the T_j are considered as tractions.

$\dot{\varepsilon}^p_{ij}$ is the strain rate field derived from the velocity field v_j. If v_j is kinematically admissible so is $\dot{\varepsilon}^p_{ij}$.

Equation (76) expresses an upper bound on the power J^* in terms of three components:

(i) Internal power of deformation, expressed as

$$\frac{2}{\sqrt{3}} Y \int_V \left[\tfrac{1}{2}\dot{\varepsilon}^p_{ij}\,\dot{\varepsilon}^p_{ij}\right]^{\frac{1}{2}} dV \tag{77}$$

(ii) Shear power losses computed along surfaces of velocity discontinuities S

$$\int_{S_\Gamma} \tau^* |\Delta v|\, dS_\Gamma \tag{78}$$

(iii) Power supplied by predetermined body tractions

$$-\int_{S_t} T_j v_j dS_t$$

Throughout the calculations the deformation process is treated as isothermal [47].

V.2 Velocity field

In the process under consideration it is assumed that the metal deforms according to Avitur's velocity field [62], [21], [22], [90]. This field involves radial flow in a spherically bounded plastic zone, where the radial velocity depends on the angular position. A geometric description of the field is shown in Fig. 21.

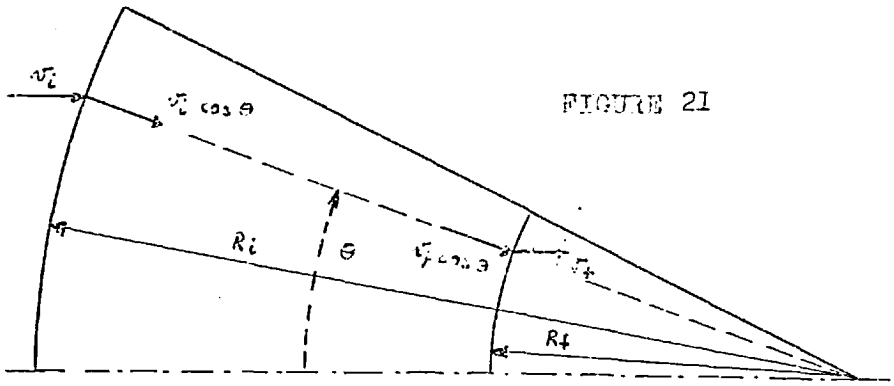

FIGURE 21

In spherical coordinates (R, φ, θ) the components of the velocity vector are:

$$V_R = v = -v_f R_f^2 \frac{\cos\theta}{R^2} \qquad (79.a)$$

$$v_\theta = v_\varphi = 0 \qquad (79.b)$$

The derivation of equation (79.a) is based on volume constancy.

The corresponding components of the strain rate tensorial field are obtained by means of equations (25.b), as follows:

$$\dot{\varepsilon}_{RR} = -2\dot{\varepsilon}_{\theta\theta} = -2\dot{\varepsilon}_{\varphi\varphi} = 2v_f R_f^2 \frac{\cos\theta}{R^3}$$

$$\dot{\varepsilon}_{R\theta} = \tfrac{1}{2} v_f R_f^2 \frac{\sin\theta}{R^3} \qquad (80)$$

$$\dot{\varepsilon}_{\theta\varphi} = \dot{\varepsilon}_{\varphi R} = 0$$

V.3 Deformation of the composite specimen

It is assumed that the composite specimen deforms following the geometry illustrated in Fig. 22:

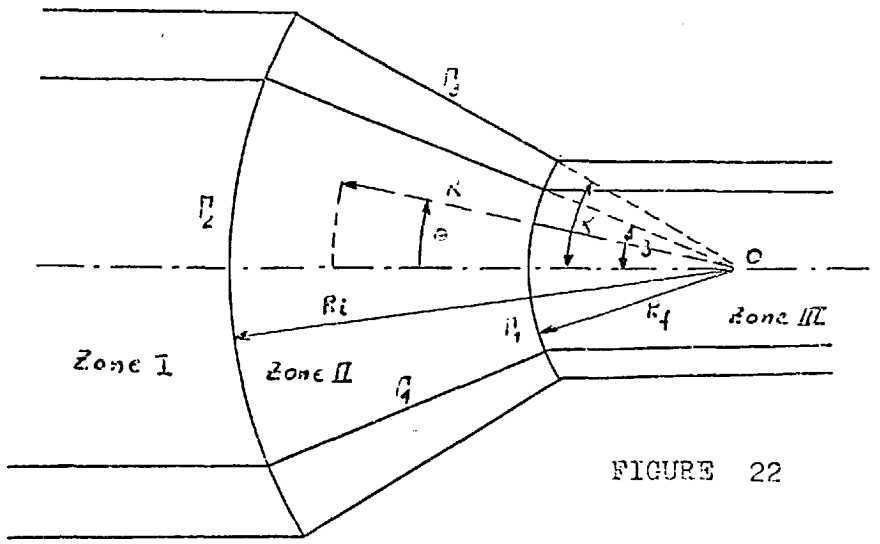

FIGURE 22

The specimen is divided into three zones in which the velocity field is continuous. In zones I and III the velocity is uniform and has an axial component only. Velocity in zone I is v_i and in zone III is v_f. In zone II, the

velocity components are described by equations (79.a) and (79.b).

In zone I deformation has not yet begun. Deformation starts when the incoming specimen crosses the boundary surface Γ_2 and ends at surface Γ_1. In the assumed Avitzur's model these surfaces are spherical with radii R_i and R_f respectively and centred at the apex O of the cone of the die.

The conical surface Γ_4 is the core-tube interface where the dragging stress, as described in Section IV.2, is developed. Again, as a consequence of this interaction both metals will move together without sliding. As has already been pointed out, under this condition both metals deform with the same extrusion ratio.

Across boundaries Γ_1 and Γ_2 there exist velocity discontinuities parallel to these surfaces:

$$\Delta v = v_f \sin\theta \qquad \text{along } \Gamma_1 \tag{81}$$

and

$$\Delta v = v_i \sin\theta \qquad \text{along } \Gamma_2 \tag{82}$$

Since the die is at rest, discontinuity along the conical surface Γ_3 is

$$\Delta v = v_f R_f^2 \frac{\cos\alpha}{R^2} \tag{83}$$

All powers involved in the deformation process of the composite specimen are next analysed separately for core and tube.

V.4 Power involved in the deformation of the core

In relation to the deformation process of the core, two different kinds of power are identified: dissipative and active powers.

The sources of dissipation or consumption of energy for the core are:

(i) Internal power of deformation of the core, and

(ii) Dissipation on the surfaces of discontinuities,

while the driving or active powers are due to:

(i) The drawing force,

(ii) The hydrostatic pressure of extrusion, and

(iii) The dragging force supplied by the tube.

Each one of these components is considered separately in the following sections. A description of the acting stresses is shown in Fig. 23.

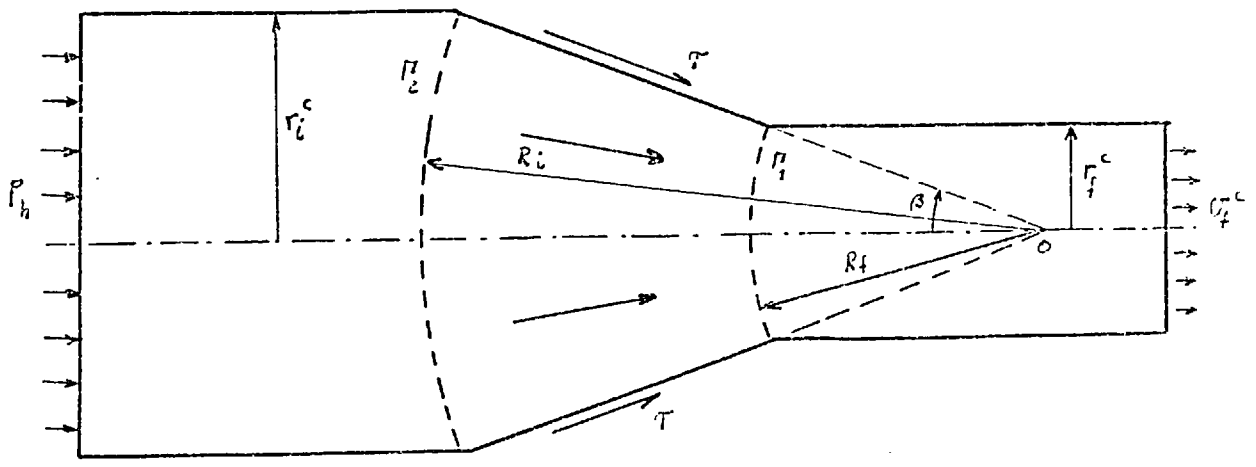

FIGURE 23

V.4.1 Internal power of deformation

The internal power of deformation involved in the deformation of the core is given by the expression

$$\dot{W}_i = \frac{2}{\sqrt{3}} Y^c \int_{V_c} \left[\tfrac{1}{2} \dot{\varepsilon}^p_{ij} \dot{\varepsilon}^p_{ij} \right]^{\frac{1}{2}} dV \qquad (84)$$

As the strain rate components are given by equation (80), the following expression is obtained (see Appendix B):

$$\dot{W}_i = \pi Y^c (r_f^c)^2 \, v_f \, F(\beta) \ln R_c \qquad (85)$$

V.4.2 Dissipation on the surfaces of discontinuities

Surfaces Γ_1 and Γ_2 are surfaces where discontinuities exist in the velocity field. Such discontinuities parallel to the surfaces have values

$$\Delta v_1 = v_f \sin\theta \qquad \text{along } \Gamma_1$$
$$\Delta v_2 = v_i \sin\theta \qquad \text{along } \Gamma_2$$

Due to this difference in velocity at both sides of Γ_1 and Γ_2, some energy is dissipated on these surfaces. Its total value per unit time is

$$\dot{W} = \int_{\Gamma_1} \tau^* \Delta v_1 dS_1 + \int_{\Gamma_2} \tau^* \Delta v_2 dS_2 \qquad (86)$$

where

$$dS_1 = 2\pi R_f \sin\theta \, d\theta \qquad (87)$$

and

$$dS_2 = 2\pi R_i \sin\theta \, d\theta$$

For a metal with the properties assumed in this section τ^* will never exceed the shear yield stress, that is

$$\tau^* \leqslant \frac{Y^c}{\sqrt{3}}$$

Consequently the maximum value for expression (86) is

$$\dot{W}_\Gamma = 4\pi v_f (r_f^2)^2 \frac{Y^c}{\sqrt{3}} \int_0^\beta \sin^2\theta \, d\theta$$

or, after integration

$$\dot{W}_\Gamma = \frac{2}{\sqrt{3}} \pi v_f (r_f^c)^2 Y^c \left[\frac{\beta}{\sin^2\beta} - \cot\beta \right] \qquad (87)$$

V.4.3 Power developed by the drawing force

In the process of hydrostatic extrusion-drawing, the driving stress is the resultant of billet augmentation due to the hydrostatic pressure, and product augmentation due to a pulling or drawing force.

The power developed by this drawing force is

$$\dot{W}_D = - \int_{S_f} T_j v_j dS_f$$

where S_f is the cross sectional area of the core at the exit of the die and T_j is in this case the drawing stress distribution across that section.

Since the drawing force is applied at the end of a long tag, it produces in the metal, at the exit of the die, a tensile stress σ_f^c that can be reasonably assumed as being uniform throughout the cross section. Consequently, the following expression is obtained:

$$\dot{W}_D = \pi v_f (r_f^c)^2 \sigma_f^c \qquad (88)$$

V.4.4 Power developed by the hydrostatic pressure

In a similar form, the power developed by the billet augmentation force, in this case supplied by the hydrostatic pressure of extrusion, is given by the expression:

$$\dot{W}_e = - \int_{S_i} T_j v_j dS_i$$

where S_i is the cross sectional area of the core before being deformed and T_j the stress distribution on that section.

Since the hydrostatic pressure p_h acts at all points of S_i, under this condition and after integration, the following expression is obtained:

$$\dot{W}_e = \pi v_f (r_f^c)^2 p_h \qquad (89)$$

V.4.5 Power developed by the dragging force

It is assumed that the dragging effect has the same characteristics as described in Section IV.2. The dragging

force is generated by a system of tangential stresses τ_j with axial symmetric properties. The power developed by such a system during the deformation process is

$$\dot{W}_d = \int_{\Gamma_4} \tau_j v_j d\Gamma_4 \qquad (90)$$

where $d\Gamma_4$ is an element of area of the conical surface Γ_4, v_j is the velocity corresponding to a generical point at the interface and τ_j is the stress distribution on that surface.

This component is considered as an active power and it is supplied by the tube on the assumption that the tube is the softer metal; otherwise the situation must be reversed.

The stress τ_j is expressed in terms of the dragging function ϑ as:

$$\tau_j = -q\vartheta$$

and is assumed to be constant along the Γ_4 surface.

The velocity of a generical point at the interface is

$$v_j = - v_f R_f^2 \frac{\cos\beta}{R^2}$$

or, as

$$R = \frac{r}{\sin\beta}$$

the following expression is obtained:

$$v_j = - v_f (r_f^c)^2 \frac{\cos\beta}{r^2} \tag{91}$$

An infinitesimal element of the conical surface is

$$d\Gamma_4 = \frac{2\pi r}{\sin\beta} dr \tag{92}$$

Substituting expressions (91) and (92) into (90), it gives:

$$\dot{W}_d = \int_{r_f^c}^{r_i^c} q\vartheta\pi v_f (r_f^c)^2 \frac{\cos\beta}{r^2} \frac{2\pi r}{\sin\beta} dr$$

and, after integration

$$\dot{W}_d = q\vartheta\pi v_f (r_f^c)^2 \cot\beta \ln R_c \tag{93}$$

In case of the tube being the harder metal, $q < 0$ and consequently this power must be considered as dissipative.

V.4.6 Balance of power in the core

Substituting expressions (85), (87), (88), (89) and (93) into the general expression of the upper bound theorem (1), it gives:

$$\sigma_f^c + p_h + q\vartheta \cot\beta \ln R_c = \frac{2}{\sqrt{3}} Y^c \left(\frac{\beta}{\sin^2\beta} - \cot\beta\right) + Y_c F(\beta) \ln R_c$$

and solving for the driving stress

$$\sigma_f^c + p_h = Y^c \left[\frac{2}{\sqrt{3}} \left(\frac{\beta}{\sin^2\beta} - \cot\beta\right) + F(\beta) \ln R_c\right] + q\vartheta \cot\beta \ln R_c \tag{94}$$

From equation (94) it follows that the additional stress acting on the core and generated by the tube is

$$q\vartheta\cot\beta \ln R_c \tag{95}$$

and it is directly comparable to a tensile stress.

In terms of the volume fraction γ_c, equation (95) can be written as:

$$\frac{q\vartheta}{\sqrt{\gamma_c}} \cot\alpha \ln R_c \tag{96}$$

Equation (96) is the same as expression (53) obtained by means of the slab method approach.

V.5 Power involved in the deformation of the tube

Following similar definitions as in the analysis of the core, the sources of dissipation of energy in the deformation process of the tube are:

(i) Internal power of deformation of the tube.

(ii) Dissipation on discontinuity surfaces.

(iii) Dragging of the core.

(iv) Friction at the die-tube interface.

The active powers in this case are due to:

(i) The drawing force.

(ii) The hydrostatic pressure of extrusion.

These points are considered next in an individual way. A description of the acting stresses is shown in Fig. 24.

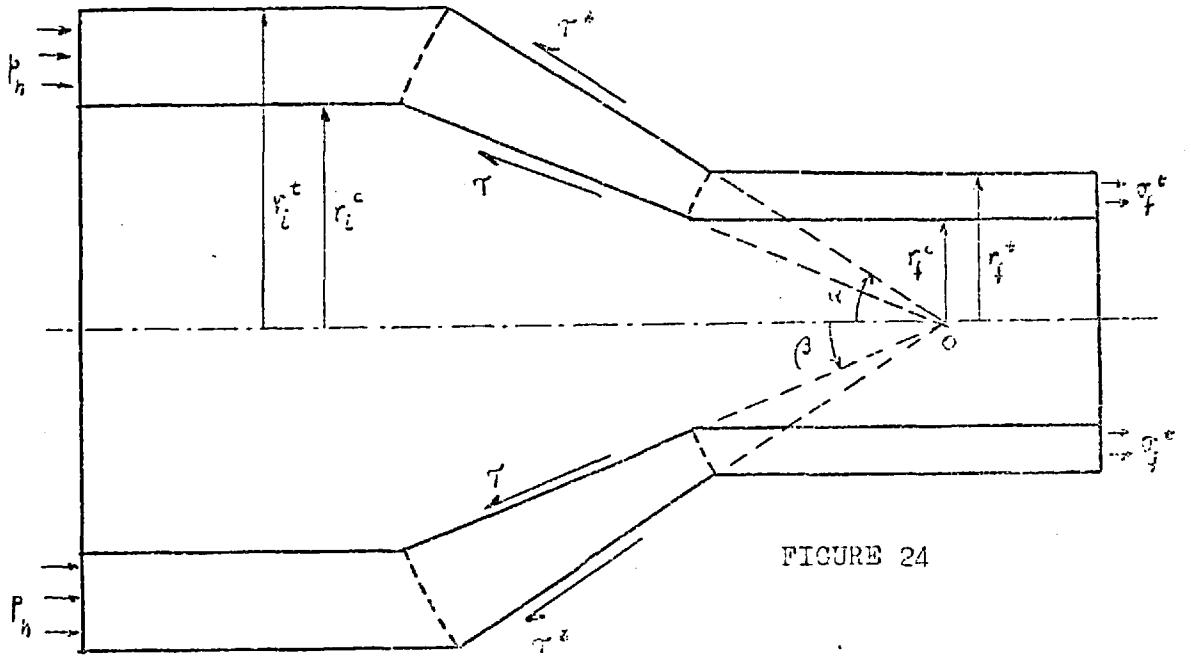

FIGURE 24

V.5.1 Internal power of deformation

The power involved in the internal deformation of the portion of tube limited by the spherical surfaces Γ_1 and Γ_2 can be calculated as the difference between the powers required to deform the whole conical volume of semi-angle α and the conical volume of semi-angle β. In analytical terms this means

$$\dot{W}_i = \frac{2}{\sqrt{3}} Y^t \left[\int_{V_t} (\tfrac{1}{2}\dot{\varepsilon}^p_{ij}\dot{\varepsilon}^p_{ij})^{\frac{1}{2}} dV - \int_{V_c} (\tfrac{1}{2}\dot{\varepsilon}^p_{ij}\dot{\varepsilon}^p_{ij})^{\frac{1}{2}} dV \right] \quad (97)$$

Substituting the values of the strain rate field components into equation (97) and integrating as has already been described (see Appendix B), the following expression is obtained:

$$\dot{W}_i = \pi Y^t v_f \left[(r_f^t)^2 F(\alpha) \ln R_t - (r_f^c)^2 F(\beta) \ln R_c \right] \qquad (98)$$

For the die angles and volume fractions used throughout the experiments carried out, the maximum error involved in assuming $F(\alpha) = F(\beta)$ is less than 0.1%.

As has already been pointed out, under the conditions being considered, both materials deform with the same extrusion ratio, that is

$$R_c = R_t = R$$

Consequently, expression (98) becomes

$$\dot{W}_i = \pi Y^t F(\alpha) v_f (r_f^t)^2 \left[1 - \left(\frac{r_f^c}{r_f^t} \right)^2 \right] \ln R$$

or, in another form

$$W_i = \pi Y^t F(\alpha) v_f (r_f^t)^2 \ln R \qquad (99)$$

since

$$1 - \left(\frac{r_f^c}{r_f^t} \right)^2 = 1 - \gamma_c = \gamma_t$$

V.5.2 Dissipation on the surface discontinuities

In this case the surfaces containing the discontinuities are the part of Γ_1 and Γ_2 limited by the conical surfaces Γ_3 and Γ_4 as shown in Fig. 25.

The general expression for the dissipation of power is

$$\dot{W} = \int \tau^* \Delta v \, dA$$

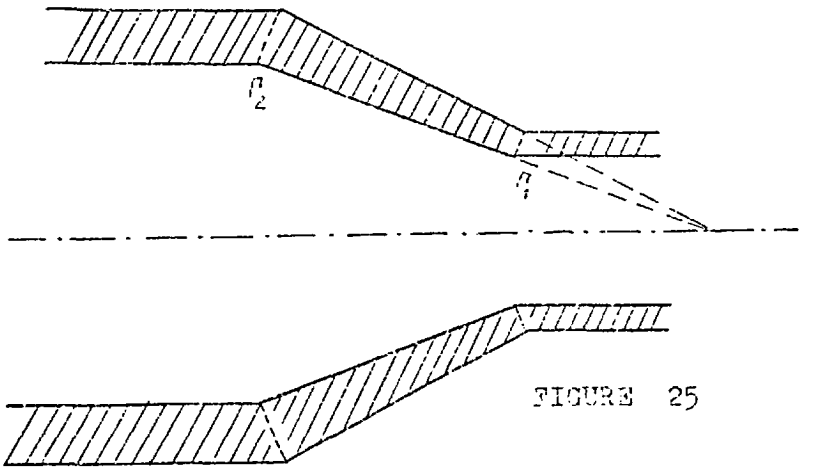

FIGURE 25

Assuming as before

$$\tau^* = \frac{Y^t}{\sqrt{3}}$$

and since for Γ_1

$$\Delta v = v_f \sin\theta$$

and $$dA = 2\pi R_f^2 \sin\theta \, d\theta$$

the above integral rewrites to

$$\dot{W}_{\Gamma_1} = \int_{\beta}^{\alpha} \frac{Y^t}{\sqrt{3}} (v_f \sin\theta)(2\pi R_f^2 \sin\theta d\theta)$$

After integration,

$$\dot{W}_{\Gamma_1} = \frac{\pi}{\sqrt{3}} Y^t R_f^2 v_f \left[(\alpha - \beta) - \sin\alpha\cos\alpha + \sin\beta\cos\beta \right]$$

or alternatively

$$\dot{W}_{\Gamma_1} = \frac{\pi}{\sqrt{3}} Y^t (r_f^t)^2 v_f \left[\frac{\alpha - \beta}{\sin\alpha} - \cot\alpha + \frac{\sin\beta\cos\beta}{\sin^2\alpha} \right] \qquad (100)$$

Similarly for Γ_2

$$\dot{W}_{\Gamma_2} = \frac{\pi}{\sqrt{3}} Y^t (r_i^t)^2 v_i \left[\frac{\alpha - \beta}{\sin^2\alpha} - \cot\alpha + \frac{\sin\beta\cos\beta}{\sin^2\alpha} \right]$$

or

$$\dot{W}_{\Gamma_2} + \frac{\pi}{\sqrt{3}} Y^t (r_f^t)^2 v_f \left[\frac{\alpha - \beta}{\sin^2\alpha} - \cot\alpha + \frac{\sin\beta\cos\beta}{\sin^2\alpha} \right] \qquad (101)$$

since, from volume constancy:

$$(r_i^t)^2 v_i = (r_f^t)^2 v_f$$

Finally, the total power involving both surfaces is:

$$W = \frac{2\pi}{\sqrt{3}} Y^t (r_f^t)^2 v_f \left[\frac{\alpha - \beta}{\sin^2\alpha} - \cot\alpha + \frac{\sin\beta\cos\beta}{\sin^2\alpha} \right] \qquad (102)$$

V.5.3 Power consumed in dragging the core

This component has the same value as calculated in (93) with the difference that here it acts as a resistance to the deformation process and consequently has the opposite sign:

$$W_d = - q\vartheta\pi v_f (r_f^c)^2 \cot\beta \ln R$$

or

$$\dot{W}_d = -q\vartheta\pi v_f (r_f^t)^2 \gamma_c \cot\beta \ln R \qquad (103)$$

V.5.4 Power dissipated by friction at the tube-die interface

The dissipation of power due to friction can be expressed as

$$\dot{W}_{\Gamma_3} = \int_{\Gamma_3} \tau^* \Delta v \, dS \qquad (104)$$

The tangential stress τ^* developed at the tube-die interface due to friction can be put in terms of the shear yield stress $\frac{Y^t}{\sqrt{3}}$ of the tube (assuming the die to be rigid in comparison to the tube). That is

$$\tau^* = g\frac{Y^t}{\sqrt{3}} \qquad 0 \leqslant g \leqslant 1 \qquad (105)$$

Under the assumption of a rigid die, the discontinuity in velocity across Γ_3 is

$$\Delta v = v_f (r_f^t)^2 \frac{\cos\alpha}{r^2} \qquad (106)$$

An element of that surface is

$$dS = \frac{2\pi r \, dr}{\sin\alpha} \qquad (107)$$

Replacing values in equation (104), the following expression is obtained after integration:

$$\dot{W}_{\Gamma_3} = \frac{1}{\sqrt{3}} g Y^t \pi v_f (r_f^t)^2 \cot\alpha \ln R \qquad (108)$$

V.5.5 Active powers acting on the tube

Again both components arising from the process of product and billet augmentation in the form of a pulling or drawing force and a hydrostatic pressure are present.

The power developed by the drawing force is

$$\dot{W}_D = \int_{S_t} T_j v_j dS_t$$

where S_t is the cross sectional area of the tube at the exit of the due, while v_j and T_j are the velocity and stress distribution on that surface.

As before, the drawing stress can be assumed as constant with a value of σ_f^t; the velocity v_f is also constant for the whole area. Consequently, the applied power is

$$\dot{W}_D = \pi v_f (r_f^t)^2 \gamma_t \sigma_f^t \qquad (109)$$

Similarly, the power applied by means of the hydrostatic pressure of extrusion is

$$\dot{W}_e = \int_{S_i} T_j v_j dS_i$$

where S_i is the cross sectional area of the tube before being deformed, while T_j and v_j are the stress and velocity distribution corresponding to that area.

As the stress T_j is in this case the hydrostatic

pressure p_h acting on all points of S_i and the velocity v_i is constant, after integration, the following expression is obtained:

$$\dot{W}_e = \pi v_i \left[(r_i^t)^2 - (r_i^c)^2\right] p_h$$

or

$$\dot{W}_e = \pi v_i (r_i^t)^2 \left[1 - \left(\frac{r_i^c}{r_i^t}\right)^2\right] p_h$$

and, finally

$$\dot{W}_e = \pi v_f (r_f^t)^2 \gamma_t \, p_h$$

since

$$1 - \left(\frac{r_i^c}{r_i^t}\right)^2 = 1 - \gamma_c = \gamma_t \qquad (110)$$

V.5.6 Balance of power in the tube

By substituting equations (99), (102), (103), (108), (109) and (110) in the general expression of the theorem (76), the following expression for the driving stress is obtained:

$$\sigma_f^t + p_h = Y^t F(\alpha) \ln R + \frac{2Y^t}{\sqrt{3}\,\gamma_t}\left[\frac{\alpha - \beta}{\sin\alpha} - \cot\alpha + \frac{\sin\beta\cos\beta}{\sin^2\alpha}\right] +$$

$$+ q\vartheta\frac{\gamma_c}{\gamma_t}\cot\beta \ln R + \frac{g}{\sqrt{3}}\frac{Y^t}{\gamma^t}\cot\alpha \ln R \qquad (111)$$

In this case, the compressive stress due to the dragging of the core is

$$q\vartheta\frac{\gamma_c}{\gamma_t}\cot\beta\ln R \qquad (112)$$

Again, in case of the tube being the harder metal, $q < 0$ and equation (112) represents a tensile stress.

V.6 Mean pulling stress

The mean pulling stress σ_p can be calculated as

$$\sigma_p = \sigma_f^t\gamma_t + \sigma_f^c\gamma_c \qquad (113)$$

Solving equation (94) for σ_f^c, equation (111) for σ_f^t and substituting these values into equation (113), the following expression is obtained:

$$\sigma_p = -p_h + Y^tF(\alpha)\ln R\gamma_t + \frac{2}{\sqrt{3}}Y^t\left[\frac{\alpha-\beta}{\sin^2\alpha} - \cot\alpha + \frac{\sin\beta\cos\beta}{\sin^2\alpha}\right]$$
$$+ \frac{g}{\sqrt{3}}Y^t\cot\alpha\ln R + Y^c\gamma_c\left[\frac{2}{\sqrt{3}}\left(\frac{\beta}{\sin^2\beta} - \cot\beta\right) + F(\beta)\ln R\right]$$

or, with the already used hypothesis

$$f(\alpha) \cong F(\beta)$$

$$\sigma_p = -p_h + \left[(Y^t\gamma_t + Y^c\gamma_c)F(\alpha) + g\frac{Y^t}{\sqrt{3}}\cot\alpha\right]\ln R +$$
$$+ \frac{2}{\sqrt{3}}Y^t\left[\frac{\alpha-\beta}{\sin^2\alpha} - \cot\alpha + \frac{\sin\beta\cos\beta}{\sin^2\alpha}\right] + \frac{2}{\sqrt{3}}Y^c\gamma_c\left(\frac{\beta}{\sin^2\beta} - \cot\beta\right) \qquad (114)$$

If only one metal is being processed, $Y^t = Y_c = Y$, $\gamma_c = 0$ and the well-known Avitzur's expression

$$\sigma_p = - p_h + (YF(\alpha) + g\frac{Y}{\sqrt{3}}\cot\alpha)\ln R + \\ + \frac{2}{\sqrt{3}}Y\left(\frac{\alpha}{\sin^2\alpha} - \cot\alpha\right) \qquad (115)$$

is obtained.

V.7 Theoretical and experimental results

The driving stress can be obtained from equation (114) and presented in a non-dimensional form by relating it to the yield stress of the core:

$$\frac{\sigma_p + p_h}{Y^c} = \left[(\omega\gamma_t + \gamma_c)F(\alpha) + g\frac{\omega}{\sqrt{3}}\cot\alpha\right]\ln R + \frac{2}{\sqrt{3}}\gamma_c\left(\frac{\beta}{\sin^2\beta} - \cot\beta\right) \\ + \frac{2}{\sqrt{3}}\omega\left[\frac{\alpha-\beta}{\sin^2\alpha} - \cot\alpha + \frac{\sin\beta\cos\beta}{\sin^2\alpha}\right] \qquad (116)$$

Expression (116) was computed for different values of the extrusion ratio and the ω relation. The results are shown in Fig. 26 in a semi-logarithmic scale together with the experimental ones.

The analysis of Fig. 26 shows that there is a reasonable agreement between the experimental and the predicted values.

This problem has been solved independently by Mellor et al. by using a similar tangential stress system to describe the dragging effect. Their approach represents the dragging stress as:

$$\tau = m \frac{Y_{soft}}{\sqrt{3}} \qquad 0 \leqslant m \leqslant 1$$

and considerations about the influence of Y_{soft}/Y_{hard} are made on the basis of experimental results.

The form of expression $\tau = q\vartheta$ used in the present work seems to have more flexibility, not only because it includes the relation ω into the theoretical formulation but also because it allows the use of different dragging functions ϑ . This has the advantage of making room for non-uniform and non-symmetric distributions of τ along the interface.

It seems apparent that τ must be influenced by the pressure distribution along the die interface and expressions like (71) or results as described in [91] should be taken into account in a future work.

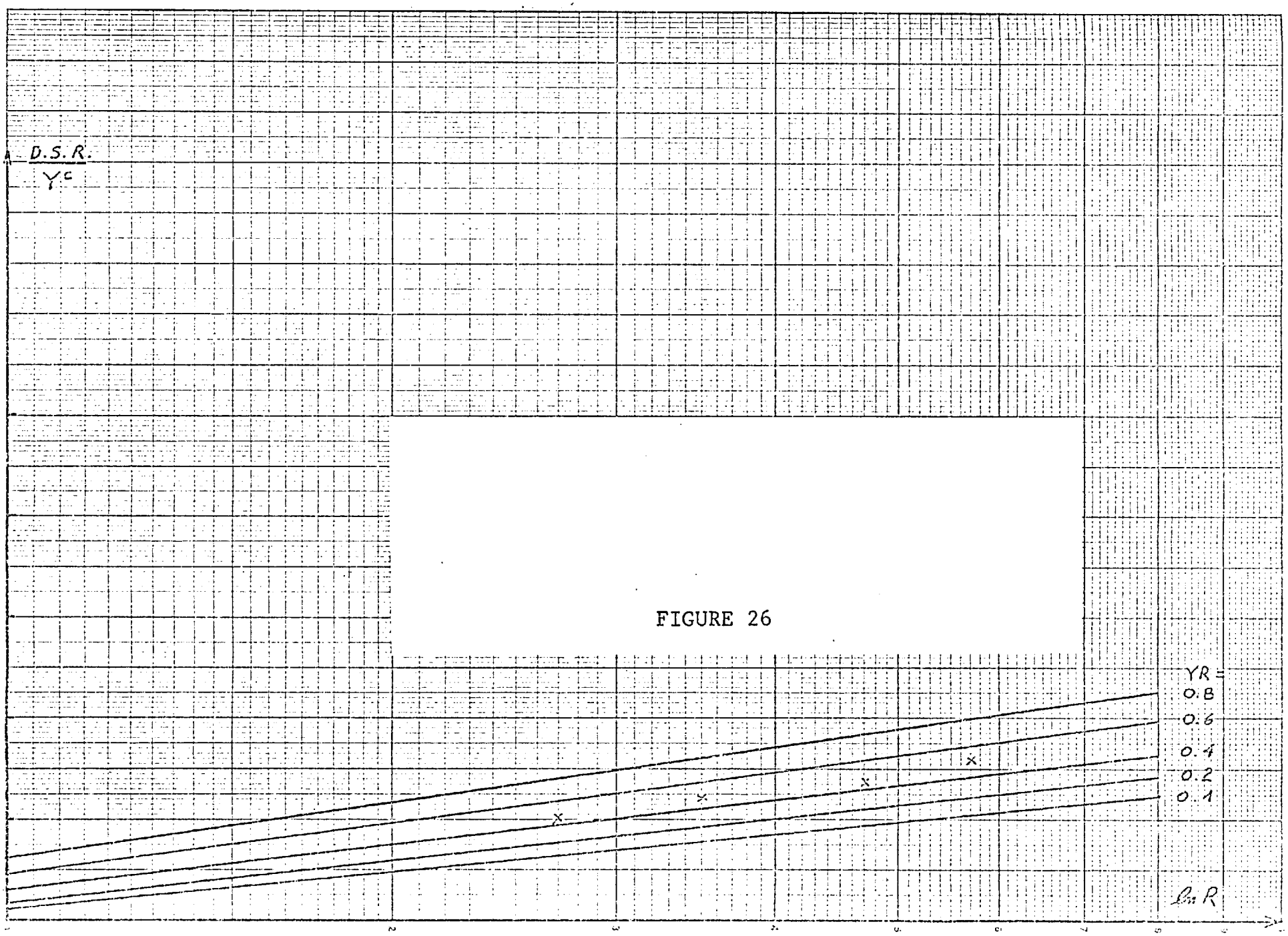

FIGURE 26

VI. THE METHOD OF WEIGHTED RESIDUALS AND ECONOMIZATION IN SEVERAL VARIABLES

VI.1 Introduction

The Method of Weighted Variables is an engineer's tool for finding approximate solutions to the equations of change of distributed systems. Experience and intuition can be distilled into a reasonable and sometimes quite accurate first guess, from which it is possible to proceed to successively improved approximations.

Briefly, the procedure consists in assuming an approximate solution in the form of a linear combination of known trial functions with unknown coefficients. By substituting the proposed solution in the governing equation, a residual function is obtained, which is then required to be orthogonal to a selected set of "weighting" functions.

The analytical form of the approximate solution is often more useful than solutions generated by numerical integration and it usually takes less computation time to generate [50], [92].

Approximate solutions of differential equations may be required to satisfy either all or only part of the conditions of the problem. For example, it may be necessary to satisfy both the differential equation and the boundary condition

approximately; in other cases the differential equation may need to be satisfied only at a few positions, rather than at each point.

The approximate solution is expanded in a set of known functions with arbitrary parameters. In order to determine these parameters by the method of weighted residuals, the differential equation and boundary condition are directly used. Two strategies may be followed:

a) A first approximation may be sufficient; its validity is assessed using our intuition and experience.

b) A sequence of approximations can be calculated to converge to the solution. In this case, calculations must be put in a form amenable to a computer [51].

In all approximate methods where we focus our attention on achieving a small equation residual, we make the tacit assumption that a small error in satisfying the equation is reflected by only a small deviation of the approximate solution from the true solution. Systems for which this assumption is justified are often said to be "well behaved" or "well conditioned" [48].

VI.2 Description of the method [51], [92]

Let us consider the differential equation for u(X):

$$N(u) = 0 \qquad X \in V \qquad (116)$$

where N(u) denotes a generical differential operator involving spatial derivatives of u, and V is a three-dimensional domain with boundary B. The boundary condition may have the form

$$u(X) = f_B(X) \qquad X \in B \qquad (117)$$

Assume a trial solution of the form:

$$u^*(X) = u_B(X) + \sum_{i=1}^{n} A_i \varphi_i(X) \qquad (118)$$

where the approximating functions, φ_i are prescribed so that they satisfy the boundary condition

$$u_B(X) = f_B(X) \quad \text{and} \quad \varphi_i(X) = 0 \qquad X \in B \qquad (119)$$

and A_i are the parameters to be determined. This means that u^* satisfies the boundary conditions for any set of values given to the so far unknown parameters.

The trial solution does not necessarily need to be linear on the A_i parameters, nevertheless this form is usually chosen for simplicity.

By substituting expression (119) in the differential equation (116), we obtain:

$$N(u^*) = R(u^*) \qquad (120)$$

$R(u^*)$ being the residual function of the differential equation and constituting a measure of the extent to which the trial solution satisfies the equation. Finally, the error R will be minimized by following certain criteria and this operation will produce the A_i parameters.

According to the requirements of a specific problem, the φ_i can be prescribed as to fit in one of the following cases:

	Satisfies approximately	Satisfies exactly	Error function corresponds to
(i)	Diff. equation	Boundary cond.	Diff. equation
(ii)	Diff. equation & Boundary cond.	-	Diff. equation & Boundary cond.
(iii)	Boundary cond.	Diff. equation	Boundary cond.
(iv)	-	Diff. equation & Boundary cond.	-

Every case corresponds to a different problem and a particular analysis of each needs to be done [93], [49].

VI.3 Criteria for minimization of the error

There are several approaches to the minimization of the total error R that we consider next:

(i) Let us express the total error in the form:

$$R = \sum_{i=1}^{n} R_i = 0 \qquad (121)$$

which we want to make zero. In this expression, "i" is a

generical nodal point corresponding to a spatial mesh which represents a discretization of the domain V, and R_i the error that the assumed solution produces in the "i" point. This criterion may lead to false conclusions because of the possibility

$$R_i^+ + R_j^- = 0$$

and, consequently, its use is not convenient.

(ii) Let us express the total error in the form:

$$R = \sum_{i=1}^{n} F(R_i) = 0 \qquad (122)$$

which expresses the total error as a function of the local errors. This form is a generalization of the case (i) and F may be any suitable function.

Example:

$$\sum_{i=1}^{n} R_i^2 = 0 \qquad (123)$$

that, in fact is also

$$\sum_{i=1}^{n} |R_i| = 0 \qquad (124)$$

(iii) Other forms:-

Expression (123) may be written as

$$\sum_{i=1}^{n} R_i^2 = \sum_{i=1}^{n} R_i \times R_i = 0 \qquad (125)$$

and may be considered a particular case of the more general expression:

$$\sum_{i=1}^{n} R_i \times (\text{something else}) = 0 \qquad (126)$$

Example: If we choose

$$\sum_{i=1}^{n} R_i \times (\text{sign of the error}) = 0$$

the expression (124) is obtained.

A general form for the expression (126) is

$$\sum_{i=1}^{n} W(X_i)R(X_i) = 0 \qquad (127)$$

or, in the case of a continuum domain V:

$$\int_V W(X)R(X)dX = 0 \qquad (128)$$

Equation (128) is the analytical expression of the Method of the Weighted Residuals which, in general terms, means that the weighted averages of the residuals must vanish. The W(X) are called "weighting functions".

In a more abstract form, equation (128) may be regarded as

$$\int_V R(X)\, d\mu = 0 \qquad (129)$$

where $d\mu = W(X)dX = d\mu(X)$.

Expression (129) is a Stieltjes's integral, where

the differential $d\mu$ "weighs" at any point the function which is to be integrated.

VI.4 Particular forms of the method of weighted residuals

The general process which is analytically described in equation (128), contains many well-known approximation methods (e.g. the methods of collocation, subdomain, Galerkin, least squares, etc.) as special cases corresponding to particular methods for choosing the weighting functions.

Let us see an illustrative example of the most common forms of the method [48]. We propose to solve the differential equation:

$$\frac{dx}{dt} = -x \qquad t > 0 \tag{130}$$

with the boundary condition

$$x = 1 \qquad t = 0 \tag{131}$$

in the interval $0 \leqslant t \leqslant 1$.

The first and most important step in the application of the method is to adopt a trial family of approximate solutions. An analysis of the different criteria for the selection of trial families will be considered further on. For this particular case we choose

$$x = 1 + A_1 t + A_2 t^2 \tag{132}$$

where A_1 and A_2 are the free parameters to be determined.

Different combinations of values for A_1 and A_2 represent different possible approximations. This trial solution (132) satisfies the boundary condition (131) for any value of the parameters.

By substituting function (132) in the differential equation (130) we obtain the expression of the residual R(t) as follows:

$$R(t) = \frac{dx}{dt} + x = 1 + (1+t)A_1 + (2t+t^2)A_2 \qquad (133)$$

The next step requires the adoption of a criterion for selecting the best approximation within the family, Several different criteria have been suggested.

(i) Collocation

In this criterion we choose as many locations within the interval as there are parameters to be determined. The assumption here is that the residual vanishes at these locations. Having in this case two free parameters, we choose two points within the interval, e.g. $\frac{1}{3}$ and $\frac{2}{3}$. Consequently, we obtain

$$R(\tfrac{1}{3}) = 1 + \frac{4}{3}A_1 + \frac{7}{9}A_2 = 0$$

$$R(\tfrac{2}{3}) = 1 + \frac{5}{3}A_1 + \frac{16}{9}A_2 = 0$$

When solving for A_1 and A_2 we get:

$$A_1 = -0.9310$$

$$A_2 = 0.3103$$

and hence, from expression (132), the corresponding approximate solution

$$x = 1 - 0.9310\,t + 0.3103\,t^2 \qquad (134)$$

(ii) Subdomain method

The desired interval is divided into as many subdomains as there are free parameters. Then they are adjusted until the average value of the residual in each subdomain is zero.

For this example, let us consider the two subdomains as: $0 \leqslant t \leqslant \frac{1}{2}$, and $\frac{1}{2} \leqslant t \leqslant 1$, and consequently:

$$\int_0^{\frac{1}{2}} R\,dt = \tfrac{1}{2} + \frac{5}{8}A_1 + \frac{7}{24}A_2 = 0$$

$$\int_{\frac{1}{2}}^{1} R\,dt = \tfrac{1}{2} + \frac{7}{8}A_1 + \frac{25}{24}A_2 = 0$$

Solving for A_1 and A_2 and substituting into expression (132) we finally obtain:

$$x = 1 - 0.947\,t + 0.3158\,t^2 \qquad (135)$$

(iii) Galerkin's method

This criterion requires that the weighted averages of the residual over the desired interval must vanish. The

weighting functions are taken to be the same functions of t as were used in constructing the trial family. In this case, these functions are t and t^2 and, therefore, we establish that:

$$\int_0^1 t\,R\,dt = \tfrac{1}{2} + \frac{5}{6}A_1 + \frac{11}{12}A_2 = 0$$

$$\int_0^1 t^2\,R\,dt = \frac{1}{3} + \frac{7}{12}A_1 + \frac{9}{20}A_2 = 0$$

Solving this system for A_1 and A_2 leads to:

$$x = 1 - 0.9143\,t + 0.2857\,t^2 \qquad (136)$$

(iv) Method of least squares

Here the free parameters are adjusted in such a way as to minimize the integral of the square of the residual, over the desired interval. Thus we establish:

$$\tfrac{1}{2}\frac{\partial}{\partial A_1}\int_0^1 R^2\,dt = \int_0^1 R\frac{\partial R}{\partial A_1}\,dt = \frac{3}{2} + \frac{7}{3}A_1 + \frac{9}{4}A_2 = 0$$

$$\tfrac{1}{2}\frac{\partial}{\partial A_2}\int_0^1 R^2\,dt = \int_0^1 R\frac{\partial R}{\partial A_2}\,dt = \frac{4}{3} + \frac{9}{4}A_1 + \frac{38}{15}A_2 = 0$$

from which we obtain:

$$x = 1 - 0.9427\,t + 0.3110\,t^2 \qquad (137)$$

All four criteria can be considered as special cases of the single general criterion (128) which states that

the weighted averages of the residual must vanish. In the case of collocation, the weighting function is the "Dirac delta": $\delta(t-a)$, "a" being the chosen location. Similarly, in the subdomain method, the weighting function is taken as one in the subdomain and zero outside. The cases corresponding to the Galerkin and least squares methods are more obviously particular forms of equation (128).

The error distribution corresponding to the different methods, over the 0 - 1 interval is shown in Fig. 27. As a matter of comparison it is also shown the truncation error of the first three terms of the Taylor's series:

$$x = 1 - t + \tfrac{1}{2}t^2$$

corresponding to the true solution: $x = e^{-t}$.

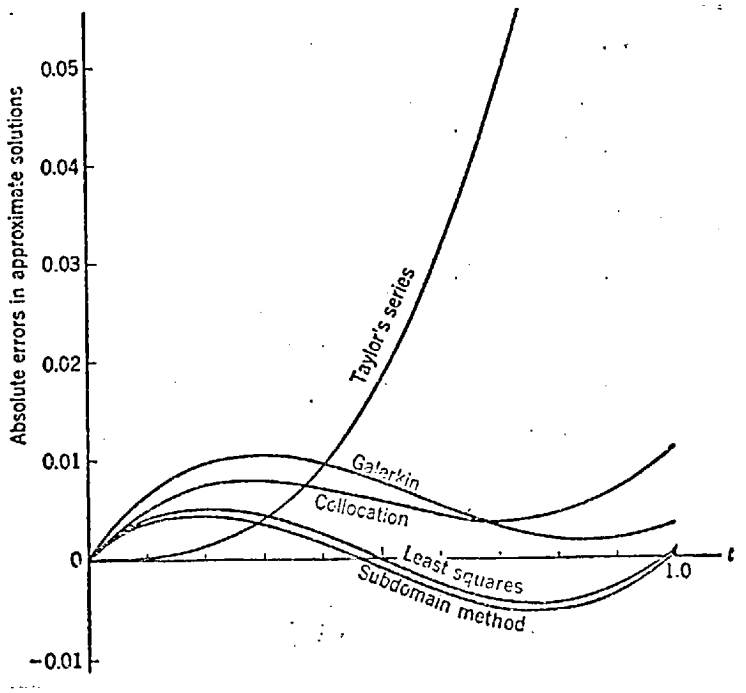

FIGURE 27

Note that the least squares method provides the most uniform distribution of the error while collocation gives the worse. Nevertheless, all of them are better approximations than Taylor's series, except near the zero end of the interval.

The selection of the weighting functions for a given set of trial functions and a particular problem is still a matter of discussion [94]. Several authors considered this question from the standpoint of the economy in computing time and ease of application and presented numerical examples showing relative accuracy [48], [93], [95], [96], [97].

VI.5 The least squares method

As was pointed out in section VI.4.(iv), the integral of the square of the residual is minimized in respect to the undetermined parameters A_k, to provide the r simultaneous equations required:

$$\frac{\partial}{\partial A_k} \int_V R^2 \, dX = 0 \qquad k = 1(1)r \qquad (138)$$

In numerical calculations it is frequent to assume the domain V represented by a discrete mesh and, accordingly, to minimize the error at the nodal points. Therefore, expression (138) is substituted by:

$$\frac{\partial}{\partial A_k} \sum_{i=1}^{n} R_i^2 = 0 \qquad k = 1(1)r \qquad (139)$$

n being the number of nodal points in the adopted mesh, while "i" represents a generical one.

This procedure involves, in fact, the idea of the collocation method.

Since a polynomial is probably the easiest form for computation, it is frequent to adopt, as trial solutions, expressions of the form:

$$u^{*}(X) = u_B(X) + \sum_{i=1}^{n} A_i X^i \qquad (140)$$

Being the differential operator N(u) linear, expression (139) leads to a set of simultaneous linear equations in the free parameters A_i.

VI.6 The trial solution

The most important and difficult stage in all the methods described here is the selection of the trial function. As the purpose of these methods is merely to choose the "best" approximation of a given family, good results cannot be obtained if good approximations are not included within the family.

Theoretically, if enough independent $\varphi_i(X)$ are included in (118), good approximations must be contained within the family; however, the principal attraction of these methods lies in the possibility of obtaining good approximations with a limited number of adjustable parameters [48].

In low-order approximations the choice may influence the results, but higher approximations are less affected since numerical convergence is desired.

The trial functions must be complete and linearly independent. A set of functions $\{\varphi_i\}$ is complete if any function of a given class can be expanded in terms of the set:

$$f(x) = \sum_i A_i \varphi_i(X)$$

Consequently, expressions of the form $\sum_i A_i \varphi_i(X)$ are inherently capable of representing the exact solution, provided enough terms are used. The polynomials are a complete set and, therefore, any continuous function can be expanded in terms of them.

The property of completeness of a set of functions ensures that, if sufficient number of terms are used, we can represent the exact solution. Otherwise, the successive approximations might converge to something which is not the solution [51].

A common expression for a trial function of polynomial form is:

$$P = P(X) = \sum_{i=1}^{n} A_i X^i$$

With a boundary condition such that

$$P = f_B \quad \text{when} \quad X = 0,$$

the estimate may be written as

$$P = f_B + \sum_{i=1}^{n} A_i X^i \tag{141}$$

Other functions such as orthogonal polynomials and transcendental functions have also been used in setting up the trial solution [98], [99]. In general, this selection may involve difficulties in the computing process, but it may be suitable for some particular problems.

The selection of approximating functions is yet somewhat dependent on the user's intuition and experience, and this is often regarded as a major disadvantage of the methods of weighted residuals. Nevertheless, some guidelines of general application may be outlined:

(a) The form of the estimate must be kept as simple and general as possible, trying to avoid the use of too rigid restrictions, even if a minor characteristic of the solution has to be lost.

(b) Consideration should be given to symmetries or any other special feature of the solution which may be known in advance from the kind of problem to be solved. This property must be kept independent of the free parameters.

(c) The highest power in the coordinates must give no preference for any one coordinate direction. The initial estimate should not predetermine a strong tendency in the solution.

(d) The trial solution must satisfy the largest possible number of boundary conditions, independently of the values taken by the set of free parameters.

VI.7 Setting up error functions

As was pointed out, it is advisable to select the trial solution in such a way as to satisfy all the boundary conditions, independently of the free parameters A_i.

Unfortunately, this is not always possible, or at least, not for all the prescribed boundary conditions. Frequently a boundary condition may constitute too strong a restriction for the more suitable trial solution for the governing equation. In other cases, the selected estimate does not simply leave room as to include some particular condition. In these circumstances, it is more convenient to have separate error functions for the boundary conditions.

Expression (128) is substituted by a linear combination of the integrals:

$$a \int_V W(X)\, R_v(X)\, dX + b \int_B W(X)\, R_B(X)\, dX = 0 \qquad (142)$$

where a and b are constants, usually called "weighting factors", R_V is the error functions corresponding to the governing equation and R_B the error functions corresponding to the boundary condition. The integral associated with the boundary condition is calculated only at boundary points.

If the least squares method is used, one obtains

$$\frac{\partial}{\partial A_k} \int_V a R_V^2(X) dX + \frac{\partial}{\partial A_k} \int_B b R_B^2(X) dX = 0 \qquad k = 1(1)r \qquad (143)$$

or, in another form:

$$\frac{\partial}{\partial A_k} \int_V \left[a R_V^2(X) + b R_B^2(X) \right] dX = 0 \qquad k = 1(1)r \qquad (144)$$

where R_B is defined in such a way that it takes the proper value at boundary points and zero on all others.

Referred to a discrete domain or a representative mesh, equation (29) becomes:

$$\frac{\partial}{\partial A_k} \sum_{i=1}^{n} \left[a R_{Vi}^2(X) + b R_{Bi}^2(X) \right] = 0 \qquad k = 1(1)r \qquad (145)$$

If linear forms in the unknown parameters A_k, have been used for the trial solutions of both, governing equation and boundary condition, expression (145) represents a linear system of equations that may be solved by means of any of the standard methods. Otherwise, a non-linear system would be obtained which in general is more difficult to solve by computer

methods. This consideration is particularly important if the method is going to be used on an iteration process, as is frequently the case when solving non-linear equations.

In general, the region over which the boundary error function is integrated is smaller than the total domain V, where the error function associated with the governing equation is integrated. Consequently, the errors in the differential equation will "weigh" more heavily in the minimization of the total error and it can be expected that the boundary conditions will be approximated with much less accuracy. A criterion may be derived from these considerations in order to give values for the constants a and b. This may be given by the ratio of the number of mesh points in the domain V to that of the boundary.

Expression (145) may be written as

$$\frac{\partial}{\partial A_k} \sum_{i=1}^{n} R_{Ti}^2 = 0 \qquad k = 1(1)r \quad (146)$$

where

$$R_{Ti}^2 = R_{vi}^2(X) + \frac{N_1}{N_2} R_{Bi}^2(X)$$

and N_1 and N_2 are the number of nodal points on V and the boundary region B respectively [54].

It is important to remark that one must be careful to choose a closer net when increasing the number of free

parameters in order to prevent waviness in the solution.

Together with the use of a finer net and a large number of parameters, a better accuracy is obtained, but the computing time and the rounding error increases very rapidly, so a compromise situation must be found between these factors.

VI.8 Economization of polynomial solutions

VI.8.1 Introduction

The use of estimates of a polynomial form as

$$P(X) = \sum_{i=1}^{n} A_i X^i \qquad X \in V$$

has several advantages in the process of computation and it is preferably used in relation with the method of weighted residuals. There is a frequent inconvenience in the use of this type of estimates: the eventually large number of terms "n" required in order to keep the maximum error of the solution, bounded by a pre-fixed value ε. This is particularly important if the solution is then going to be computed at a large amount of nodal points.

In general the number of terms required to get the total error bounded by a pre-fixed value is not known in advance. Consequently, "n" will be increased until an admissible level of accuracy is attained and then the polynomial solution is economized in order to reduce the computing time and to

avoid the instabilities arising from operating with an excessively laborious arithmetic [100]. These problems involve the use of high powers and too many multiplications, which increase the rounding errors considerably.

The aim of the economization process is to reduce the complexity in the calculation of P while allowing for a small permissible error of amplitude ε to be distributed in the domain V.

The method was originally proposed by C. Lanczos, [101] and [102], for the case of one variable, where economization was achieved when the degree of a given polynomial could be reduced in at least one unit.

In the following we extend Lanczos's method for economization to the case of more than one variable and find a second possible criterion which we call "carving" or vectorial economization. The purpose of carving is to induce as many zeros as possible in the lowest or extreme right lines of the coefficients matrix A, associated with P (see section VI.8.2). Then we discuss, for the case of two variables, sufficient conditions for the economization process to be feasible, in terms of the coefficients of the original polynomial. These results are condensed in simple rules for the case of two variables. The construction of the economized polynomial and the possibility of block economization are also discussed.

Since many polynomials used in the approximate solution of partial differential equations or in optimization problems come from the truncation of convergent power series expansions in several variables, where the coefficients decrease rapidly, the method describing the existence of a ε-economized expression of a given polynomial $P(x,y)$ is applicable to a wide variety of problems.

VI.8.2 Economization in several variables

Economization is essentially based on the idea of representing the original polynomial in terms of a polynomial basis which emphasizes the contribution of the first components.

The shifted Chebyshev polynomials of the first kind:

$$T_n^*(x) = \cos n\theta, \quad x = \cos^2\frac{\theta}{2} \qquad 0 \leqslant x \leqslant 1$$

are such that

$$x^n = 2 \times 4^{-n}\left[T_n^*(x) + \binom{2n}{1}T_{n-1}^*(x) + \ldots + \binom{2n}{n}T_0^*(x)\right] \quad (147)$$

and clearly constitute a basis with such a property.

In our approach we consider a given finite hypercubic domain V in which the economization is required, and we represent in it each variable of $P = P(x,y,\ldots)$ in terms of Chebyshev polynomials defined in suitable intervals. This gives a polynomial P^{Ch} in the new basis. Then we define P_ε^{Ch} such that

$$|P - P_\varepsilon^{Ch}| < \varepsilon$$

in V. P_ε^{Ch} is called the ε-economized form of P. Eventually P_ε^{Ch} is reconverted into powers of the original variables and is referred to as P_ε. For the sake of simplicity we shall restrict our discussion to the case when $P = P(x,y)$ is a polynomial of two variables x and y, and the economization process takes place in the square:

$$Q = \{(x,y): \quad 0 \leqslant x \leqslant 1, \qquad 0 \leqslant y \leqslant 1\},$$

an approach which can be extended without essential difficulties when the number of variables is greater than two.

Let us write P in the following form:

$$P = X^T A Y \tag{148}$$

where

$$X = \begin{bmatrix} x^0 \\ x^1 \\ x^2 \\ . \\ . \\ . \\ x^I \end{bmatrix} \qquad Y = \begin{bmatrix} y^0 \\ y^1 \\ y^2 \\ . \\ . \\ . \\ y^J \end{bmatrix} \qquad A = ((a_{ij})) \begin{cases} i = 0 \ (1) \ I \\ j = 0 \ (1) \ J \end{cases}$$

Then P is expressed in terms of Chebyshev polynomials by means of the linear transformations

$$\begin{aligned} X &= B\, T_x^* \\ Y &= B\, T_y^* \end{aligned} \tag{149}$$

where

$$T^*(t) = \begin{bmatrix} T_0^*(t) \\ T_1^*(t) \\ T_2^*(t) \\ \vdots \\ T_M^*(t) \end{bmatrix}$$

$T_n^*(t)$, n = 0 (1) M, are Chebyshev polynomials of the first kind as defined above. The elements of $B = ((b_{ij}))$ are generated by means of (147).

From (148) and (149) we obtain:

$$P^{Ch} = T_x^* C T_y^* \qquad (150)$$

that is the expression of P in terms of Chebyshev polynomials where

$$C = B^T A B$$

is the coefficients matrix of P^{Ch}.

VI.8.3 The process of economization

Two possible ways will be considered in which economization can be achieved. In the first we look for the largest possible reduction in the degree of the given polynomial compatible with the permissible error bound. In this case we

conduct in the matrix C a search along a diagonal path and terminate it when the accumulated error exceeds ε. We call this process triangular economization. In the second case we assume that the polynomial P is given in a double nested form in the variable x:

$$P(x,y) = ((p_1(r)y - p(r))y - \ldots)y + p_n(r) \quad (151)$$

or, in y:

$$P(x,y) = ((g_1(y)x - g_2(y))x - \ldots)x + g_n(y) \quad (152)$$

In this case, the cancellation of every coefficient in a border line of the matrix A, will result in a reduction of one in the number of multiplications required to evaluate P. We call this process "carving or vectorial economization".

(i) Triangular economization

We arrange the elements of matrix C in a diagonal sequence

$$\sigma = \left\{c_{ij}^{(k)}\right\}, \quad k = 1,2,\ldots N = (I+1)(J+1)$$

such that $C_{i,j}$ is identified with the leading coefficient c_{IJ} and in every secondary diagonal, the coefficients are of the same degree r+s in $T_r^*(x)T_s^*(y)$.

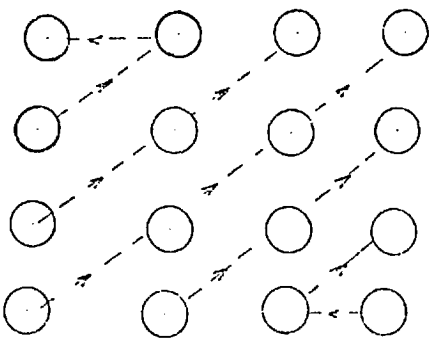

Given the admissible error bound ε, we then proceed to compute the sums

$$S_1^E = \sum_{k \in \bar{\sigma}} \left| c_{ij}^{(k)} \right| \qquad E = 1 \ (1) \ N$$

and look for the separation index such that:

$$S_1^E \leqslant \varepsilon \leqslant S_1^{E+1}$$

Since the maximum possible absolute value of $T_n^*(t)$ for all positive integers n and $0 \leqslant t \leqslant 1$ is one, S_1^E will be the maximum error arising from deleting all the E terms from P^{Ch}. Consequently, S_1^E defines the sequence σ_E of best ε-economization for P in Lanczos's sense.

(ii) Carving or vectorial economization

The algorithmic process is similar to the one just described, except for the fact that the search is now conducted along the farthermost right column or the lowest row, starting always with the element a_{IJ}. The separation index is found as in the triangular economization and the choice of row or column is made on the basis of the efficiency of the process which is measured by the number of zeros induced in the extreme lines of C. The polynomial P_ε is then evaluated in either the double nested form (151) or (152).

VI.8.4 Construction of the economized polynomial P_ε

Once σ_E have been found, we define a new matrix C^E with elements c^E_{ij} such that:

$$c^E_{ij} = 0 \qquad \text{if } c_{ij} \in \sigma_0$$

$$c^E_{ij} = c_{ij} \qquad \text{otherwise}$$

This matrix C^E defines the ε-economized polynomial $P^E_\varepsilon(x,y)$ as:

$$P^E_\varepsilon = P^E_\varepsilon(x,y) = (T^*_x)^T \, C^E \, T^*_y \tag{153}$$

and for every $(x,y) \in Q$,

$$|P(x,y) - P^E_\varepsilon(x,y)| < \varepsilon$$

The ε-economized polynomial $P_\varepsilon(x,y)$ is defined as a polynomial in x and y by the expression:

$$P_\varepsilon = P_\varepsilon(x,y) = X^T(B^{-1})^T \, C^E \, B^{-1} \, Y \tag{154}$$

VI.8.5 Sufficient conditions for the existence of an ε-economization process in terms of the coefficients of P

Let us assume that P(x,y) is defined in Q. If we take into account expression (147) and assume that I = J = n, we see that the leading coefficient c_{nn} of P^{Ch} is given by:

$$c_{nn} = \left(\frac{2}{4^n}\right)^2 a_{nn} = \frac{1}{4^{2n-1}} a_{nn}$$

Therefore, an ε-economization process involving a_{nn}, i.e., reducing the overall degree of P from 2n to 2n-1, will only be possible if:

$$|a_{nn}| < 4^{2n-1}\varepsilon \tag{155}$$

If this condition is satisfied, we then analyze the possibility of ε-economization involving the terms $x^n y^n$ and $x^n y^{n-1}$ (or $x^{n-1} y^n$). That will only be possible if a_{nn} and $a_{n\,n-1}$ (or $a_{n-1\,n}$) are such that:

$$\frac{2n+1}{4}|a_{nn}| + |a_{nn-1}| < 4^{2n-2}\varepsilon \tag{156}$$

or

$$\frac{2n+1}{4}|a_{nn}| + |a_{n-1\,n}| < 4^{2n-2}\varepsilon \tag{157}$$

Inequalities (155) to (157) will be used to give sufficient conditions in the two following cases.

(i) <u>ε-economization on a border line of matrix A</u>

In the case of ε-economization involving $x^n y^n$, $x^n y^{n-1}$, ..., $x^n y^{n-j}$ where $0 < j \leqslant n$, i.e. along the farthermost right column of A, the condition for a reduction in the number of multiplications in (151) is:

$$\sum_{s=0}^{j} \sum_{k=0}^{v-s} 4^s \, |a_{nn-s}| \, \binom{2(n-s)}{k} < 4^{2n-1}\varepsilon \tag{158}$$

where n-j = v. This follows from (155)-(157) by an inductive argument.

If we introduce the auxiliary function:

$$\psi(\alpha,\beta) = \sum_{k=0}^{\beta} \binom{\alpha}{k},$$

α and β positive integers, we can easily show that:

$$\psi(\alpha+1,\beta+1) = \psi(\alpha,\beta) + \psi(\alpha,\beta+1)$$

$$\psi(0,\beta) = 1 \qquad \alpha \neq \beta \quad \beta = 0, 1, 2, \ldots$$

and

$$\psi(\alpha,\beta) = 2^{\alpha} \qquad \alpha = \beta = 0, 1, 2, \ldots$$

Therefore, condition (158) can be stated more simply in terms of the recurrent expression $\psi(\alpha,\beta)$:

$$\sum_{s=0}^{n-j} 4^{s} |a_{nn-s}| \psi(2(n-s), n-j-s) < 4^{2n-4}\varepsilon \qquad (159)$$

For example, if n = 4 and j = 1, from Table I we get the following condition for the possibility of ε-economization of the four coefficients of P(x,y) in the farthermost right column of A, starting with a_{nn}:

$$a_{nn}\psi(8,3) + 4a_{n\,n-1}\psi(6,2) + 4^{2}a_{n\,n-2}\psi(4,1) +$$

$$4^{3}a_{n\,n-3}\psi(2,0) = 93a_{nn} + 88a_{n\,n-1} + 80a_{n\,n-2}$$

$$+ 64a_{n\,n-3} < 16384\,\varepsilon$$

where the a_{ij} are taken in absolute value.

To get a condition for the ε-economization involving coefficients in the lowest row of A, we only have to switch indices in (159).

TABLE I

$\psi(\alpha,\beta)$

α = \ β =	0	1	2	3	4	5	6	7	8
0	1								
1	1	2							
2	1	3	4						
3	1	4	7	8					
4	1	5	11	15	16				
5	1	6	16	26	31	32			
6	1	7	22	42	57	63	64		
7	1	8	29	64	99	120	127	128	
8	1	9	37	93	163	219	247	255	256

(ii) ε-economization on a triangular corner of matrix A

For the three coefficients a_{nn}, $a_{n\ n-1}$ and $a_{n-1\ n}$, from (155)-(157), the condition for the possibility of ε-economization is:

$$\frac{4n+1}{4}\left|a_{nn}\right| + \left|a_{n\ n-1}\right| + \left|a_{n-1\ n}\right| < 4^{2n-2}\varepsilon$$

In the case of a triangular sector of A, this expression generalizes as follows:

$$\frac{1}{4^{2n-1}} \sum_{s+u=0} 4^s \, 4^n \, a_{n-u \; n-s} \sum_{i+j=0}^{r-(s+u)} \binom{2(n-u)}{i} \binom{2(n-s)}{j} < 4^{2n-1}\varepsilon \qquad (160)$$

where $r-1$ is the number or rows (or columns) involved in the triangle under consideration.

From inequalities (159) and (160) we can give easy empirical rules for the ε-economization. For instance, we can say that ε-economization in the triangular case is possible for a_{nn} if:

$$|a_{nn}| < 10^n \varepsilon$$

anf for the first triangular corner, if:

$$n\,|a_{nn}| + |a_{n\;n-1}| + |a_{n-1\;n}| < 10^n \varepsilon$$

Similar rules can be found in the case of economization in one variable. From the previous formulae, it is easy to deduce analagous rules for the case of carving in one variable.

VI.8.6 Block economization

Conditions (159) and (160) give the possibility of ε-economization of a polynomial P considering only the set of coefficients a_{ij} for which, according to the method chosen for

the economization, the first or second condition is satisfied.

The polynomial P is thus divided into two segments P_1 and P_2, such that the coefficients of P_2 satisfy one of the conditions. Then P_2 is expressed in terms of the Chebyshev polynomials and ε-economized. The resulting expression is reconverted in powers of the original variables and added to P_1 to get P_ε.

This procedure is particularly suitable when either the number of variables, the size of the stored information or the computing time impose heavy restrictions on the economization process.

In the subroutine described in the next chapter, the ε-economization process involves the entire polynomial.

It is important to point out that when the difference between the times required to perform addition and multiplication is not too great, it may be preferable to carve the polynomial, inducing as many zeros as possible, everywhere in A.

VII. NUMERICAL INTEGRATION OF THE PRANDTL-REUSS EQUATION BY MEANS OF THE METHOD OF WEIGHTED RESIDUALS

VII.1 Introduction

In this chapter, the method of weighted residuals will be used in order to obtain approximate polynomial solutions to the Prandtl-Reuss equation. The procedure will then be used in the particular case of the hydrostatic extrusion-drawing of a bimetallic specimen, with the aim of obtaining the stress distribution on the deformating area. It is assumed that the flow pattern of deformation is described by Avitzur's velocity field and the materials are homogeneous and with an isotropic rule of hardening.

As was pointed out in equation (38) of Section II.4.3, the Prandtl-Reuss equation may be written as:

$$\sigma'_{ij} = \frac{k}{\sqrt{I_2}} \dot{\varepsilon}^P_{ij}$$

or, by means of symbolic notation:

$$T' = \frac{k}{\sqrt{I_2}} V \qquad (160)$$

T' being the deviatoric stress tensor and V the strain rate tensor. In a scalar form and under conditions of axial-symmetry, equation (160) becomes:

$$\sigma_r = \sigma_m + \frac{k}{\sqrt{I_2}} \dot{\varepsilon}_r \tag{161.a}$$

$$\sigma_\theta = \sigma_m + \frac{k}{\sqrt{I_2}} \dot{\varepsilon}_\theta \tag{161.b}$$

$$\sigma_z = \sigma_m + \frac{k}{\sqrt{I_2}} \dot{\varepsilon}_z \tag{161.c}$$

$$\tau_{rz} = \frac{k}{\sqrt{I_2}} \dot{\varepsilon}_{rz} \tag{161.d}$$

These equations are not independent if constancy of volume is assumed, that is,

$$\dot{\varepsilon}_z = -(\dot{\varepsilon}_r + \dot{\varepsilon}_\theta) \tag{162}$$

and consequently:

$$\sigma'_z = -(\sigma'_r + \sigma'_\theta) \tag{163}$$

VII.2 Process of calculation

Since the Prandtl-Reuss's equation is a non-linear one, the use of polynomial forms as trial solution leads to non-linear systems of equations in the unknown parameters. This fact constitutes an important obstacle in the application of the method of weighted residuals because non-linear systems of equations are hardly possible to be solved by means of a computing routine.

The way chosen for the solution of that problem is a process of linearization [53] and the use of the least squares criterion, within a routine of iteration.

Let us assume that, in a first approach, equation (160) may be written as:

$$T' = kV \tag{164}$$

where k is a constant that here may take the initial value of the shear yield stress of the material.

In this hypothesis, equations (161) are not exactly satisfied and, hence, there will be some difference between both sides of these equations. Let us express these differences by means of the error functions R_i. Equation (161.c) will not be considered due to constancy of volume.. Therefore, if "n" identifies a generical nodal point of the mesh that represents the deformating area, equations

$$R_{1n} = \sigma_r - \sigma_m - k\dot{\varepsilon}_r \tag{165.a}$$

$$R_{2n} = \sigma_\theta - \sigma_m - k\dot{\varepsilon}_\theta \tag{165.b}$$

$$R_{3n} = \tau_{rz} - k\dot{\varepsilon}_{rz} \tag{165.c}$$

are obtained, which must all be calculated for every modal point.

Squaring these equations, according to the least squares method, and summing up the error at all points of the mesh, we obtain:

$$R_1 = \sum_n (R_{1n})^2 \geqslant 0 \tag{166.a}$$

$$R_2 = \sum_n (R_{2n})^2 \geqslant 0 \qquad (166.b)$$

$$R_3 = \sum_n (R_{3n})^2 \geqslant 0 \qquad (166.c)$$

The total error in the whole deformating zone may be expressed as a linear combination of the error functions corresponding to each of the equations involved, that is:

$$R_T = g_1 R_1 + g_2 R_2 + g_3 R_3 = \sum_i g_i R_i \qquad (167)$$

where the g_i coefficients are the weighting factors.

As was pointed out in Section II.1.2.2, an axi-symmetrical state of stresses, referred to a cylindrical set of coordinates, can be expressed in terms of two stress functions: $\phi_1 = \phi_1(r,z)$ and $\phi_2 = \phi_2(r,z)$. In Section II.3.1 it was shown that the corresponding strain rate field can be put in terms of a stream function $\psi = \psi(r,z)$. Hence, if polynomial forms are adopted to represent approximately these three functions, such as:

$$\phi_1 = \phi_1(r,z,A_{ij}) = \phi_1^* + \sum_i \sum_j A_{ij} r^i z^j \qquad (168.a)$$

$$\phi_2 = \phi_2(r,z,B_{kl}) = \phi_2^* + \sum_k \sum_l B_{kl} r^k z^l \qquad (168.b)$$

$$\psi = \psi(r,z,C_{mn}) = \psi^* + \sum_m \sum_n C_{mn} r^m z^n \qquad (168.c)$$

the state of stress and strain rate can be put in terms of

the free parameters A_{ij}, B_{kl} and C_{mn}, according to equations (11) and (26).

This allows us to express the total error function R_T in terms of those parameters, as

$$R_T + R_T(r,z,A_{ij},B_{kl},C_{mn})$$

In this next step, following the least squares criterion, we calculate:

$$\frac{\partial R_T}{\partial A_{ij}} = 0 \qquad (169.a)$$

$$\frac{\partial R_T}{\partial B_{kl}} = 0 \qquad (169.b)$$

$$\frac{\partial R_T}{\partial C_{mn}} = 0 \qquad (169.c)$$

which constitutes a system of linear equations in the free parameters. By solving the system we obtain the values of the free parameters $A_{ij}^{(1)}$, $B_{kl}^{(1)}$, $C_{mn}^{(1)}$ that minimize the error in the whole deformating zone. Consequently they give an approximate form to the stress and stream functions and also to the stress and strain fields. Those values define a first approximation to the strain rate field $V^{(1)}$ and the corresponding stress field $T^{(1)}$ satisfying the governing equation (164).

A "better" set of parameters may be found if the error functions (165) are recalculated with

$$\frac{k}{\sqrt{I_2^{(1)}}}$$

instead of k, where the value of $I_2^{(1)}$ is derived from $V^{(1)}$. In this way, repeating equations (165)-(169), a new set of parameters $A_{ij}^{(2)}$, $B_{kl}^{(2)}$ and $C_{mn}^{(2)}$ is obtained which improves the solutions for the stress and strain rate tensor fields $T^{(2)}$ and $V^{(2)}$. In general, this second set of values is different from the first one and, therefore, it gives a new value for

$$\frac{k}{\sqrt{I_2^{(2)}}}$$

where $I_2^{(2)}$ is derived from $V^{(2)}$. With this value the process is reinitiated from equation (165) onwards and will continue as described until the absolute value of the difference between any parameter of the cycle "n+1" and the corresponding to the cycle "n" becomes smaller than a prefixed value Ω, that is

$$\left| A_{pq}^{(n+1)} - A_{pq}^{(n)} \right| < \Omega \qquad (170)$$

where A_{pq} is a generical parameter of the group. The value of Ω may also be expressed in terms of percentage of variation of A_{pq}, as criterion for establishing convergence. Another useful criterion of convergence is to determine the cycle in which R_T reaches its minimum value:

$$R_T^{(n+1)} > R_T^{(n)} \qquad (171)$$

Once this situation is obtained, by means of the velocity field (equation (23)), it is possible to determine the new positions of the nodal points by:

$$\Delta r = v_r \Delta t$$
$$\Delta z = v_z \Delta t$$

where Δt is a small interval of time.

The final coordinates are:

$$\begin{aligned} r_1 &= r_o + \Delta r \\ z_1 &= z_o + \Delta z \end{aligned} \qquad (172)$$

where r_o and z_o correspond to the coordinates of the mesh points at $t = 0$.

The application of expression (172) to all nodal points of the original mesh will produce a new mesh that represents the "picture" of the deformating zone after a time Δt.

The sequence of iteration is restarted for this new mesh, from equation (165) onwards, using

$$\frac{k}{\sqrt{I_2^{(n)}}}$$

as first value, n being the last cycle of iteration.

The same value of k is used throughout the process

if the problem is solved under the hypothesis of non-hardening materials. If the material work-hardens, k must be modified at this stage as described in the next item.

This routine continues until the total deformation time is covered.

VII.3 Work hardening materials

The procedure used up to here is valid for a rigid perfectly-plastic material; eventually k may be considered as the mean yield stress of a work hardening metal.

Let us now take into account the real behaviour of metals and introduce work hardening into the theory.

As von Mises's yield criterion was used when developing the theory, the effective stress $\bar{\sigma}$ may also be considered as a yielding function, that is:

$$\bar{\sigma} = Y = \sqrt{3}\,k \tag{173}$$

According to the definition, the effective strain rate is:

$$\dot{\bar{\varepsilon}} = \frac{2}{\sqrt{3}}\sqrt{I_2} \tag{174}$$

and, consequently

$$\bar{\varepsilon} = \frac{2}{\sqrt{3}}\int \sqrt{I_2}\,dt \tag{175}$$

Assuming the relationship $\bar{\sigma} = \bar{\sigma}(\bar{\varepsilon})$ as being known for the material we are dealing with, this may be expressed as:

$$\bar{\sigma} = \bar{\sigma}_o + \bar{\sigma}(\bar{\varepsilon}) \tag{176}$$

where $\bar{\sigma}_o$ is a constant.

The derivative of equation (176) with respect to time is:

$$\frac{d\bar{\sigma}}{dt} = \frac{d\bar{\sigma}}{d\bar{\varepsilon}} \cdot \frac{d\bar{\varepsilon}}{dt} = H.\dot{\bar{\varepsilon}} \tag{177}$$

where H is the slope of the $\bar{\sigma}$-$\bar{\varepsilon}$ curve, as in Fig. 28.

Expression (177) can be written as:

$$d\bar{\sigma} = H\,\dot{\bar{\varepsilon}}\,dt \tag{178}$$

and introducing equation (174) in (178) we get:

$$d\bar{\sigma} = \frac{2}{\sqrt{3}} H \sqrt{I_2}\, dt \tag{179}$$

FIGURE 28

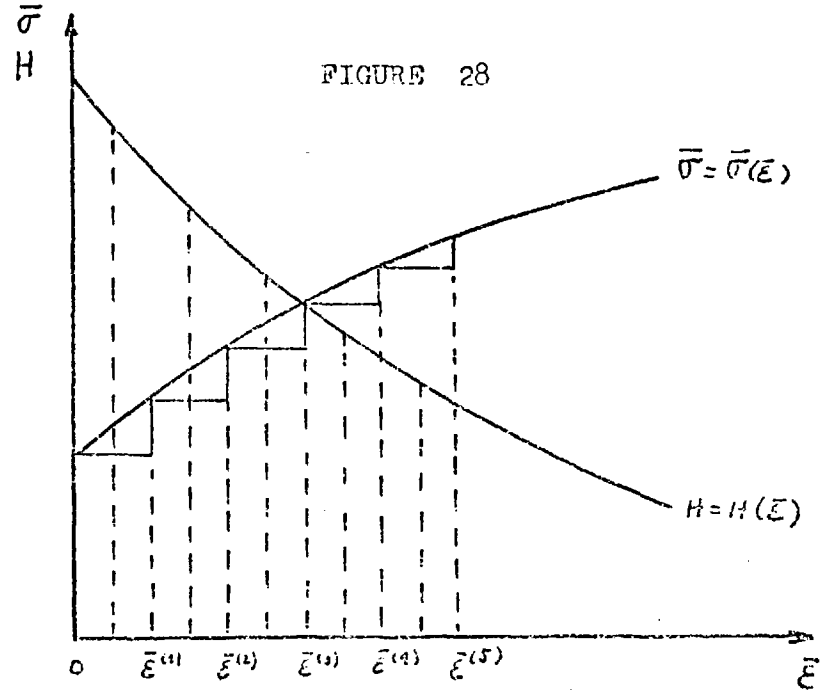

Differentiating (173) and replacing in (179)

$$dk = \frac{2}{3} H \sqrt{I_2}\, dt \tag{180}$$

is obtained, or, in terms of finite increments:

$$\Delta k = \frac{2}{3} H \sqrt{I_2}\, \Delta t \tag{181}$$

A time interval Δt must be adopted according to the velocity of displacement of the cross-section in which we are interested.

If a linear rule of hardening is admissible, $H(\bar{\varepsilon}) =$ constant, equation (181) may be written as:

$$\Delta k = C_k \sqrt{I_2}\, \Delta t \tag{182}$$

where C_k is a constant. In this case, a unique value for H will be used throughout the calculations.

Equation (181) will be used to take into account modifications in the value of k in equations (165) due to work hardening, as follows:

The total range of deformation will be divided into small intervals: $0 - \bar{\varepsilon}^{(1)}$, $\bar{\varepsilon}^{(1)} - \bar{\varepsilon}^{(2)}$, etc. These intervals are determined by the Δt increment chosen and the velocity of the specimen. It is assumed that the shear stress will take a constant value within each interval, that is:

Step	$t = 0$	$0 - \bar{\varepsilon}^{(1)}$	$k = k_1$
	$t = \Delta t$	$\bar{\varepsilon}^{(1)} - \bar{\varepsilon}^{(2)}$	$k = k_2 = k_1 + \Delta k_1$
	.....	.....	.....
	$t = n\Delta t$	$\bar{\varepsilon}^{(n-1)} - \bar{\varepsilon}^{(n)}$	$k = k_n = k_{n-1} + \Delta k_{n-1}$

VII.4 Modifications to the error functions due to work hardening

Once convergence was achieved for the first step, corresponding to $t = 0$, by using the first value of $k = k_1$ and the last value for $I_2^{(n)}$, it is possible to calculate:

$$\Delta k = C_k \sqrt{I_2^{(n)}}\, \Delta t \tag{183}$$

assuming a linear rule of hardening. Consequently, the next value for $k = k_2$ to be used during the second step will be:

$$k_2 = k_1 + \Delta k$$

With this new value for k and the new mesh obtained according to:

$$\begin{aligned} r_1 &= r_o + v_r^{(n)}\, \Delta t \\ z_1 &= z_o + v_z^{(n)}\, \Delta t \end{aligned} \tag{184}$$

the procedure is reinitiated from equations (165) onwards. The value

$$\frac{k_2}{\sqrt{I_2^{(n)}}}$$

is used in these equations.

Sequence of operations:

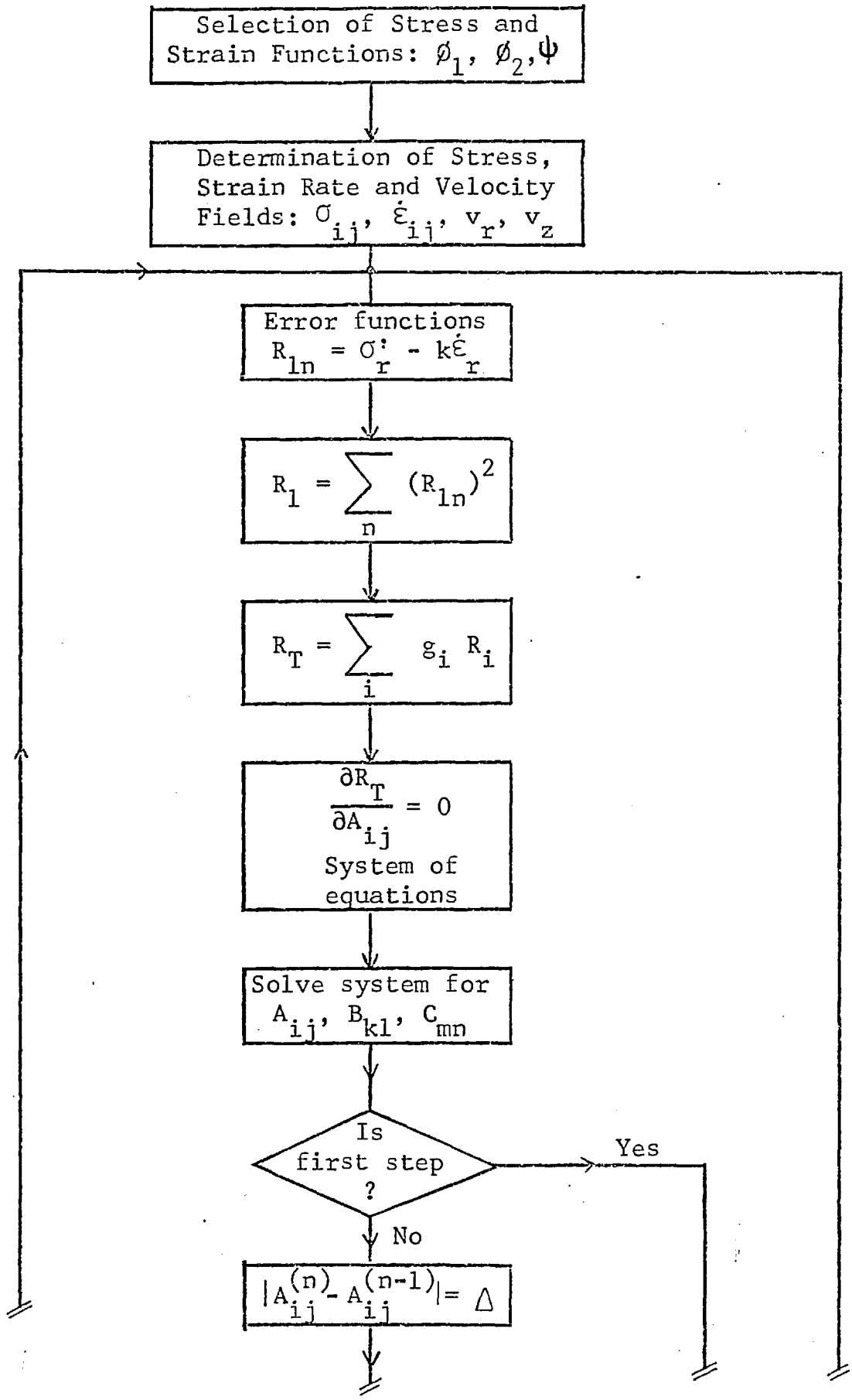

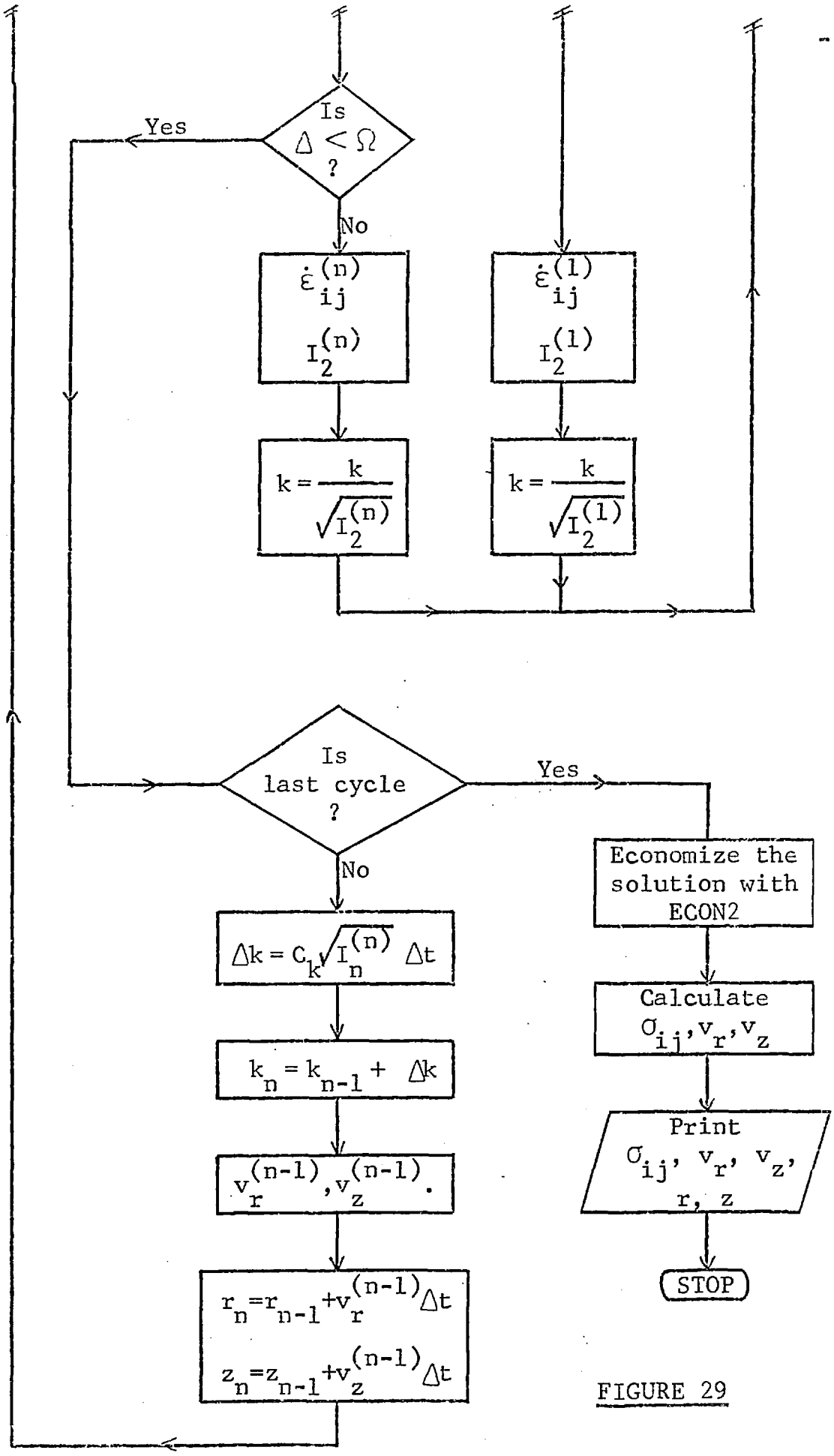
Is
$\Delta < \Omega$
?
Yes
No
$\dot{\varepsilon}_{ij}^{(n)}$
$I_2^{(n)}$
$\dot{\varepsilon}_{ij}^{(1)}$
$I_2^{(1)}$
$k = \frac{k}{\sqrt{I_2^{(n)}}}$
$k = \frac{k}{\sqrt{I_2^{(1)}}}$
Is
last cycle
?
Yes
No
Economize the solution with ECON2
Calculate
σ_{ij}, v_r, v_z
Print
σ_{ij}, v_r, v_z,
r, z
STOP
$\Delta k = C_k \sqrt{I_n^{(n)}}\ \Delta t$
$k_n = k_{n-1} + \Delta k$
$v_r^{(n-1)}, v_z^{(n-1)}$
$r_n = r_{n-1} + v_r^{(n-1)} \Delta t$
$z_n = z_{n-1} + v_z^{(n-1)} \Delta t$

FIGURE 29

If the hypothesis of linear hardening is not satisfactory, equation (181) must be used in order to calculate Δk, by means of the corresponding value of H in each step, as shown in Fig. 28.

As was pointed out before, the procedure continues until the total time of deformation is covered.

The whole sequence of calculations is summarized in the flow chart presented in Fig. 29.

VII.5 Economization of the solutions

Once the polynomial expressions for the different fields have been obtained, we next proceed to economize them in order to reduce the incidence of high powers and rounding errors. With this purpose, we use a procedure presented as a computing subroutine, described as follows:

VII.5.1 Description of the subroutine

In the first part of the subroutine the polynomial P is rearranged in terms of Chebyshev polynomials and P^T is generated.

In the second part a search is made for the special term $a^T_{ij} = a^*$ for which the number of elements in a set π_a^* is maximum; an element $a^T_{ij} \in \pi_a^*$ if

$$\left|a^{T}_{ij}\right| \leqslant \left|a^{*}\right| \qquad \text{and} \qquad \sum \left|a^{T}_{ij}\right| \leqslant \varepsilon$$

ε being the permissible error bound read in the main programme.

If the polynomial P(x,y) comes from the truncation of a convergent power series expansion, as is often the case, this part of the subroutine will tend to select the terms of higher orders and then reduce the total number of multiplications. A FORTRAN list of the subroutine is presented in Fig. 30 with the name ECON2.

VII.5.2 Data for the subroutine

The coefficients a_{ij} of the polynomial P are supplied in array DYX. The subroutine reads the elements of the matrix transforming powers of x and y in Chebyshev expansions and its inverse matrix, from the main programme, in the form of arrays DX and DT.

When the subroutine is called, the parameters

(i) ND = dimension of arrays,

(ii) NT = highest exponent in P plus 1,

(iii) ERRMAX = permissible error bound ε,

must be fixed in its argument.

VII.5.3 Output of the subroutine

The subroutine commands the following printout:

```
      SUBROUTINE  ECON2
     1           (ND,NT,NC,ERRMAX,ERRTOT,DX,DT,DYX,FCT,FCX)
C
C     ECONOMIZATION OF A POLYNOMIAL IN TWO VARIABLES
C
C     ----------------------------------------------
C
C     ND - DIMENSION OF ARRAYS
C     NT - HIGHEST EXPONENT IN THE EXPRESSION +1
C     NC - NUMBER OF TERMS IGNORED FROM CHEBYSHEV EXPANSION
C     ERRMAX - PERMISSIBLE MAXIMUM ERROR
C     ERRTOT - ACTUAL TOTAL ERROR
C     DYX - ARRAY CONTAINING GIVEN EXPRESSION
C           DYX(1,N)   (X**0)(Y**0)  (X**0)(Y**1) ...
C           DYX(2,N)   (X**1)(Y**0)  (X**1)(Y**1) ...
C           ...
C     DX - CONTAINS COEFFICIENTS OF VARIABLES IN CHEBYSHEV
C          POLYNOMIALS
C     DT - CONTAINS INVERSE OF DX
C     FCT - CONTAINS CHEBYSHEV EXPANSION
C     FCX - CONTAINS ECONOMIZED EXPRESSION
C           IN THE SAME SEQUENCE AS DYX
C     ALL PARAMETERS EXCEPT NC,ERRTOT,FCT,AND FCX SHOULD BE
C     SUPPLIED IN THE MAIN PROGRAMME
C
C
C
C
      DIMENSION FCT(ND,ND),FCX(ND,ND),DYX(ND,ND),DT(ND,ND)
     1   ,  DX(ND,ND)
      DOUBLE PRECISION DT,FCX,FCT,A,ERRMAX,ERR,AERR,BERR
     1, ERRTOT,ERRTN,ERRN
C     COMPUTE CHEBYSHEV EXPANSION
      DO 100  I= 1,NT
      DO 100  J= 1,NT
  100 FCT(I,J)= 0.0
      DO 101 I= 1,NT
      DO 101 J= 1,NT
      A= DYX(I,J)
      IF( A .EQ. 0.0 ) GO TO 101
      DO 102 N=1,I
      DO 102 M= 1,J
      FCT(N,M) = FCT(N,M) + DT(I,N) * DT(J,M) * A
  102 CONTINUE
  101 CONTINUE
      ERRN = 0.0
      NCN= 0
      DO 103 I= 1,NT
      DO 103 J= 1,NT
      ERR= DABS(FCT(I,J))
      ERRTOT = 0.0
      NC= 0
      DO 115 II= 1,NT
      DO 115 IJ= 1,NT
      A = FCT (II,IJ)
      IF(DABS(A) . GT. ERR) GO TO 115
      ERRTOT = ERRTOT + DABS(A)
      NC = NC + 1
  115 CONTINUE
      IF(ERRTOT .GT.ERRMAX) GO TO 103
      IF(NC . LE . NCN) GO TO 103
      NCN = NC
      ERRN = ERR
  103 CONTINUE
C     COMPUTE ECONOMIZED EXPRESSION
      ERRTOT = 0.0
      NC = 0
      ERR= ERRN
      DO 113 I = 1,NT
      DO 113 J = 1,NT
  113 FCX(I,J) = 0.0
      DO 106 I = 1,NT
      DO 106 J = 1,NT
      A= FCT(I,J)
      IF(DABS(A) . LE. ERR) GOTO 109
      DO 107  N= 1,I
      DO 107 M= 1,J
      FCX(N,M)= FCX(N,M) + DX(I,N)*DX(J,M)*A
  107 CONTINUE
      GOTO 106
  109 NC = NC + 1
      ERRTOT = ERRTOT + DABS(A)
  106 CONTINUE
      RETURN
      END
```

FIGURE 30

(i) ERRTOT = total error in P,

(ii) NC = number of terms either deleted or zero in the Chebyshev expansion of P,

(iii) CFT = Chebyshev expansion of P,

(iv) FCX = double array with the coefficients of the economized polynomial P .

VII.5.4 Test results

As an example, the first 36 terms of the power series expansion of exp(x + y) are considered:

$$P(x,y) = 1 + x + y + \tfrac{1}{2}(x^2 + 2xy + y^2) + (x^3 + 3x^2y + 3xy^2 + y^3)/6 + (x^4 + 4x^3y + 6x^2y^2 + 4xy^3 + y^4)/24 + (x^5 + 5x^4y + 10x^3y^2 + 10x^2y^3 + 5xy^4 + y^5)/120 + (x^6 + 6x^5y + 15x^4y^2 + 20x^3y^3 + 15x^2y^4 + 6xy^5 + y^6)/720 + (x^7 + 7x^6y + 21x^5y^2 + 35x^4y^3 + 35x^3y^4 + 21x^2y^5 + 7xy^6 + y^7)/5040.$$

After being economized, the polynomial with an error bound ε equal to 0.005, the expression

$$P_\varepsilon(x,y) = 1.000 + 0.995(x+y) + 0.125xy + 0.466(x^2+y^2) + 0.042(x^2y+xy^2) + 0.687x^2y^2 + 0.254(x^3+y^3) + 0.46(x^3y+xy^3)$$

is obtained, with only 13 terms. Figures were rounded to 3D and the economy is 23 terms.

Table II shows the values of the percentage relative error:

	1	1/9	2/9	3/9	4/9	5/9	6/9	7/9	8/9	1
0	-5.6462	2.5206	10.6247	15.0569	14.9159	11.1076	5.6596	1.2086	0.6233	6.7361
1/9	2.5206	-7.0368	-6.9042	-4.3099	-2.8183	-3.4360	-5.4648	-7.1500	-6.1655	0.0297
2/9	10.6247	-6.9042	-9.8091	-7.3399	-4.5243	-3.3977	-3.9560	-4.8846	-4.1079	0.8031
3/9	15.0569	-4.3099	-7.3399	-4.1589	-0.4093	1.4588	1.1870	-0.0598	-0.2747	2.9612
4/9	14.9159	-2.8183	-4.5243	-0.4093	3.8468	5.7882	5.1074	3.1848	1.8718	3.6851
5/9	11.1076	-3.4360	-3.3977	1.4588	5.7882	7.3807	6.1680	3.4615	1.3774	2.4114
6/9	5.6596	-5.4648	-3.9560	1.1870	5.1704	6.1680	4.3653	1.2272	-1.0511	0.0485
7/9	1.2086	-7.1500	-4.8846	-0.0598	3.1848	3.4615	1.2272	-1.9059	-3.6891	-1.6151
8/9	0.6233	-6.1655	-4.1079	-0.2747	1.8718	1.3774	-1.0511	-3.6891	-4.2729	-0.3500
1	6.7361	0.0297	0.8031	2.9612	3.6851	2.4114	0.0485	-1.6151	-0.3500	6.1969

TABLE II: The values of $\rho(\%)$ are multiplied by 100.

$$\rho(\%) = \frac{P(x,y) - P_{\varepsilon}(x,y)}{P(x,y)} 100$$

calculated in 100 equidistant points of the square Q:(1,1). In no entry of the table the error exceeds 0.151%.

Some results related to the evaluation of numerical solutions of partial differential equations will be considered further on.

VIII. ANALYSIS OF THE HYDROSTATIC EXTRUSION-DRAWING OF A COMPOSITE WIRE BY THE METHOD OF WEIGHTED RESIDUALS

VIII.1 Introduction

The procedure described in the preceding Section is now being used to calculate the stress field developed in the deforming zone during the extrusion of a composite wire constituted by two different metals. From the stress field required for having plastic deformation under steady state conditions, values for the "pulling stress-hydrostatic pressure" relationship for different extrusion ratios are obtained. These values allow a direct comparison with the experimental ones. The geometric characteristics of the specimen are as described in Chapter III.

It is assumed that the pattern of deformation follows Avitzur velocity field. It is also assumed that no relative movement between both metals exists on the interface and, hence, the interface is considered as the superposition of the limit surfaces of both metals.

During the process of calculation, mesh points are considered with the physical constants of the corresponding metal, according to its position in the wire.

A mesh point located on the interface is taken into account twice: first as belonging to one metal and then to the other, and finally, the value attributed to that point is the

average of both situations.

A rigid-plastic model with a linear rule of hardening is assumed for both metals. As the elastic strains are neglected, the plastic strains coincide with the total strains.

VIII.2 Velocity field and stream function

Avitzur's velocity field is described in a cylindrical coordinate system by the stream function:

$$\psi = - v_f R_f^2 \frac{z^2 - r^2}{4(r^2+z^2)} \tag{185}$$

which gives, according to expression (23), the following velocity equations:

$$v_r = - v_f R_f^2 \frac{rz}{(r^2+z^2)^2} \tag{186.a}$$

$$v_z = - v_f R_f^2 \frac{z^2}{(r^2+z^2)^2} \tag{186.b}$$

and the strain rate field:

$$\dot{\varepsilon}_r = - v_f R_f^2 \frac{z^2-3r^2z}{(r^2+z^2)^2} \tag{187.a}$$

$$\dot{\varepsilon}_\theta = - v_f R_f^2 \frac{z}{(r^2+z^2)^2} \tag{187.b}$$

$$\dot{\varepsilon}_z = - 2 v_f R_f^2 \frac{r^2z - z^3}{(r^2+z^2)^3} \tag{187.c}$$

$$\dot{\varepsilon}_{rz} = - \tfrac{1}{2} v_f R_f^2 \frac{r^3 - 7rz^2}{(r^2+z^2)^3} \tag{187.d}$$

The corresponding second principal deviatoric invariant is then calculated by means of:

$$I_2 = -(\dot{\varepsilon}'_r\dot{\varepsilon}'_\theta + \dot{\varepsilon}'_\theta\dot{\varepsilon}'_z + \dot{\varepsilon}'_z\dot{\varepsilon}'_r) + \dot{\varepsilon}'^2_{rz} \qquad (188)$$

VIII.3 Stress field

For the description of an axisymmetric stress field, two stress functions are required. Let us propose the following polynomial forms as trial functions:

$$\phi_1(r,z) = \frac{\sqrt{3}}{6} k r^3 + P^3 \sum_i \sum_j A_{ij}\, r^{2i+3}\, z^j \qquad (189.a)$$

$$\phi_2(r,z) = P^2 \sum_m \sum_n B_{mn}\, r^{2m+1}\, z^n \qquad (189.b)$$

where $P = R_i^2 - r^2 - z^2$, A_{ij} and B_{mn} are parameters to be determined and k the shear yield stress corresponding to a generical material point.

From these stress functions, according to expressions (11), the trial functions corresponding to the stress field are obtained as follows:

$$\sigma_\theta = \sum_m \sum_n B_{mn} z^n r^{2m} \left[-4Pr^2 + (2m+1)P^2\right] \qquad (190.a)$$

$$\sigma_z = \sqrt{3}\, k + \sum_i \sum_j A_{ij} P z^j r^{2i} \left[24r^4 - 6(4i+z)Pr^2 + (2i+3)(2i+2)P^2\right] \qquad (190.b)$$

$$\sigma_r = \sum_i \sum_j A_{ij} r^{2i+2} z^{j-z} P \left[24z^4 - 6Pz^2(2j+1) + j(j+1)P^2\right]$$

$$+ \sum_m \sum_n B_{mn} r^{2m} z^n \qquad (190.c)$$

$$\tau_{rz} = \sum_i \sum_j A_{ij} r^{2i+1} z^{j-1} P \left[-24r^2z^2 + 6jPr^2 + 6(2i+3)Pz^2\right.$$

$$\left. - j(2i+3)P^2\right] \qquad - \qquad (190.d)$$

The ϕ_1 and ϕ_2 expressions have been chosen in such a way as to have a general polynomial form and, at the same time, allow the stress field to accomplish the following boundary conditions for any set of values of their free parameters:

(i) For mesh points on the entry boundary (P = 0) belonging to the core or the sleeve:

$$\sigma_z = \sqrt{3}k$$

$$\sigma_r = \sigma_\theta = \tau_{rz} = 0$$

These are the conditions required for having plastic flow under the particular state of stresses existing on that surface.

(ii) For mesh points on the z-axis (r = 0), conditions of axisymmetry require:

$$\sigma_z = f(z)$$

$$\tau_{rz} = \sigma_\theta = \sigma_r = 0$$

where f(z) is the expression of $\sigma_z(r,z)$ for r = 0.

(iii) The axial symmetry condition also requires that the functions σ_r, σ_θ and σ_z be even in the r variable, while τ_{rz}

be odd in this variable.

VIII.4 Boundary condition on the tube-die interface

The conical surface corresponding to the tube-die interface may be characterized as follows:

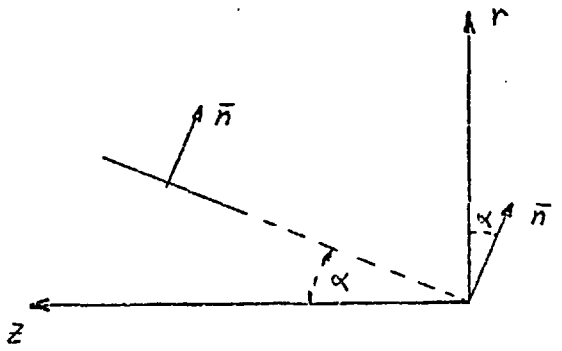

where α is the semi-angle of the die and $\bar{n}$ a normal vector given by:

$$\bar{n} = (\cos\alpha,\ 0, -\sin\alpha)$$

The stress components at a generical point on that surface are:

$$S_i = \sigma_{ij}\, n_j$$

and in this particular case:

$$S_r = \sigma_r \cos\alpha - \tau_{rz} \sin\alpha$$

$$S_\theta = 0$$

$$S_z = \tau_{rz} \cos\alpha - \sigma_z \sin\alpha$$

The stress component tangent to that surface is:

$$\tau_{\alpha} = \frac{\sigma_r - \sigma_z}{2} \sin 2\alpha + \tau_{rz} \cos 2\alpha \qquad (191)$$

The frictional stress at the interface may be expressed in terms of a fraction of the shear yield stress of the tube, i.e.

$$\tau_{\alpha} = q\, k^t \qquad (192)$$

q being $0 \leqslant q \leqslant 1$.

Substituting expression (191) into (192), the equation conditions stresses on the boundary

$$\frac{\sigma_r - \sigma_z}{2} \sin 2\alpha + \tau_{rz} \cos 2\alpha = q\, k^t \qquad (193)$$

is obtained.

VIII.5 The error functions

By substituting expressions (187), (188) and (190) into Prandtl-Reuss's equation, the following error functions are obtained:

$$R_{1n} = \sigma_r - \sigma_m - \frac{k}{\sqrt{I_2}} \dot{\varepsilon}_r \qquad (194.a)$$

$$R_{2n} = \sigma_\theta - \sigma_m - \frac{k}{\sqrt{I_2}} \dot{\varepsilon}_\theta \qquad (194.b)$$

$$R_{3n} = \tau_{rz} - \frac{k}{\sqrt{I_2}} \varepsilon_{rz} \qquad (194.c)$$

n representing a generical node point and $\sigma_m = \frac{1}{3}(\sigma_r + \sigma_\theta + \sigma_z)$.

The expression corresponding to σ_z does not appear to constancy of volume, since

$$\sigma_z = -(\sigma_r + \sigma_\theta)$$

Another error function is obtained from the boundary condition at the tube-die interface:

$$R_{4n} = \frac{\sigma_r - \sigma_z}{2} \sin 2\alpha + \tau_{rz} \cos 2\alpha - q\, k^t \qquad (195)$$

where σ_z, σ_r and τ_{rz} are to be substituted by expressions (190.b), (190.c) and (190.d) respectively.

Equations (194.a) are to be calculated in the whole deformed volume while equation (195) is to be considered only at the tube-die interface.

These four error functions are to be joined together in a general error function R_n, as a linear combination of them with weighting factors:

$$R_n = g_1 R_{1n} + g_2 R_{2n} + g_3 R_{3n} + g_4 R_{4n} \qquad (196)$$

In this case is $g_1 = g_2 = g_3$ and, hence:

$$R_n = g_1 (R_{1n} + R_{2n} + R_{3n}) + g_4 R_{4n} \qquad (197)$$

The values of g_4 and g_1 are adopted proportional to the number of nodal points existing at the interface and in

the whole deforming zone respectively. In the process of calculation, expression R_{4n} is taken into account only at the interface nodal points.

After all substitutions have been made, an expression of R_n in terms of the coordinates and free parameters A_{ij} and B_{mn} is obtained:

$$R_n = R_n(r, z, A_{ij}, B_{mn})$$

This expression of the total error function is to be squared and minimized with respect to the free parameters, in the volume of the deforming zone. The corresponding sequence of calculations will be programmed by using a least squares approach, in the frame of the method of weighted residuals, as was already described.

VIII.6 Process of deformation

Based on Avitzur's velocity field, the mesh adopted for representing the deforming zone under steady state condition is shown in Fig. 31.

According to this pattern of deformation, it is assumed that the final hardening of the specimen is achieved in eight steps, that is, hardening takes place only when the material reaches a spherical surface and no strain hardening occurs in between them.

FIGURE 31

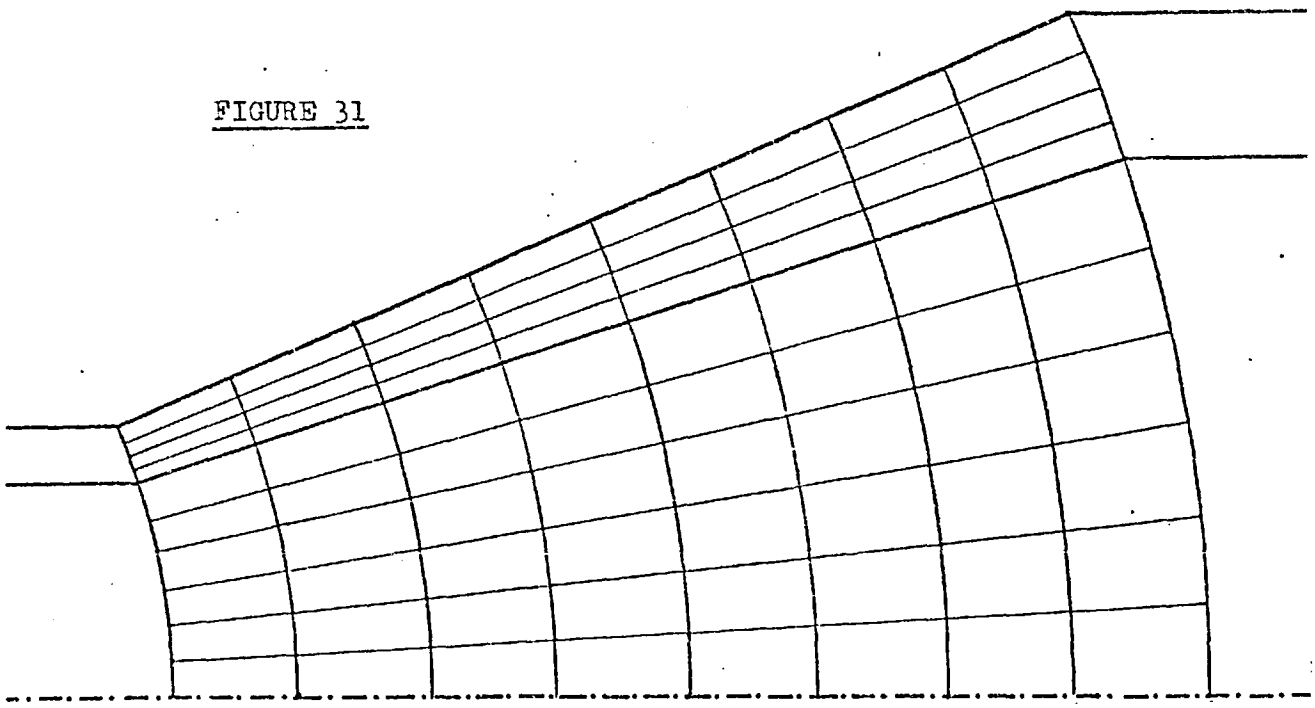

Assuming a linear rule of hardening, it is possible to calculate the shear yield stress of the metals at each point by means of the expression:

$$k = k_o + C_k \sqrt{I_2(r,z)}\ \Delta t \qquad (198)$$

where k_o is the initial shear yield stress, C_k is a constant defined in equation (182) and Δt the time increment. The material moves from the entry boundary I towards the exit boundary IX, crossing nine equidistant spherical surfaces, with a velocity field given by equation (187).

Adopting an axial velocity V_E for the specimen at the exit and the geometrical dimensions of the die, the time increment Δt required for the material to move from one surface

to the next can be obtained for each nodal point by means of the expression:

$$\Delta t_j(r,z) = \left[\frac{(r_j - r_{j-1})^2 + (z_j - z_{j-1})^2}{v_{r_j}^2 + v_{z_j}^2}\right]^{\frac{1}{2}} \qquad (199)$$

VIII.7 Pulling stress-hydrostatic pressure relationship

The numerical procedure described so far provides a description of the stress components required for having plastic flow at each point of the deforming zone.

Particularly we obtain the axial stress components at the entry and exit boundaries. Let them be expressed by functions $\sigma_z^{(I)}$ and $\sigma_z^{(II)}$ respectively, according to the following diagram:

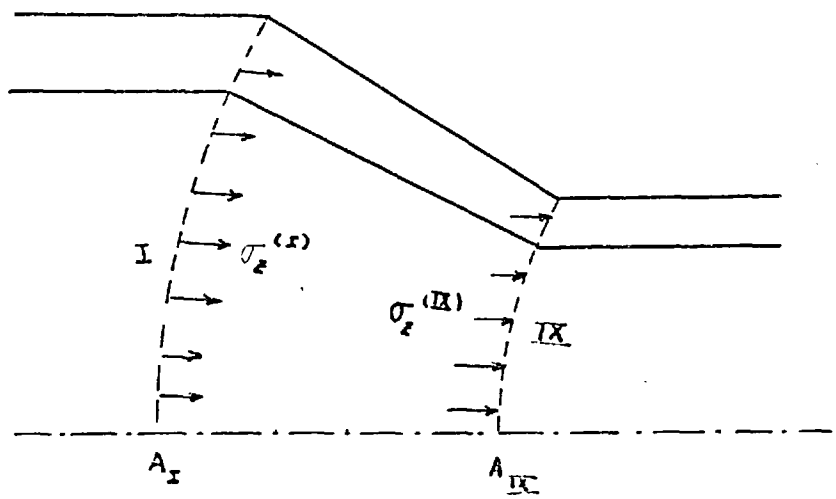

The average stress acting on each boundary is given by:

$$\sigma_I = \frac{1}{A_I}\iint_{A_I} \sigma_z^{(I)}\, r\, dr\, d\theta$$

and

$$\sigma_{II} = \frac{1}{A_{II}} \iint_{A_{II}} \sigma_z^{(II)} \, r \, dr \, d\theta$$

respectively, where A_I and A_{II} are the cross sectional areas. In practice, stress σ_I is provided by the hydrostatic pressure p_h while σ_{II} by the pulling stress σ_p. Hence, the driving stress may be expressed as:

$$\sigma_p + p_h = \frac{1}{A_I} \iint_{A_I} \sigma_z^{(I)} \, r \, dr \, d\theta + \frac{1}{A_{II}} \iint_{A_{II}} \sigma_z^{(II)} \, r \, dr \, d\theta$$

These integrals are evaluated numerically as follows:

$$\sigma_I = \frac{1}{r_I^2} \iint_{A_I} \sigma_z^{(I)} \, r \, dr \, d\theta = \frac{2}{r_I^2} \int_0^{r_I} \sigma_z^{(I)} \, r \, dr$$

with a discrete approach:

$$\sigma_I \cong \frac{2}{r_I^2} \sum_{j=1}^{N} (\sigma_z^{(I)} . r)_j \left(\frac{r_{j+1} - r_{j-1}}{2} \right)$$

or

$$\sigma_I \cong \frac{1}{r_I^2} \sum_{j=1}^{N} (\sigma_z^{(I)} . r)_j \, (r_{j+1} - r_{j-1}) \qquad (200)$$

and, similarly:

$$\sigma_{II} = \frac{1}{r_{II}^2} \sum_{j=1}^{N} (\sigma_z^{(II)} . r)_j \, (r_{j+1} - r_{j-1}) \qquad (201)$$

Finally, the driving stress is given by:

$$\sigma_p + p_h = \sigma_I + \sigma_{II} \qquad (202)$$

The values of σ_I and σ_{II} depend upon materials

involved, conditions of friction, deformation velocities, extrusion ratio, etc. If all parameters except the extrusion ratio are kept constant, equation (202) can be expressed as a function φ of this parameter:

$$\sigma_p + p_h = \varphi(R) \qquad (203)$$

This equation allows a direct comparison with the experimental values.

VIII.8 Temperature distribution

VIII.8.1 Introduction

The steady state temperature distribution developed during the process of deformation is now considered by using the method of weighted residuals.

It is assumed that heat is generated at nodal points, due to the plastic work involved in the process of deformation already described and at the tube-die interface, due to friction. It is also assumed that work is entirely converted into heat.

Both metals are considered isotropic and homogeneous, from the thermal point of view.

VIII.8.2 Theoretical considerations [110], [111]

Let us define in a material medium a spatial velocity

field $\bar{v} = \bar{v}(x,y,z)$, referred to some particular coordinate system of reference:

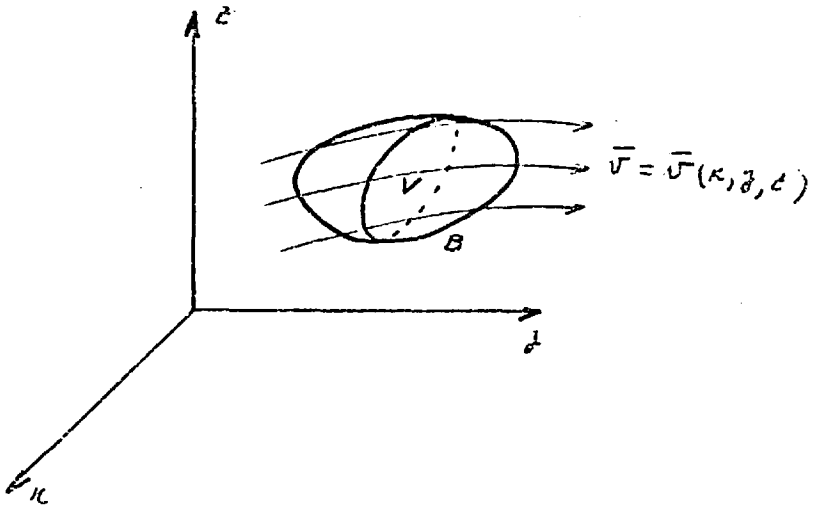

Let us pay attention to a particular volume $V(x,y,z)$ limited by a surface $B(x,y,z)$ and fixed with respect to the frame of reference. It is assumed the existence at any point of this volume of a source of heat characterized by the function $h_v(x,y,z,t)$, the amount of heat generated per unit volume. The amount of heat produced at points on the surface B is measured by the function $h_s(x,y,z,t)$, where h_s is the heat produced per unit area.

As a consequence of these sources of heat, a temperature field $T(x,y,z,t)$ is obtained, which we aim to describe.

It is an experimental fact that the amount of heat accumulated in V at a given time may be expressed as:

$$H = \iiint_V \vartheta c\, T\, dV \qquad (204)$$

where ϑ represents the density of the medium and c its specific heat. The time derivative of expression (204) is:

$$\frac{dH}{dt} = \frac{d}{dt} \iiint_V \vartheta c\, T\, dV = \iiint_V \vartheta c \left(\frac{\partial T}{\partial t} + \bar{v} \times \text{grad} T\right) dV \qquad (205)$$

The heat transferred by conduction through the surface B, per unit area and unit time in the n-direction, is proportional to the temperature gradient in this direction:

$$\frac{d^2 H_1}{ds\,dt} = k_n \frac{\partial T}{\partial t} \qquad (206)$$

where k_n is the thermal conductivity of the medium in the n-direction. If the material is thermally isotropic, k_n has the same value for any direction, say k. Hence, expression

$$\frac{d^2 H_1}{dt} = k \frac{\partial T}{\partial n} dS = k \nabla T \times \overline{dS} \qquad (207)$$

is obtained.

By integration of expression (207) over the whole boundary surface B, the expression

$$\frac{dH_1}{dt} = \iint_B (k \nabla T) . \overline{dS} \qquad (208)$$

is obtained. On the other hand, the amount of heat generated per unit time within V and its boundary surface is:

$$\frac{dH_2}{dt} = \iiint_V \dot{h}_v dV + \iint_B \dot{h}_s ds \qquad (209)$$

where $\dot{h}_v = \frac{\partial h_v}{\partial t}$ and $\dot{h}_s = \frac{\partial h_s}{\partial t}$, h_v being the amount of heat generated per unit volume and h_s the heat generated per unit area. Adding expressions (208) and (209), the total rate of change of the heat in V is obtained:

$$\frac{dH}{dt} = \iint_B (k\nabla T) \times \bar{dS} + \iiint_V \dot{h}_v dV + \iint_B \dot{h}_s dS \qquad (210)$$

Assuming a flux vector as:

$$\dot{\bar{h}}_s = \bar{n}\dot{h}_s$$

$\bar{n}$ being the unit normal vector to the surface element dS. The last term of expression (210) rewrites as:

$$\iint_B \dot{h}_s dS = \iint_B \dot{h}_s dS(\bar{n} \times \bar{n}) = \iint_B \dot{\bar{h}}_s \times d\bar{S} \qquad (211)$$

By substituting expression (211) into (210) we get:

$$\frac{dH}{dt} = \iint_B (k\nabla T) \times d\bar{S} + \iint_V \dot{h}_v dV + \iint_B \dot{\bar{h}}_s = d\bar{S}$$

which, by means of Gauss's theorem may be transformed into:

$$\frac{dH}{dt} = \iiint_V \left[\mathrm{div}(k\nabla T) + \dot{h}_v + \mathrm{div}\,\dot{\bar{h}}_s\right] dV \qquad (212)$$

According to the conservation of energy principle, equations (205) and (212) may be equated and hence:

$$\iiint_V \vartheta c \left[\frac{\partial T}{\partial t} + \bar{v} \times \mathrm{grad} T\right] dV = \iiint_V \left[k\nabla^2 T + \dot{h}_v + \mathrm{div}\,\dot{\bar{h}}_s\right] dV$$

(213)

As equation (213) must hold for any volume V, expression

$$\vartheta c \left[\frac{\partial T}{\partial t} + \bar{v} \times \text{grad} T\right] = k \nabla^2 T + \dot{h}_v + \text{div}\, \dot{\bar{h}}_s \qquad (214)$$

is obtained.

If only the steady state is to be considered, equation (214) becomes:

$$\nabla^2 T - \beta(v \times \text{grad} T) = - \frac{1}{k}(\dot{h}_v + \text{div}\, \dot{\bar{h}}_s) \qquad (215)$$

where $\beta = \frac{\vartheta c}{k}$.

Under conditions of axial symmetry and referred to a cylindrical system of coordinates, expression (215) is written as:

$$\frac{\partial^2 T}{\partial r^2} + \frac{\partial^2 T}{\partial z^2} + (\frac{1}{r} - \beta v_r)\frac{\partial T}{\partial r} - \beta v_z \frac{\partial T}{\partial z} = - \frac{1}{k}\left[\dot{h}_v + \frac{\partial(\dot{\bar{h}}_s)_r}{\partial r} + \frac{(\dot{\bar{h}}_s)_r}{r} + \frac{\partial(\dot{\bar{h}}_s)_z}{\partial z}\right] \qquad (216)$$

which is the equation to be integrated for this case.

VIII.8.3 Proposed estimates and error functions

In order to calculate the temperature distribution in the deforming zone of a composite wire, it is adopted the geometry shown in Fig. 32, which includes the die.

The value of $\dot{h}_v$ corresponding to each nodal point is

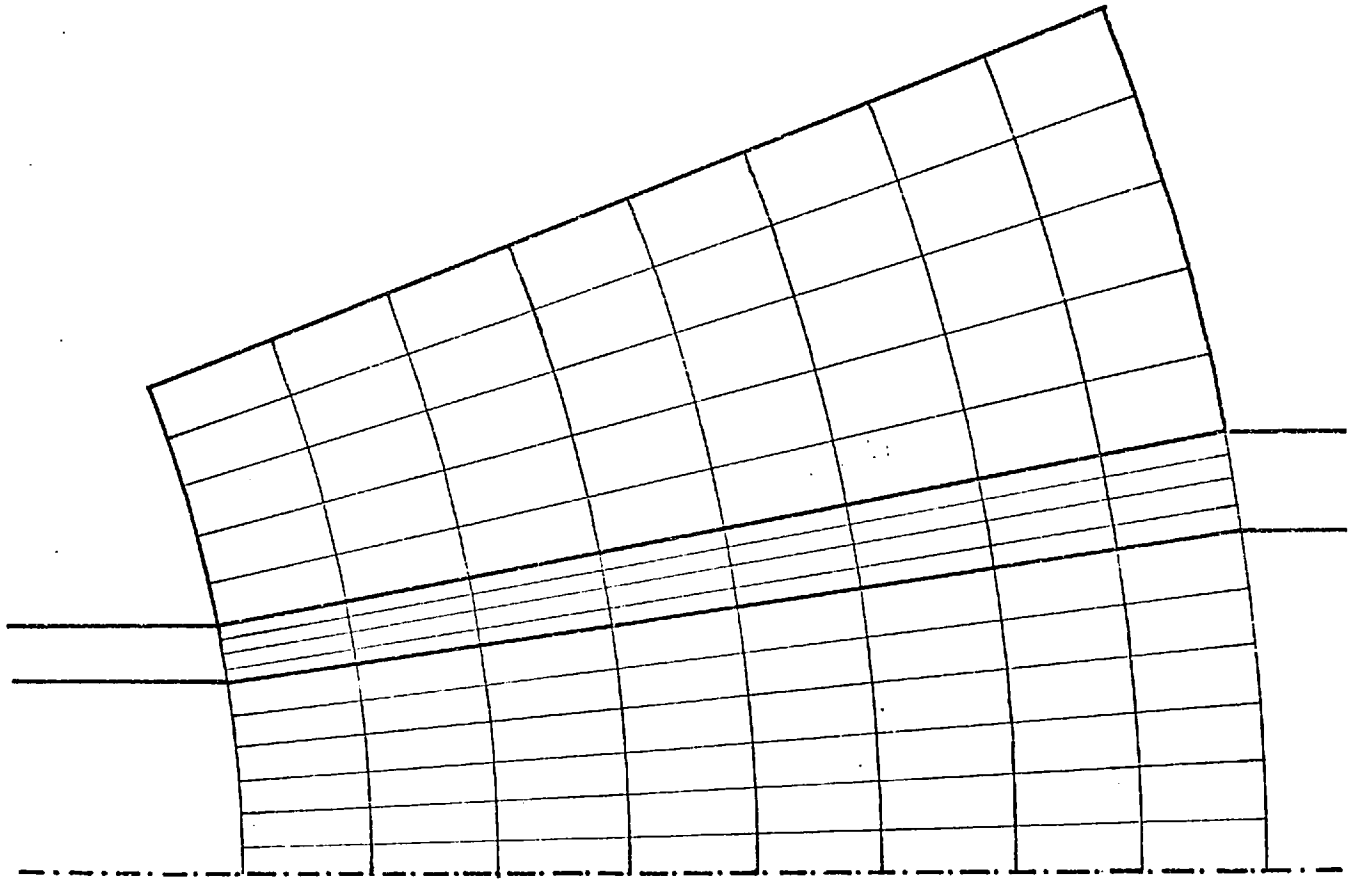

FIGURE 32

calculated assuming that all plastic work involved in the process is converted into heat and, consequently, its expression is given by:

$$\dot{h}_v = \sigma'_{ij}\,\dot{\varepsilon}_{ij}$$

where tensors σ'_{ij} and $\dot{\varepsilon}_{ij}$ have already been obtained. The expression for the heat generated on the tube-die interface due to friction is:

$$\dot{h}_s = \tau_\alpha v_\alpha$$

where τ_α is the shear stress at the tube-die interface and v the velocity corresponding to points on that surface. These values are assumed as being given by the expressions:

$$\tau_\alpha = q\,k^t$$

$$v_\alpha = V_E\,R_E^2\,\frac{\cos\alpha}{(r^2+z^2)}$$

and, hence, for that surface the expression for $\dot{h}_s$

$$\dot{h}_s = V_E R_E q k^t\,\frac{\cos\alpha}{r^2+z^2}\,(\cos\alpha\,,\ 0,\ -\sin\alpha) \qquad (217)$$

is obtained.

The boundary conditions to be considered in the process of integration are as follows:

(i) On surfaces I and II: $T = T_o$ (room temperature).

(ii) On surface III $\frac{\partial T}{\partial z} = 0$. It implies no variation of temperature immediately after leaving the boundary of the deforming zone.

(iii) Due to symmetry, at all points of the z-axis (r = 0) is $\frac{\partial T}{\partial r} = 0$ and also $T = f(z)$.

The proposed trial family for this problem is chosen as:

$$T = T_o + (R_I^2 - r^2 - z^2)(z.\tan\alpha_E - r) \sum_{i=0}^{N} \sum_{j=1}^{M} r^{2i} z^j$$

or, in another form:

$$T = T_o + P.L \sum_{i=0}^{N} \sum_{j=1}^{M} D_{ij} r^{2i} z^j \qquad (219)$$

where $P = R_I^2 - r^2 - z^2$ and $L = z \tan\alpha_E - r = z.a - r$.

Factors P and L ensure the fulfillment of condition (i). It can be shown that condition (iii) is automatically satisfied while condition (ii) needs to be taken into account through an error function.

By substituting expression (218) into the governing equation (216), the following error function arises:

$$R_{ln} = \sum_{i} \sum_{j} D_{ij} r^{2i-z} \left[(2i-1)z^2(-2r^2L-Pr+ziPL)+z^2r(-4rL \right.$$
$$+4r^2-P-4irL-2iP)+r^2(j-1)(-2z^2L+aPz+jPL)$$
$$+r^2z(-4zL-4az+aP+jaP-zjzL)+(\frac{1}{r}-\beta v_r)z^2r(-zr^2L$$
$$\left. -Pr+2iPL)+\beta v_z r^2 z(-2z^2L+aPz+jPL) \right] + \frac{1}{k}\left[\dot{h}_v + \mathrm{div}\dot{h}_s \right]$$

(219)

In this expression, the values of the physical constants for each point are properly selected during the computing process. For simplicity sake the same values are assigned for the die and the stainless steel core since they are quite similar.

For points on the tube-die interface, the expression

$$\operatorname{div} \dot{\bar{h}}_s = V_E R_E^2 q k^t \cos \left(-\frac{2r\cos\alpha}{(r^2+z^2)^2} + \frac{\cos\alpha}{r(r^2+z^2)} + \frac{2z\sin\alpha}{(r^2+z^2)^2}\right) \tag{220}$$

is obtained, which must vanish for any other point.

The boundary condition (ii) gives birth to the second error function:

$$R_{2n} = \sum_i \sum_j D_{ij} r^{2i} z^{j-1} (-2z^2 L + aPz + jPL) - 0.0 \tag{221}$$

The total error function is:

$$R_n = g_1 R_{1n} + g_2 R_{2n} \tag{222}$$

g_1 and g_2 being weighting factors proportional to the involved nodal points respectively. This error function is to be squared, computed at all points, and minimized through the least squares criterion.

VIII.9 Description of the computing programme

The process of calculation is programmed in FORTRAN IV language, for the C.D.C. 6400 computer of the Imperial College.

For simplicity sake the programme is designed with a Main Programme and three subroutines performing the following operations:

Subroutine MESH:

It generates the coordinates of the nodal points selected in the composite wire for the analysis of stress and also, in the die, for the analysis of temperatures.

Subroutine STRESS:

It calculates the stress distribution, according to the method of weighted residuals already described.

Subroutine TEMPD:

It determines the temperature distribution which arises from the stress and strain rates previously calculated.

The calculations are performed for different extrusion ratios.

After the polynomial solutions are obtained, they are economized by means of the subroutine ECON2, already described.

The detailed sequence of operations performed during

the process by each subroutine can be seen in the corresponding flow charts and listings.

VIII.9.1 Main Programme

The Main Programme reads the data related to the physical and geometrical characteristics of the problem, which are expressed as FORTRAN variables with the following names:

Input Data:

Number of error functions (stress)	NERRFN
Maximum power in R (stress 1)	NTERM1
Maximum power in z (stress 2)	NTERN2
Number of variables (stress)	NVAR
Number of error functions (temperature)	NERFT
Maximum power in R (temperature 1)	NTERM3
Maximum power in z (temperature 2)	NTERM4
Number of variables (temperature)	NVART
Number of total nodes	NDNODE
Number of nodes in billet	NNODE
Number of nodes in the core	NFNODE
Number of nodes in the interface	NCNODE
Number of divisions of angle (core)	NADIVC
Number of divisions of angle (tube)	NADIVT
Number of divisions of angle (die)	NADIVD
Radius at exit	RF

Radius at entry	RI
Semi-core angle	ALPHAC
Semi-die angle	ALPHA
Semi-external angle	ALPHAE
Velocity at exit	VE
Constant Q (friction)	Q
Shear yield stress of core	AK1
Shear yield stress of tube	AK2
Constant CK for the core	CK1
Constant CK for the tube	CK2
Initial temperature	TIN1
Thermal conductivity (tube)	TC1
Thermal conductivity (core)	TC2
Constant beta - 1	BETA1
Constant beta - 2	BETA2
Weighting factor - 1 (stress)	G(1)
Weighting factor - 2 (stress)	G(2)
Weighting factor - 3 (stress)	G(3)
Weighting factor - 4 (stress)	G(4)
Weighting factor - 1 (temperature)	WF(1)
Weighting factor - 2 (temperature)	WF(2)

It also performs several preliminary operations which are enumerated in the corresponding flow chart. This flow

chart is presented as Fig. 33 while the FORTRAN listing is presented as Fig. 34.

At the end of the calculations the subroutine GRAFIT is called as required to plot results. This subroutine is a standard one of the Computing Centre.

VIII.9.2 Subroutine MESH

The coordinates of the nodal points are calculated with reference to a cylindrical system of coordinates (r,z), according to the following diagram.

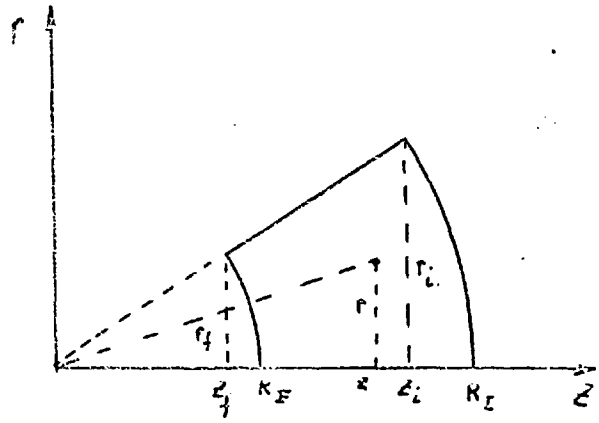

The RF coordinate defines the exit spherical surface and, consequently, the extrusion ratio. By selecting adequate values for RF, it is possible to obtain the different extrusion ratios:

$$R_F = \frac{r_i}{\sin 15^o \sqrt{R}}$$

In the case of our specimens:

$$R_F = 9.4358\ R^{-\frac{1}{2}}$$

The flow chart and the FORTRAN listing are presented as Figs. 35 and 36 respectively.

VIII.9.3 Subroutine STRESS

It performs the whole sequence of the method of weighted residuals with the numerical values for the variables read in the Main Programme and the coordinates generated in MESH. All these variables are contained in a COMMON declaration statement.

In order to solve the linear system of equations, this subroutine calls another subroutine SIMQ, which is a standard one of the IBM System Subroutine Package.

Since we are using linear expressions in the unknown parameters A_i as trial function, the arising error functions have a form like:

$$F = A_i X_i$$

which squares as:

$$F^2 = A_i A_j X_i X_j$$

The least squares method requires that the derivatives of this expression with respect to the parameters must vanish, that is:

$$\frac{\partial F^2}{\partial A_p} = \delta_{ip} A_j X_i X_j + \delta_{jp} A_i X_i X_j = A_j X_p X_j + A_i X_i X_p = 0$$

and, finally:

$$\frac{\partial F^2}{\partial A_p} = 2 A_i X_i X_p = 0$$

which is a generical equation of the system to be solved. It is interesting to point out that the coefficient matrix of the system contains the same elements $[X_i X_p]$ as in F^2, making the derivative operation unnecessary.

The corresponding flow chart and the FORTRAN listing are presented as Figs. 37 and 38 respectively.

VIII.9.4 Subroutine TEMPD

The sequence of operations performed by this subroutine is similar to the subroutine STRESS, solving the temperature distribution equation (216) as already described. The numerical data come from Main Programme through a COMMON declaration statement.

The corresponding flow chart and FORTRAN listing are presented as Figs. 39 and 40 respectively.

VIII.10 Verification of the algorithm

The temperature or stress field in the wire cannot be measured by experimental means. Consequently, in order to have a true idea about the accuracy of the numerical procedure to be used in the analysis of these fields, we consider next the

numerical solution of the elliptic equation

$$\nabla^2 f = \frac{\partial^2 f}{\partial x^2} + \frac{\partial^2 f}{\partial y^2} = -A \qquad (223)$$

with f/D = 0 and A = 2, of which solutions are very well known.

This equation corresponds to the torsion problem of Saint-Venant, discussed by Southwell [103] using relaxation methods, and by Mason [104], [105] using Chebyshev methods. A theoretical analysis of this problem is given by Knudsen and Katz [106]. That equation also describes the temperature distribution on a plane section, with a uniform source of heat all over the surface, in which case the governing equation is:

$$\nabla^2 T = -\frac{H}{k}$$

H being the source of heat. This equation is a particular case of the equation

$$\nabla^2 T - \beta(\bar{v} \times \nabla T) = -\frac{H}{k} \qquad (224)$$

to be integrated in the temperature distribution, in which the convective term is zero.

We solve equation (223) by means of the method of weighted residuals in a square section as follows:

As trial solution we use an expression of the form:

$$f(x,y) = (x-z)(y-z)\sum_{i=1}\sum_{j=1} A_{ij}x^i y^j \qquad (225)$$

valid in a square domain $D = \{0 \leqslant x \leqslant 2,\ 0 \leqslant y \leqslant 2\}$. The factors preceding the polynomial make certain that the boundary condition is fulfilled. The A_{ij} are the unknown parameters we then evaluate with a least squares approach.

For the numerical application we use a square mesh with a set of 121 equidistant points.

We start with an approximate solution of degree 6 in x (N = 6) and 6 in y (M = 6) and then economize it in the square domain $D_1 = \{0 \leqslant x \leqslant 1,\ 0 \leqslant y \leqslant 1\}$ with a permissible error bound $\varepsilon = 0.8\ 10^{-3}$, to a degree of 4 in x and 4 in y. We restrain our study to the domain D_1 because, due to symmetry, in the domain D there are four equivalent sectors as D_1.

The original polynomial solution is shown in Table III and that corresponding to the economized polynomial in Table IV.

In Table V we give values of $f(x_i,y_i)$ for x_i, y_i = 0 (0.25) 1, computed using:

a. The analytical solution (top line).

b. Our solution (middle line in brackets).

c. Chebyshev selected points solution (low line) as given in [107] rounded to 3D.

TABLE III

0.4968E+01	(X** 1)	(Y** 1)
-.1001E+02	(X** 1)	(Y** 2)
0.1356E+02	(X** 1)	(Y** 3)
-.1092E+02	(X** 1)	(Y** 4)
0.4521E+01	(X** 1)	(Y** 5)
-.7536E+00	(X** 1)	(Y** 6)
-.1001E+02	(X** 2)	(Y** 1)
0.3572E+02	(X** 2)	(Y** 2)
-.6029E+02	(X** 2)	(Y** 3)
0.5203E+02	(X** 2)	(Y** 4)
-.2218E+02	(X** 2)	(Y** 5)
0.3697E+01	(X** 2)	(Y** 6)
0.1356E+02	(X** 3)	(Y** 1)
-.6029E+02	(X** 3)	(Y** 2)
0.1089E+03	(X** 3)	(Y** 3)
-.9653E+02	(X** 3)	(Y** 4)
0.4157E+02	(X** 3)	(Y** 5)
-.6928E+01	(X** 3)	(Y** 6)
-.1092E+02	(X** 4)	(Y** 1)
0.5203E+02	(X** 4)	(Y** 2)
-.9653E+02	(X** 4)	(Y** 3)
0.6657E+02	(X** 4)	(Y** 4)
-.3746E+02	(X** 4)	(Y** 5)
0.6242E+01	(X** 4)	(Y** 6)
0.4521E+01	(X** 5)	(Y** 1)
-.2218E+02	(X** 5)	(Y** 2)
0.4157E+02	(X** 5)	(Y** 3)
-.3746E+02	(X** 5)	(Y** 4)
0.1624E+02	(X** 5)	(Y** 5)
-.2706E+01	(X** 5)	(Y** 6)
-.7536E+00	(X** 6)	(Y** 1)
0.3697E+01	(X** 6)	(Y** 2)
-.6928E+01	(X** 6)	(Y** 3)
0.6242E+01	(X** 6)	(Y** 4)
-.2706E+01	(X** 6)	(Y** 5)
0.4511E+00	(X** 6)	(Y** 6)

TABLE IV

0.1818D-04	(X** 0)	(Y** 0)
0.3843D-02	(X** 0)	(Y** 1)
-.1557D-01	(X** 0)	(Y** 2)
0.2015D-01	(X** 0)	(Y** 3)
-.8496D-02	(X** 0)	(Y** 4)
0.3843D-02	(X** 1)	(Y** 0)
0.4622D+01	(X** 1)	(Y** 1)
-.7132D+01	(X** 1)	(Y** 2)
0.6249D+01	(X** 1)	(Y** 3)
-.2291D+01	(X** 1)	(Y** 4)
-.1557D-01	(X** 2)	(Y** 0)
-.7132D+01	(X** 2)	(Y** 1)
0.1878D+02	(X** 2)	(Y** 2)
-.2081D+02	(X** 2)	(Y** 3)
0.8156D+01	(X** 2)	(Y** 4)
0.2015D-01	(X** 3)	(Y** 0)
0.6250D+01	(X** 3)	(Y** 1)
-.2081D+02	(X** 3)	(Y** 2)
0.2490D+02	(X** 3)	(Y** 3)
-.1004D+02	(X** 3)	(Y** 4)
-.8496D-02	(X** 4)	(Y** 0)
-.2291D+01	(X** 4)	(Y** 1)
0.8156D+01	(X** 4)	(Y** 2)
-.1004D+02	(X** 4)	(Y** 3)
0.4119D+01	(X** 4)	(Y** 4)

TABLE V

y = \ x =	0	0.25	0.50	0.75
0	0.589 (0.585) 0.600	0.558 (0.553) 0.562	0.459 (0.456) 0.450	0.280 (0.279) 0.262
0.25	0.558 (0.553) 0.562	0.528 (0.524) 0.530	0.436 (0.434) 0.431	0.267 (0.266) 0.258
0.50	0.459 (0.456) 0.450	0.436 (0.434) 0.431	0.362 (0.362) 0.356	0.226 (0.225) 0.234
0.75	0.279 (0.279) 0.262	0.267 (0.266) 0.258	0.225 (0.225) 0.234	0.146 (0.146) 0.163

Comparison of our solution and the one given in [107] based on Manson's extension of Lanczos's selected points method, with the analytical solution [106] (see Appendix C) being, in this case, favourable to our results.

The maximum error detected in our solution in the mesh described in [107] is 0.89% and for the Chebyshev collocation solution, 11.64%. In this case of the ε-economized solution, error estimates can be deduced from estimates on the least squares approximations (see Picone [108], Fichera [109] and Collatz [93]).

This application shows that our numerical procedure is adequate to solve this type of equation and, hence, we can confidently use it with equation (224) which governs the temperature distribution in our problem.

VIII.11 Stress fields in the composite wire

By means of the described programme, the stress and temperature distributions produced during the extrusion process of a bimetallic wire under different extrusion ratios are obtained. This means the description of the stress tensor component fields: σ_r, σ_θ, σ_z, τ_{rz}, and the temperature field. The strain hardening distribution in the wire, according to the adopted rule of hardening, is also described.

Except for the extrusion ratio all other parameters involved in the process are kept constant.

The numerical values selected for the physical and geometrical parameters which characterized the experiments carried out are as follows, in S.I. units wherever relevant.

Number of error functions (Stress)	4
Number of indices (Stress 1)	3
Number of indices (Stress 2)	3
Number of variables (Stress)	2
Number of total nodes	144
Number of nodes in billet	99
Number of nodes in the core	63
Number of nodes in the interface	9
Number of divisions of angle (core)	6
Number of divisions of angle (tube)	4
Number of divisions of angle (die)	5
Radius at exit	according to extrusion ratio
Radius at entry	.9500E-02
Semi-core angle	.2000E+00
Semi-die angle	.2600E+00
Semi-external angle	.5220E+00
Velocity at exit	.1000E-02
Constant Q (friction)	.5000E-01

Shear yield stress of core	according to extrusion ratio
Shear yield stress of tube	.2000E+09
Constant CK for the core	according to extrusion ratio
Constant CK for the tube	.3400E+08
Time increment (hardening)	.5625E+00
Weighting factor - 1 (stress)	.1000E+01
Weighting factor - 2 (stress)	.1000E+01
Weighting factor - 3 (stress)	.1000E+01
Weighting factor - 4 (stress)	.1000E+01

In Figs. 41 and 42 the experimental stress-strain curves of the two metals are shown together with the linear approximations chosen to be used in this theoretical approach. These straight lines have been chosen with a least square criterion, within the approximate range of deformation covered by our extrusion experiments, and the following expressions were obtained:

$$\bar{\sigma} = 320 + 51\bar{\varepsilon} \qquad (MN/m^2)$$

for copper. Similarly

$$\bar{\sigma} = 950 + 750\bar{\varepsilon} \qquad (MN/m^2)$$

for the stainless steel and deformation up to the extrusion ratios 5 and 6. For extrusion ratios up to 4 the following expression was used:

$$\bar{\sigma} = 650 + 770\bar{\varepsilon} \qquad (MN/m^2)$$

These equations correspond to the theoretical form adopted to follow the strain hardening of the metals, according to von Mises's yield criterion and a linear rule of hardening (see equation (182)).

As far as the polynomial solution is concerned, a polynomial of nine terms has been adopted for the determination of the unknown parameters in the expressions of the stress functions:

$$\phi_1 = \frac{\sqrt{3}}{6} k r^3 + P^3 \sum_{I=1}^{3} \sum_{J=1}^{3} A_{IJ} r^{2I} z^J$$

$$\phi_2 = P^2 \sum_{M=1}^{3} \sum_{N=1}^{3} B_{MN} r^{2M+1} z^N$$

This is achieved in the computer programme by making I = J = 3 and also M = N = 3. In this case, maximum powers of 10 in r and 8 in z are produced, which are on the recommended upper limit, as far as rounding errors are concerned.

The calculations have also been made with higher values of indices (4 and 5) and, since no significant differences with the previous results arise, the value 3 has been adopted for the final results. This fact is considered as a convergence test by several authors [51], [48].

These polynomials are then economized to power 7 in r and 6 in z, thus obtaining the set of values for the unknown parameters to be used in the calculation of the stress field.

The contour corresponding to equi-stress lines for the different stress components and extrusion ratios are shown in Figs. 43 to 62 . The values have been divided by the initial yield stress of the tube in order to put them in a non-dimensional form.

In order to check how well the solution satisfies the governing equations, a direct numerical substitution for all nodal points was made. The resulting error was expressed as a percentage of the calculated values.

From this analysis it clearly shows two zones of the mesh where the higher errors are obtained, being located at both ends of the tube. The maximum and average percentage errors for the different stress components and extrusion ratios are shown in the table on the following page. The economization process adds a maximum of 2% to the corresponding average errors.

In order to be compared with the experimental results the pulling stress-hydrostatic pressure relationship has been calculated from the theoretical stress field for different extrusion ratios, by means of expression (202). In Fig.68 the theoretical lines are shown together with the experimental ones presenting a reasonable agreement.

Extrusion Ratio	σ_r		σ_θ		σ_z		τ_{rz}	
	Maximum error (%)	Average error (%)	Maximum error (%)	Average error (%)	Maximum error (%)	Average error (%)	Maximum error (%)	Average error (%)
2	21	16	23	17	18.6	13	19	15
3	18	14	21	15	17	12	18	14
4	16	11	19	16	15	14	20	16
5	19	12	20	14	15	12	21	17
6	18	15	21	15	16	13	17	13

VIII.12 Temperature field in the composite wire

The temperature field was calculated by direct integration of the equation (216) by means of the method of weighted residuals, using the following trial function:

$$T = T_o + (R_I^2 - r^2 - z^2)(z.\tan\alpha_E - r)\sum_{i=0}^{N}\sum_{j=1}^{M} r^{2i}\, z^j$$

as was explained in Section VII.8.3.

The error function arising from the use of that expression was calculated with the following numerical values, in S.I. units wherever relevant (MKS system):

Number of error functions	2
Maximum index (temperature 1)	3
Maximum index (temperature 2)	3
Number of variables (temperature)	1
Initial temperature	.2000E+02
Thermal conductivity (tube)	.1600E+02
Thermal conductivity (core)	.3860E+03
Constant beta - 1	.3600E+12
Constant beta - 2	.1445E+11
Weighting factor - 1 (temperature)	.1000E+01
Weighting factor - 2 (temperature)	.2200E+03

The contours corresponding to the isothermal lines for the different extrusion ratios are presented in Figs. 64 to 67 .

The maximum temperatures predicted are of the same order as the ones obtained by R.M. Guha and B. Lengyel [47] by a finite difference approach in the case of hydrostatic extrusion of a single metal wire.

VIII.13 Pressure welding conditions

VIII.13.1 Introduction

The basic process variables involved in solid state welding are pressure, temperature and level of superficial contamination. A metallurgical variable must also be taken into account when the welding of dissimilar metals is considered. These variables, together with the physico-chemical properties of the materials to be welded, determine the course of the joint formation process [113], [114], [115]. Although the experimental parameters involved in several welding processes are well estbalished, the mechanism operating in the formation of the joint still remains unclear [116].

There are two aspects in the formation of a pressure weld:

(i) The presence of surface oxide films that prevents bonding.

(ii) The difficulty of forming a bond between metallic areas exposed by fragmentation of the oxide during the deformation.

The several reasons proposed to account for the second point can be seen in [114] and they can be briefly summarized as follows:

(i) An energy barrier has to be overcome for the formation of the bond.

(ii) Bonds do form but are broken by elastic stresses on release of the load.

(iii) The metallic surfaces become contaminated by adsorbed contaminants transferring from particles of the original surface.

These mechanisms are in a close relationship with the existence of a minimum or threshold deformation required to produce the joint, below which the welding of the surfaces does not seem to take place.

VIII.13.2 Surface preparation and threshold deformation

Whenever metals are to be pressure welded at room temperature the question of surface preparation arises, for it is invariably found that welding will not take place without some sort of surface treatment.

An extensive consideration of this problem has been done by L.R. Vaidyanath and D.R. Milner [117]. In their experiments it has been found that degreasing followed by scratch brushing immediately before welding gives the highest bond

strengths. It is often stated that scratch-brushing removes scale and oxide films; although this may be true, it cannot produce a surface which is free from oxide, for the scratch-brushing operation heats the surface layers, so that a further film will be rapidly reformed before welding can be carried out.

It has also been postulated that the main effect of scratch-brushing is the removal of adsorbed contaminant surface layers [118]. This finds support in Milner's work [119] where it was shown that if scratch-brushed surfaces were exposed to the atmosphere before welding for periods exceeding about two minutes, the bond strength progressively decreased owing to the adsorption of contaminants, mainly water vapour.

In Ref. [117] there is presented an illustrative diagram showing the influence that different surface treatments have on the bond strength of aluminium roll-bonded composites. It is found that degreasing followed by scratch-brushing gave the best bonding properties. It is also established that if the procedure is reversed, with scratch-brushing followed by degreasing, the threshold deformation for bonding is higher, and lower bond strengths are obtained. Machined surfaces gave intermediate bond strengths, while electropolished surfaces and the "as received" commercial surfaces, either with or without a degreasing treatment, did not weld even with an 80% deformation.

In the same reference, [117], another series of experiments analyse the influence of heating the "as received" specimens followed by a cooling period in a dessicator, on the bond strength. It was shown that temperature does not seem to be as effective as scratch-brushing in removing contaminants or that there must be another significant factor associated with the scratch-brushing process.

In some papers by H. Helman and C. Martinez Vidal it was experimentally studied the influence of the moisture and the specimen exposure time to this, time covering from the end of the scratch-brushing process to the bonding process, on the threshold deformation of aluminium specimens bonded by rolling [120] and by indentation [121]. In Figs. 69 and 70 can be seen how relevant to the threshold deformation is the adsorbed moisture and also the importance of avoiding delays after the scratch-brushing process is finished.

Perhaps one of the more conclusive experimental works in favour of the superficial contamination as being mainly responsible for the existence of a threshold deformation was done by W.C. Sherwood and D.R. Milner [122]. In this work the effect on pressure welding of reducing the level of contamination has been examined by rolling strips together immediately after machining off the contaminated surface layer. The operation

was carried out in a vacuum chamber so as to minimize the possibility of reformation of a contaminated layer. It was shown that when operating in a vacuum of 3×10^{-5} torr the threshold deformation for aluminium, copper and cadmium was reduced to less than 1%, while for stronger metals it went up to 7% for nickel and 24% for iron.

Another similar experiment has been done by D.V. Keller and T. Spalvins [123]: in an ultra-high vacuum chamber, contaminants were removed from the surfaces by argon-ion and electron bombardment, in a vacuum of 10^{-11} torr. They have found that when the surfaces were brought together under light loads, many, but not all, metals and combinations of metals adhered together.

In industrial practice much more highly contaminated surfaces are welded together to give full strength, but this is accomplished by greater pressures and deformations, and sometimes also by operating at high temperatures.

Very little is known about how contaminants behave during the process of deformation. There is some information about oxides' behaviour during the rolling process [124] and also there has been proposed a mechanism for the joint formation related to such behaviour [125]. Briefly, it was stated that for surfaces prepared by degreasing and scratch-brushing,

cold pressure welding is essentially a three-stage process involving:

(i) Coherent fracture of the surface layers resulting from extension of the interface during rolling.

(ii) Extrusion of underlying surfaces through interfacial cracks from both sides of the interface under the action of normal roll pressure.

(iii) Metallic bonding between freshly created surfaces that approach to within interatomic distances.

It also pointed out that welding is initiated at a deformation slightly below the threshold deformation, i.e. that at which the bonds formed become sufficiently strong to withstand the forces acting to separate the strips as they emerge from the roll gap. The principal effects of increasing the degree of deformation are to enlarge the interfacial area available for bonding and to increase the bonded area of individual junctions.

Nevertheless, there still remains unclear the role played by other inhibiting factors such as moisture, trapped and adsorbed gases, etc. Since most of the research effort has been oriented towards the form of eliminating such interferences, mainly by the process of degreasing followed by scratch-brushing, there is little information about cold welding conditions for

the "as received" commercial surfaces processed by conventional methods (rolling, indentation, etc.). It is only known that the threshold deformation is very high: more than 80% for cold rolled aluminium [17] and we know that a still higher deformation did not produce bonding in aluminium deformed by indentation [21].

The basic problem to be considered, therefore, is the welding of two surfaces having a certain amount of contaminant present between them that must in some way be dispersed by the operating variables of deformation, pressure and temperature. Such information is relevant to some cases where the scratch-brushing operation is difficult to carry out. This is the case of our specimens, which consist of small diameter tubes and a wire as core, for the process of coextrusion.

However, there exists a pressure welding method where the surfaces received no special treatment prior to the welding process, as is the case of explosive cladding. Nevertheless, in this process a jet or spray of metal is formed at the apex of the collision of both plates and is forced outward from the space between the colliding plates, at a very high velocity.

The explosion-welding process can be considered as a two-step process. Firstly, the jet breaks up and cleans the inhibiting surface layers and, secondly, the high pressure

produced forces the clean metal surfaces into such close contact that the interatomic forces can be established across the bond interface [126].

The impact pressure developed during the welding process required for the joint to be formed are 44.7 Kb for low carbon steel, 48 Kb for medium carbon steel, and 44 Kb for Ti, involving kinematic energies in the order of 150 Nm/cm^2 [127], [128], [129]. These values tend to increase with the yield stress of the metals to be welded.

The other parameters involved in pressure welding are less critical, as far as cold welding is concerned. Increasing pressure primarily increases the development of bonding above the threshold deformation, having little effect on the threshold deformation itself [130].

If high temperature is developed during the process of deformation it may have an important influence on the bonding: the threshold deformation decreases as temperature increases. This incidence seems to be directly related to the yield stress. With metals which dissolve their oxide films at high temperature (e.g. iron, copper, titanium, etc.) welding is greatly enhanced at these temperatures, because the oxide on the mating surfaces dissolves into the adjacent metal, thus decreasing the area over which the bonding is inhibited. This

dissolution starts to occur at welding temperatures of about 0.5 Tm (Tm is the absolute melting temperature) [130].

VIII.14 Coextrusion of copper-stainless steel specimens

VIII.14.1 Experimental preparation

The specimens to be processed are those described in Section III.3

The superficial treatment given to the copper tube was as follows:

1. Degreasing by means of trichlorethylene.

2. Chemical removal of oxides by means of the solution

$$80\%\ NO_3H \qquad 20\%(PO_3)_4H_3$$

After being carefully washed with water the tubes were left in a dessicator with silica gel during at least 24 hours.

This treatment is known to have poor results because of the amount of contaminants, mainly adsorbed water, left at the end of the process on the surfaces to be welded. Unfortunately it was not possible to use, without special devices, the procedure of baking followed by scratch-brushing. The adequate temperature required for the contaminents to be baked off is too high to avoid softening the copper tube [17] (see Section III.3) and the scratch-brushing operation of the

internal surfaces of tubes of small diameters requires the use of special devices.

The stainless steel wire was heated in vacuum furnace at 600°C and scratch-brushed immediately before the composite specimen was assembled.

The preparation of the composite specimen takes some time since it involves several operations; in a minor degree also the assembly of the extrusion rig imposes a delay before the deformation process.

After all these steps have been fulfilled, the surfaces to be welded have surely been recontaminated. Consequently, as far as the bonding operation is concerned, the surfaces of the tube and core may reasonably be considered to be in a similar condition to the "as received" state.

VIII.14.2 Pressures and temperatures at the interface

From the theoretical description obtained for the stress and temperature fields, it is possible to calculate the normal stress or pressure acting along the interface and also the temperature distribution developed on this surface.

The pressure distributions are presented in Figs. 71-75 while the temperature distributions are shown in Fig. 76. In Fig. 77 is presented the "maximum temperature-extrusion ratio"

relationship, and in Fig. 78 the "maximum pressure-extrusion ratio" relationship.

VIII.14.3 Conditions for cold welding and experimental results

The described specimens were extruded with the extrusion ratios 2.7, 4.3 and 5.6. It was intended to reach still higher extrusion ratios; however, it was not possible to obtain further reductions since even with an extrusion pressure of 110 ton/in^2 the stainless steel was broken without the specimen starting to extrude, for an extrusion ratio of 7. For safety reasons the use of higher pressures was not considered.

In all cases the minimum speed was used; for the extrusion ratio 5.6 several specimens were obtained free extruded with an estimated velocity of 1 m/s.

IX. GENERAL CONCLUSIONS

The process of hydrostatic extrusion of bimetallic composites was analysed by the Method of Weighted Residuals. Pressure, stress and temperature distribution in the deforming zone were computed.

The metals were assumed to obey the von Mises yield criterion, a linear rule of isotropic hardening and Prandtl-Reuss stress-strain relationship. Avitzur's velocity field was assumed to characterise the flow of metals through the dies.

The theoretically predicted pulling stress-hydrostatic pressure relationship is in reasonable agreement with the experimental results. The maximum temperatures computed in the deforming zone are comparable to those obtained by others.

The pressure distribution at the core/tube interface of the composite was calculated for different extrusion ratios and the influence of this parameter on the pressure welding of the two metals was discussed.

Metallurgical bonding was not achieved during the experiments. Adequate preparation of contact surfaces to ensure satisfactory welding conditions was not possible to obtain with the available equipment due to the difficult geometry of the specimen and the mechanical properties of the metals used. Neither the required pressure (60-100 Kb) nor

sufficiently high temperature ($> 500^{o}C$) which might have allowed pressure welding to take place without removing the contaminated layer could be reached during the experiments.

The chosen Method of Weighted Residuals has proved to be easy to handle and suitable to solve the two types of equations encountered in this work. It is also much less demanding in terms of computation and consequently less expensive in comparison with other numerical methods. About 12 seconds of processing time (CDC 6400) was required to obtain the stress and temperature distributions mentioned above, whereas the central processing time required to obtain the same information by the method of Finite Elements would probably be several orders of magnitude higher.

Whenever a solution to a system of partial differential equations (or tensor differential equation) is to be approximated by a polynomial to within an acceptable level of accuracy, it is usually necessary to use high order expansions. This condition could lead to high rounding errors and excessive computing time. Aiming to lessen these difficulties a new method for the numerical solution of partial differential equations based on the economization of several variables was developed [133]. This procedure combines the operational simplicity of the Method of Weighted Residuals with the high accuracy of the

Chebyshev methods, which are difficult to use in the numerical solution of partial differential equations, as has been pointed out by several authors [131], [132].

Main Programme

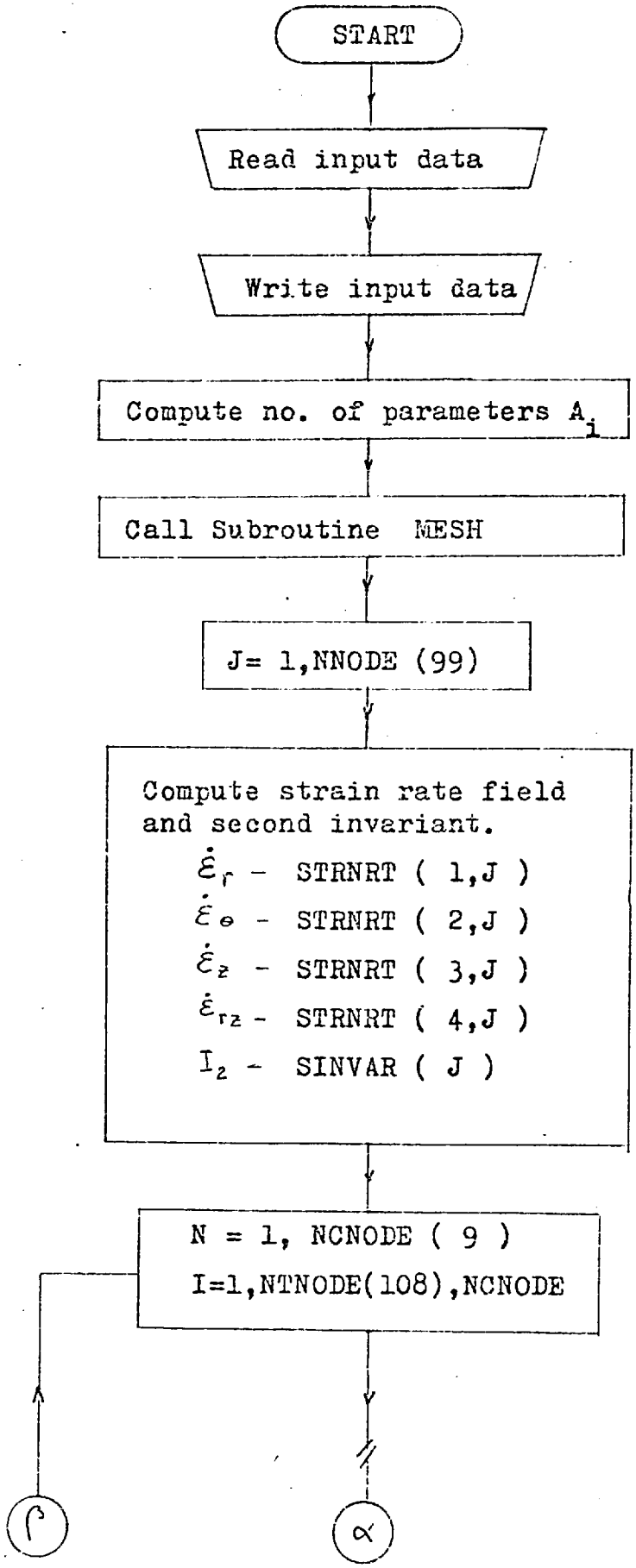

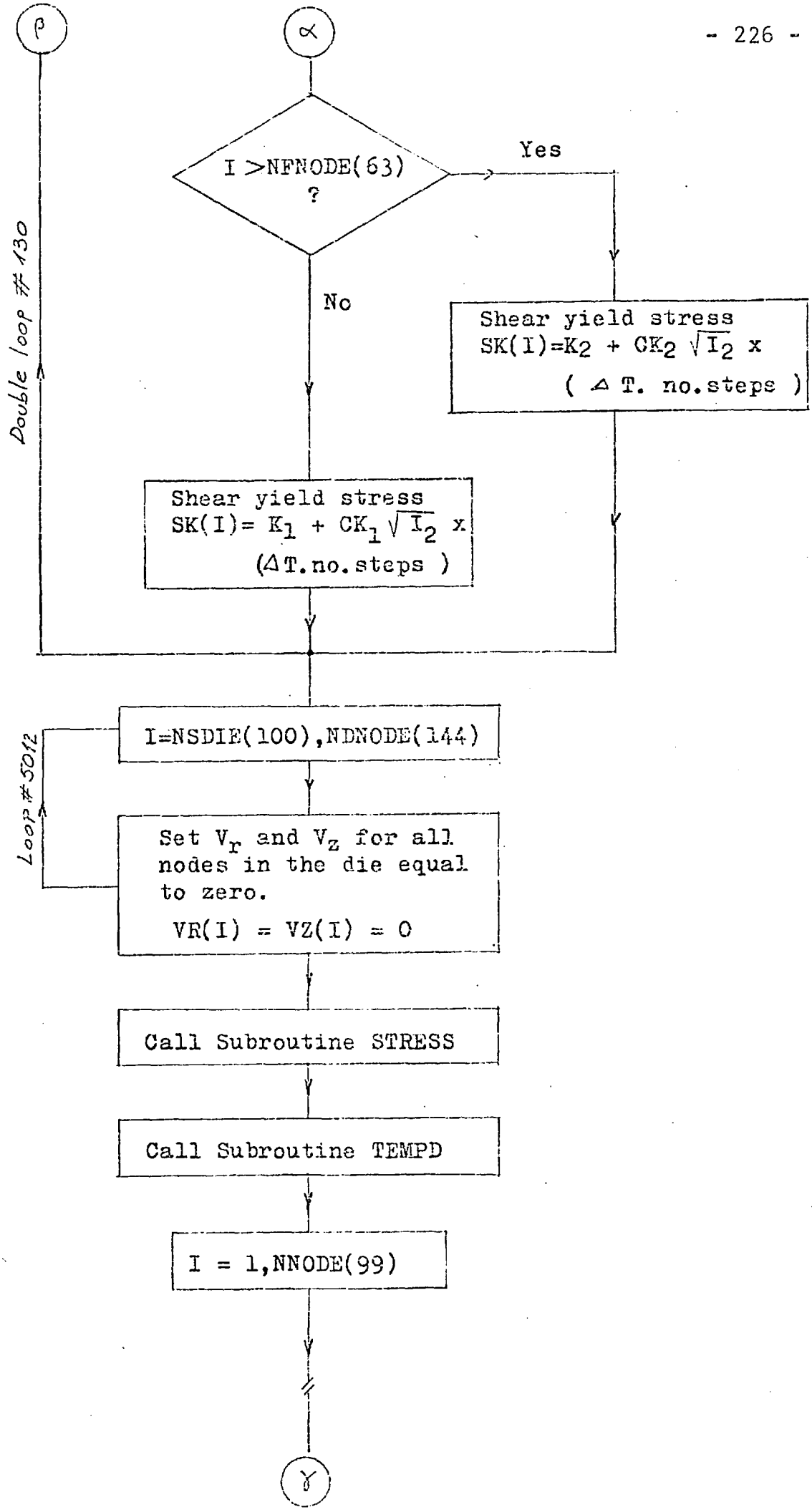
β
α
Double loop #130
I >NFNODE(63) ?
Yes
No
Shear yield stress SK(I)=K2 + CK2 √I2 x (Δ T. no.steps)
Shear yield stress SK(I)= K1 + CK1 √I2 x (Δ T. no.steps)
Loop #5012
I=NSDIE(100),NDNODE(144)
Set Vr and Vz for all nodes in the die equal to zero.
VR(I) = VZ(I) = 0
Call Subroutine STRESS
Call Subroutine TEMPD
I = 1,NNODE(99)
γ

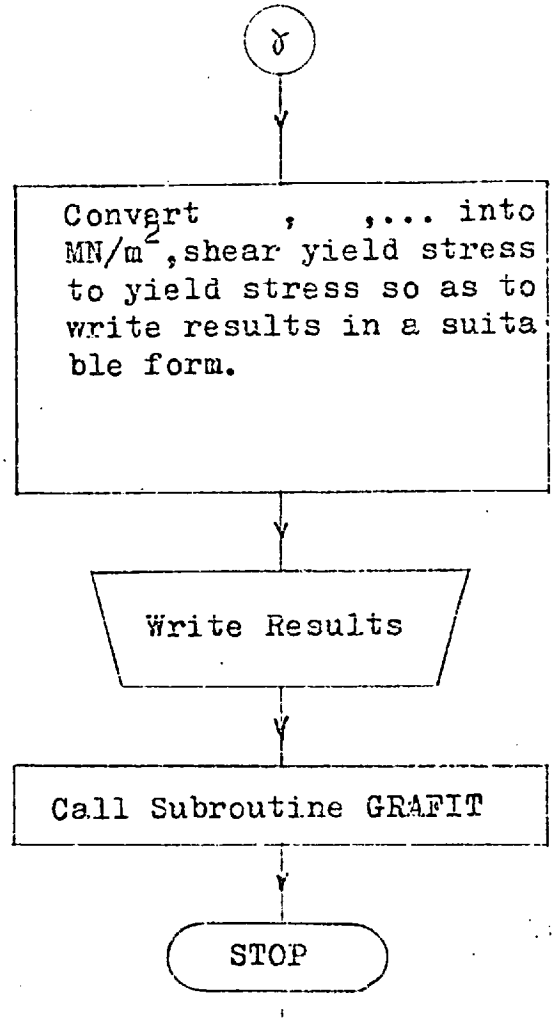
γ
Convert , ,... into MN/m², shear yield stress to yield stress so as to write results in a suitable form.
Write Results
Call Subroutine GRAFIT
STOP

FIGURE 33

```
      PROGRAM HIRES1 (INPUT, OUTPUT, TAPE5=INPUT, TAPE6=OUTPUT)
C      WEIGHTED RESIDUALS PROGRAMME
      COMMON NTERM,NTERM1,NTERM2,NVAR,NCREF,NTERM3,NTERM4,NVART,
     1    NDNODE,NNODE,NFNODE,NCNODE,NADIVC,NADIVT,NADIVD,NSINT,
     2    RF, RI, ALPHAS, ALPHA, ALPHAE, VE, C, AK1, AK2, CK1, CK2, TINI,
     3    TC1, TC2, BETA1, BETA2, NTNODE, NSCOND, NGNODE, NPARAM,NPARA1,
     4    A(2,[illegible]), B([illegible]), C([illegible]), I([illegible]), G(4), WF(2), X([illegible]),
     5    ORGR(144), ORGZ(144), RADS([illegible]), STRNRT(4,99), STNVAR(126),
     6    SX([illegible]), VR(144), VZ(144), SIGMAR(99), SIGMAZ(99),
     7    SIGMAT(99), SIGMRZ(99),TEMP(144) ,AVER, AVER1, AVER2
      READ(5,1001) NTERM,NTERM1,NTERM2,NVAR,NCREF,NTERM3,NTERM4,NVART,
     1    NDNODE, NNODE, NFNODE, NCNODE, NADIVC,NADIVT,NADIVD,
     2    RF, RI, ALPHAS, ALPHA, ALPHAE, VE, C, AK1, AK2, CK1, CK2,
     3    TINI, TC1, TC2, BETA1, BETA2, DELTAT, G(1), G(2), G(3), G(4),
     4    WF(1), WF(2)
 1001 FORMAT(15I5,5X/2(7E10.4) , 7E10.4)
      WRITE(6,1002)NTERM,NTERM1,NTERM2,NVAR,NCREF,NTERM3,NTERM4,NVART,
     1    NDNODE, NNODE, NFNODE, NCNODE, NADIVC,NADIVT,NADIVD,
     2    RF, RI, ALPHAS, ALPHA, ALPHAE, VE, C, AK1, AK2, CK1, CK2,
     3    TINI, TC1, TC2, BETA1, BETA2, DELTAT, G(1), G(2), G(3), G(4),
     4    WF(1), WF(2)
 1002 FORMAT(1H1/5X,12H  INPUT DATA/ 5X,12H -----------//
     1          5X,39H  NUMBER OF ERROR FUNCTIONS (STRESS) ..,I12//
     2          5X,39H  NUMBER OF INDICIES (STRESS 1) ........,I12//
     3          5X,39H  NUMBER OF INDICIES (STRESS 2) ........,I12//
     4          5X,39H  NUMBER OF VARIABLES (STRESS) .........,I12//
     5          5X,39H  NUMBER OF ERROR FUNCTIONS (TEMP.) ....,I12//
     6          5X,39H  NUMBER OF INDICIES (TEMP. 1) .........,I12//
     7          5X,39H  NUMBER OF INDICIES (TEMP. 2) .........,I12//
     8          5X,39H  NUMBER OF VARIABLES (TEMP.) ..........,I12//
     9          5X,39H  NUMBER OF TOTAL NODES ................,I12//
     1          5X,39H  NUMBER OF NODES IN BILLET ............,I12//
     2          5X,39H  NUMBER OF NODES IN THE CORE ..........,I12//
     3          5X,39H  NUMBER OF NODES IN THE INTERFACE .....,I12//
     4          5X,39H  NUMBER OF DIVISIONS OF ANGLE (CORE) ..,I12//
     5          5X,39H  NUMBER OF DIVISIONS OF ANGLE (TUBE) ..,I12//
     6          5X,39H  NUMBER OF DIVISIONS OF ANGLE (DIE) ...,I12//
     7          5X,39H  RADIUS AT EXIT .......................,E12.4//
     8          5X,39H  RADIUS AT ENTRY ......................,E12.4//
     9          5X,39H  SEMI-CORE ANGLE ......................,E12.4//
     1          5X,39H  SEMI-DIE ANGLE .......................,E12.4//
     2          5X,39H  SEMI-EXTERNAL ANGLE ..................,E12.4//
     3          5X,39H  VELOCITY AT EXIT .....................,E12.4//
     4          5X,39H  CONSTANT C (FRICTION) ................,E12.4//
     5          5X,39H  SHEAR YIELD STRESS OF CORE ...........,E12.4//
     6          5X,39H  SHEAR YIELD STRESS OF TUBE ...........,E12.4//
     7          5X,39H  CONSTANT CK FOR THE CORE .............,E12.4//
     8          5X,39H  CONSTANT CK FOR THE TUBE .............,E12.4//
     9          5X,39H  INITIAL TEMPRATURE ...................,E12.4//
     1          5X,39H  TERMAL CONDUCTIVITY (TUBE) ...........,E12.4//
     2          5X,39H  TERMAL CONDUCTIVITY (CORE) ...........,E12.4//
     3          5X,39H  CONSTANT BETA - 1 ....................,E12.4//
     4          5X,39H  CONSTANT BETA - 2 ....................,E12.4//
     5          5X,39H  TIME INCREMENT (HARDENING) ...........,E12.4//
     6          5X,39H  WEIGHTING FACTOR - 1 (STRESS) ........,E12.4//
     7          5X,39H  WEIGHTING FACTOR - 2 (STRESS) ........,E12.4//
     8          5X,39H  WEIGHTING FACTOR - 3 (STRESS) ........,E12.4//
     9          5X,39H  WEIGHTING FACTOR - 4 (STRESS) ........,E12.4//
     1          5X,39H  WEIGHTING FACTOR - 1 (TEMP.) .........,E12.4//
     2          5X,39H  WEIGHTING FACTOR - 2 (TEMP.) .........,E12.4//)
      NGNODE = NDNODE + NFNODE + NCNODE
      NTNODE = NNODE + NCNODE
      NSCOND = NNODE - NCNODE +1
      NSINT = NFNODE - NCNODE + 1
      NPARAM = NTERM1*NTERM2 * 2
      NPARA1 = NTERM3*NTERM4
      NSDIE= NNODE + 1
      CALL MESH
      DO 120 J = 1, NNODE
   21 R = ORGR(J)
      Z = ORGZ(J)
      R2 = R*R
      R3 = R2 *R
      R4= R2*R2
      Z2 = Z*Z
      Z3 = Z2 *Z
      P1 = R2 +Z2
      FAC4 = - VE * RF * RF
      FAC5 = P1 * P1
      FAC6 = FAC5 * P1
C      STRAIN RATE FIELD


      STRNRT(1,J) =  FAC4*(Z3-R2*Z*3.)/FAC6
      STRNRT(2,J) =  FAC4*Z/FAC5
      STRNRT(3,J) = 2.*FAC4*(R2*Z-Z3)/FAC6
      STRNRT(4,J) = 1.5 * FAC4*(R3-4.*R*Z2)/FAC6
C     COMPUTE STRAINRATE INVARIANT (I2) AND DEVIATORIC STRESS TENSOR
      STNVAR(J)=ABS(STRNRT(4,J)*STRNRT(4,J) - STRNRT(1,J)*STRNRT(2,J)-
     1 STRNRT(2,J)*STRNRT(3,J)-STRNRT(3,J)*STRNRT(1,J))
  120 CONTINUE
      DO 133 N= 1,NCNODE
      DO 133 I = N,NTNODE ,NCNODE
      IF(I.GT.NFNODE) GO TO 200
      SK(I) = AK1 +CK1 * SQRT(STNVAR(I)) * DELTAT * (NCNODE-N)
      GO TO 133
  200 SK(I)= AK2+CK2*SQRT(STNVAR(I-NCNODE))*DELTAT*(NCNODE-N)
  133 CONTINUE
      DO 5012  I= NSDIE,NGNODE
      VR(I)= 0.0
 5012 VZ(I)= 0.0
      CALL STRESS
      CALL TEMPO
      DO 555 I = 1,NNODE
      SIGMAR(I) = SIGMAR(I) * 1.0E-6
      SIGMAT(I) = SIGMAT(I) * 1.0E-6
      SIGMAZ(I) = SIGMAZ(I) * 1.0E-6
      SIGMRZ(I) = SIGMRZ(I) * 1.0E-6
  555 SK(I) = SK(I) * SQRT(3.0) * 1.0E-6
      WRITE(6,1003)
 1003 FORMAT(1H1/5X,18H  COMPUTED RESULTS/5X,18H  ----------------  /)
      WRITE(6,1004) (I,A(I), I = 1,NPARAM)
 1004 FORMAT(5X,29H  FREE PARAMETER (STRESS) A -,I3,7H.......,E12.4/)
      WRITE(6,1005) (I,B(I), I = 1,NPARA1)
 1005 FORMAT(5X,29H  FREE PARAMETER (TEMP.)  A -,I3,7H.......,E12.4/)
      WRITE(6,1011)
 1011 FORMAT(1H1/5X,13H  NO          R              Z       VELOCITY-R  VELOCIT
     1Y-Z       SIGMA-R       SIGMA-T       SIGMA-Z     SIGMA-RZ   YLD.STRESS
     2     TEMP.                                              /)
      WRITE(6,1006)(I,ORGR(I),ORGZ(I),VR(I),VZ(I),SIGMAR(I),SIGMAT(I),
     1    SIGMAZ(I),SIGMRZ(I),SK(I),TEMP(I) , I = 1,NNODE)
 1006 FORMAT(5X,I4,10E12.4)
      M = NNODE+1
      WRITE(6,1007)(I,ORGR(I),ORGZ(I),TEMP(I), I= M,      NGNODE)
 1007 FORMAT(5X,I4,2E12.4,[illegible]     ---         ---         ---         --
     1-         ---                  ---            ,E12.4)
      WRITE(6,1020) AVER1,AVER2, AVER
 1020 FORMAT(//5X,39H  AVERAGE PULLING STRESS ..............,E12.4//
     1          5X,39H  HYDROSTATIC PRESSURE ...............,E12.4//
     2          5X,39H  TOTAL STRESS .......................,E12.4//)
      CALL GRAFIT( ORGR,ORGZ,[illegible],TEMP,8)
      CALL GRAFIT( [illegible],SIGMAR,7)
      CALL GRAFIT( [illegible],SIGMAZ,7)
      CALL GRAFIT( [illegible],SIGMAT,7)
      CALL GRAFIT( [illegible],SIGMRZ,7)
      CALL GRAFIT( ORGR,ORGZ,[illegible],SK,7)
      STOP
      END
```

FIGURE 34

Subroutine MESH

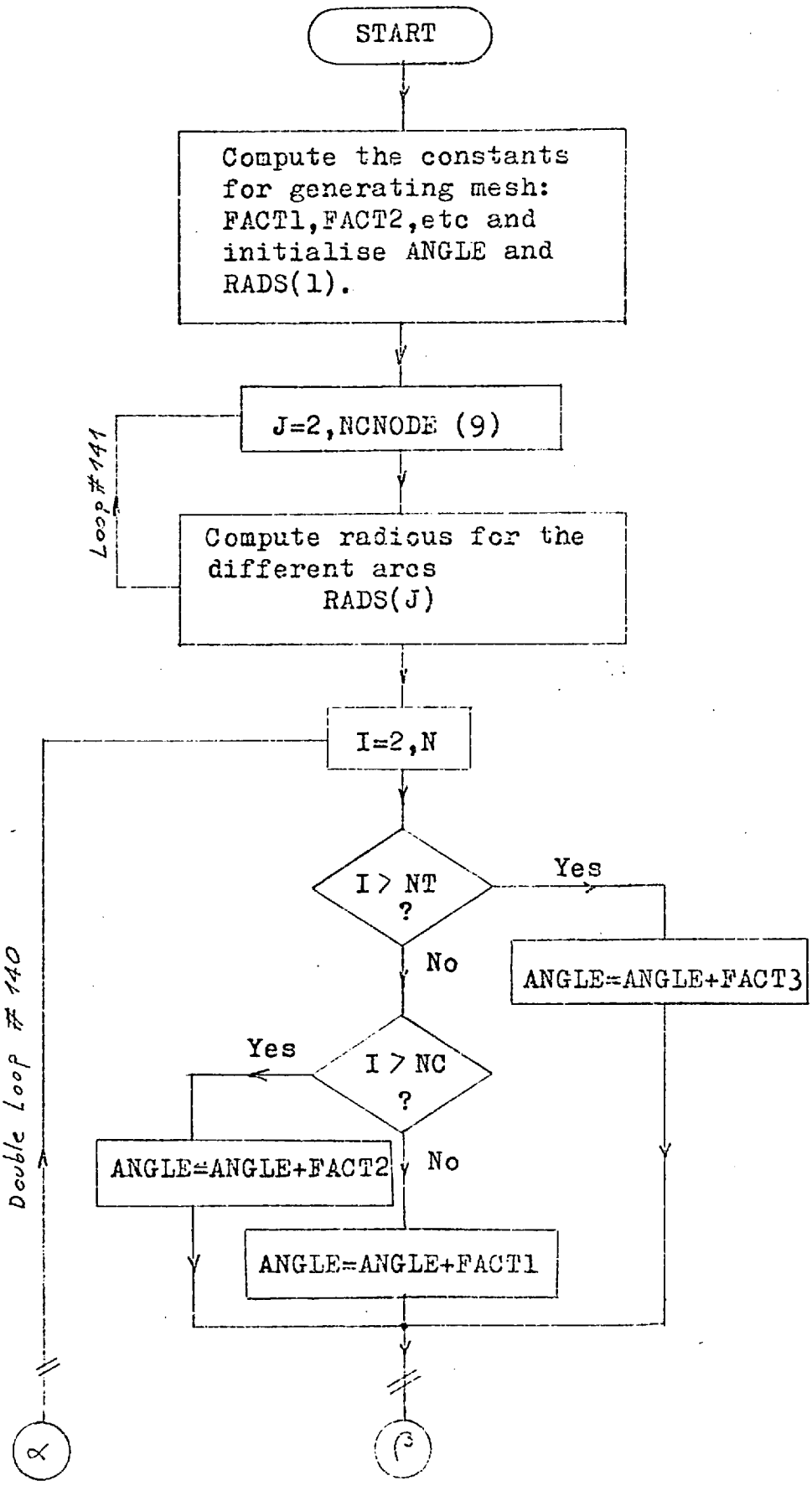

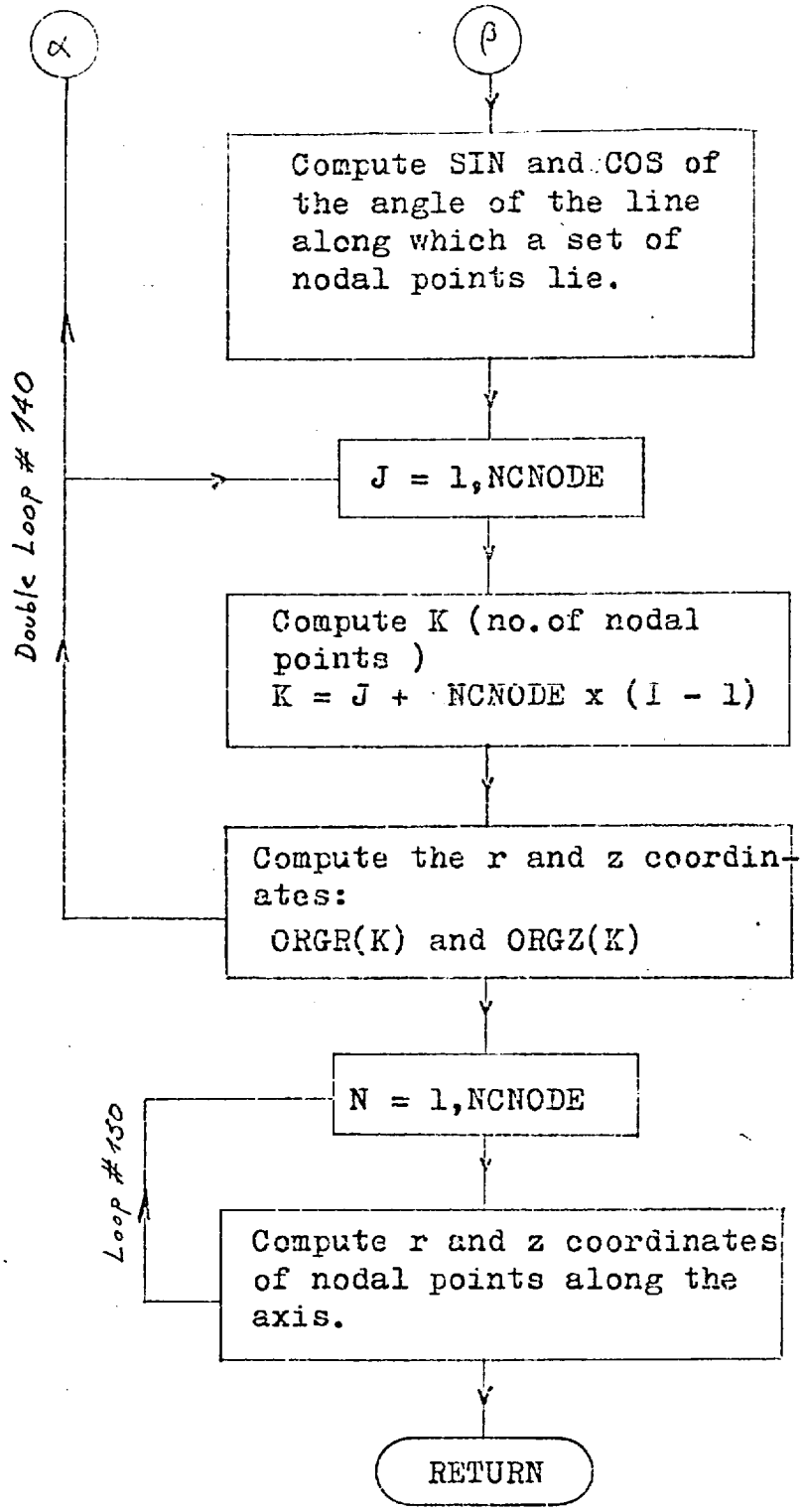
α
β
Compute SIN and COS of the angle of the line along which a set of nodal points lie.
Double Loop # 140
J = 1,NCNODE
Compute K (no.of nodal points)
K = J + NCNODE x (I - 1)
Compute the r and z coordinates:
ORGR(K) and ORGZ(K)
N = 1,NCNODE
Loop #150
Compute r and z coordinates of nodal points along the axis.
RETURN

FIGURE 35

```
      SUBROUTINE  MESH
      COMMON NEARBY,NTERM1,NTERM2,NVAR,NEART,NTERM3,NTERM4,NVART,
     1   NDNODE,NNODE,MENODE,NCNODE,NADIVC,NADIVT,NADIVD,NSINT,
     2   RF, RI, ALPHAC, ALPHA, ALPHAE, VE, G, AK1, AK2, CK2, CK3, TINI,
     3   TC1, TC2, BETA1, BETA2,  NTNODE, NSECND, NGNODE, NPARAM,NPAREI,
     4   A(20,20), B(400), C(20), D(20), G( 4), WF( 2), X(4,20),
     5   ORGR(144), ORGZ(144), RADS( 9), STRART(4,99), SINVAR(1:8),
     6   SK(400), VR(144), VZ( 4), SIGMAR(99), SIGMAZ(99),
     7   SIGMAT( 99), SIGMRZ( 99),TEMD(144) ,AVER, AVER1, AVER2
      NC = NADIVC + 1
      NT = NC + NADIVT
      N = NT + NADIVD
      ALPHAT = ALPHA - ALPHAC
      ALPHAD= ALPHAE - ALPHA
      FACT = (RI-RF)/(NDNODE-1)
      FACT1 = ALPHAC/NADIVC
      FACT2 = ALPHAT/NADIVT
      FACT3 = ALPHAD/NADIVD
      RADS(1) = RF
      ANGLE = 0.0
      DO 141 J = 2,NDNODE
  141 RADS(J) = RADS(J-1) + FACT
      DO 140 I = 2,N
      IF(I.GT. NT) GO TO 120
      IF(I.GT.NC) GO TO 130


      ANGLE = ANGLE+FACT1
      GO TO 135
  130 ANGLE = ANGLE + FACT2
      GOTO 135
  120 ANGLE = ANGLE + FACT3
  135 SIGNN = SIN(ANGLE)
      COSIGN = COS(ANGLE)
      DO 140 J = 1, NDNODE
      K = J + NDNODE * (I-1)
      ORGR(K)= RADS(J) * SIGNN
      ORGZ(K) = RADS(J) * COSIGN
  140 CONTINUE
      DO 150 N = 1,NDNODE
      ORGZ(N) = RADS(N)
  150 ORGR(N) = 0.000001
      RETURN
      END
```

FIGURE 36

Subroutine STRESS

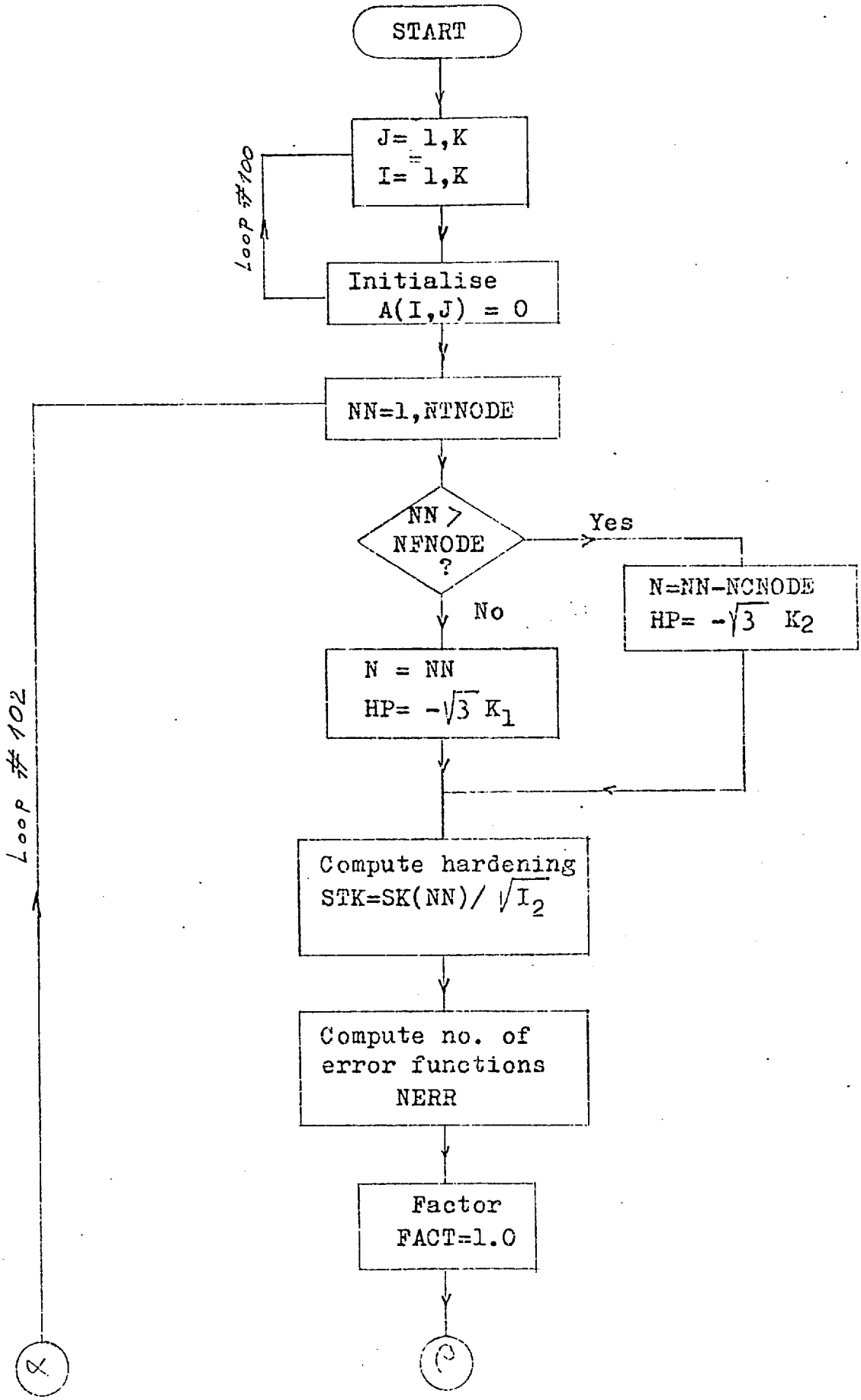

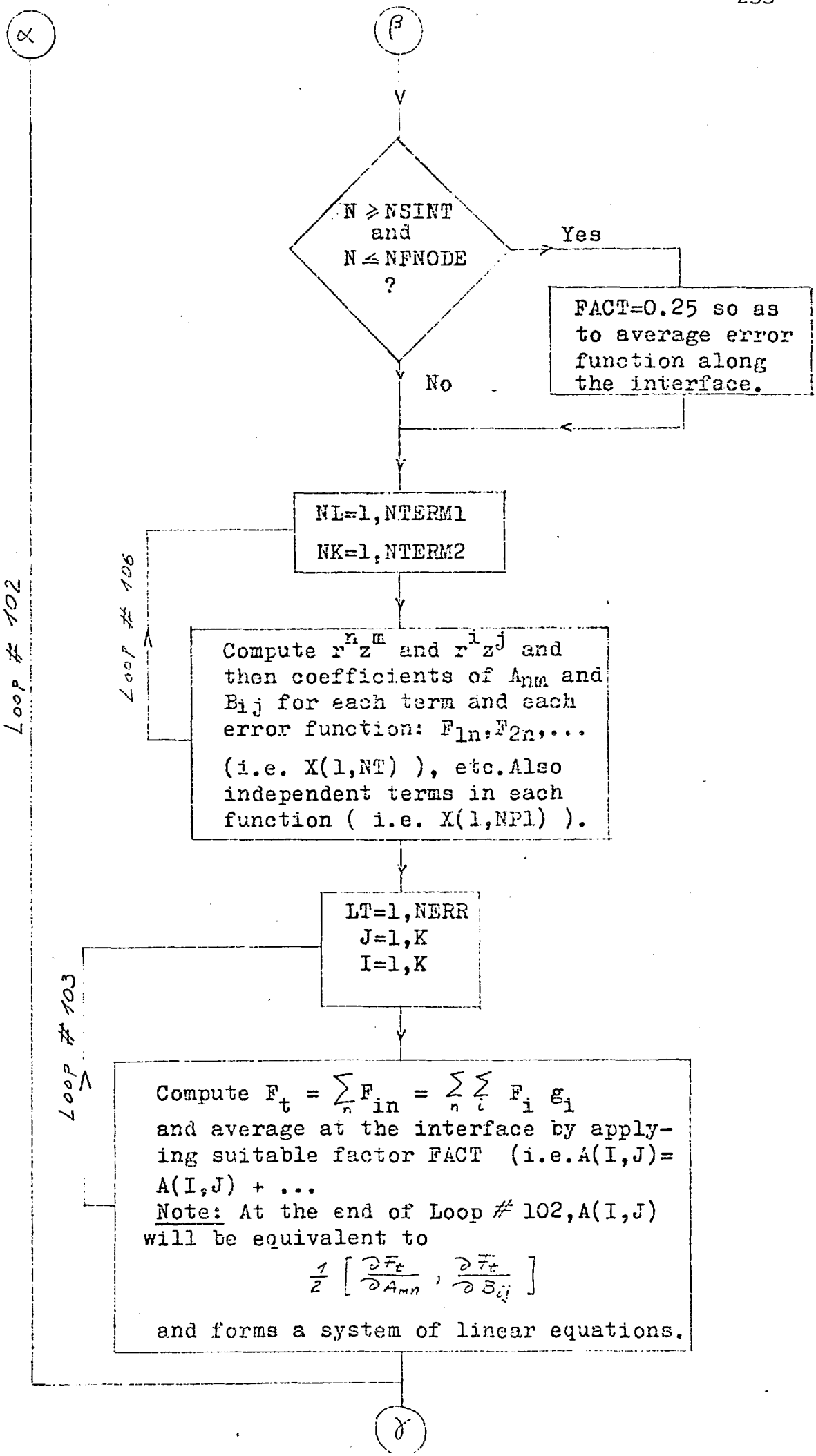
α
β
N ≥ NSINT and N ≤ NFNODE ?
Yes
No
FACT=0.25 so as to average error function along the interface.
NL=1,NTERM1
NK=1,NTERM2
Loop # 106
Compute $r^n z^m$ and $r^l z^j$ and then coefficients of A_{nm} and B_{ij} for each term and each error function: $F_{1n}, F_{2n}, \ldots$ (i.e. X(1,NT)), etc. Also independent terms in each function (i.e. X(1,NP1)).
LT=1,NERR
J=1,K
I=1,K
Loop # 103
Compute $F_t = \sum_n F_{in} = \sum_n \sum_i F_i g_i$ and average at the interface by applying suitable factor FACT (i.e. A(I,J)= A(I,J) + ...
Note: At the end of Loop # 102, A(I,J) will be equivalent to
$\frac{1}{2}\left[\frac{\partial F_t}{\partial A_{mn}}, \frac{\partial F_t}{\partial B_{ij}}\right]$
and forms a system of linear equations.
Loop # 102
γ

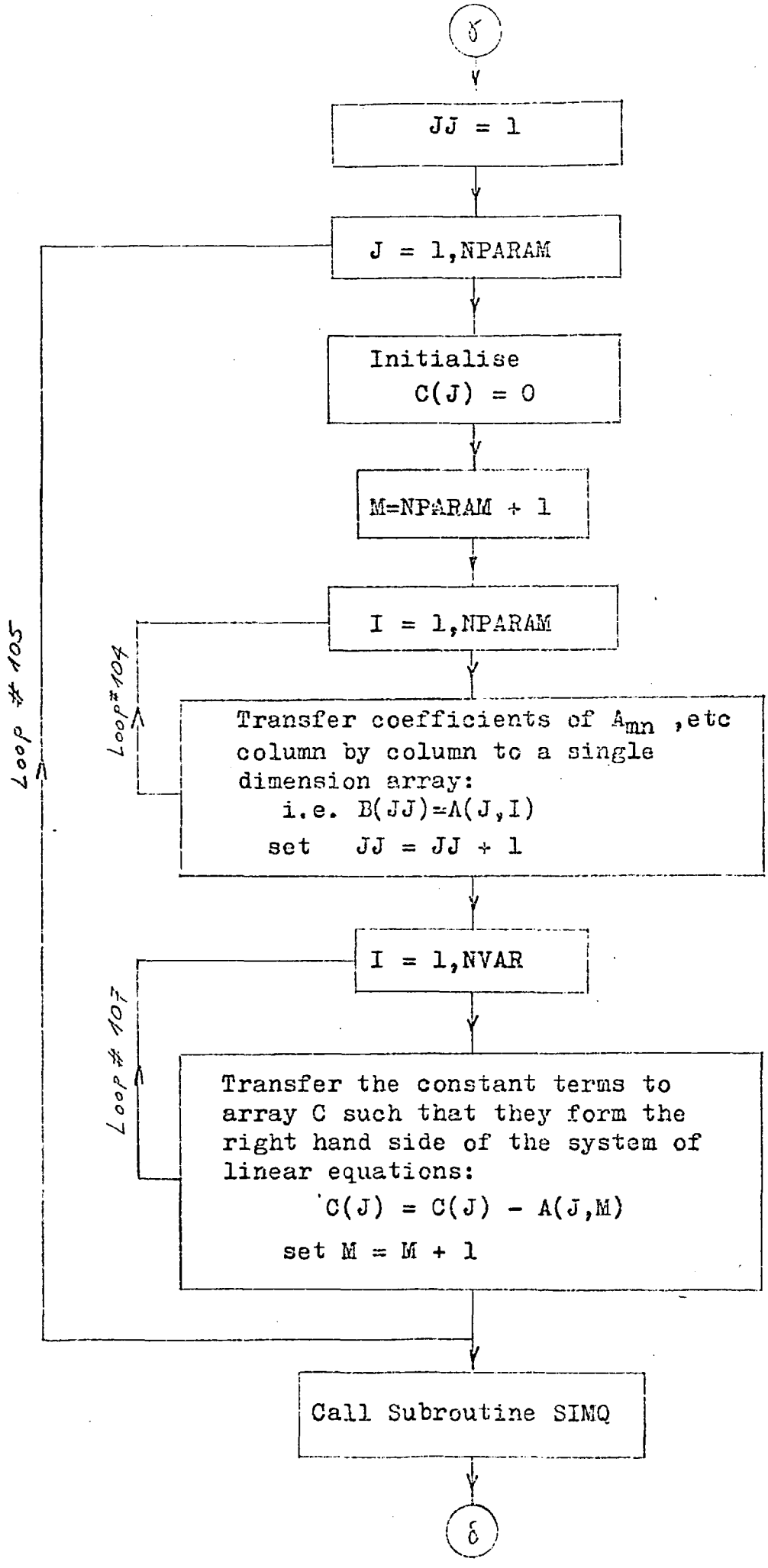
δ
JJ = 1
J = 1,NPARAM
Initialise
C(J) = 0
M=NPARAM + 1
I = 1,NPARAM
Loop #104
Transfer coefficients of A_{mn} ,etc column by column tc a single dimension array:
i.e. B(JJ)=A(J,I)
set JJ = JJ + 1
I = 1,NVAR
Loop # 107
Transfer the constant terms to array C such that they form the right hand side of the system of linear equations:
C(J) = C(J) - A(J,M)
set M = M + 1
Loop # 105
Call Subroutine SIMQ
ε

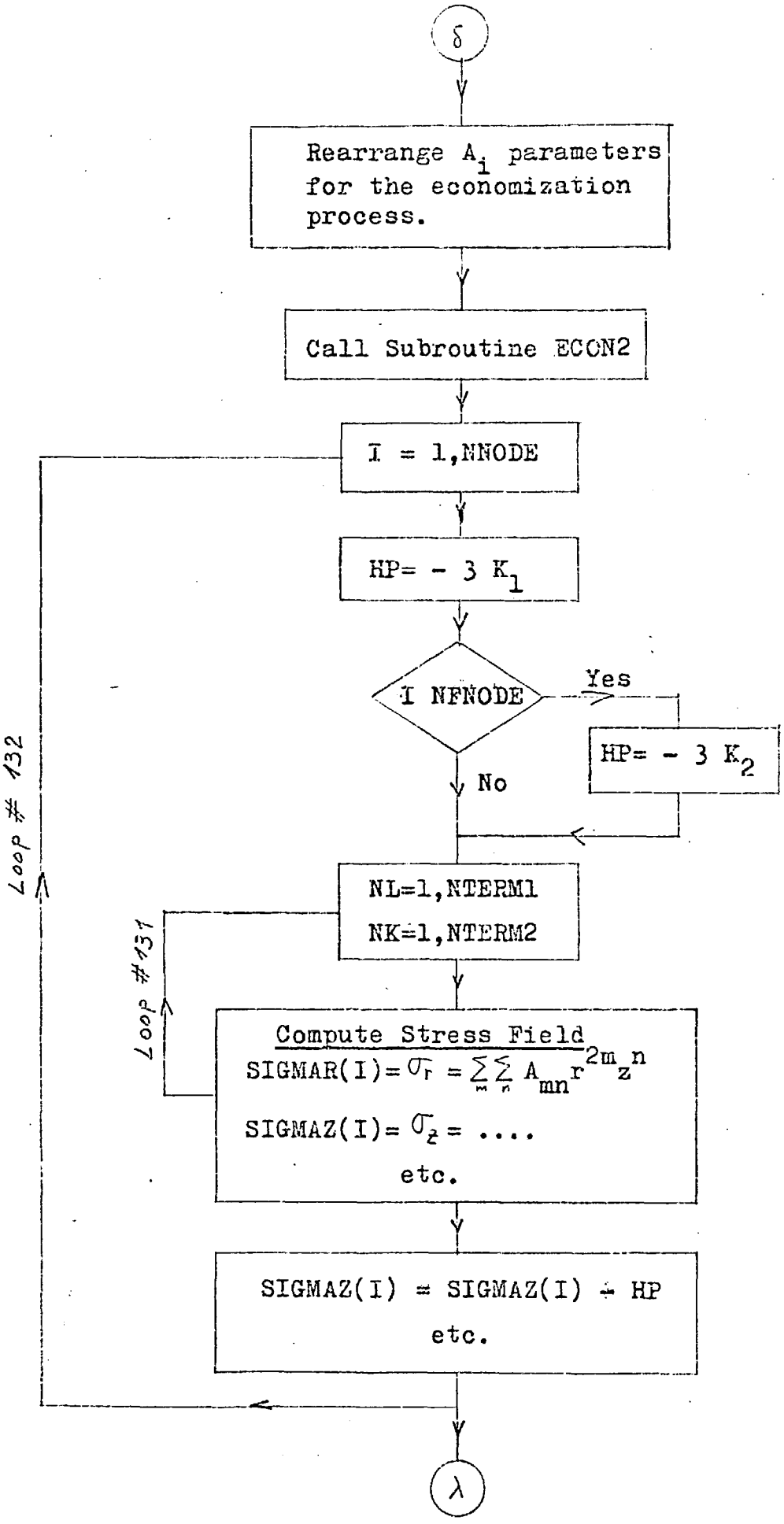
δ
Rearrange A_i parameters for the economization process.
Call Subroutine ECON2
I = 1,NNODE
HP= - 3 K_1
I NFNODE
Yes
HP= - 3 K_2
No
NL=1,NTERM1
NK=1,NTERM2
Compute Stress Field
SIGMAR(I)= $\sigma_r = \sum_m \sum_n A_{mn} r^{2m} z^n$
SIGMAZ(I)= σ_z = ...
etc.
SIGMAZ(I) = SIGMAZ(I) + HP
etc.
λ
Loop # 132
Loop #131

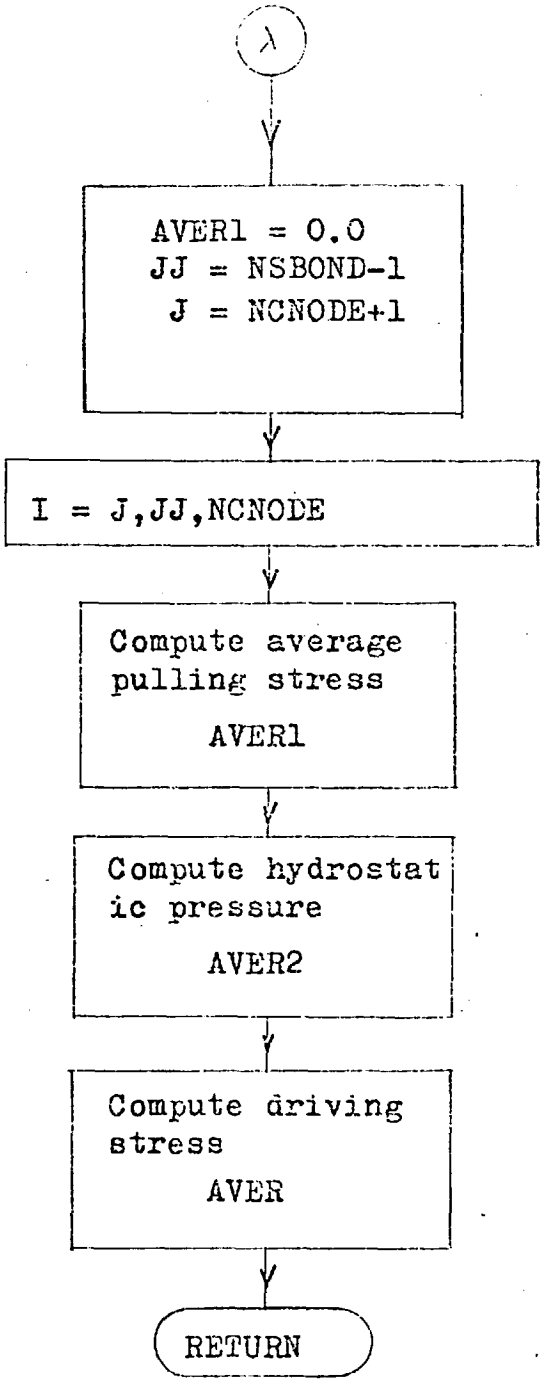
λ
AVER1 = 0.0
JJ = NSBOND-1
J = NCNODE+1
I = J,JJ,NCNODE
Compute average pulling stress
AVER1
Compute hydrostatic pressure
AVER2
Compute driving stress
AVER
RETURN

FIGURE 37

```
      SUBROUTINE STRESS
      COMMON NERRFN,NTERM1,NTERM2,NVAR,NEFFI,NTERM3,NTERM4,NVART,
     1   NONODE,NNODE,NFNODE,NONODE,NADIVO,NADIV1,NADIV2,NSINT,
     2   RF, RI, ALPHAO, ALPHA, ALPHAF, VE, C, AK1, AK2, CK1, CK2, TINI,
     3   TOL, TOL2, DETAL, DTIME, NTNODE, NSECND, NSNODE, NPARAM,NPARA1,
     4   A(24,24), B(400), D(20), Q(20), G( 4), WF( 2), X(4,20),
     5   ORGR(144), ORGZ(144), RADS( 9), STRNRT(4,99), SINVAR(100),
     6   SK(100), VR(144), VZ(144), SIGMAR(99), SIGMAZ(99),
     7   SIGMAT( 99), SIGNRI( 99),TEMD(144) ,AVER, AVER1, AVER2
      K = NPARAM + NVAR
      DO 101 J = 1,K
      DO 100 I = 1,K
  100 A(I,J) = 0.0
C     LOOP 101 TO SQUARE ERROR FUNCTION FOR EACH NODE
      NP1 = NPARAM + 1
      NP2 = NPARAM + 2
      X(3,NP2) = 0.0
      DO 102 NN = 1,NTNODE
      IF(NN .GT. NFNODE) GOTO 108
      HP = - SQRT(3.0) * AK1
      N = NN
      GOTO 109
  108 N = NN-NONODE
      HP = - SQRT(3.0) * AK2
  109 STK = SK(NN)/SQRT(SINVAR(N))
      NERR= NERRFN - 1
      FACT = 1.0
      IF(N .GE. NSINT .AND. N  .LE. NFNODE) FACT = 0.25
      R= ORGR(N)
      Z =ORGZ(N)
      Z2 = Z**2
      Z3 = Z2*Z
      Z4 = Z2 * Z2
      R2 = R**2
      R3 = R2 * R
      R4 = R2*R2
      P1 = R2 + Z2
      P= RI*RI - P1
      DO 106  NL= 1,NTERM1
      DO 106  NK= 1,NTERM2
      INDN = NK -1
      INDM= NL
      INDI= NK-1
      INDJ = NL - 1
      NI=NK+(NL - 1 )*NTERM1
      NTT=NI+(NTERM1 * NTERM2)
      SIGRA=(R**(2*INDI))*(Z**(INDJ-2))*P*(24*R4*R2-6*P*Z2*(2*INDJ+1)
     1 *R2+ INDJ*(INDJ+1)*P*P*R2)
      SIGRS =  P*P*(R**(2*INDM))*(Z**INDN)
      SIGTS=(Z**INDN)*(R**(2*INDM-2))*(-4*P*R4+(2*INDM+1)*R2*P*P)
      SIGZA = P*(R**(2*INDI))*(Z**(INDJ))*(24*R4-6*(4*INDI+7)*P*R2+
     1 (2*INDI+3)*(2*INDI+2)*P*P)
      SIGRZA= (R**(2*INDI))*(Z**(INDJ-1))*P*(-24*R3*Z2+6*P*INDJ*R3+
     1 6*(2*INDI+3)*P*Z2*R-(2*INDI+3)*INDJ*P*P*R)
      X(1,NT)= (2./3.) * SIGRA - SIGZA / 3.
      X(1,NTT) = -SIGTS/3. + (2./3.)*SIGRS
      X(2,NT) = -SIGRA/3.0 - SIGZA/3.0
      X(2,NTT) = (2./3.)*SIGTS - SIGRS/3.0
      X(3,NT) = SIGRZA
      X(3,NTT) = 0.0
      IF(N.LT.NSBOND) GO TO 106
      X(4,NT)= (SIGRA-SIGZA)*SIN(2.0*ALPHA)/2.0 + SIGRZA*COS(2.0*ALPHA)
      X(4,NTT) = SIGRS*SIN(2.0*ALPHA) / 2.
  106 CONTINUE
```

```
      X(1,NP1)       = HP/3.
      X(1,NP2)  =( STK          *VE*RF*RF*(Z3-3.*R2*Z))/(P1*P1*P1)
      X(2,NP1)  = HP/3.
      X(2,NP2)  =( STK          *VE*RF*RF*Z)/(P1*P1)
      X(3,NP1)  =(STK           *VE*RF*RF*(R3-7.*R*Z2))/(2.0*P1*P1*P1)
      X(4,NP1)  = -Q*STK
      X(6,NP2)       = HP*SIN(2.*ALPHA)/2.
      IF(N.GE. NSBCND) NERR= NERREN
      DO 103 LT= 1,NERR
      DO 101  J= 1,K
      DO 101 I = 1, K
      A(I,J)= A(I,J) + X(LT,I) *  X(LT,J) * G(LT) * FACT
  101 CONTINUE
  103 CONTINUE
  102 CONTINUE
      JJ = 1
      DO 105 J = 1, NPARAM
      C(J) =0.0
      M = NPARAM + 1
      DO 104 I = 1, NPARAM
      B(JJ) = A(J,I)
      JJ = JJ + 1
  104 CONTINUE
      DO 107 I = 1, NVAR
      C(J) = C(J) - A(J,M)
      M = M+1
  107 CONTINUE
  105 CONTINUE
      CALL SIMQ (B, C, NPARAM, 1)
  122 CONTINUE
      DO 132 I = 1, NNODE
      HP = -SQRT(3.0) * AK1
      IF(I .GT. NENODE) HP = -SQRT(3.0) * AK2
      R = ORGR(I)
      Z = ORGZ(I)
      SIGMAR(I)=0.0
      SIGMAT(I)=0.0
      SIGMAZ(I)=0.0
      SIGMRZ(I)=0.0
      Z2 = Z*Z
      Z3 = Z2*Z
      Z4 = Z2 * Z2
      R2 = R*R
      R3 = R2 * R
      R4 = R2*R2
      P1 = R2 + Z2
      P= RI*RI - P1
      VR(I)=-(VE*RF*RF*P*Z) / (P1*P1)
      VZ(I) = -(VE*RF*RF*Z2)/(P1*P1)
      DO 131 NL= 2,NTERM1
      DO 131 NK= 1,NTERM2
      INDN = NK -1
      INDM= NL
      INDI= NK-1
      INDJ = NL - 1
      IND=NK+ (NL - 1)*NTERM1
      INDD = IND+NTERM1*NTERM2
      SIGRA=(R**(2*INDI))*(Z**(INDJ-2))*P*(24*R4*R2-6*P*Z2*(2*INDJ+1)
     1 *R2+ INDJ*(INDJ+1)*P*P*R2)
      SIGRB  =  R**(2*INDM)*(Z**INDN)
      SIGTB=(Z**INDN)*(R**(2*INDM-2))*(-4*P*R4+(2*INDM+1)*R2*P*P)
      SIGZA = R**(2*INDI)*(Z**(INDJ))*(24*R4-6*(4*INDI+7)*P*R2+
     1 (2*INDI+3)*(2*INDI+5)*P*P)
      SIGRZA= (R**(2*INDI))*(Z**(INDJ-1))*P*(-24*R3*Z2+6*P*INDJ*R3+
     1 6*(2*INDI+3)*P*Z2*R-(2*INDI+3)*INDJ*P*P*R)
      SIGMAR(I)=SIGMAR(I) + C(IND)*SIGRA + C(INDD)*SIGRB
      SIGMAT(I)= SIGMAT(I) + C(IND)*SIGTB
      SIGMAZ(I)= SIGMAZ(I) + C(IND)*SIGZA
      SIGMRZ(I)= SIGMRZ(I) + C(IND)*SIGRZA
  131 CONTINUE
      SIGMAZ(I)= SIGMAZ(I) - HP
  132 CONTINUE
      AVER1 = 0.0
      JJ = NSBCND - 1
      J = NCNODE + 1
      DO 200 I = J,JJ,NCNODE
  200 AVER1=AVER1+SIGMAZ(I)*ORGR(I)*(ORGR(I+NCNODE)-ORGR(I-NCNODE))
      AVER1= AVER1/(ORGR(NSBCND)*ORGR(NSBCND))
      R = ORGR(NENODE) * ORGR(NENODE)
      RR = ORGR(NNODE) * ORGR(NNODE)
      AVER2 =(SIGMAZ(NENODE-NCNODE)*R+SIGMAZ(NNODE-NCNODE)*(RR-R))/RR
      AVER = AVER1 + AVER2
  124 RETURN
      END
```

FIGURE 38

Subroutine TEMPD

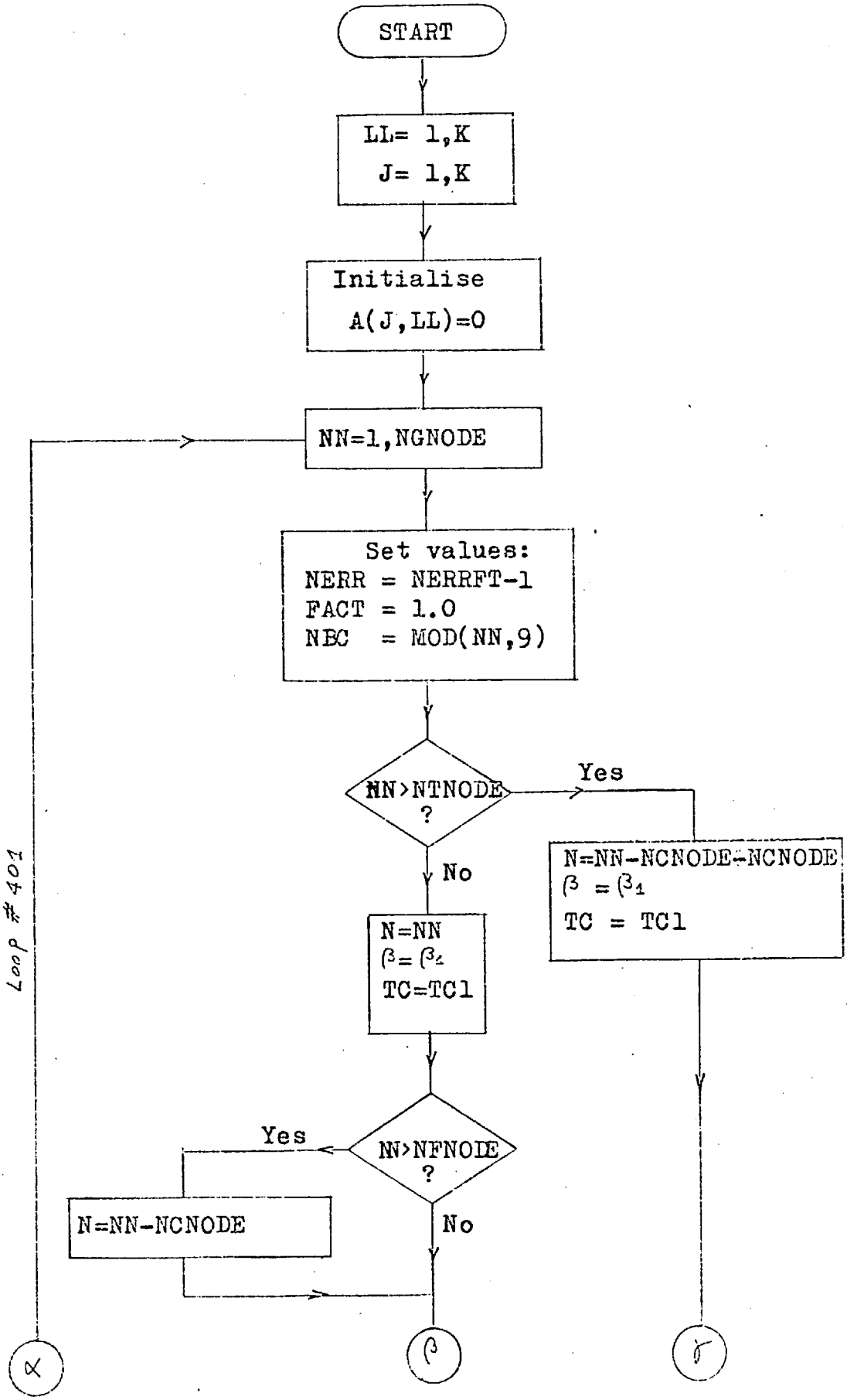

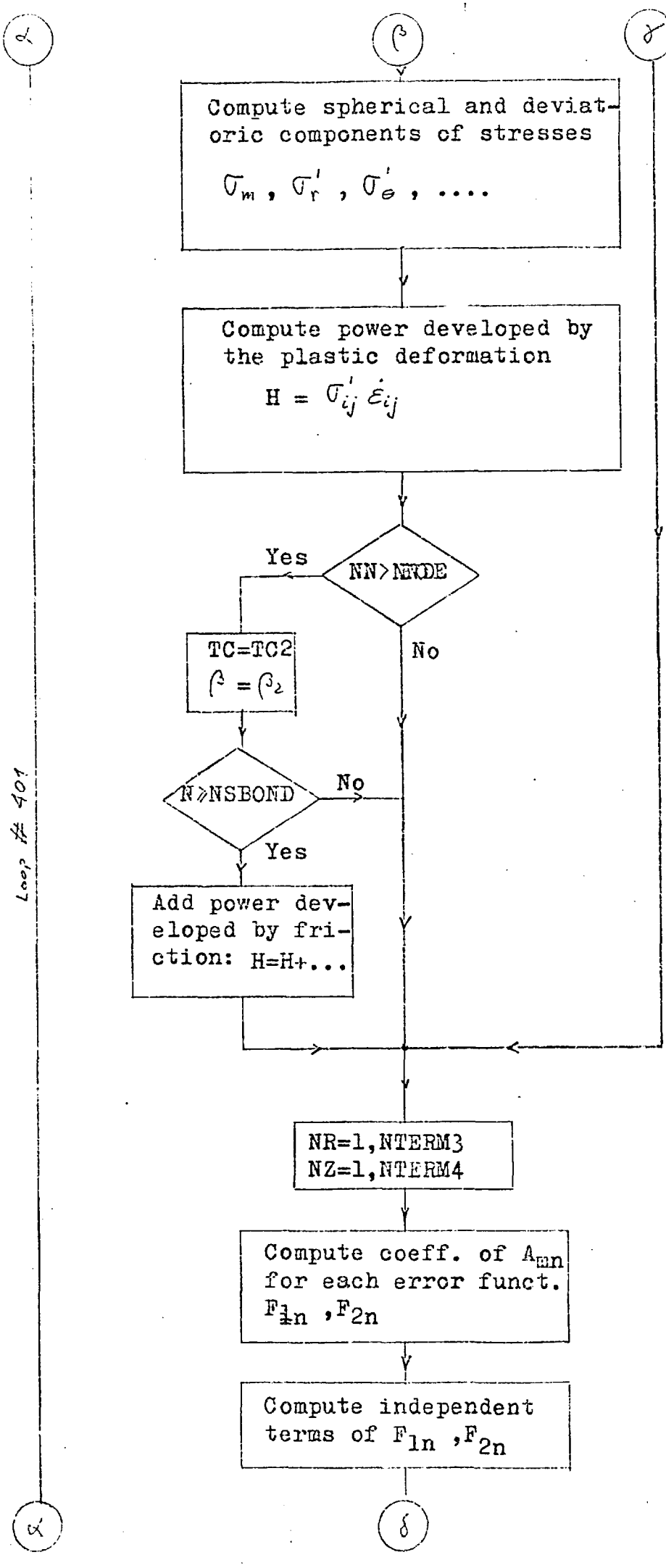
α
β
γ
Compute spherical and deviatoric components of stresses
σ_m , σ_r' , σ_θ' , ...
Compute power developed by the plastic deformation
H = $\sigma_{ij}' \dot{\varepsilon}_{ij}$
Yes
NN>NEXDE
No
TC=TC2
$\beta = \beta_2$
N≥NSBOND
No
Yes
Add power developed by friction: H=H+...
NR=1,NTERM3
NZ=1,NTERM4
Compute coeff. of A_{mn} for each error funct. F_{1n} , F_{2n}
Compute independent terms of F_{1n} , F_{2n}
δ
Loop # 401

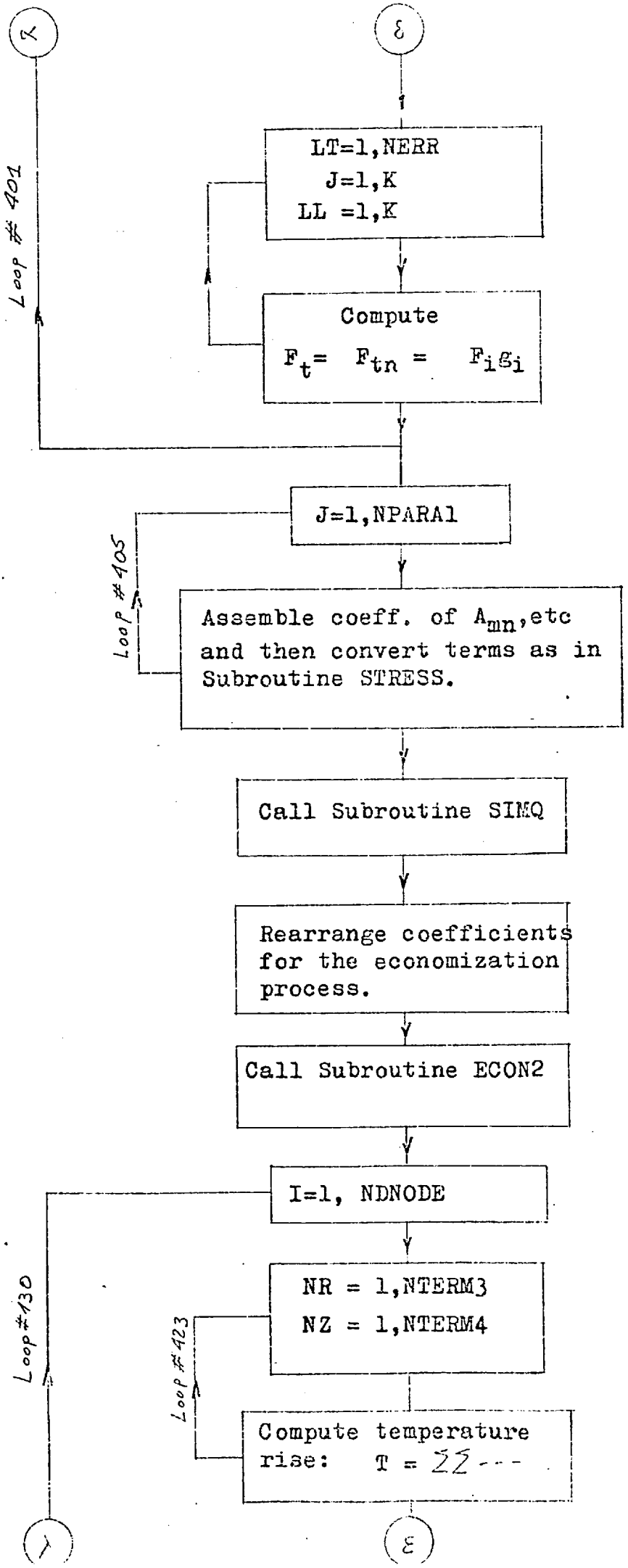
κ
ε
LT=1,NERR
J=1,K
LL =1,K
Loop # 401
Compute
$F_t = F_{tn} = F_i g_i$
J=1,NPARA1
Loop #405
Assemble coeff. of A_{mn},etc and then convert terms as in Subroutine STRESS.
Call Subroutine SIMQ
Rearrange coefficients for the economization process.
Call Subroutine ECON2
I=1, NDNODE
Loop #130
NR = 1,NTERM3
NZ = 1,NTERM4
Loop #423
Compute temperature rise: T = ΣΣ---
λ
ε

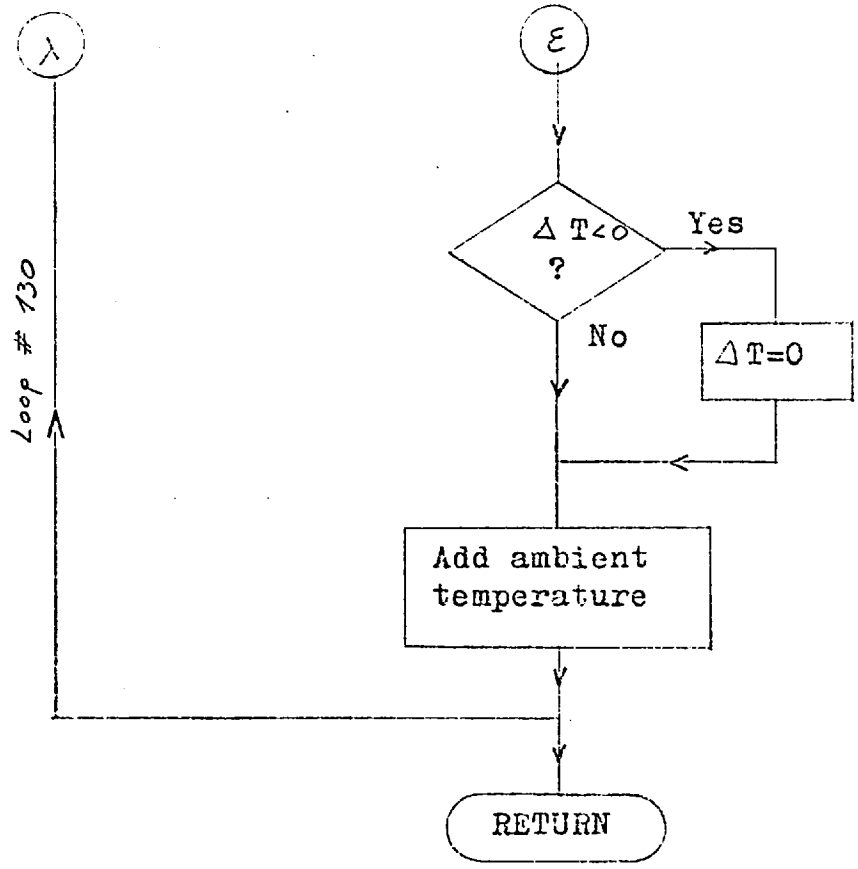

FIGURE 39

```
      SUBROUTINE TENSO
      COMMON NEFFN,NTERM1,NTERM2,NVAR,NEFF1,NTERM3,NTERM4,NVART,
     3   NONODE,NNODE,NFNODE,NSBOND,NADIVT,NADIVB,NSINT,
     2   RF, PI, ALPHA2, ALPHA, ALPHA1, AE, G, AK1, AK2, CK1, CK2, TINI,
     3   TC1, TC2, BETA1, BETA2, NTNODE, NSLOND, NSNODE, NPARA1,NPARA2,
     4   A(2,2),B(2),D(2),E(2),E(4), WF( 2), X(4,2),
     5   ORGR(144), ORGZ(144), RADS( 9), STRNRT(4,99), SINVEF(144),
     6   SK(2,2), VR(144), VZ(144), SIGMAR(99), SIGMAZ(99),
     7   SIGMAT( 99), STRAZT( 99),TEMP(144) ,AVER, AVER1, AVER2
      REAL L
      K= NTERM3 * NTERM4 + NVART
      DO 4 9  LL=1,K
      DO 409 J=1,K
  409 A(J,LL) = 0.0
      DO 401 NN = 1,NONODE
      NERR = NEFFT - 1
      FACT = 1.0
      NBC = MOD(NN,9)
      IF(NN .GT. NTNODE) GOTO 3200
      N=NN
      IF(NN .GT. NFNODE) N = NN-NONODE
      SIGMAM = (SIGMAR(N)+SIGMAT(N)+SIGMAZ(N))/3.0
      DSTR1 = SIGMAR(N) - SIGMAM
      DSTR2 = SIGMAT(N) - SIGMAM
      DSTR3 = SIGMAZ(N) - SIGMAM
      DSTR4 = SIGMAZ(N)
      H = (ABS(DSTR1*STRNRT(1,N)) + ABS(DSTR2*STRNRT(2,N))+ ABS(DSTR3*
     1  STRNRT(3,N)) + ABS(DSTR4*STRNRT(4,N))) * 1.0E-6
      IF(NN.GT. NFNODE) GO TO 3200
      TC= TC1
      BETA= BETA1
      R = ORGR(N)
      Z = ORGZ(N)
      GO TO 3115
 3200 TC = TC2
      BETA=BETA2
      R = ORGR(N)
      Z = ORGZ(N)
      P1= R*R + Z*Z
      IF(N.GE.NSBOND)H   =1   -VE*RF*RF*0*AK2*COS(ALPHA)*((2*R*
     1  COS(ALPHA)/(P1**2)) - (COS(ALPHA)/(R*P1)) - (2*Z*SIN(ALPHA)/
     2  (P1*P1 )))*1.0E-6
      GO TO 3115
 3105 N = NN - NONODE  - NONODE
      TC=TC1
      BETA= BETA1
      H = 0.0
      R= ORGR(N)
      Z= ORGZ(N)
 3115 Z2= Z*Z
      Z3=Z2*Z
      Z4=Z2*Z2
      R2= R*R
      R3=R2*R
      R4= R2*R2
      P1= R2 + Z2
      PI= RI*RI - P1
      TA= TAN(ALPHAE)
      L= TA * Z - R
      VRR=ABS(VR(N))
      VZZ= ABS(VZ(N))
      DO 409 NR = 1,NTERM3
      DO 402 NZ = 1,NTERM4
      INDR= NR-1
      INDZ= NZ
      NT= NZ+ (NR-1) * NTERM4
   21 X(1,NT)  =  (R**(2*INDR-2))*(Z**(INDZ-2))*
     1  ((2*INDR-1)*Z2*(-2*Z2*L-2*R2+2*INDR*P*L)+
     2  R*Z2*(-4*R*L+4*Z2-P-4*TA*R*L-2*INDR*P)+
     3  Z2*(-2*R2*L-2*R*P+2*INDR*P*L)+
     4  R2*(INDZ-1)*(-2*Z2*L+TA*R*Z+INDZ*R*L)+
     5  Z*R2*(-L*Z*L-4*R*Z+TA*P+INDZ*TA*P-2*INDZ*Z*L)+
     6  BETA*VRR*Z2*R*(-2*R2*L-3*R+2*INDR*P*L)+
     7  BETA*VZZ*Z*R2*(-2*Z2*L+TA*R*Z+INDZ*P*L))
   22 IF(NBC .NE. 1) GOTO 402
      X(2,NT)=(R**(2*INDR))*(Z**(INDZ-1))*(-2*Z2*L+TA*R*Z+INDZ*P*L)
  402 CONTINUE
  408 CONTINUE
      X(1,NPARA1+1) = H/TC
      X(2,NPARA1+1) = 0.0
      IF(NBC .EQ. 1 ) NERR = NEFFT
      IF((N.GE.NSINT.AND.N.LT.NFNODE).OR.(N.GE.NSBOND.AND.N. LE.NNODE))

     1 FACT = 0.25
      DO 1003 LT = 1,NERR
  416 DO 403  J= 1,K
      DO 403  LL=1,K
      A(J,LL) = A(J,LL)+X(LT,J)*X(LT,LL)*WF(LT)*FACT
  403 CONTINUE
 1003 CONTINUE
  401 CONTINUE
      JJ=1
      DO 4 5  J= 1,NPAR*1
      D(J) = 0.0
      M=NPARA1+1
      DO 406 I= 1,NPARA1
      B(JJ)= A(J,I)
      JJ=JJ+1
  406 CONTINUE
      DO 407 I=1,NVART
      D(J)= D(J) - A(J,M)
      M=M+1
  407 CONTINUE
  405 CONTINUE
      CALL SIMQ (B,D,NPARA1,1)
      DO 13  I = 1,NONODE
      TEMP1 = 0.0
      R = ORGR(I)
      Z = ORGZ(I)
      P = RI*RI -R*R -Z*Z
      TA= TAN(ALPHAE)
      L= TA * Z - R
      DO 423 NR=1,NTERM3
      DO 423 NZ=1,NTERM4
      INDR=NR-1
      INDZ=NZ
      NT= NZ* (NR-1)*NTERM4
  423 TEMP1 = TEMP1+P*L*(R**(2*INDR))*(Z**INDZ)*D(NT)
      IF( TEMP1 .LT. 0.0)  TEMP1 = 0.0
      TEMP(I) = TEMP1 + TINI
  130 CONTINUE
      RETURN
      END
```

FIGURE 40

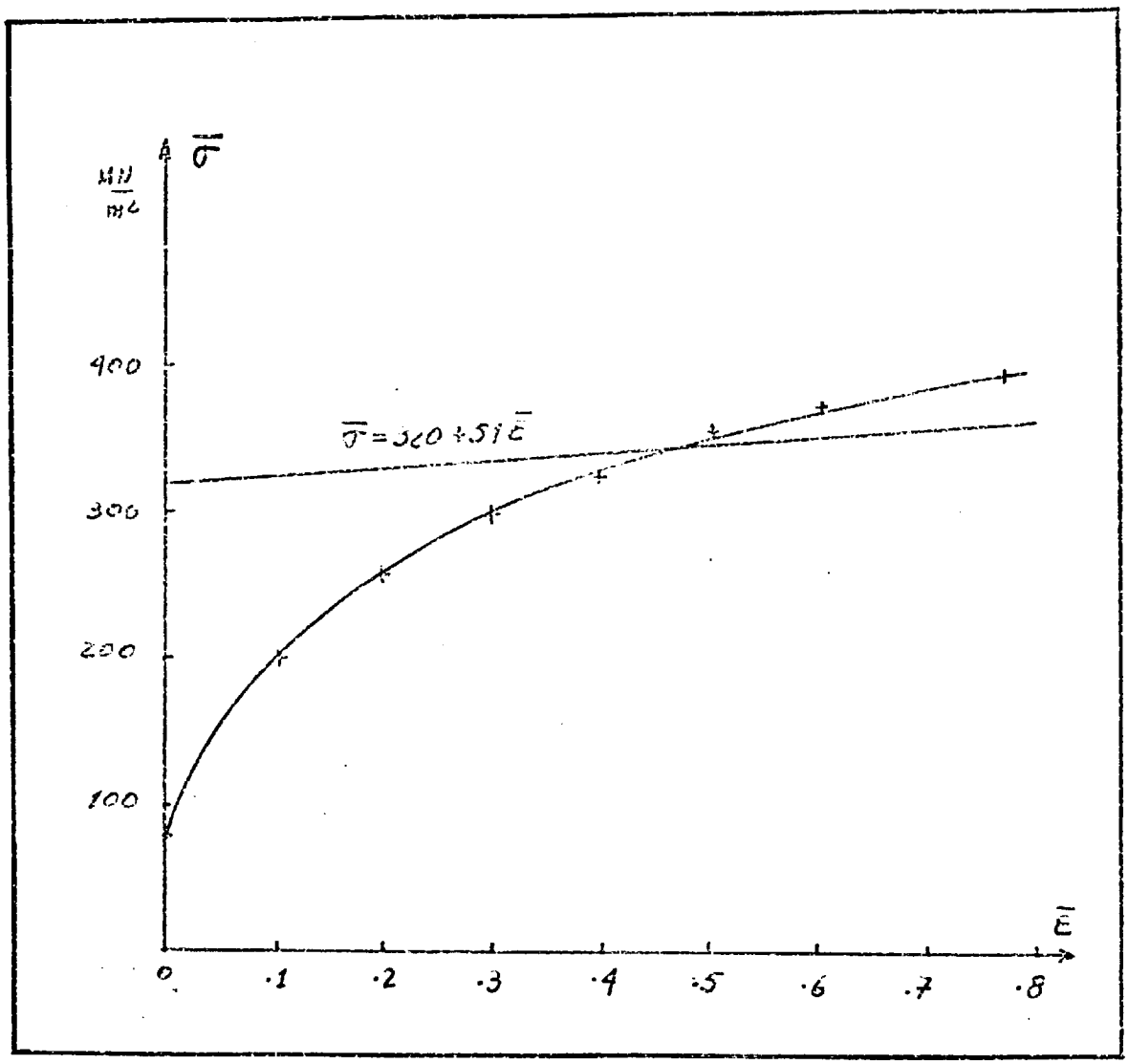

FIGURE 41 . Stress-strain curve for copper wire.

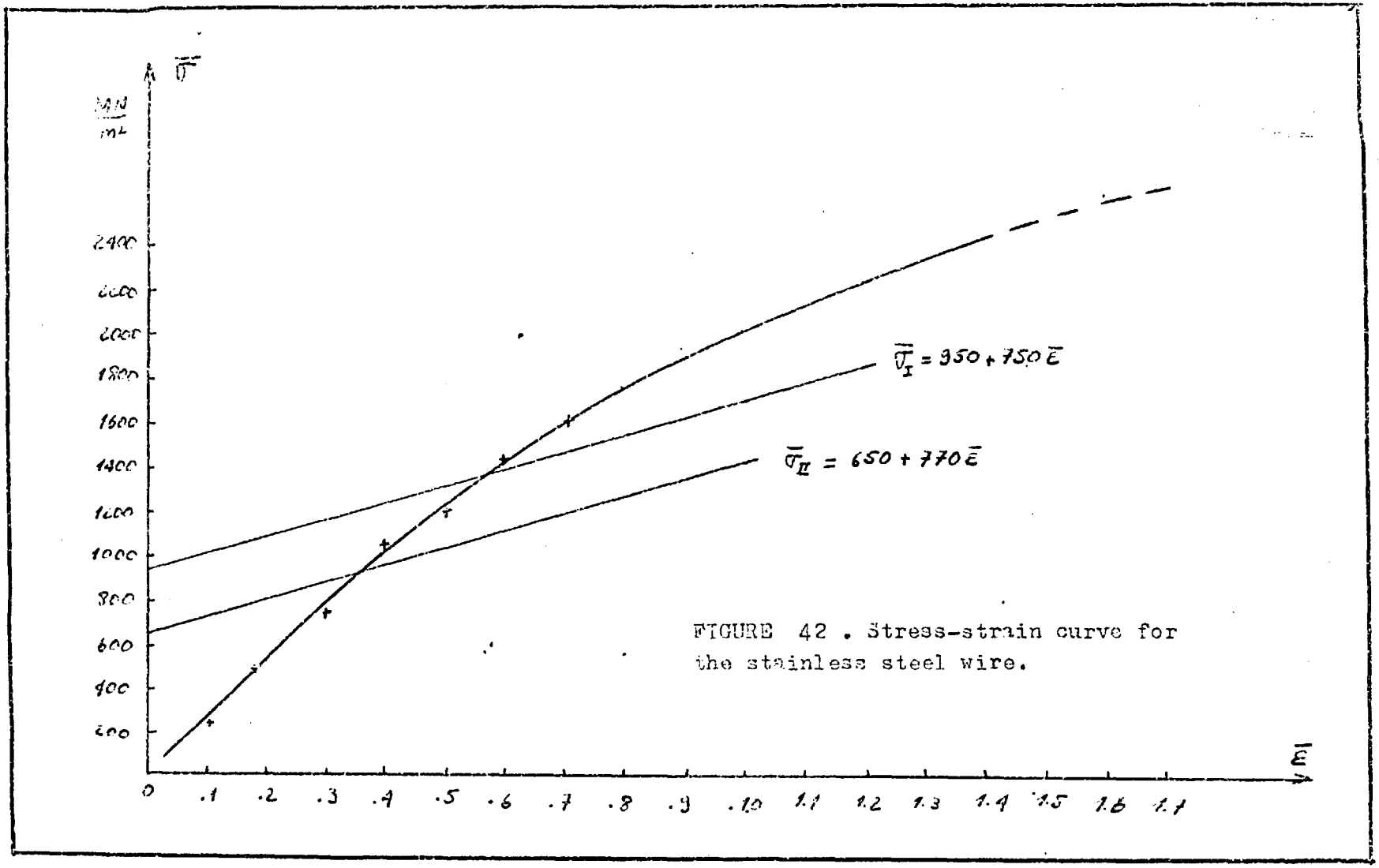

FIGURE 42 . Stress-strain curve for the stainless steel wire.

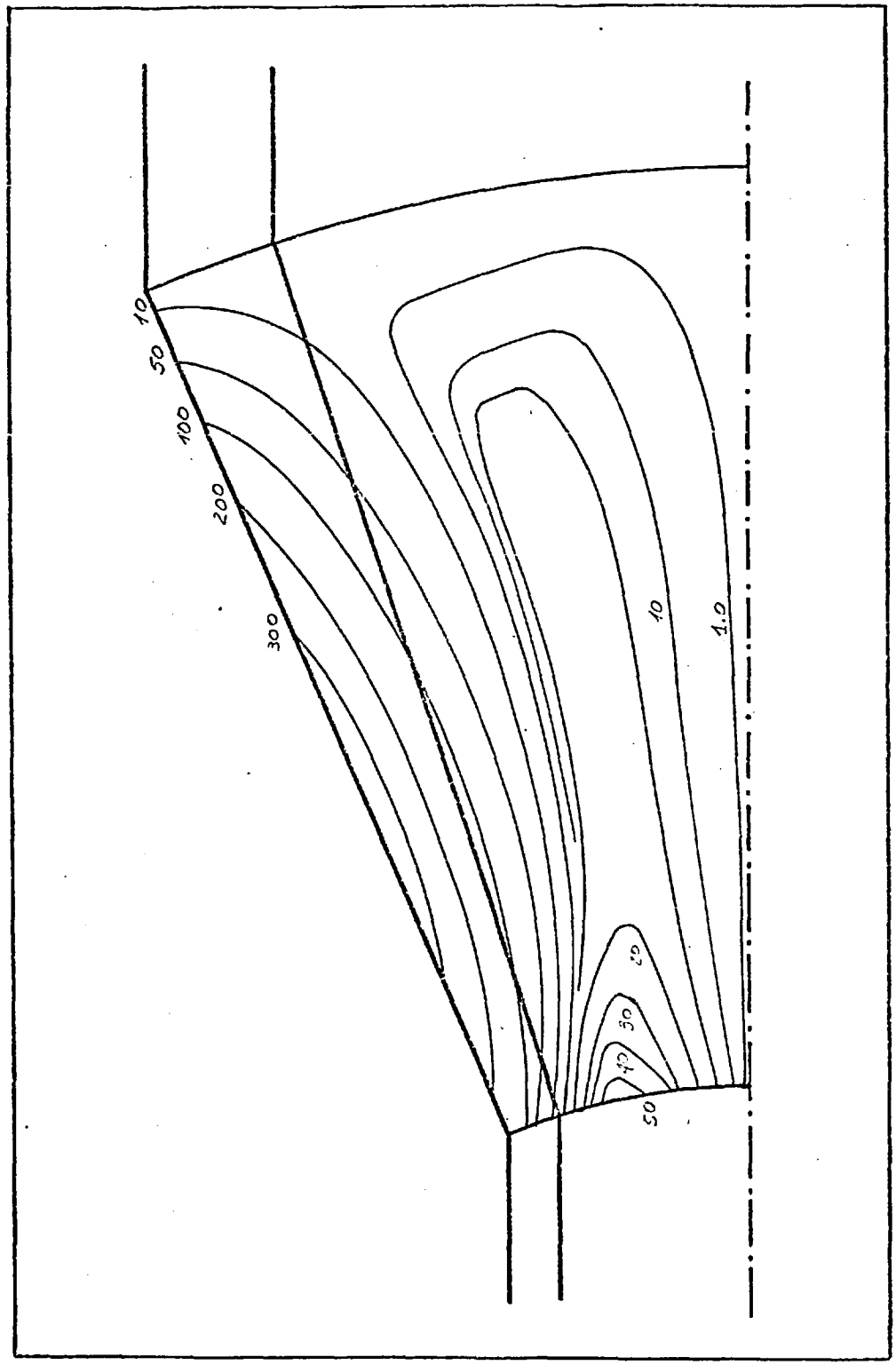

FIGURE 43: Stress distribution corresponding to $\frac{\sigma_r}{Y_o^c} \times 10^3$. Extrusion ratio 2.

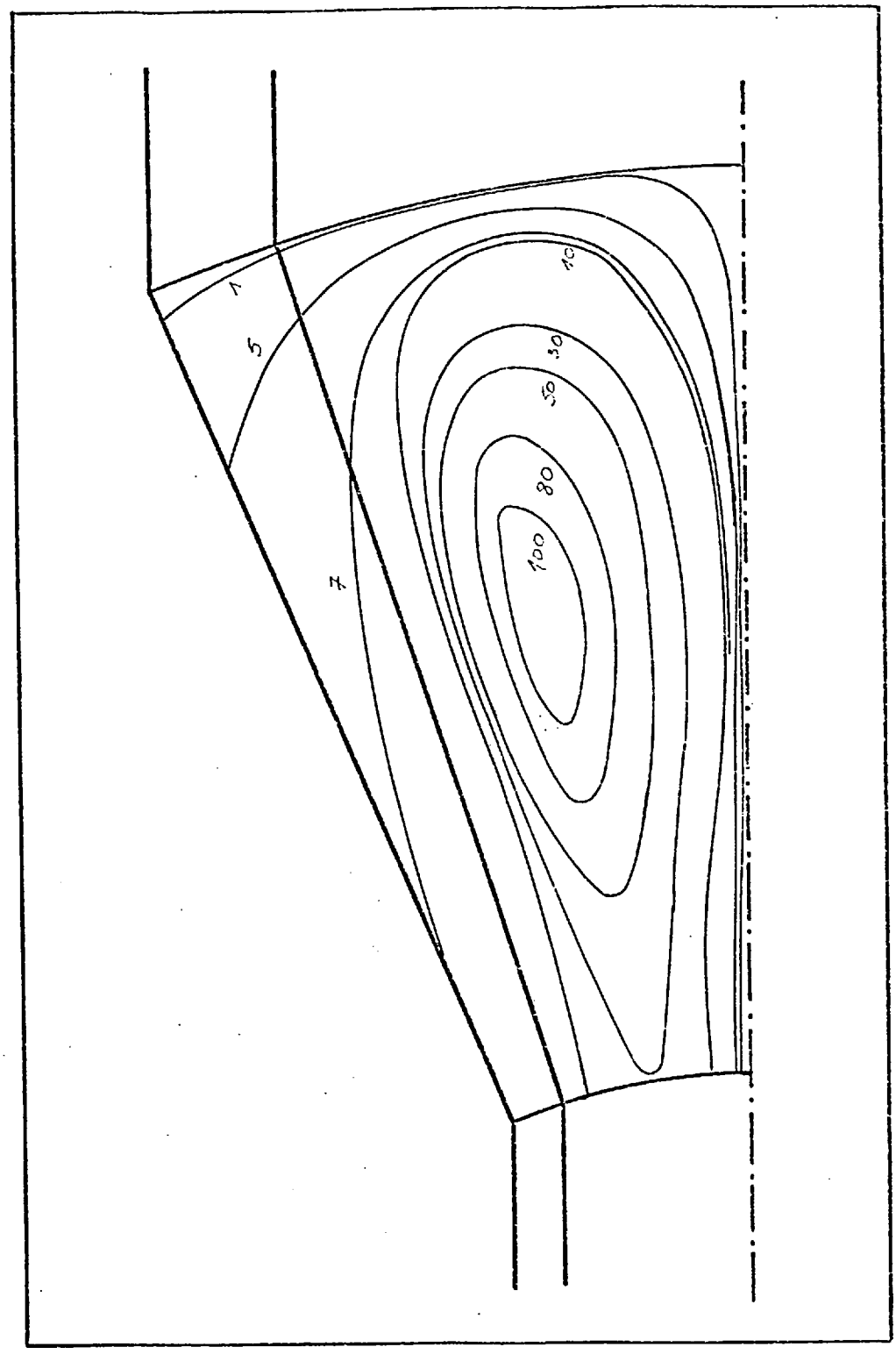

FIGURE 44: Stress distribution corresponding to $\frac{\sigma_\theta}{Y^c_o} \times 10^3$. Extrusion ratio 2.

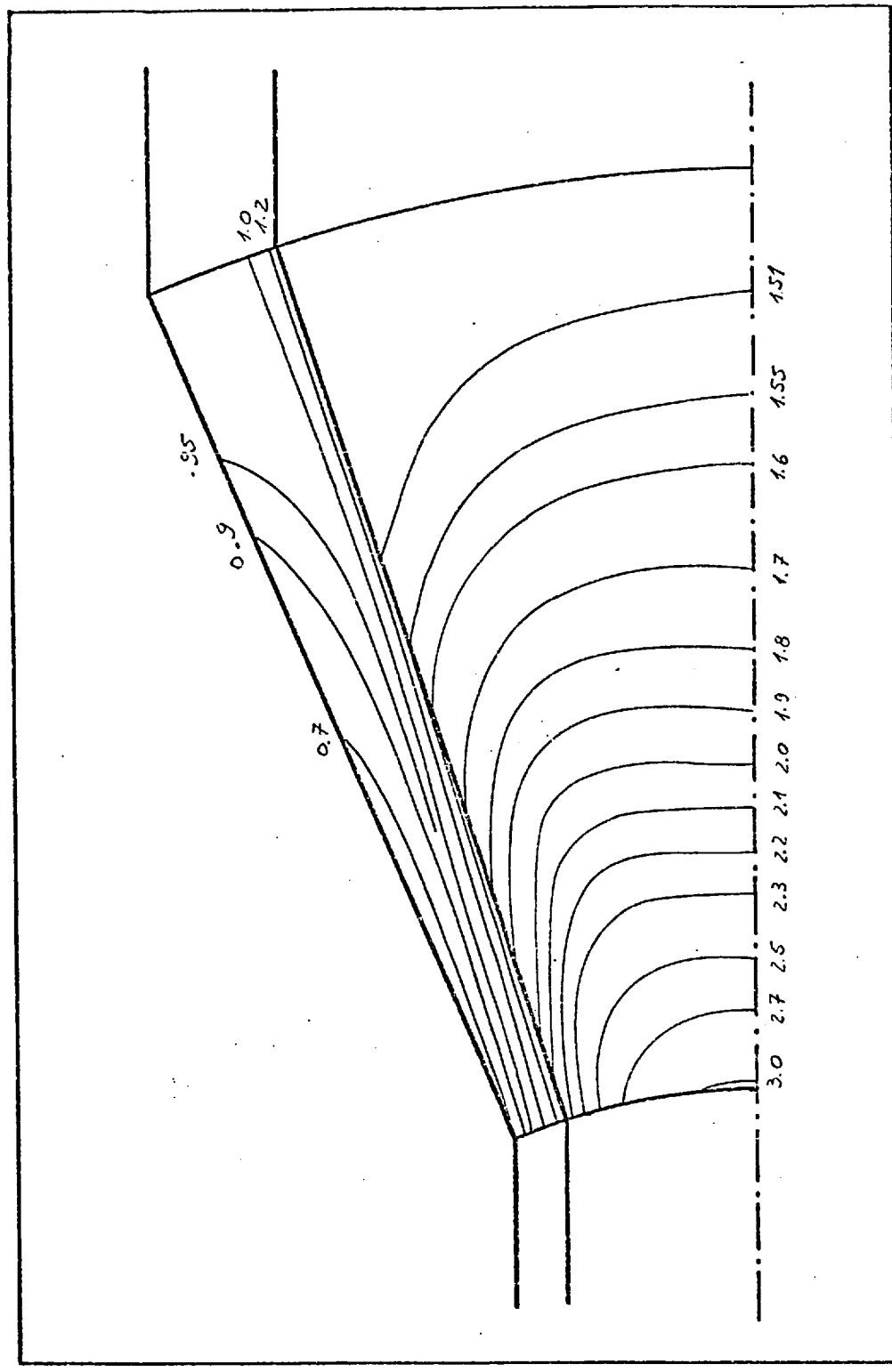

FIGURE 45: Stress distribution corresponding to $\frac{\sigma_z}{Y_o^c}$. Extrusion ratio 2.

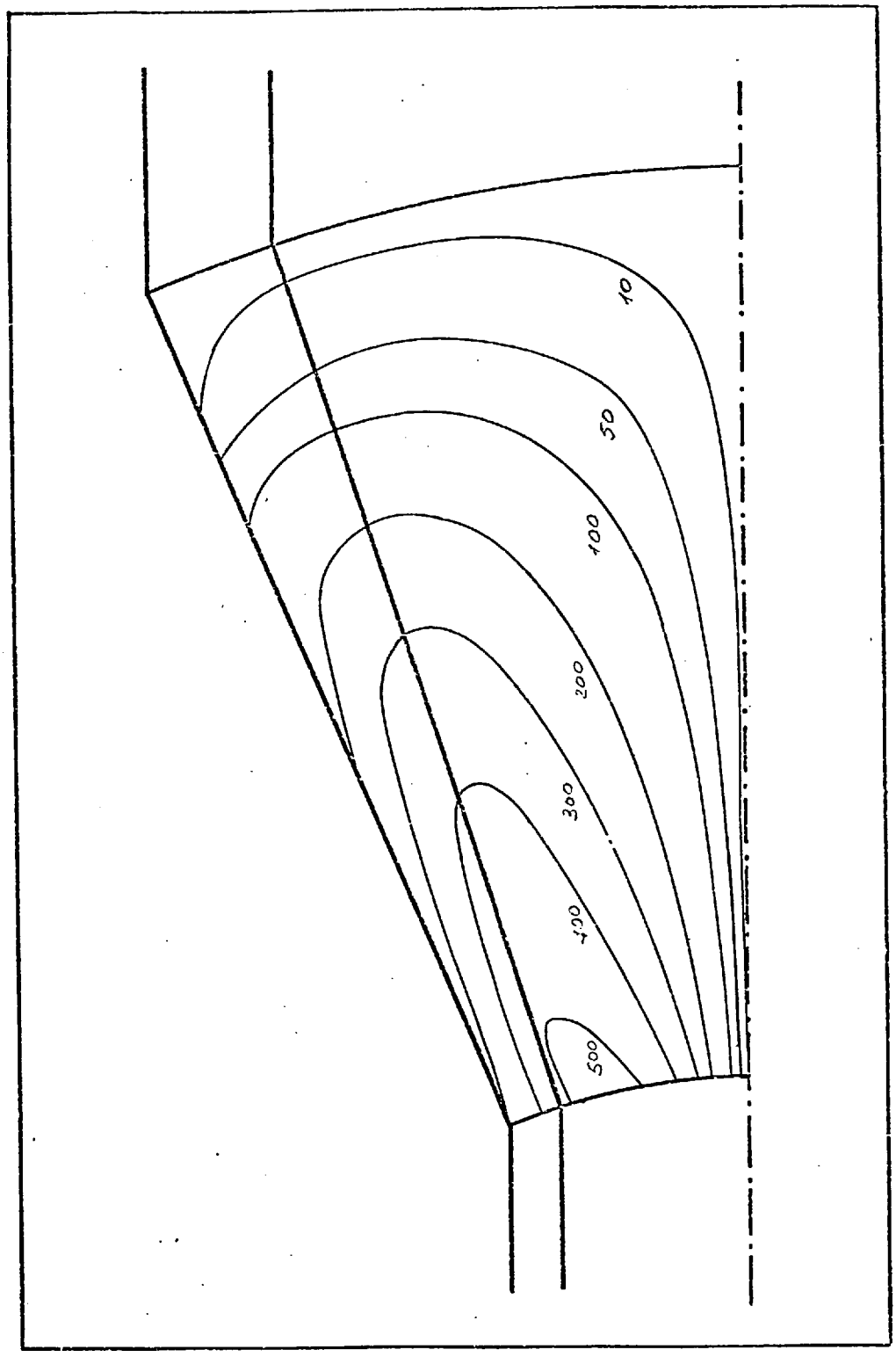

FIGURE 46: Stress distribution corresponding to $\frac{\tau_{rz}}{Y_o^c} \times 10^3$. Extrusion ratio 2.

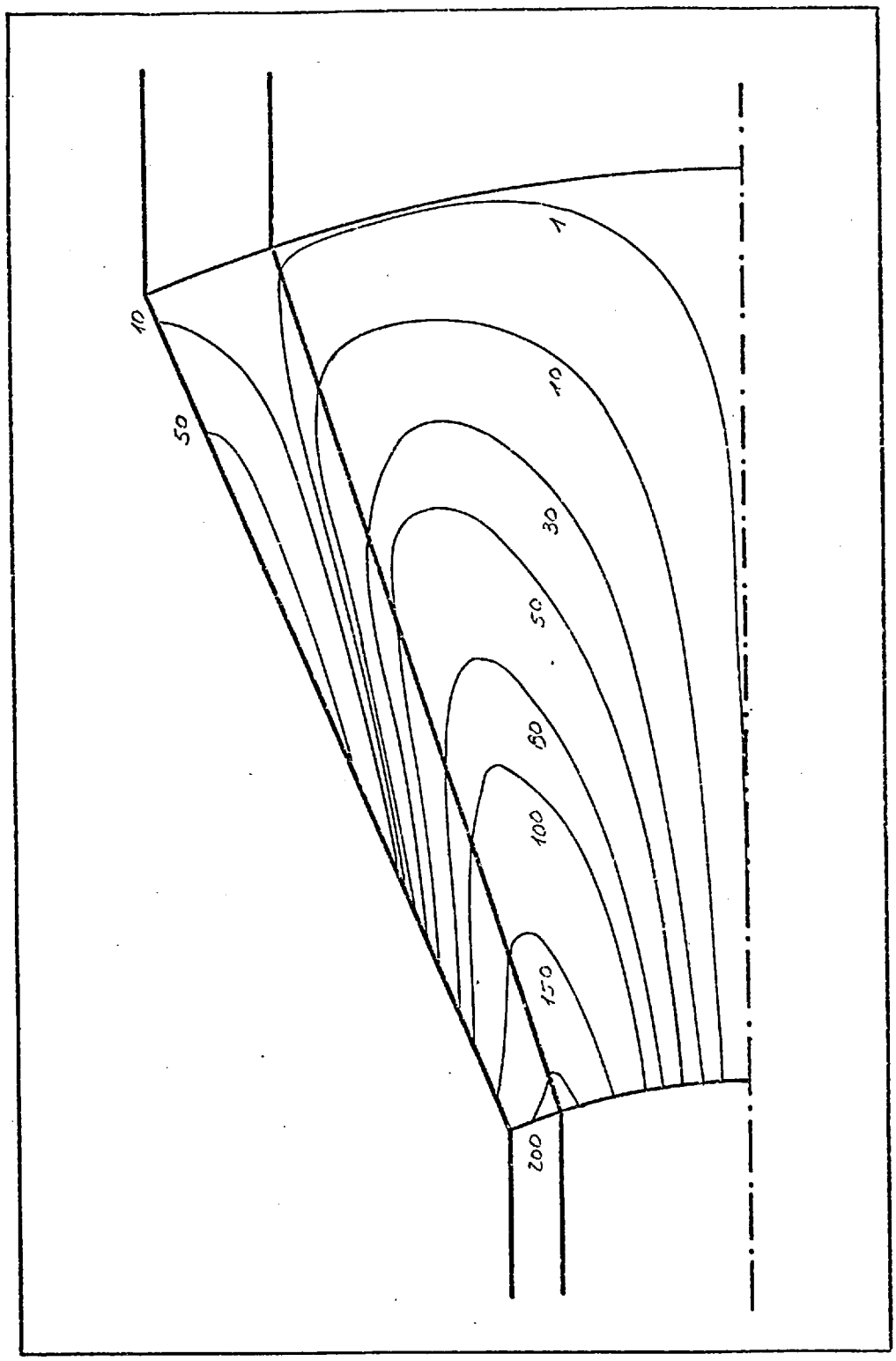

FIGURE 47: Stress distribution corresponding to $\frac{\sigma_r}{Y_o^c} \times 10^3$. Extrusion ratio 3.

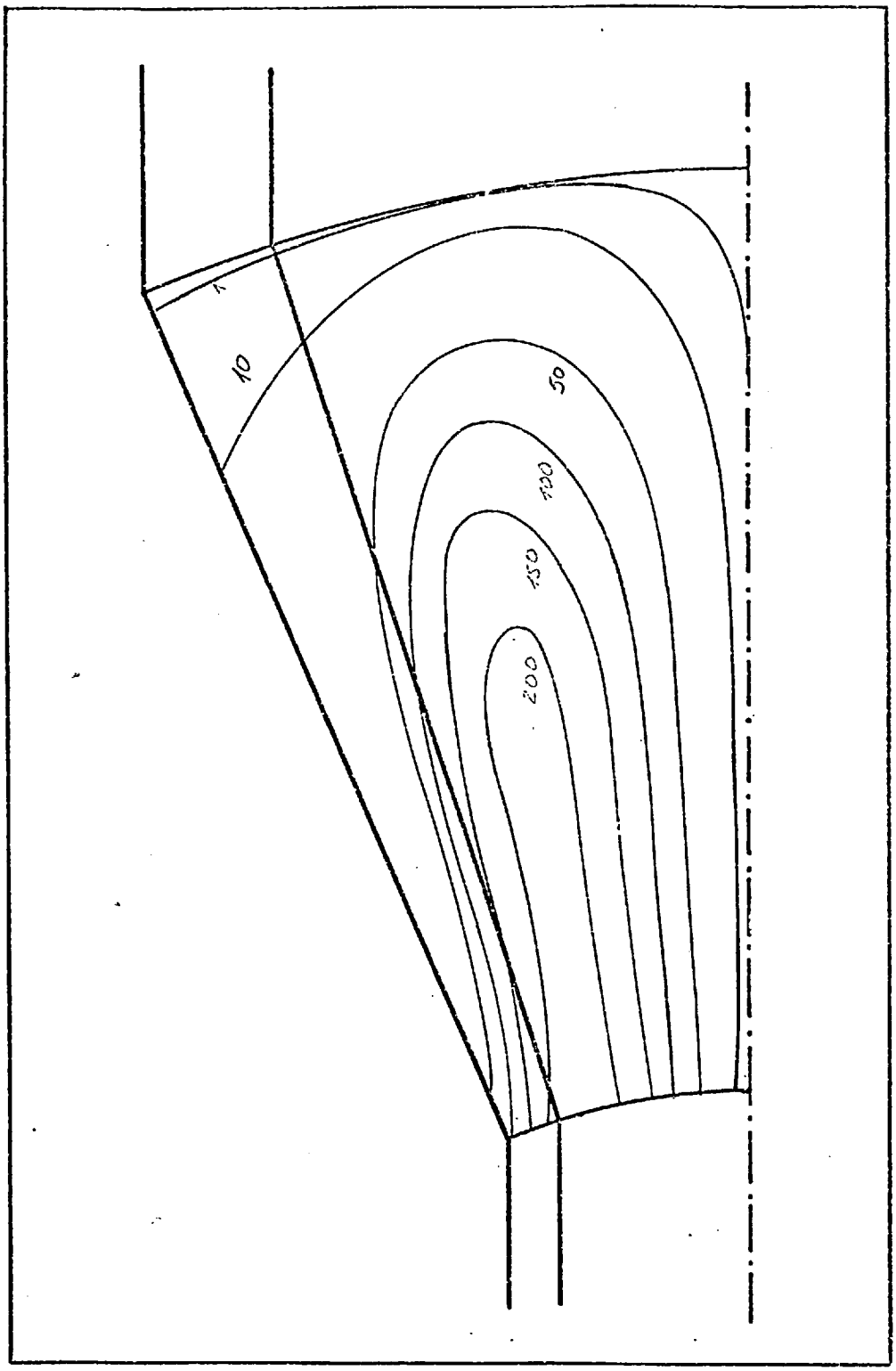

FIGURE 48: Stress distribution corresponding to $\frac{\sigma_\theta}{Y_o^c} \times 10^3$. Extrusion ratio 3.

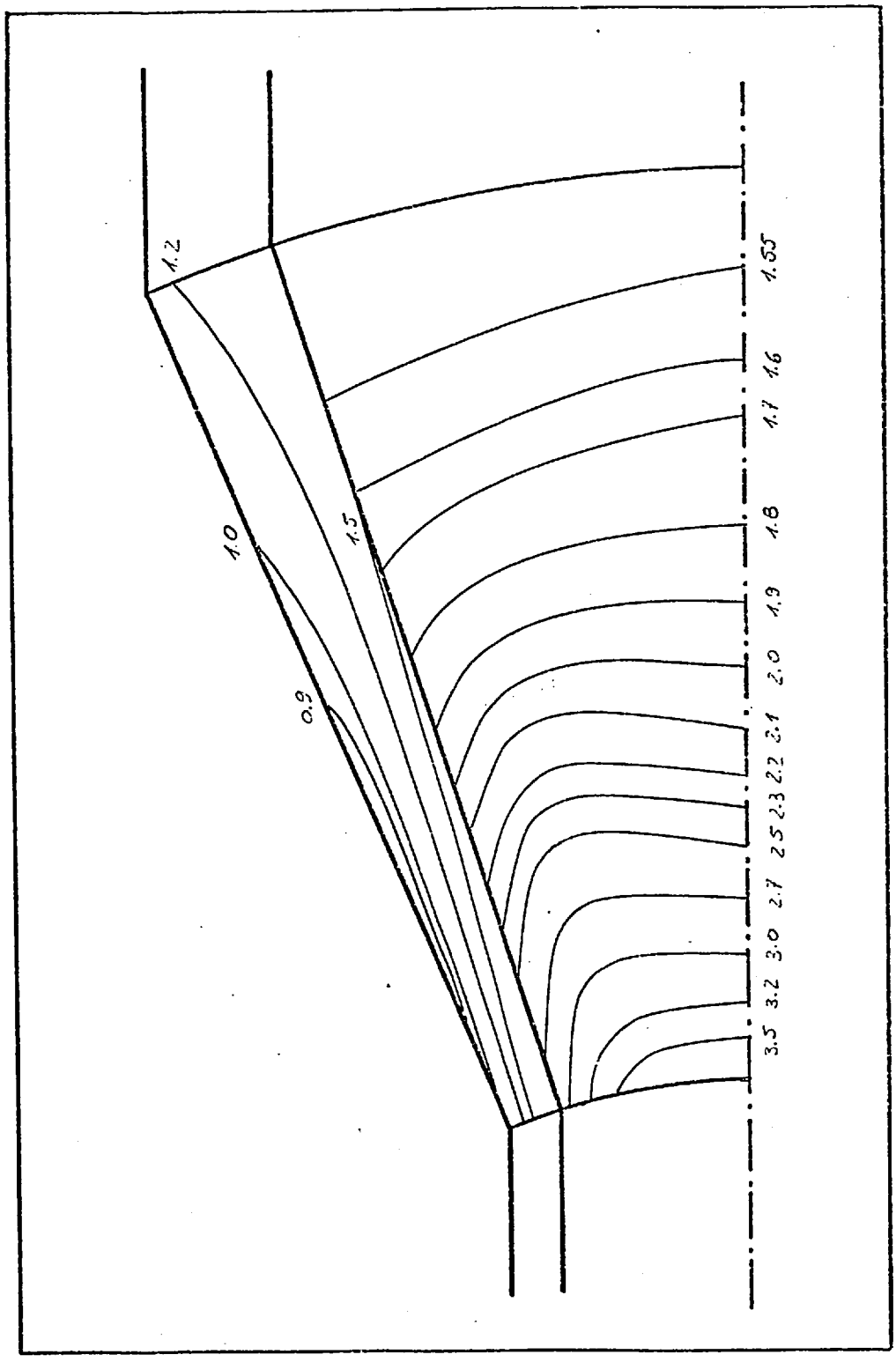

FIGURE 49: Stress distribution corresponding to $\frac{\sigma_z}{Y_o^c}$. Extrusion ratio 3.

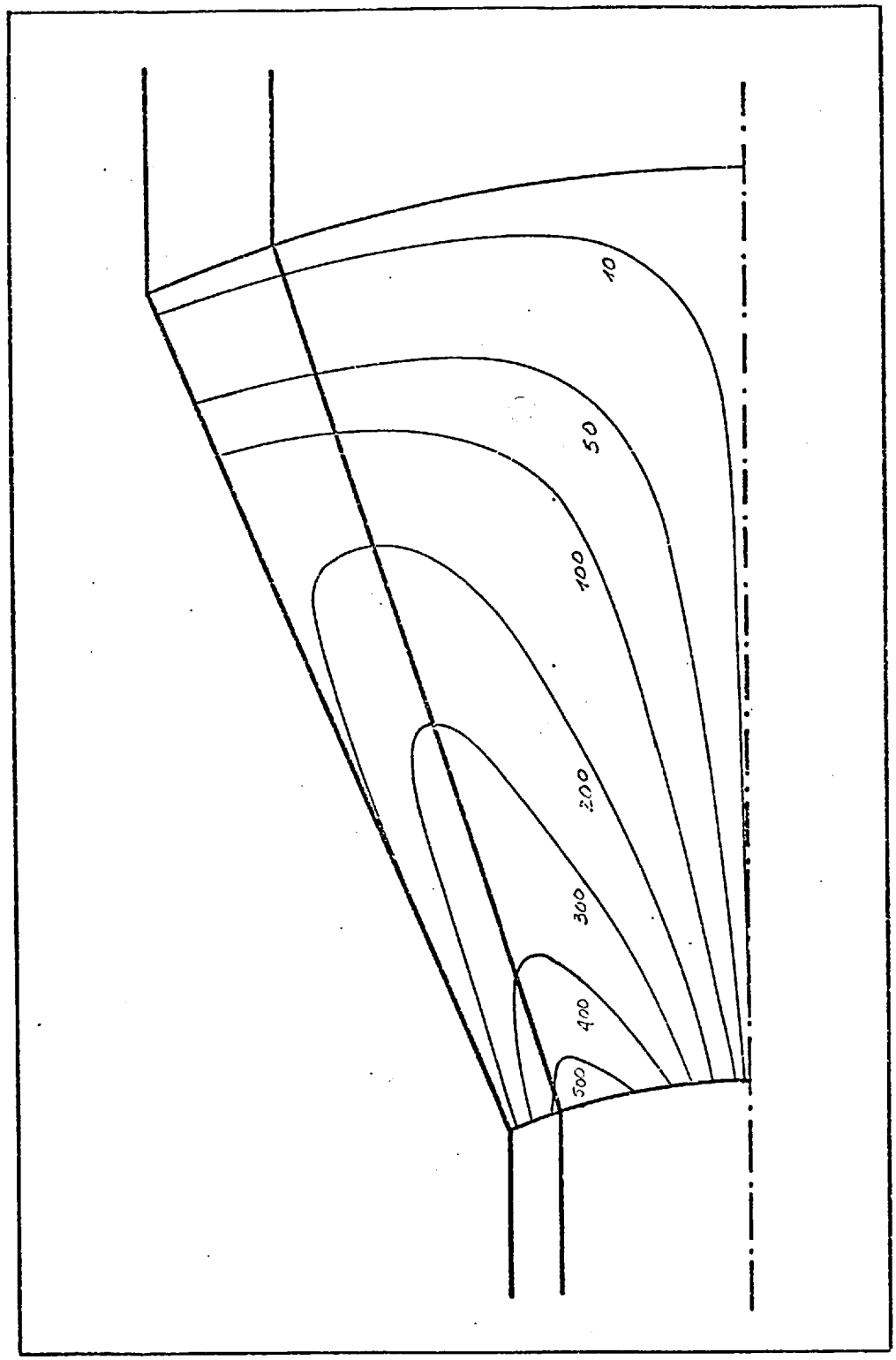

FIGURE 50: Stress distribution corresponding to $\frac{\tau_{rz}}{Y_o^c} \times 10^3$. Extrusion ratio 3.

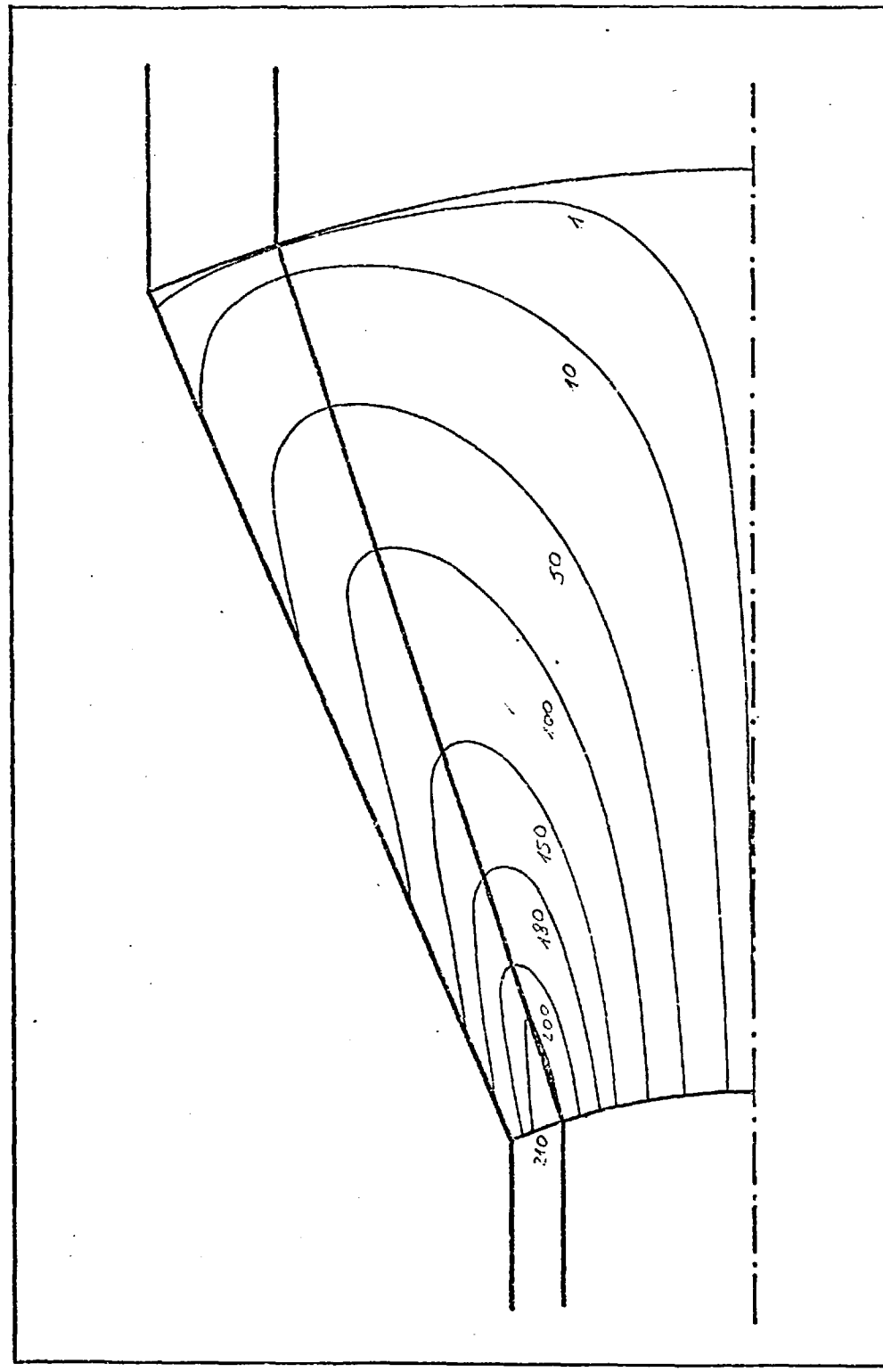

FIGURE 51: Stress distribution corresponding to $\frac{\sigma_r}{Y_o^c} \times 10^3$. Extrusion ratio 4.

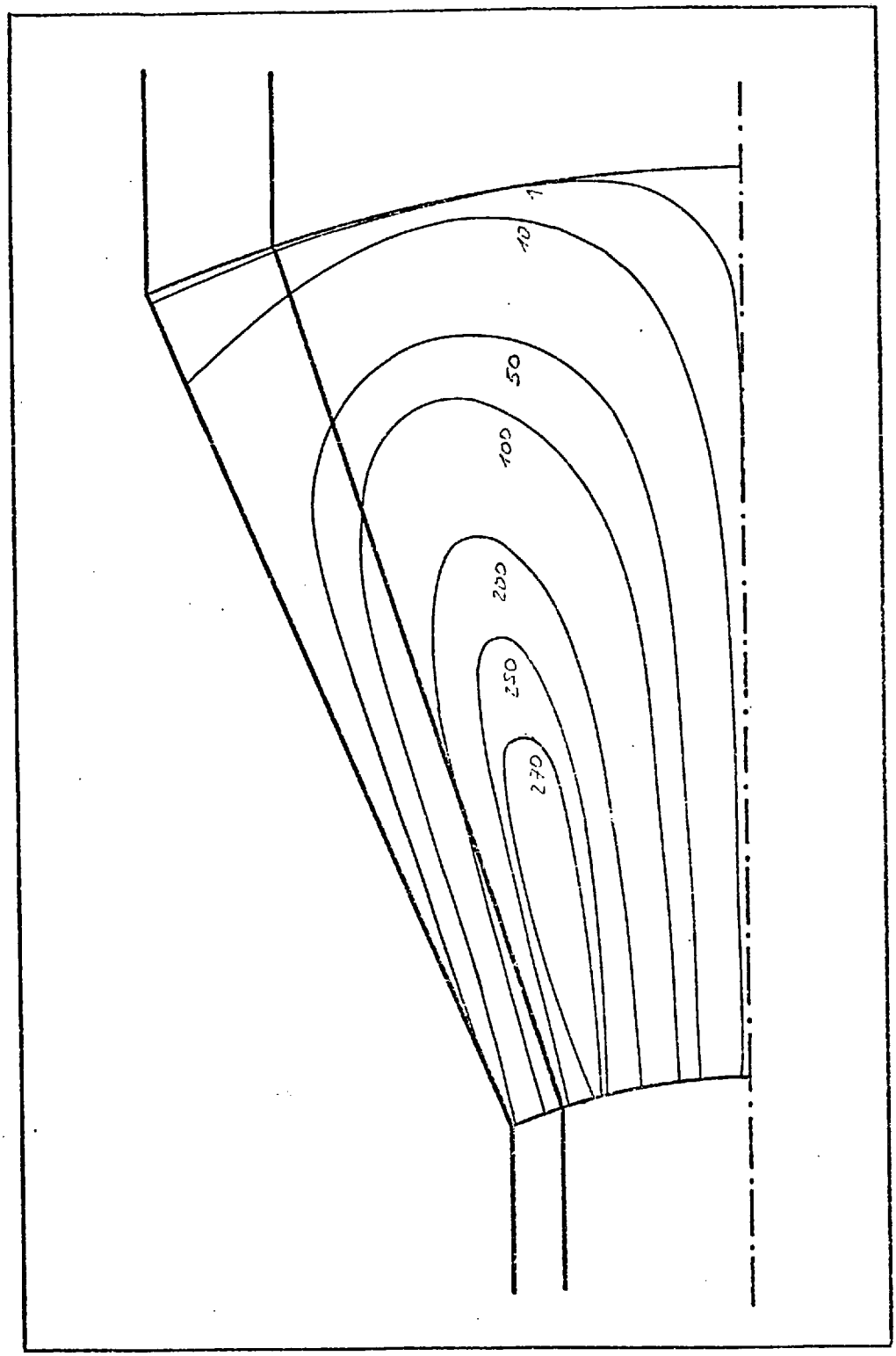

FIGURE 52: Stress distribution corresponding to $\frac{\sigma_\theta}{Y_o^c} \times 10^3$. Extrusion ratio 4.

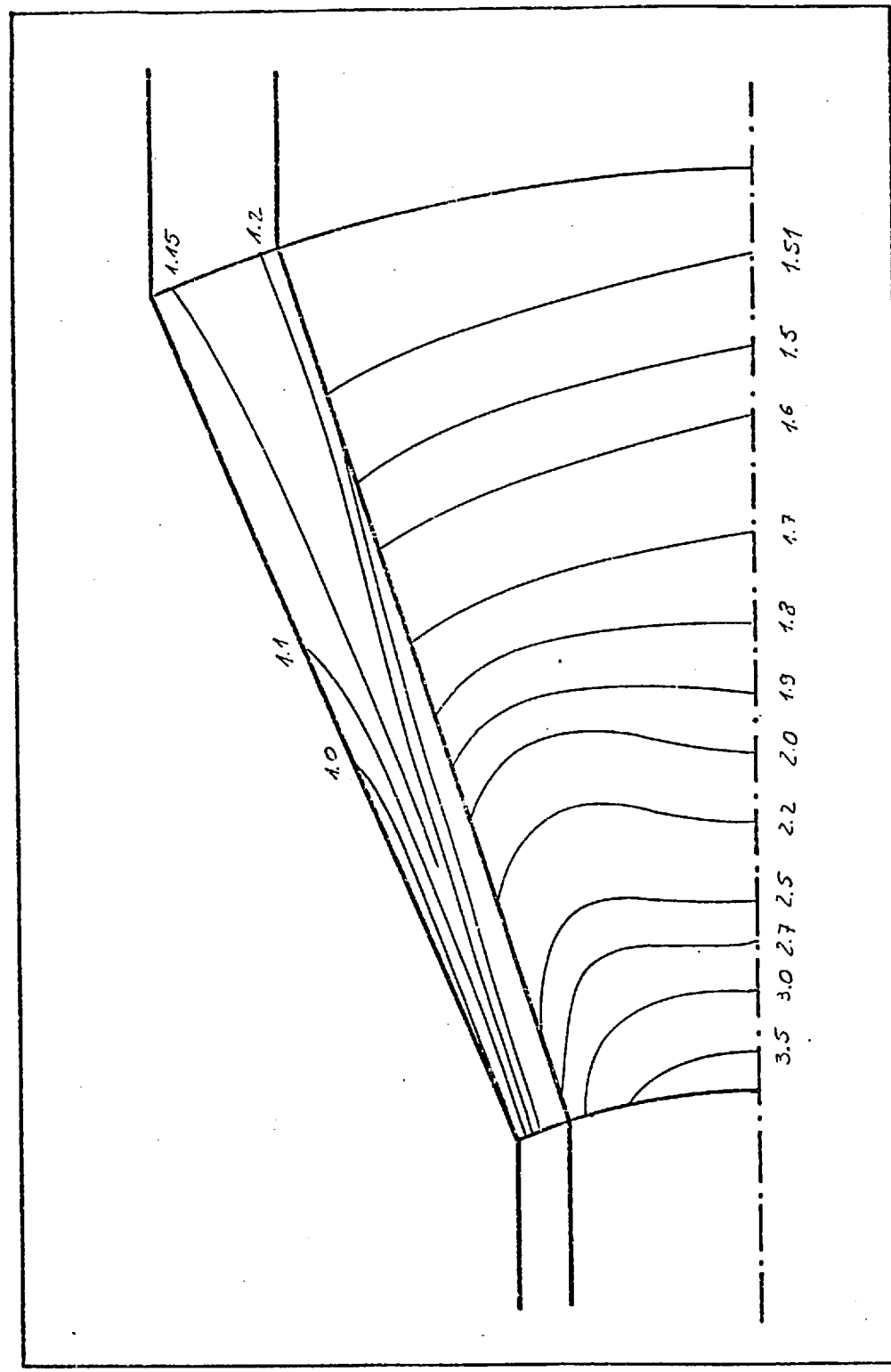

FIGURE 53: Stress distribution corresponding to $\frac{\sigma_z}{Y_o^c}$. Extrusion ratio 4.

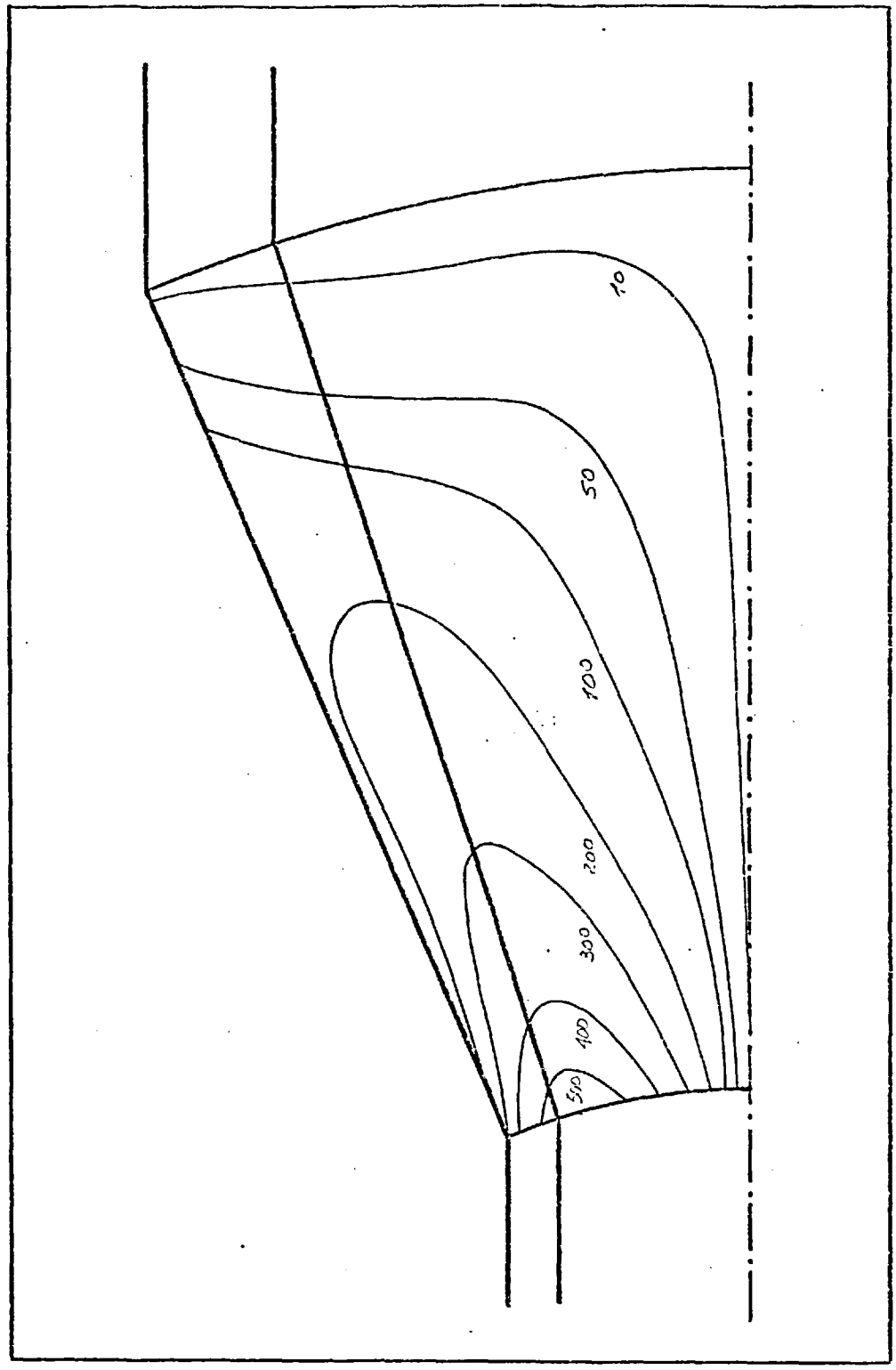

FIGURE 54: Stress distribution corresponding to $\frac{\tau_{rz}}{Y_o^c} \times 10^3$. Extrusion ratio 4.

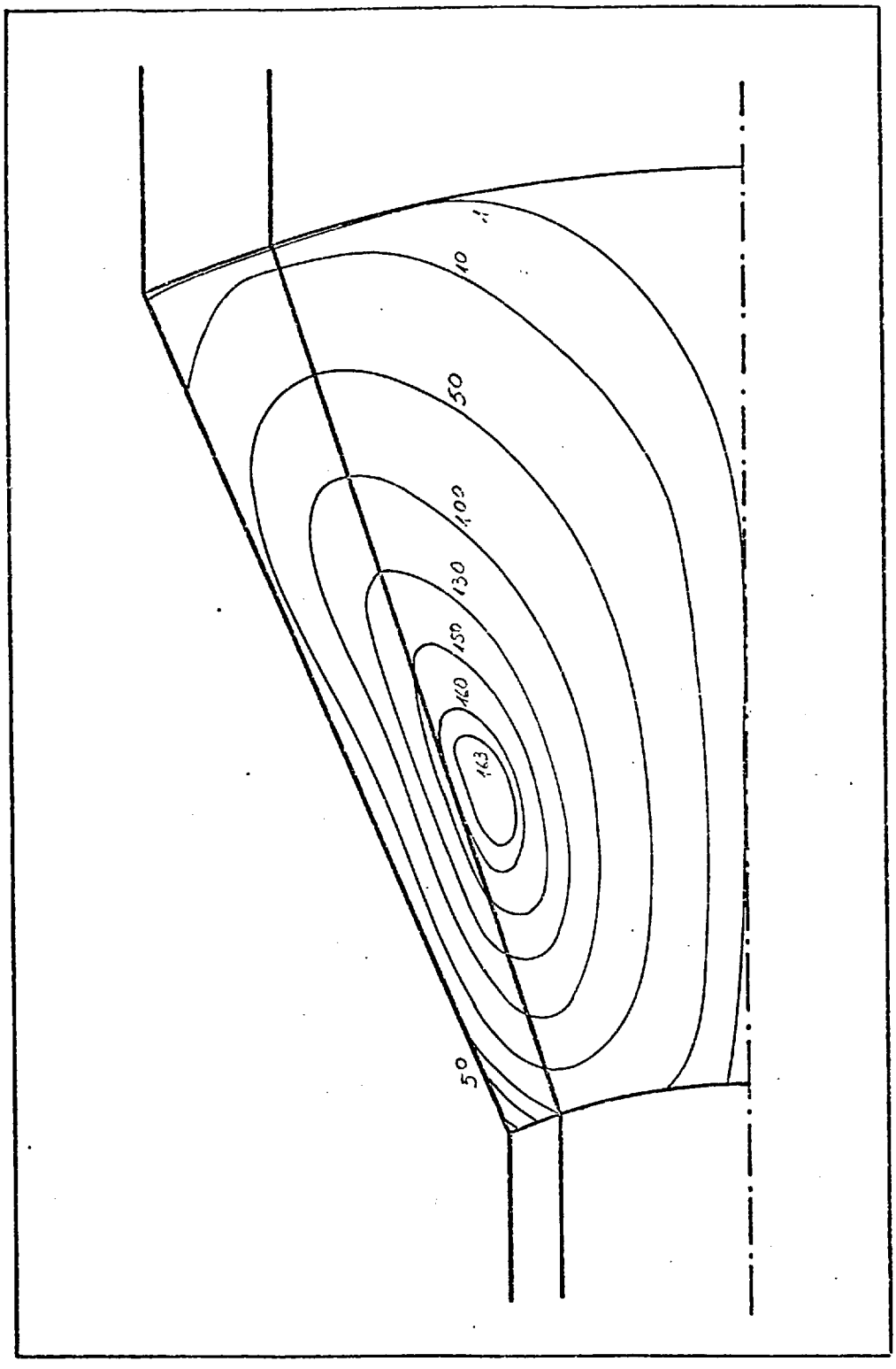

FIGURE 55: Stress distribution corresponding to $\frac{\sigma_r}{Y_o^c} \times 10^3$. Extrusion ratio 5.

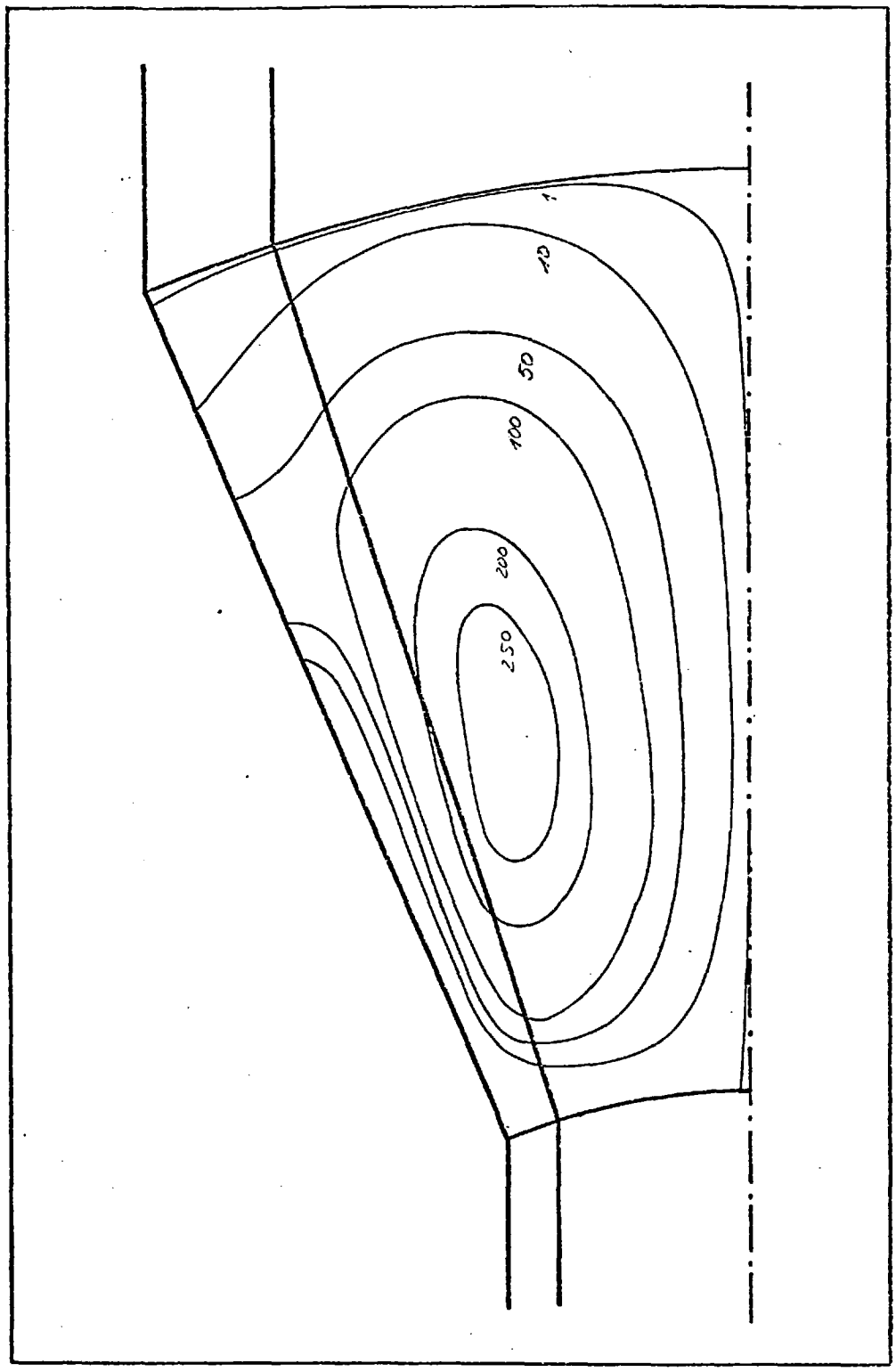

FIGURE 56: Stress distribution corresponding to $\frac{\sigma_\theta}{Y_o^c} \times 10^3$. Extrusion ratio 5.

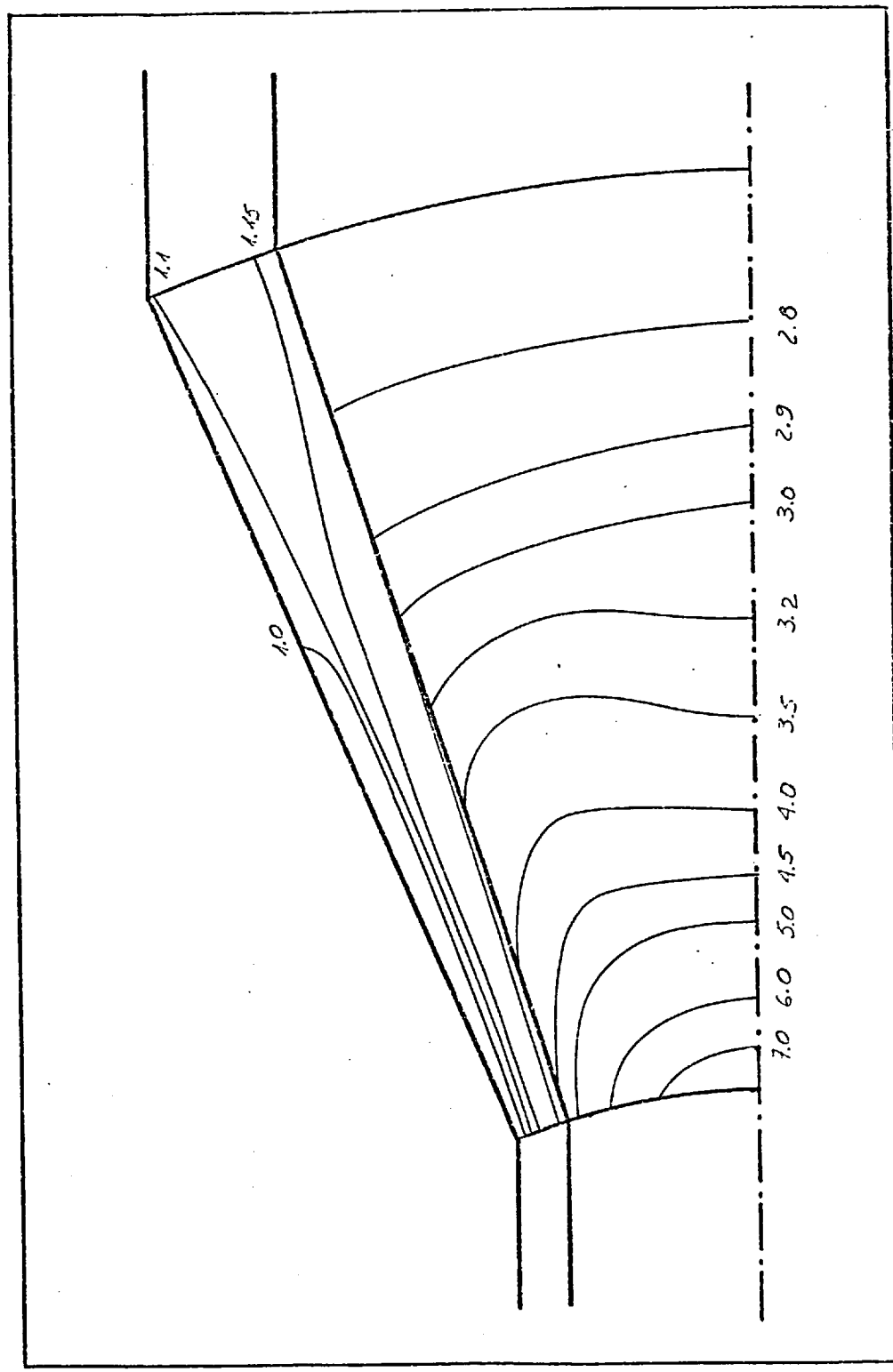

FIGURE 57: Stress distribution corresponding to $\frac{\sigma_z}{Y_o^c}$. Extrusion ratio 5.

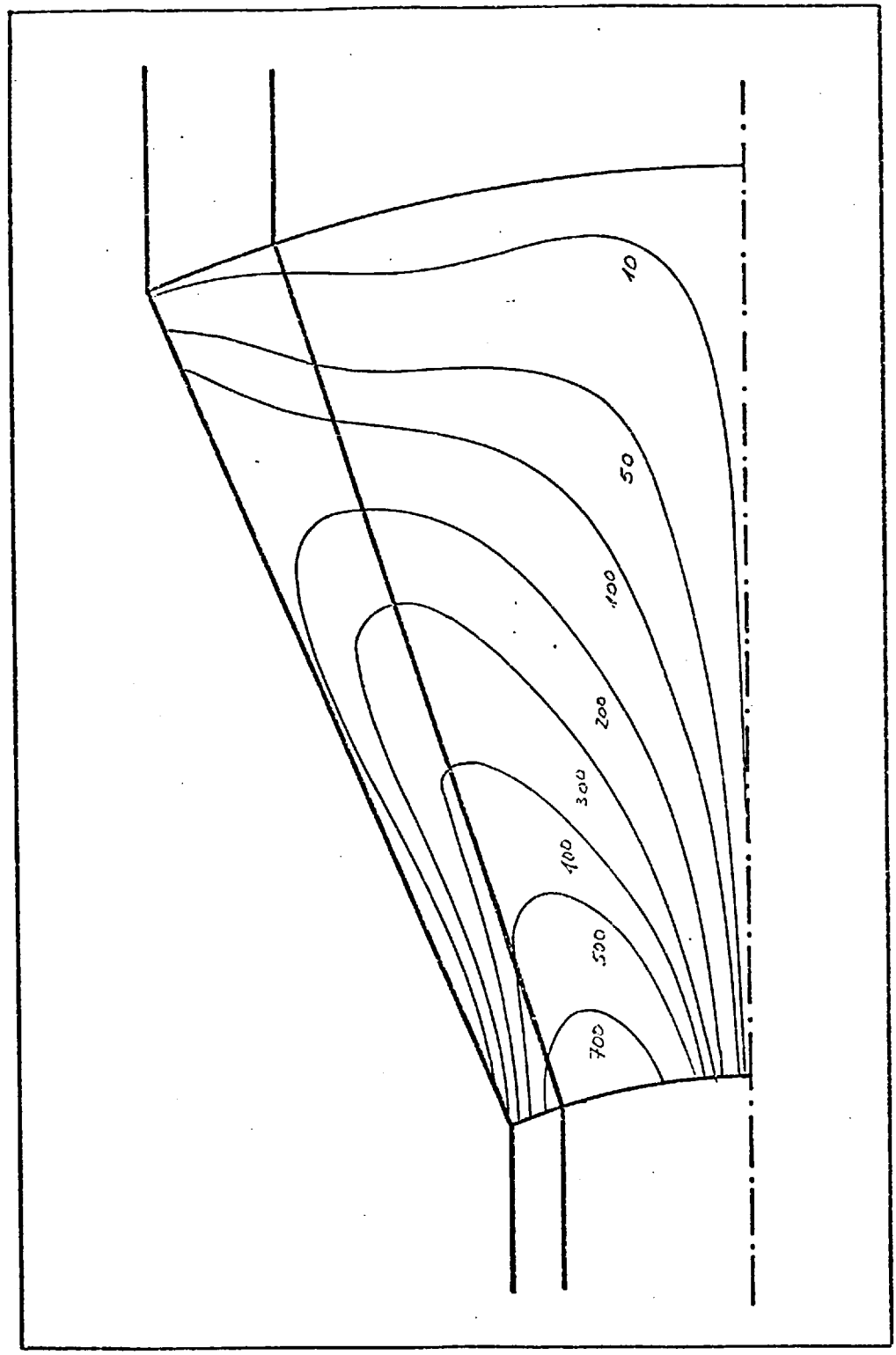

FIGURE 58: Stress distribution corresponding to $\frac{\tau_{rz}}{Y_o^c} \times 10^3$. Extrusion ratio 5.

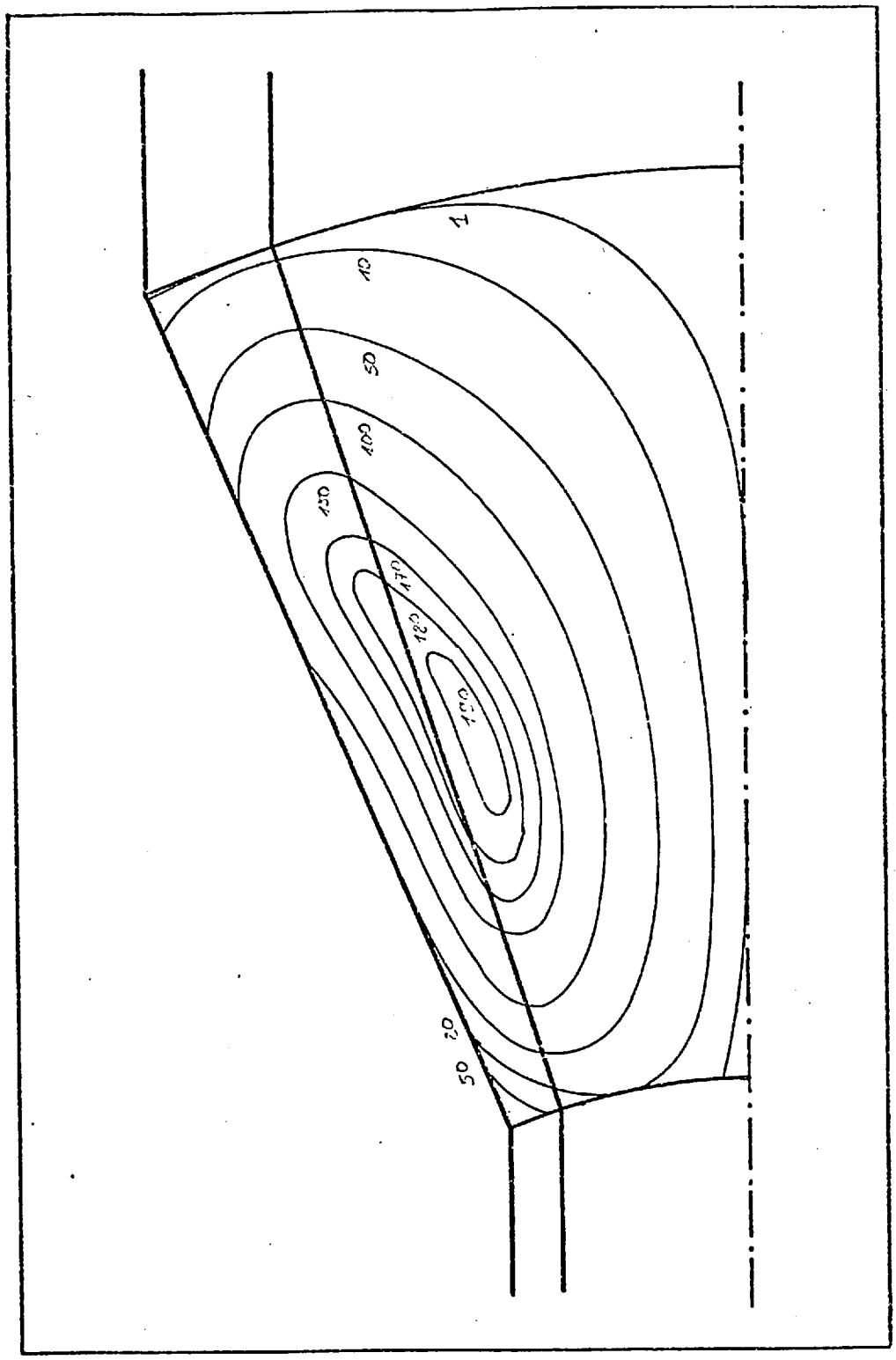

FIGURE 59: Stress distribution corresponding to $\frac{\sigma_r}{Y_o^c} \times 10^3$. Extrusion ratio 6.

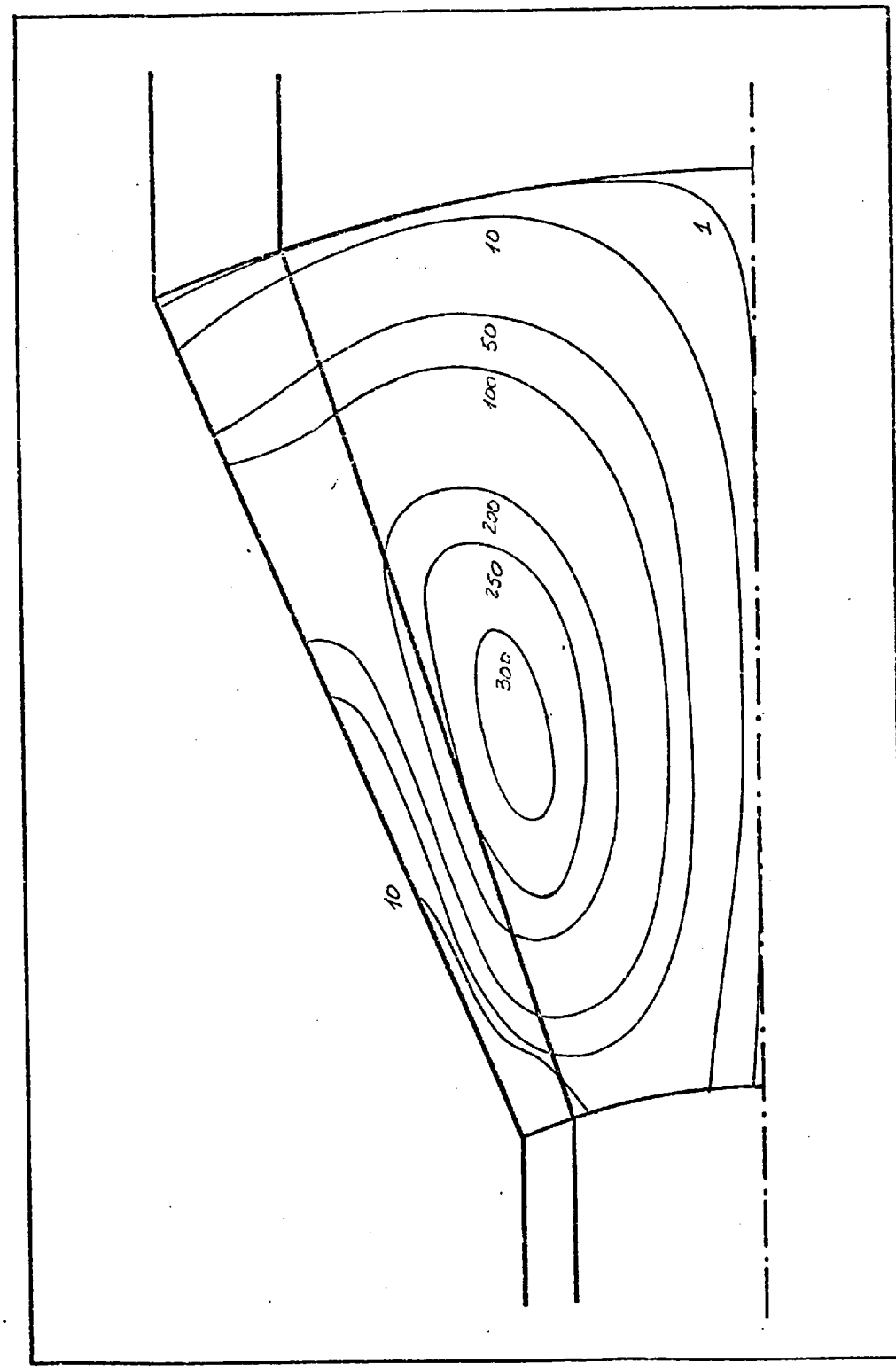

FIGURE 60: Stress distribution corresponding to $\frac{\sigma_\theta}{Y_o^c} \times 10^3$. Extrusion ratio 6.

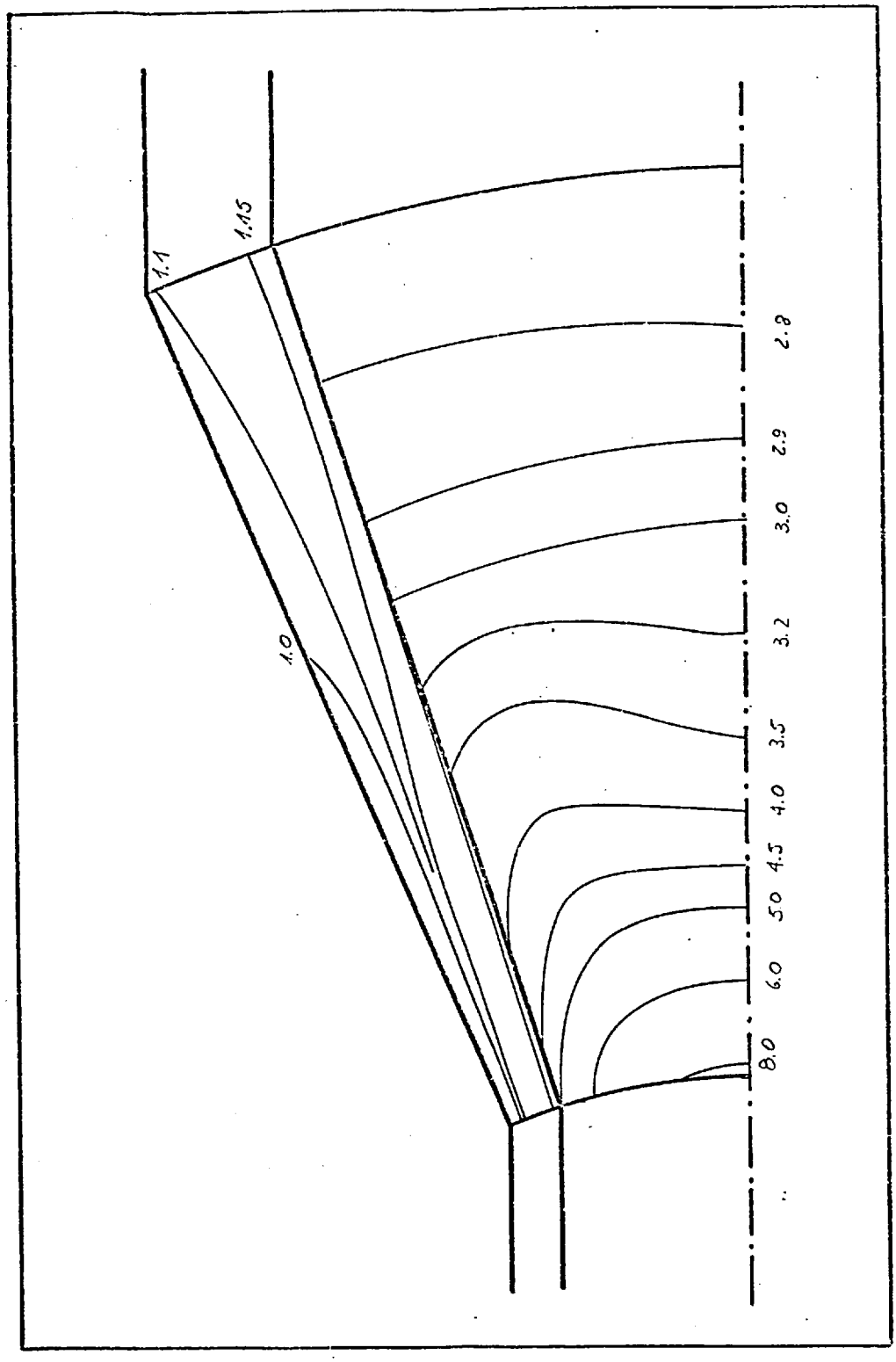

FIGURE 61: Stress distribution corresponding to $\frac{\sigma_z}{Y_o^c}$. Extrusion ratio 6.

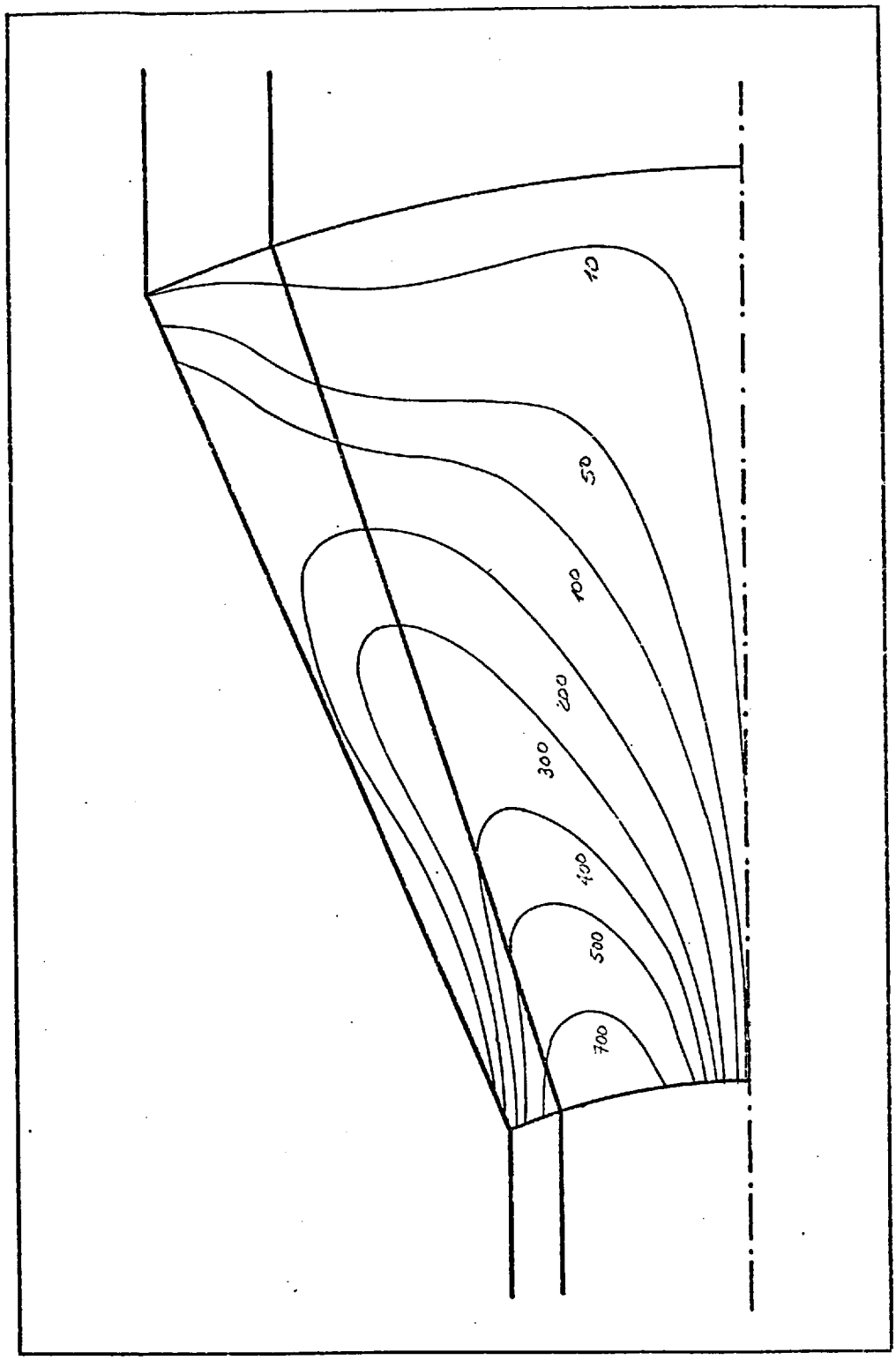

FIGURE 62: Stress distribution corresponding to $\frac{\tau_{rz}}{Y_o^c} \times 10^3$. Extrusion ratio 6.

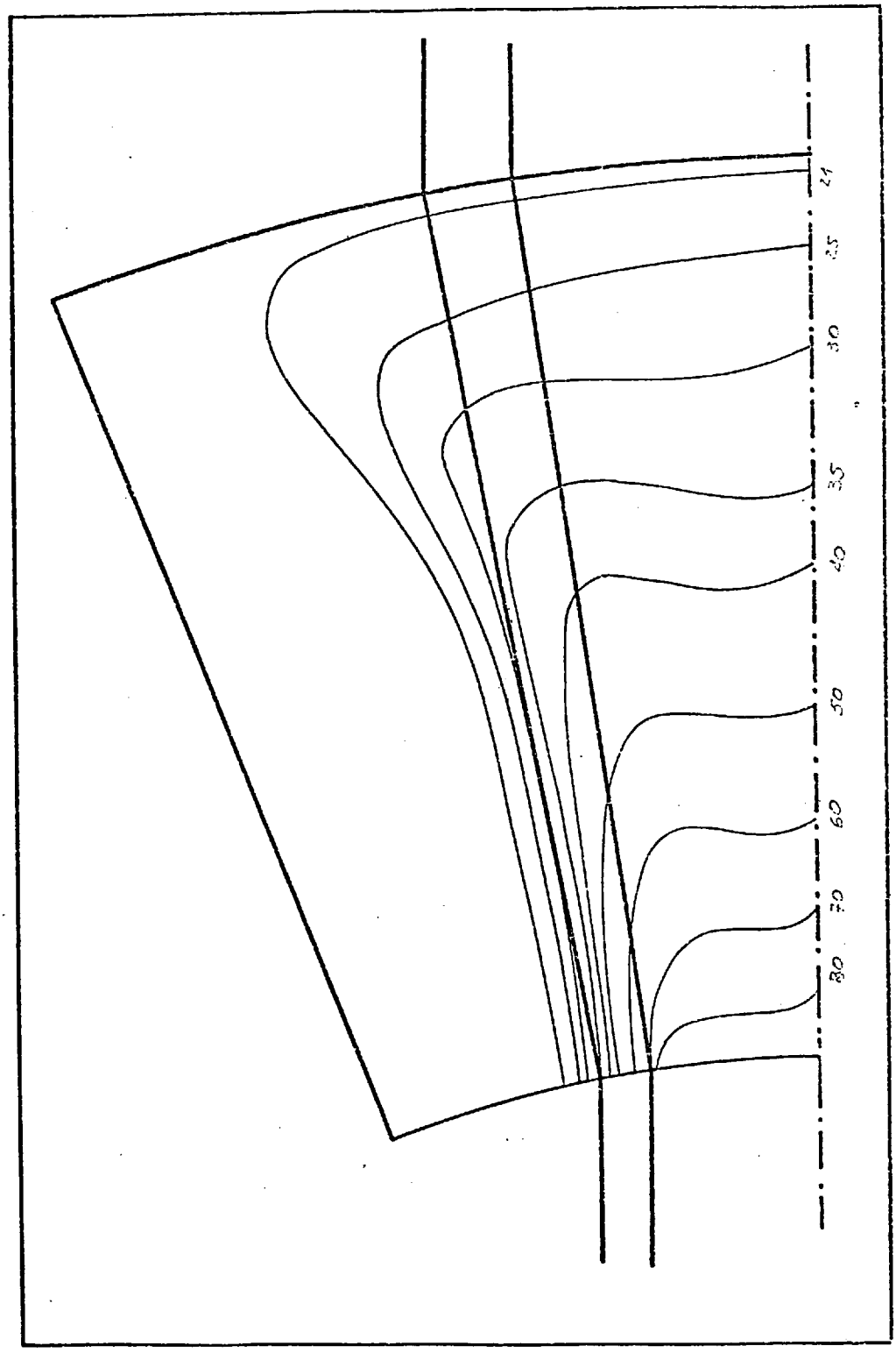

FIGURE 63: Isothermal lines for extrusion ratio 2.

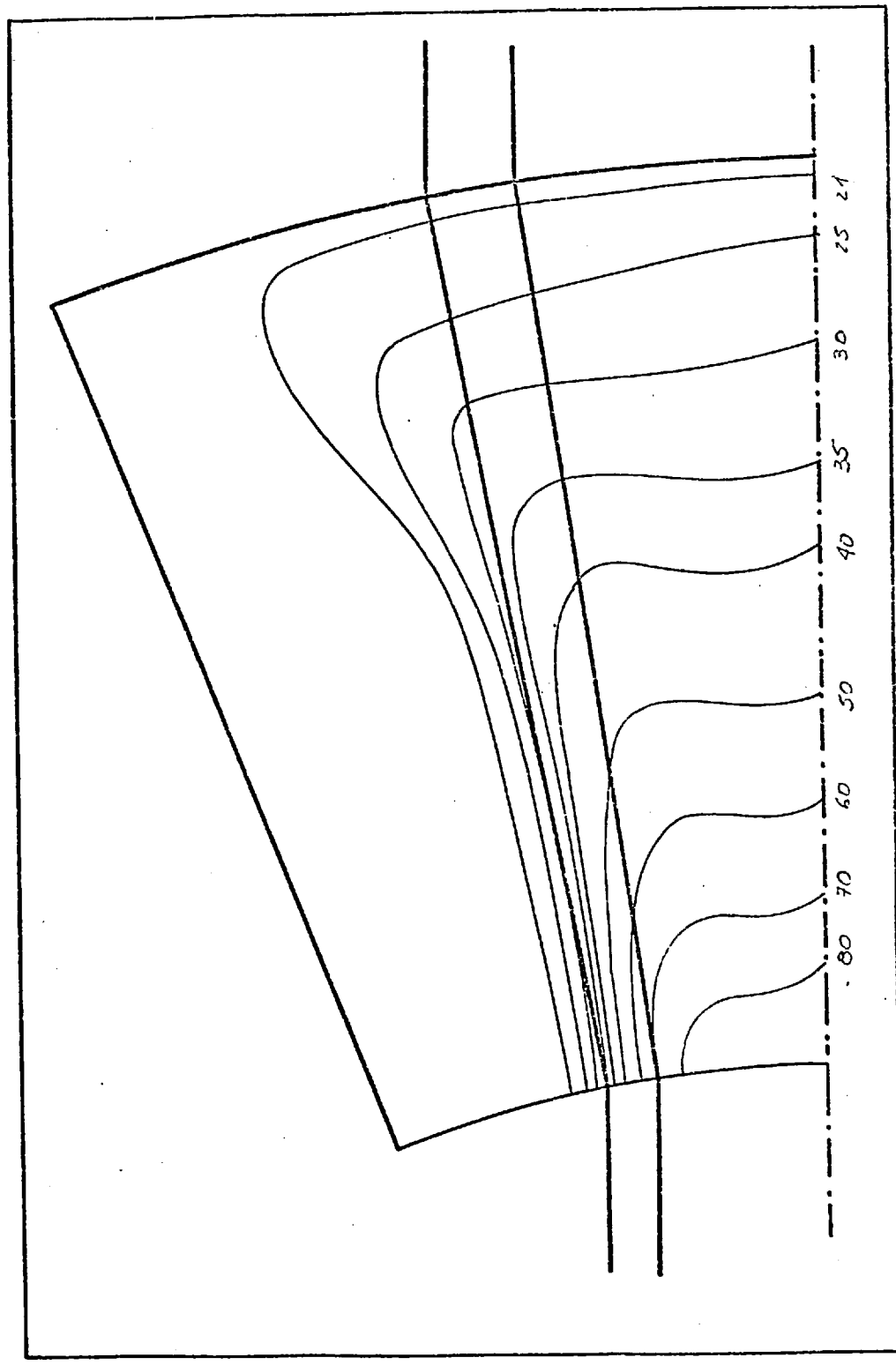

FIGURE 64: Isothermal lines for extrusion ratio 3.

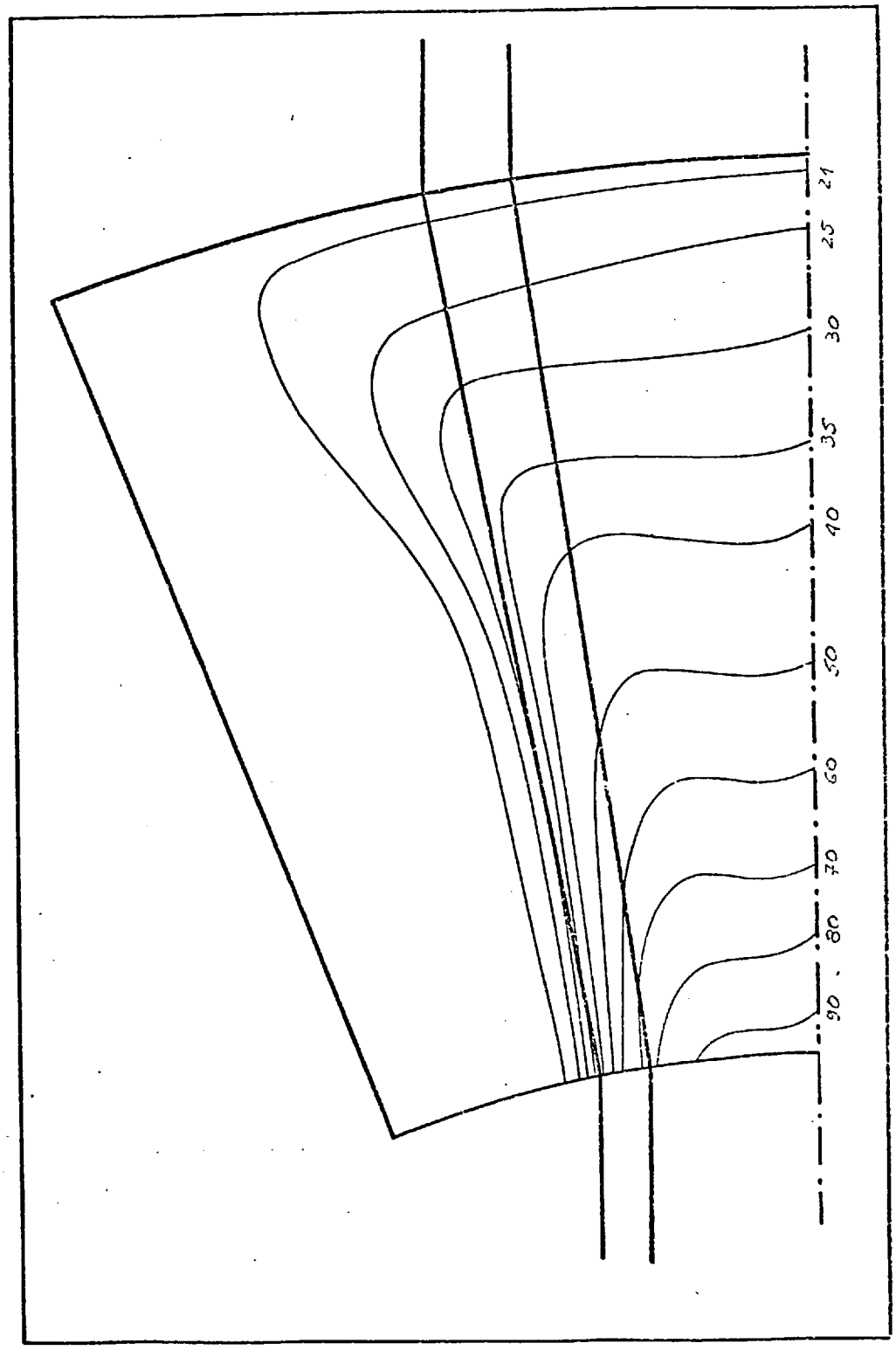

FIGURE 65: Isothermal lines for extrusion ratio 4.

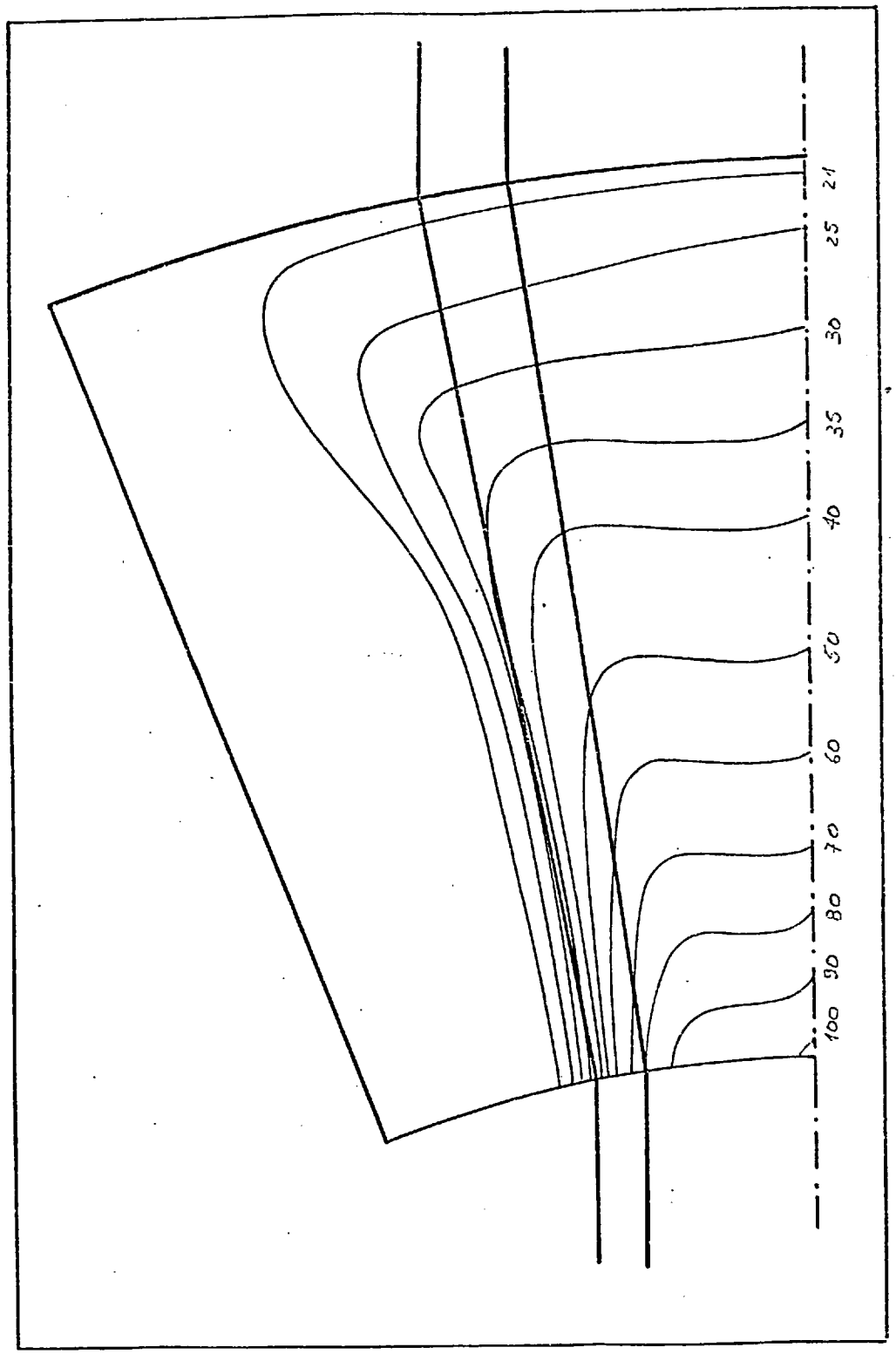

FIGURE 66: Isothermal lines for extrusion ratio 5.

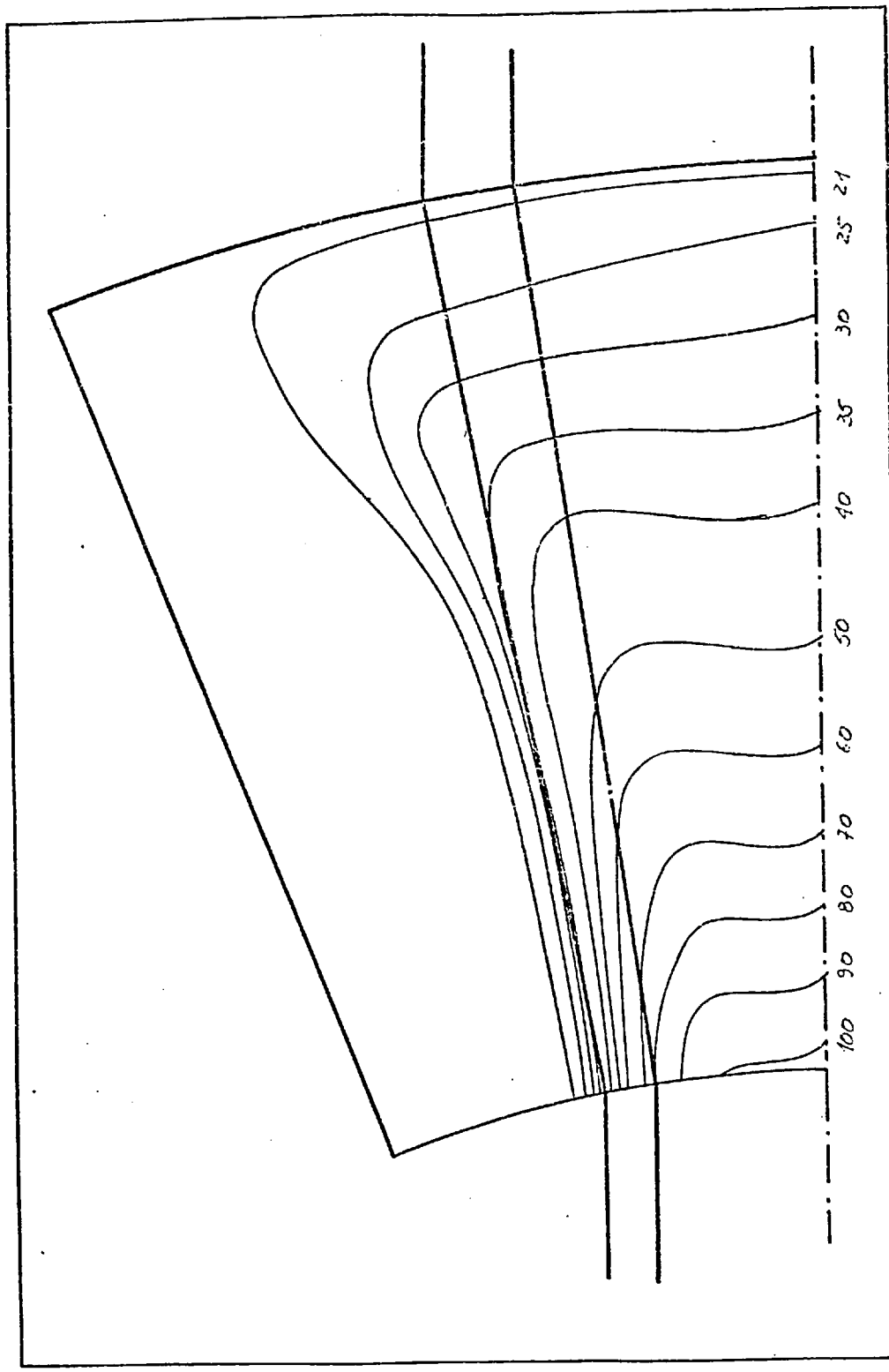

FIGURE 67: Isothermal lines for extrusion ratio 6.

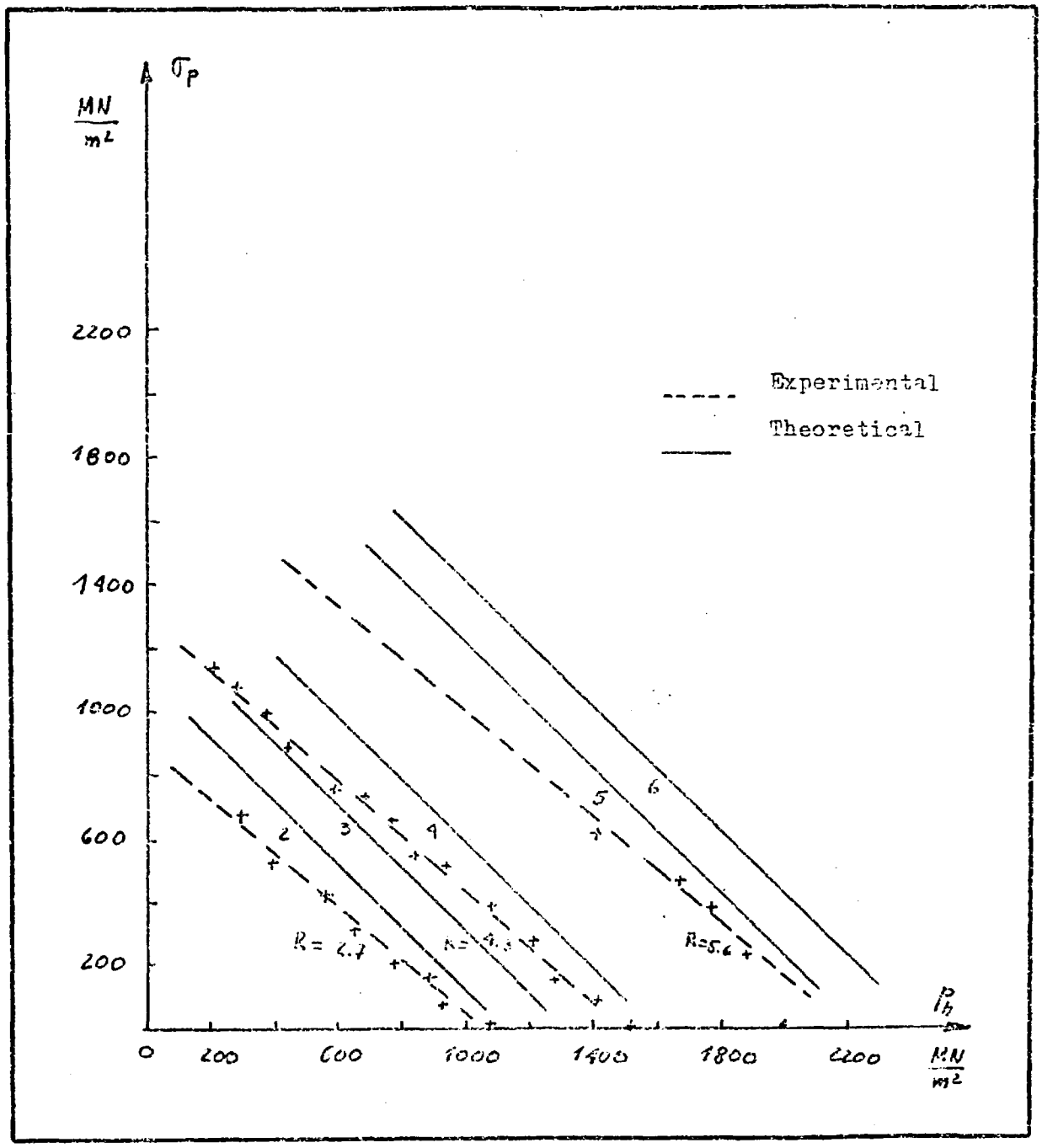

FIGURE 68 . Theoretical and experimental results for copper tube-s.steel core specimens (method of weighted residuals)

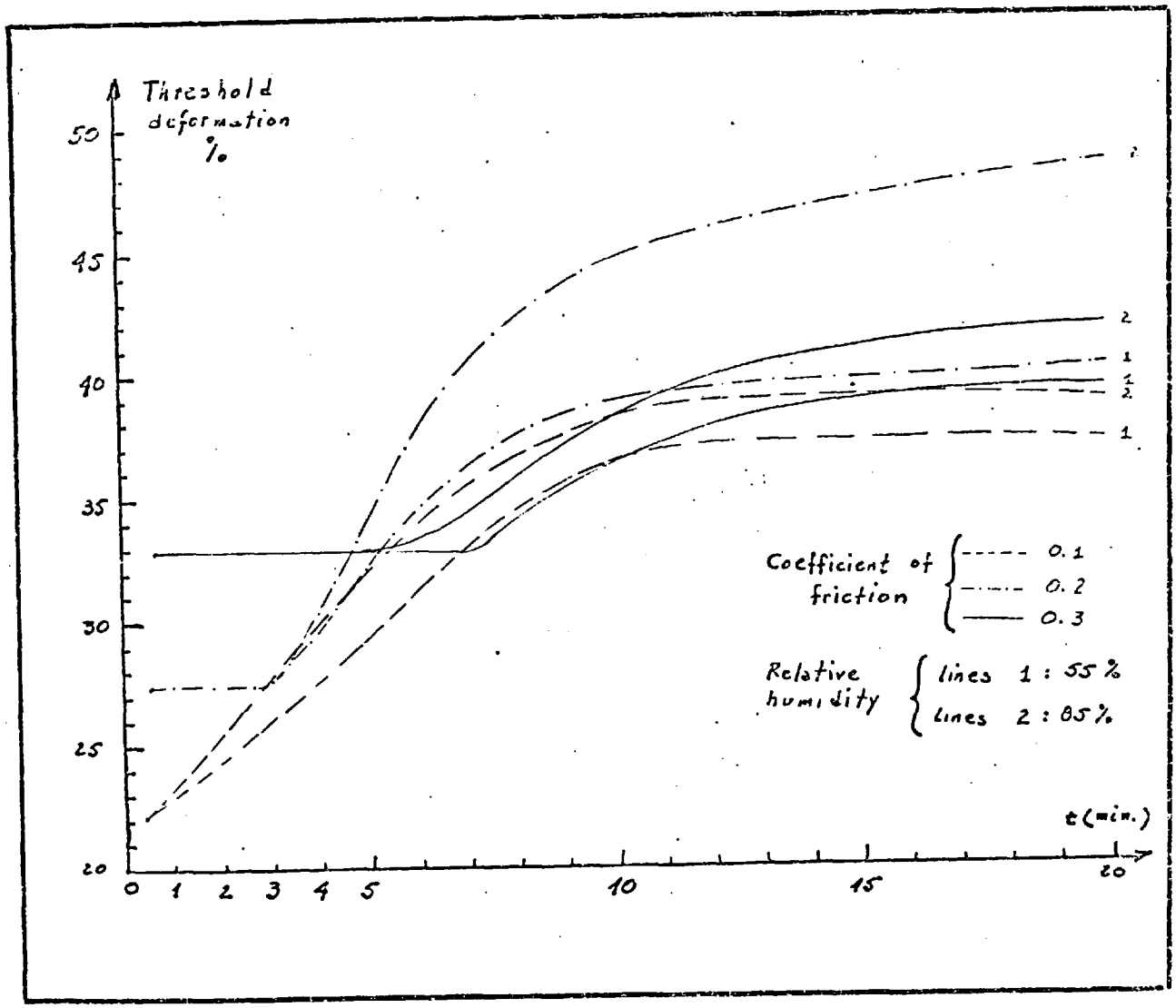

FIGURE 69: Influence of humidity on the process of welding by indentation.

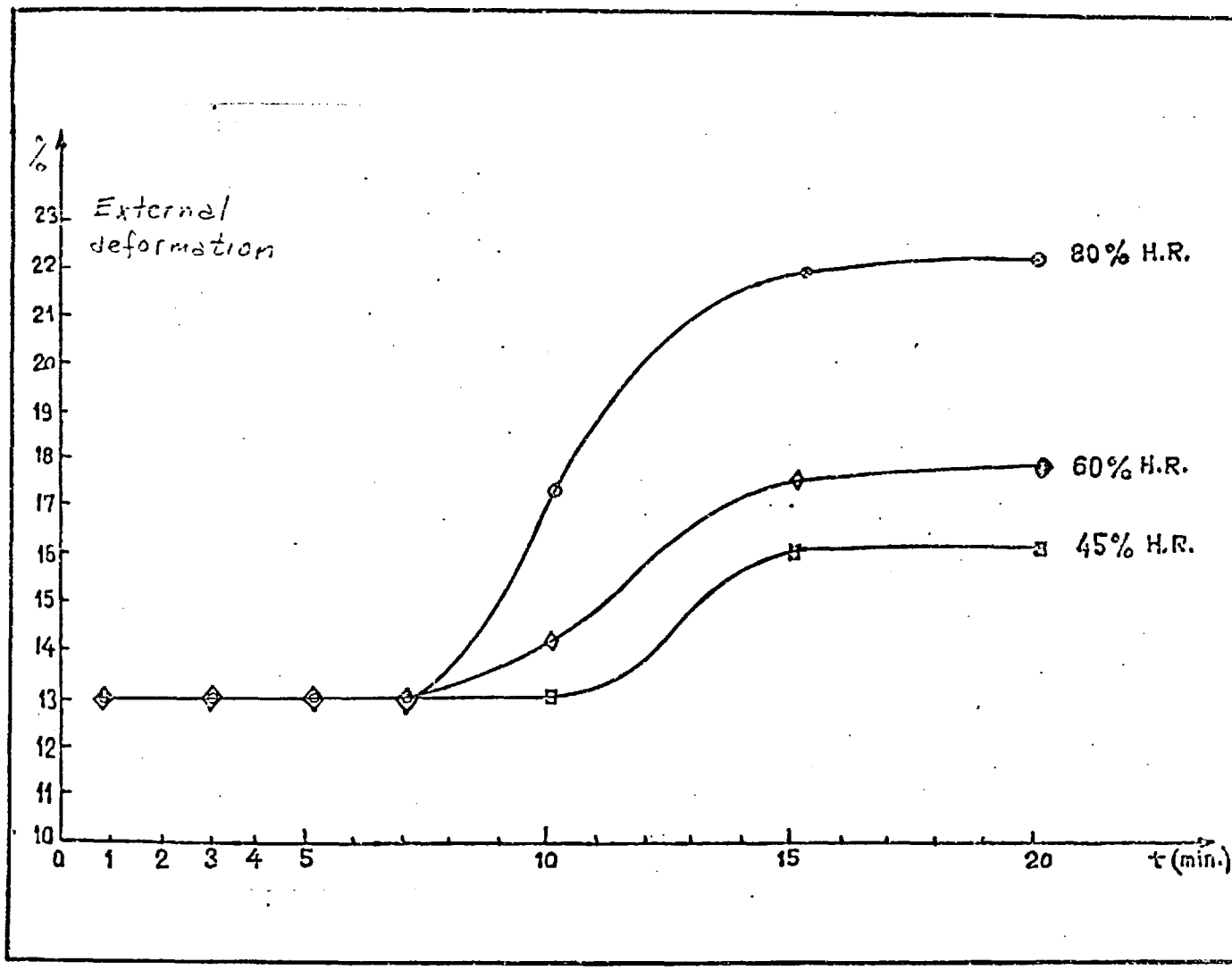

FIGURE 70: Influence of humidity on the process of welding by indentation.

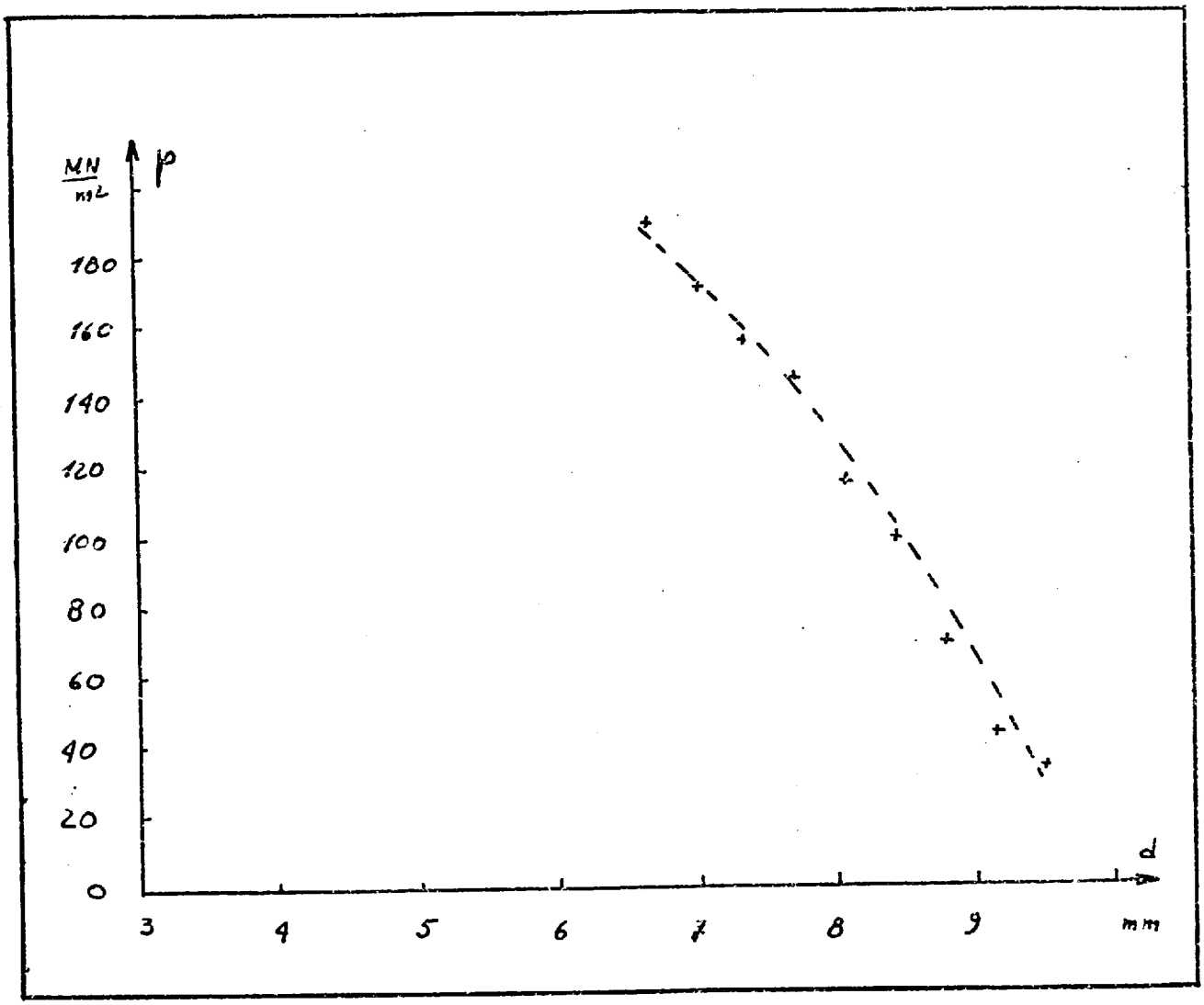

FIGURE 71 . Pressure distribution along the core-tube interface (d:distance from the apex). Extrusion ratio 2.

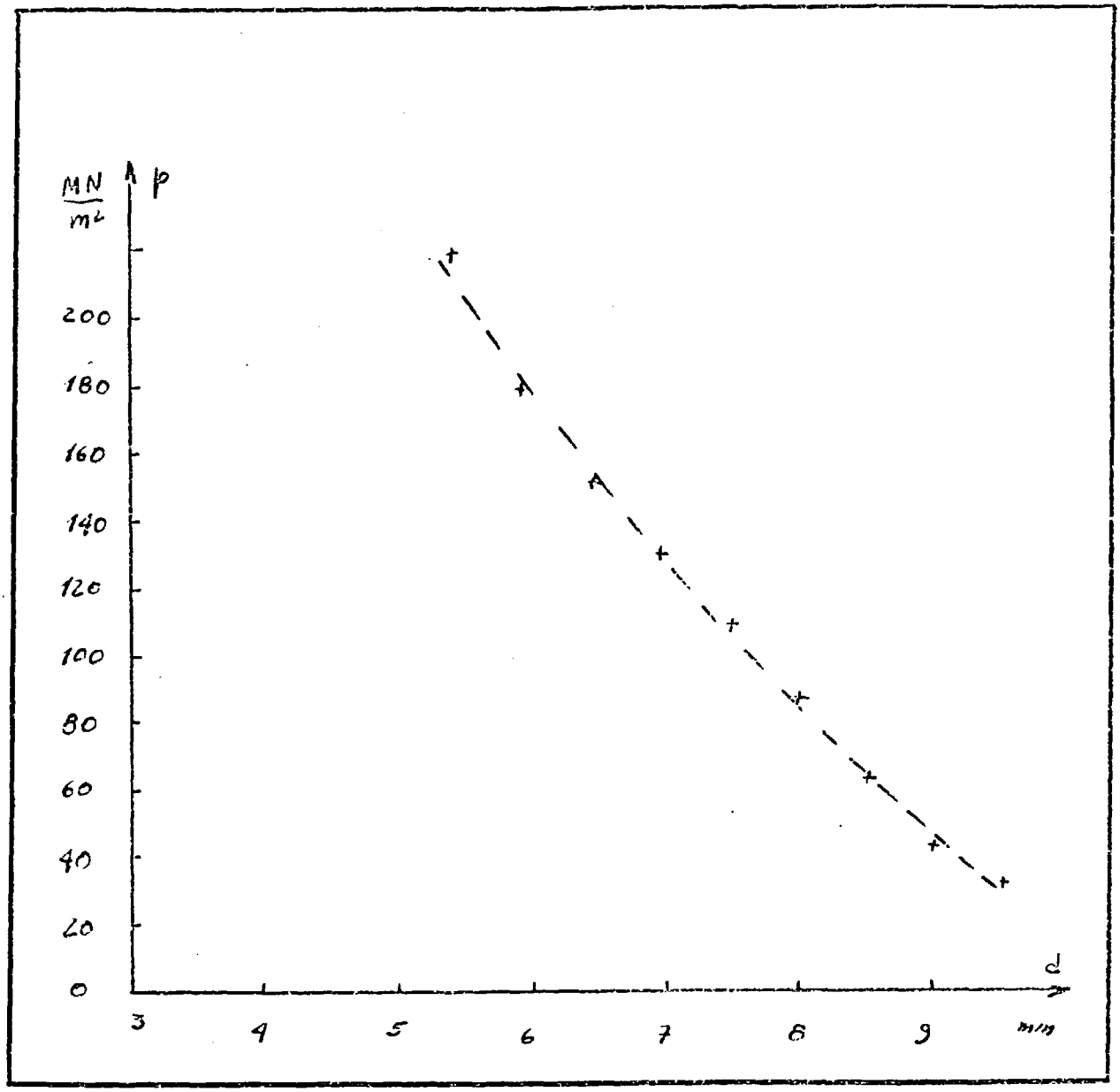

FIGURE 72 . Pressure distribution along the core-tube interface (d:distance from the apex). Extrusion ratio 3.

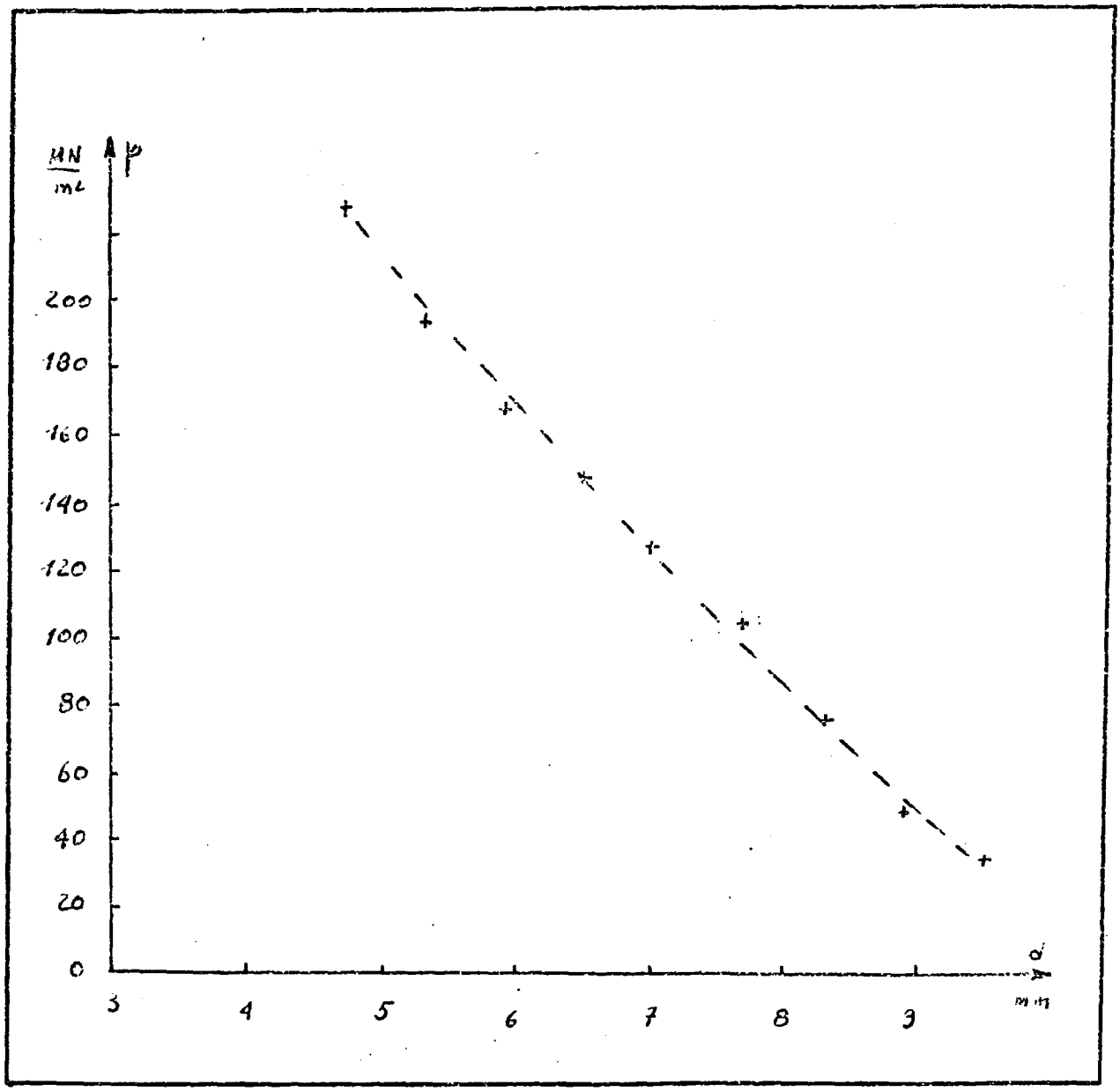

FIGURE 73 . Pressure distribution along the core-tube interface (d:distance from the apex). Extrusion ratio 4 .

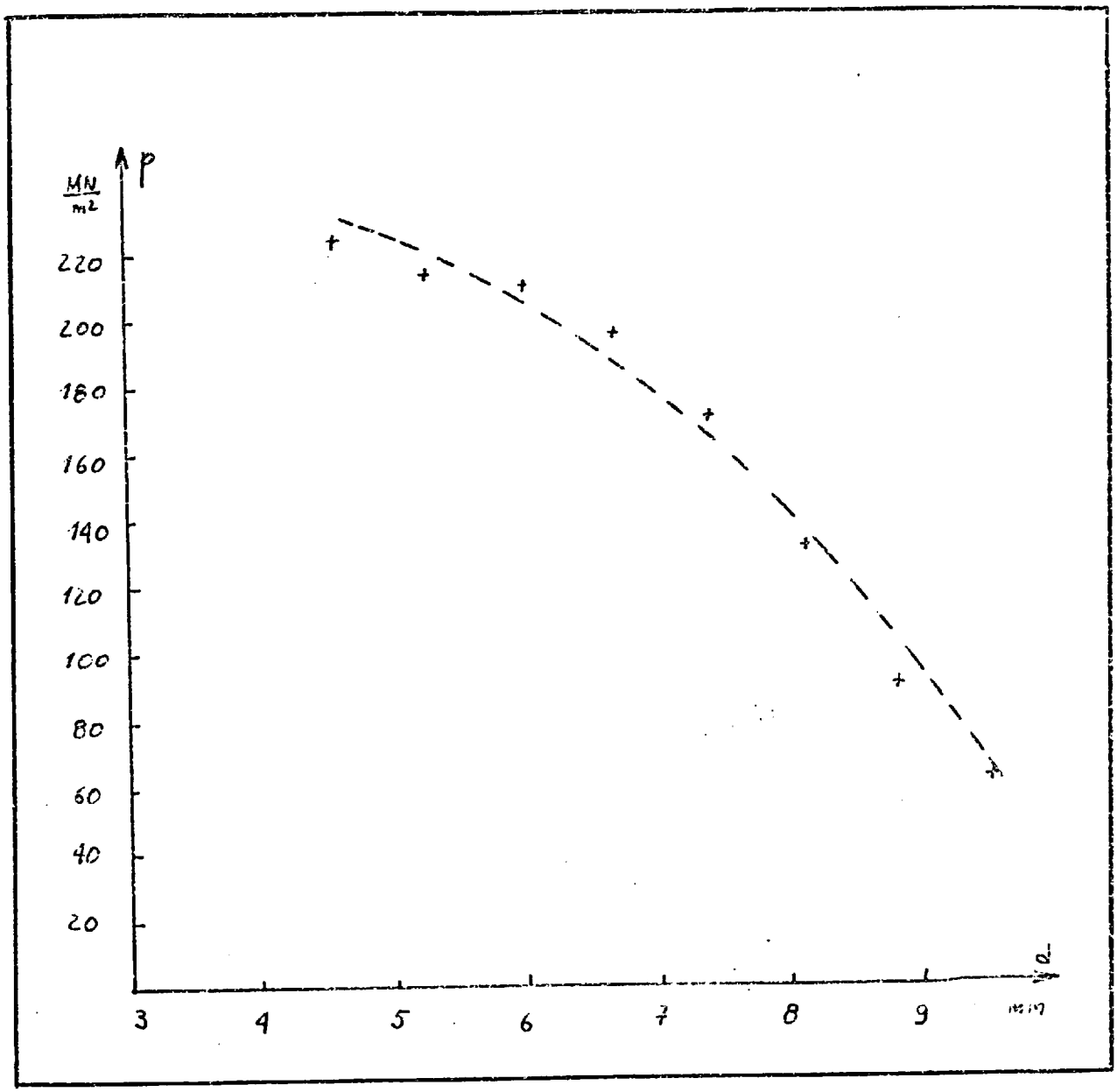

FIGURE 74 . Pressure distribution along the core-tube interface (d:distance from the apex). Extrusion ratio 5.

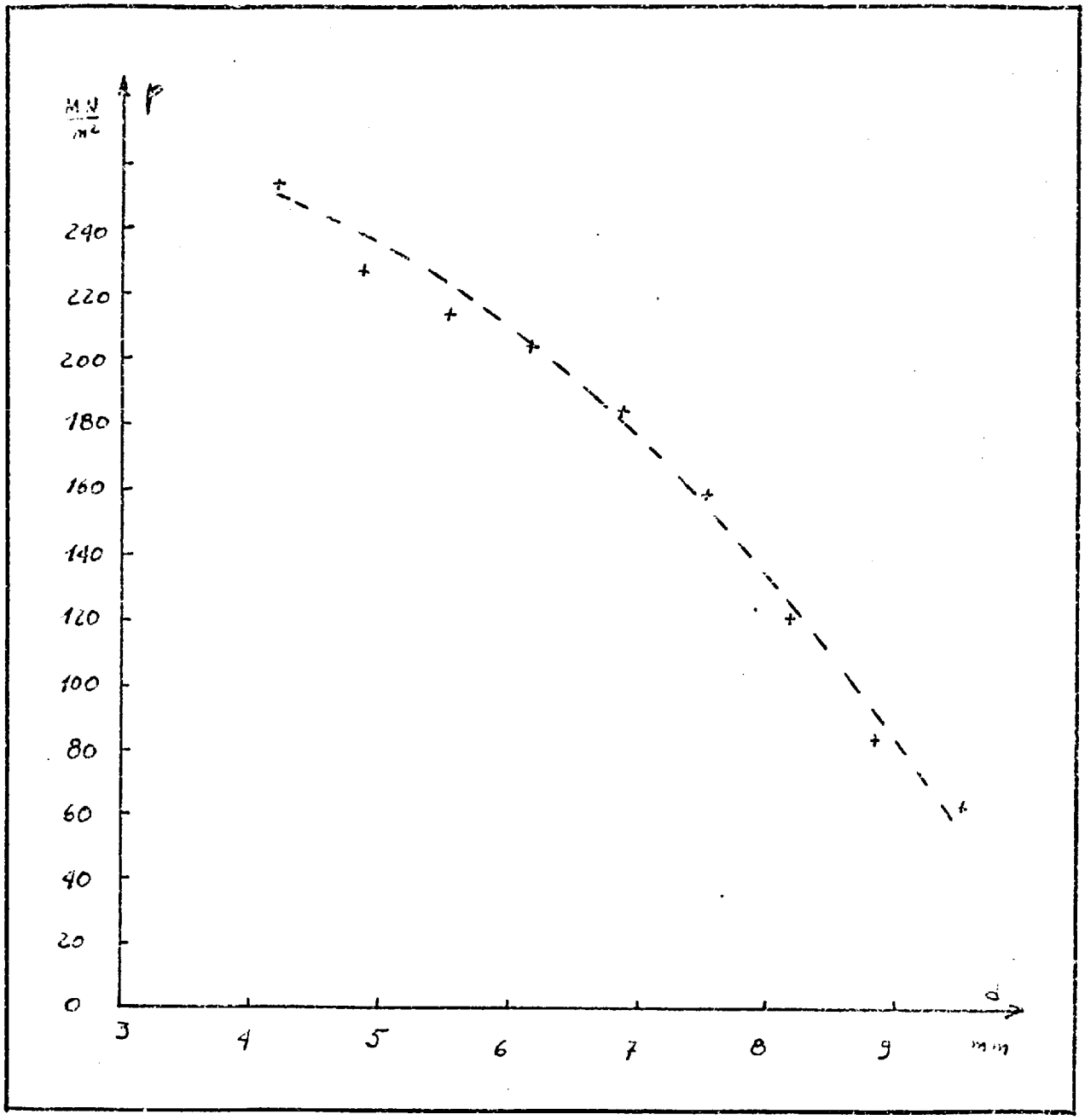

FIGURE 75 . Pressure distribution along the core-tube interface (d:distance from the apex). Extrusion ratio 6.

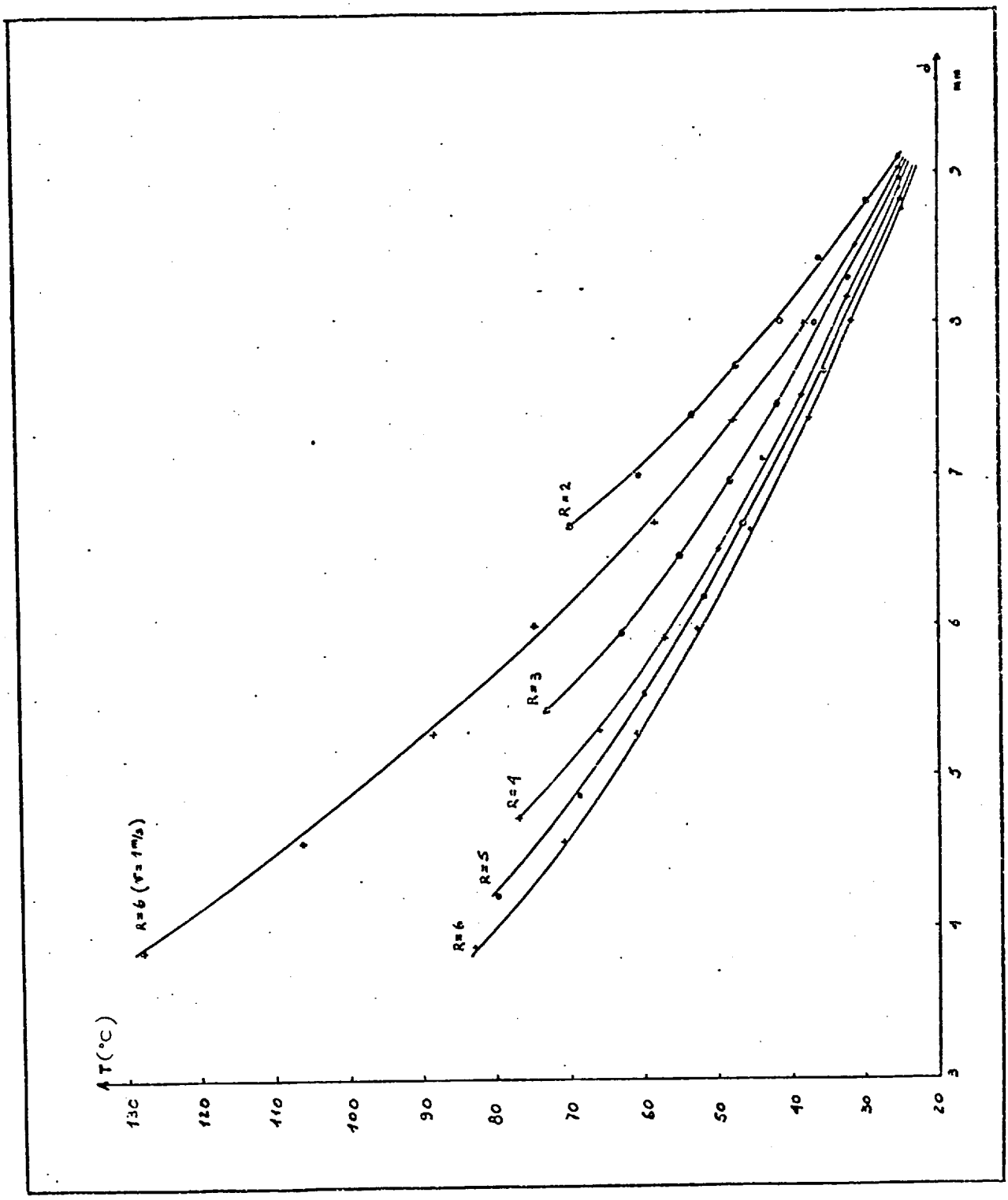

FIGURE 76: Temperature distributions along the core-tube interface for different extrusion ratios.

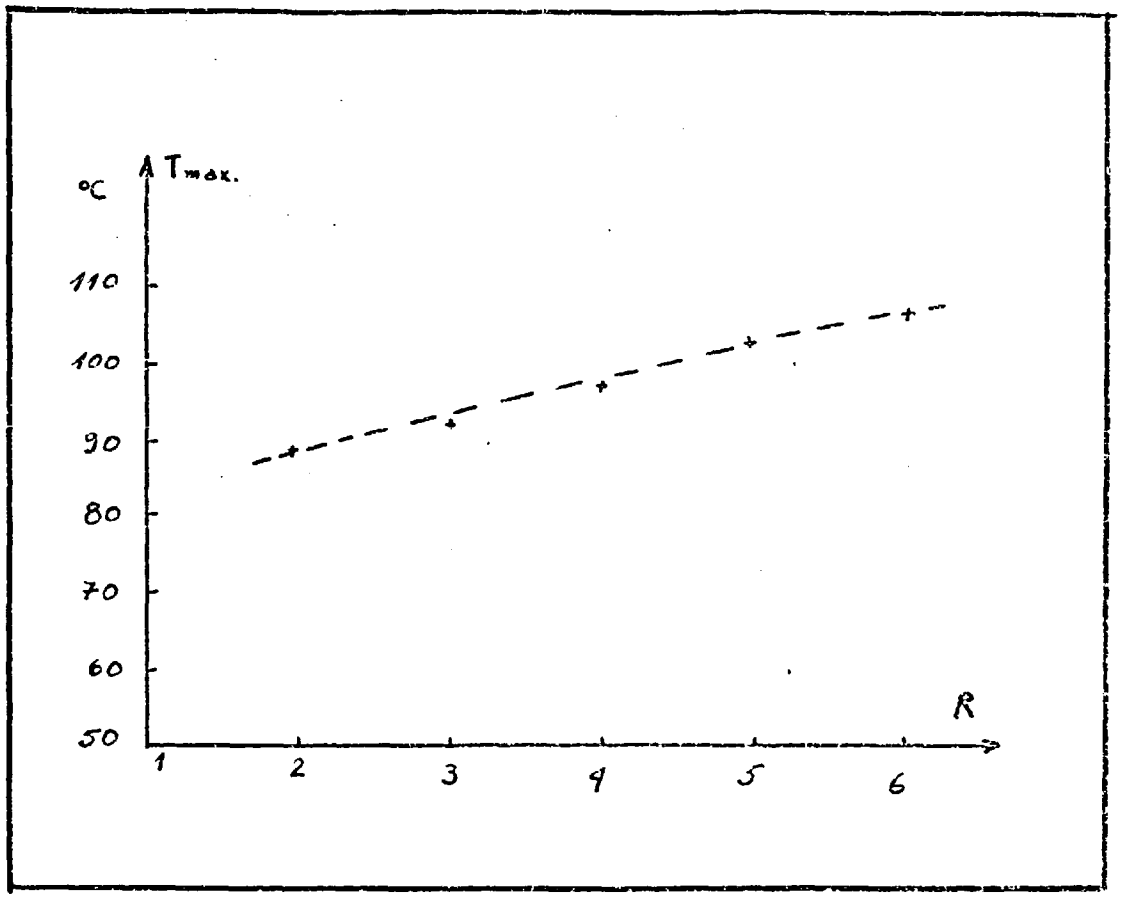

FIGURE 7 7. Maximum temperatures at the core-tube interface for different extrusion ratios.

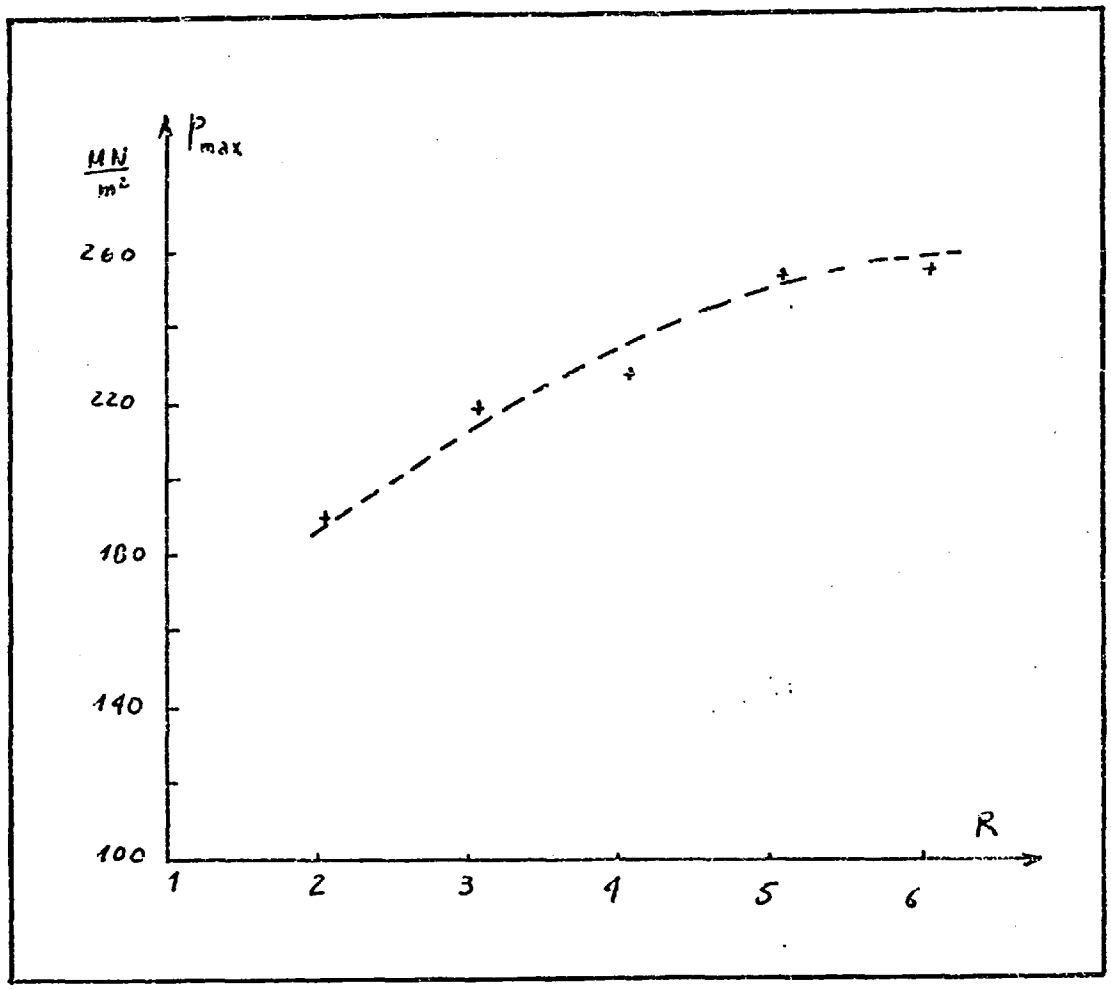

FIGURE 78 . Maximum pressures at the core-tube interface for different extrusion ratios.

X.1 APPENDIX A

Geometrical conditions for uniform deformation

Uniform deformation implies that the specimen is subjected to the same extrusion ratio at all points of a plane normal to the axis die. Consequently, both metals must deform with the same extrusion ratio.

Let us show that, in this case, the apex of the conical surface limiting the core at the deformation zone should coincide with the apex of the die conical surface. The geometrical situation is illustrated in the following diagram:

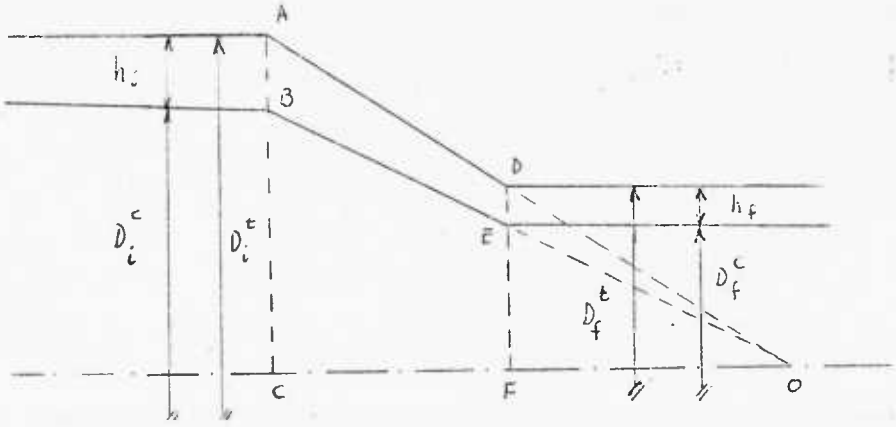

The convergence of both conical surfaces was verified by observation with adequate magnification meridional sections as shown in the following picture:

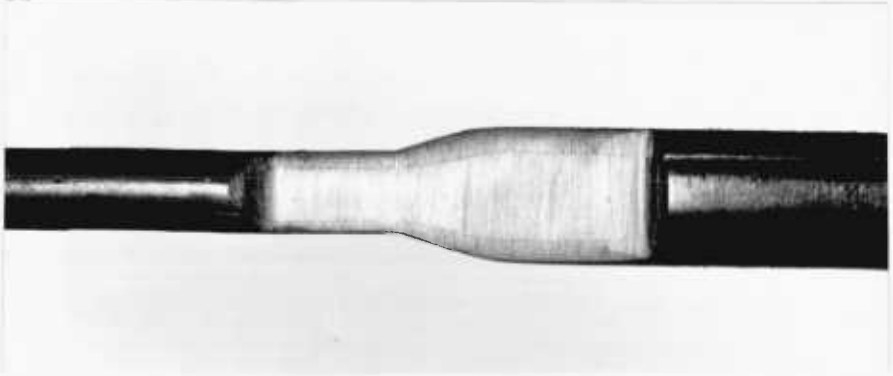

The extrusion ratio of the core is:

$$R_c = \frac{(D_i^c)^2}{(D_f^c)^2} \qquad \text{(i)}$$

The extrusion ratio of the tube is:

$$R_t = \frac{(D_i^t)^2 - (D_i^c)^2}{(D_f^t)^2 - (D_f^c)^2} \qquad \text{(ii)}$$

From a direct proportionality between elements of the triangles $A\hat{O}C$ and $B\hat{O}C$, expression

$$\frac{D_i^t}{D_i^c} = \frac{D_f^t}{D_f^c} \qquad \text{(iii)}$$

is obtained. In other form

$$D_i^t = \frac{D_i^c}{D_f^c} D_f^t = \sqrt{R_c}\, D_f^t \qquad \text{(iv)}$$

Replacing (iv) and (i) into (ii), one gets

$$R_t = \frac{R_c (D_f^t)^2 - (D_i^c)^2}{(D_f^t)^2 \; \frac{(D_i^c)^2}{R_c}} = R_c \qquad \text{(v)}$$

Consequently, if both materials have undergone the same extrusion ratio, both apices should coincide.

Another relationship to calculate is

$$r = \frac{h_f}{h_i} = \frac{D_f^t - D_f^c}{D_i^t - D_i^c} \qquad \text{(vi)}$$

By substituting (i) and (iv) into (vi), the expression

$$r = \frac{D_f^t - D_f^c}{\sqrt{R_c}\, D_f^t - \sqrt{R_c}\, D_f^c} = \frac{1}{\sqrt{R_c}} = \frac{1}{\sqrt{R_t}}$$

is obtained. Calling with $R = R_c = R_t$, we finally obtain

$$r = R^{-\frac{1}{2}} \qquad \text{(vii)}$$

Ley us finally calculate the relationship between the angles α, β and the proportion of the component metals:

$$\tan\alpha = \frac{D_i^t}{CO}$$

$$\tan\beta = \frac{D_i}{CO}$$

hence,

$$\frac{\tan\alpha}{\tan\beta} = \frac{D_i^t}{D_i^c}$$

The fraction of volume of the core is

$$\gamma_c = \left(\frac{D_i^c}{D_i^t}\right)^2$$

and hence,

$$\tan\beta = \sqrt{\gamma_c}\, \tan\alpha$$

or

$$\tan\beta = \sqrt{1 - \gamma_t}\, \tan\alpha \qquad \text{(viii)}$$

X.II APPENDIX B

Internal power of deformation using Avitzur's velocity field

The general expression for the internal power consumed in the plastic deformation of a volume V is:

$$\dot{W}_i = \int_V \sigma_{ij} \dot{\varepsilon}_{ij} \, dV \qquad \text{(i)}$$

For a material obeying the Prandtl-Reuss's relationship it is:

$$\sigma_{ij} = \frac{Y}{\sqrt{3}} \frac{\dot{\varepsilon}^P_{ij}}{\sqrt{I_2}}$$

and, consequently, expression (i) rewrites as:

$$\dot{W}_i = \int_V \frac{Y}{\sqrt{3}} \frac{\dot{\varepsilon}^P_{ij}}{\sqrt{I_2}} \dot{\varepsilon}^P_{ij} \, dV$$

or

$$\dot{W}_i = \int_V \frac{2}{\sqrt{3}} Y \sqrt{I_2} \, dV \qquad \text{(ii)}$$

since $I_2 = \frac{1}{2} \dot{\varepsilon}^P_{ij} \dot{\varepsilon}^P_{ij}$.

For a non-hardening material, the yield stress is constant throughout V, and hence

$$\dot{W}_i = \frac{2}{\sqrt{3}} Y \int_V \sqrt{I_2} \, dV \qquad \text{(iii)}$$

The expression of I_2 in a spherical system of coordinates (R, φ, θ) and conditions of axial symmetry is:

$$I_2 = -(\dot{\varepsilon}_{RR}\dot{\varepsilon}_{\theta\theta} + \dot{\varepsilon}_{\theta\theta}\dot{\varepsilon}_{\varphi\varphi} + \dot{\varepsilon}_{\varphi\varphi}\dot{\varepsilon}_{RR}) + \dot{\varepsilon}^2_{R\theta} \qquad \text{(iv)}$$

Replacing equations (6) into (iv) gives:

$$I_2 = -\left[2(v_f R_f^2 \frac{\cos\theta}{R^3})^2 + (v_f R_f^2 \frac{\cos\theta}{R^3})^2 - 2(v_f R_f^2 \frac{\cos\theta}{R^3})^2\right] + (\tfrac{1}{2} v_f R_f^2 \frac{\sin\theta}{R^3})^2$$

or

$$I_2 = (\frac{v_f R_f^2}{R^3})^2 \left[3\cos^2\theta + \tfrac{1}{4}\sin^2\theta\right]$$

and, consequently expression (iii) becomes

$$\dot{W}_i = \frac{2}{\sqrt{3}} Y \int_V v_f \frac{R_f^2}{R^3} \sqrt{3\cos^2\theta + \tfrac{1}{4}\sin^2\theta}\, dV$$

By using suitable trigonometric transformations, the following expression is obtained:

$$\dot{W}_i = 2\, Y\, v_f\, R_f^2 \int_V \frac{1}{R^3} \sqrt{1 - \frac{11}{12}\sin^2\theta}\, dV$$

where $dV = 2\pi R \sin\theta\, R\, dR\, d\theta$.

Equation (v) can be written as:

$$W_i = 4\pi Y v_f R_f^2 \int_0^{\beta} (\sqrt{1 - \frac{11}{12}\sin^2\theta}\, \sin\theta \int_{R_f}^{R_i} \frac{dR}{R}) d\theta$$

Taking into account that:

$$r_f^c = \frac{R_f}{\sin} \quad \text{and} \quad \frac{R_i}{R_f} = \frac{r_i^c}{r_f^c}$$

after integration, the expression

$$W_i = \pi Y (r_f^c)^2 v_f F(\beta) \ln R_c$$

is obtained, where

$$F(\beta) = \frac{1}{\sin^2\beta}\left[1 - \cos\beta\sqrt{1 - \frac{11}{12}\sin^2\beta} + \frac{1}{\sqrt{11.12}}\cdot \ln \frac{1 + \sqrt{\frac{11}{12}}}{\sqrt{\frac{11}{12}}\cos\beta + \sqrt{1 - \frac{11}{12}\sin^2\beta}}\right]$$

A table with values of $F(\beta)$ for different values of the angle is presented as Table I.

TABLE I

α	$F(\alpha)$	$\frac{\alpha}{\sin^2\alpha} - \cot\alpha$	α	$F(\alpha)$	$\frac{\alpha}{\sin^2\alpha} - \cot\alpha$
1	1.00001	0.011636	46	1.01679	0.58587
2	1.00003	0.024375	47	1.01772	0.60111
3	1.00006	0.034920	48	1.01869	0.61655
4	1.00010	0.046573	49	1.01970	0.63217
5	1.00016	0.058237	50	1.02075	0.64800
6	1.00023	0.069915	51	1.02185	0.66403
7	1.00031	0.081611	52	1.02300	0.68027
8	1.00041	0.093327	53	1.02420	0.69674
9	1.00052	0.10507	54	1.02546	0.71344
10	1.00064	0.11683	55	1.02677	0.73037
11	1.00078	0.12862	56	1.02814	0.74755
12	1.00093	0.14045	57	1.02958	0.76498
13	1.00109	0.15231	58	1.03108	0.78268
14	1.00127	0.16421	59	1.03265	0.80066
15	1.00146	0.17614	60	1.03430	0.81891
16	1.00167	0.18813	61	1.03603	0.83746
17	1.00189	0.20016	62	1.03784	0.85632
18	1.00212	0.21223	63	1.03974	0.87549
19	1.00237	0.22437	64	1.04174	0.89500
20	1.00264	0.23656	65	1.04384	0.91484
21	1.00292	0.24881	66	1.04605	0.93503
22	1.00322	0.26112	67	1.04838	0.95559
23	1.00354	0.27350	68	1.05082	0.97653
24	1.00387	0.28595	69	1.05340	0.99787
25	1.00422	0.29848	70	1.05613	1.01961
26	1.00459	0.31108	71	1.05900	1.04178
27	1.00498	0.32377	72	1.06204	1.06438
28	1.00538	0.33653	73	1.06526	1.08745
29	1.00581	0.34939	74	1.06867	1.11099
30	1.00625	0.36234	75	1.07228	1.13503
31	1.00672	0.37539	76	1.07611	1.15958
32	1.00721	0.38854	77	1.08018	1.18467
33	1.00772	0.40180	78	1.08451	1.21031
34	1.00825	0.41516	79	1.08912	1.23653
35	1.00881	0.42864	80	1.09404	1.26335
36	1.00939	0.44224	81	1.09928	1.29080
37	1.01000	0.45596	82	1.10488	1.31890
38	1.01063	0.46981	83	1.11087	1.34768
39	1.01129	0.48380	84	1.11727	1.37717
40	1.01198	0.49792	85	1.12413	1.40740
41	1.01270	0.51218	86	1.13148	1.43840
42	1.01345	0.52660	87	1.13935	1.47020
43	1.01423	0.54117	88	1.14780	1.50284
44	1.01505	0.55590	89	1.15687	1.53636
45	1.01590	0.57080	90	1.16660	1.57080

X.III APPENDIX C

Temperature distribution in a rectangular section

Let us consider a rectangular section as described in the following diagram:

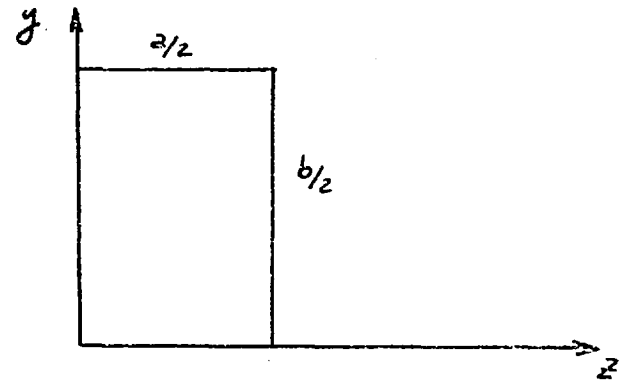

The temperature distribution in this section generated by a source of heat $\dot{h}$ is governed by the elliptic partial differential equation:

$$\frac{\partial^2 T}{\partial y^2} + \frac{\partial^2 T}{\partial z^2} = -\frac{\dot{h}}{k}$$

Let us assume as boundary conditions that:

(i) Temperature is uniform all over the boundary:

$$z = \pm \frac{a}{2}$$
$$y = \pm \frac{b}{2} \qquad \text{is} \quad T = T_o$$

(ii) If $\dot{h}$ is constant all over the surface, conditions of symmetry are such that temperature gradients across both axes should vanish, that is:

$$y = 0 \qquad \frac{\partial T}{\partial z} = 0$$

$$z = 0 \qquad \frac{\partial T}{\partial y} = 0$$

In this condition and if for simplicity sake we choose $T_o = 0$, the theoretical solution for the temperature distribution is given by:

$$T = \frac{4a^2 h}{\pi^3 k} \sum_{n=1,3,5} \frac{1}{n^3}(-1)^{\frac{n-1}{2}} \left[1 - \frac{\cosh(n\pi \frac{y}{a})}{\cosh(n\pi \frac{b}{2a})} \right] \cos \frac{n\pi z}{a}$$

XI. REFERENCES

1. PUGH, H.Ll.D. (1970) Mechanical behaviour of materials under pressure. Chapter 9, Elsevier.

2. BRIDGMAN, P.W. (1952) Studies in large plastic flow and fracture. McGraw-Hill.

3. ROBERTSON, J. (1893) Improvements on the manufacture of metal tubes and hollow articles, plates, rods, bars, wires and the like, and in means and apparatus therefor. British Patent Spec. No. 19356.

4. PUGH, H.L.D. (1964/65) The hydrostatic extrusion of difficult metals. J. Inst. Metals, 93, pp. 201-217.

5. ALEXANDER, J.M. and LENGYEL B. (1971) Hydrostatic extrusion. London, Mills and Boon Ltd.

6. SIEBEL, E. and FANGMAIER, E. (1931) Researches on power consumption in the extrusion and punching of metals. Mitt. K.W. Inst. für Eisenforschung, 13.

7. SACHS, G. (1927) Beitrag zur Theorie des Ziehvorganges. Z. Angew. Math. Mechanik, 7, pp. 235-236.

8. HOFFMAN, O. and SACHS, G. (1953) Introduction to the theory of plasticity for engineers. McGraw-Hill.

9. HILL, R. (1950) The mathematical theory of plasticity. Oxford, Clarendon Press.

10. JOHNSON, W. (1955) Extrusion through wedge-shaped dies, Part I. J. of Mech. and Physics of Solids, 3, pp. 218-223.

11. JOHNSON, W. (1956) Extrusion through square dies of large reductions. J. of Mech. and Physics of Solids, 4, pp. 191-198.

12. JOHNSON, W. (1957) The plain extrusion of short slugs. J. Mech. and Physics of Solids, 5, pp. 202-214.

13. THOMSEN, E.G. YANG, C.T. and KOBAYASHI, S. (1965) Mechanics of plastic deformation in metal processing. MacMillan Co.

14. THOMSEN, E.G. (1956) Comparison of slip-line solutions with experiment. Trans. ASME, J. Appl. Mech., 23, pp. 225-230.

15. THOMSEN, E.G., YANG, C.T. and BIERBOWER, J.B. (1954) An investigation of the mechanics of plastic deformation of metals. Univ. of California. Pub. in Engineering, 5, (4), p. 89.

16. THOMSEN, E.G. and FRISCH, J. (1954) An experimental study of metal extrusion at various strain rates. Trans. ASME, 76, pp. 599-606.

17. THOMSEN, E.G. (1955) A new approach to metal forming problems - experimental stress analysis of tubular extrusion. Trans. ASME, 77, pp. 515-522.

18. THOMSEN, E.G. and FRISCH, J. (1955) Stress and strains in cold extruding 2S-O aluminium. Trans. ASME, 77, pp. 1343-1353.

19. SHABAIK, A., LEE, C.H. and KOBAYASHI, S. (1966) Application of the visioplasticity method to extrusion through a conical die. 7th Int. M.T.D.R. Conference.

20. SHABAIK, A. and KOBAYASHI, S. (1967) Computer application to the visioplasticity method. J. of Eng. Ind., Trans ASME, pp. 339-346.

21. AVITZUR, B. (1963) Analysis of wire drawing and extrusion through conical dies of small cone angle. J. of Eng. Ind., Trans. ASME, 85, pp. 89-96.

22. AVITZUR, B. (1964) Analysis of wire drawing and extrusion through conical dies of large angle. J. of Ind. Eng., Trans. ASME, pp. 305-316.

23. ZEEV ZIMERMAN and AVITZUR, B. (1970) Metal flow through conical converging dies - a lower bound approach using generalised boundaries of the plastic zone. J. of Ind. Eng., Trans. ASME, pp. 119-129.

24. LAMBERT, E.R. and KOBAYASHI, S. (1968) A theory on the mechanics of axisymmetric extrusion through conical dies. J. Mech. Eng. Sci., 10, (5), pp. 367-380.

25. AVITZUR, B. (1965) Hydrostatic extrusion. J. of Engg. for Industry, Trans. ASME, pp. 487-499.

26. PUGH, H.Ll.D. (1964) Redundant work and friction in the hydrostatic extrusion of pure aluminium and an aluminium alloy. J. of Mech. Eng. Sci., 6, (4), pp. 362-370.

27. AVITZUR, B. (1974) Study of flow through conical converging dies. Inst. for Metal Forming, Dept. of Metallurgy and Material Science, Leign Univ., Bethlehem, Penn., U.S.A.

28. WHITFIELD, E. (1967) A preliminary study of the co-extrusion of dissimilar metals. N.E.L. Report No. 265.

29. WHITFIELD, E. (1967) Effect of plating thickness on cold extrusion of copper plated En 2E steel, N.E.L. Report No. 268.

30. ALEXANDER, J.M. and WHITLOCK, B.C. (1965/66) Extrusion of a bimetallic strip from separate containers. Proc. Inst. Mech. Engrs., 180, Part 31.

31. AVITZUR, B. (1970) The production of bi-metal wire. The Wire Journal, 3, (8), pp. 42-49.

32. ZOERNER, W., AUSTEN, A. and AVITZUR, B. (1972) Hydrostatic extrusion of hard core clad rod. Trans of ASME, J. of Basic Engineering, Series D, 94, (1), pp. 78-80.

33. STORY, J.M., AVITZUR, B. and HAHN, W.C. (1975) The effect of receiver pressure on the observed flow pattern in the hydrostatic extrusion of bi-metal rods. J. of Eng. for Industry, Trans. ASME, Paper No. 75, WA/Prod. 15

34. OSAKADA, K., LIMB, M. and MELLOR, P.B. (1973) Hydrostatic extrusion of composite rods with hard cores. Int. J. of Mech. Sci., 15, pp. 291-307.

35. HARTLEY, C.S. (1973) Upper bound analysis of extrusion of axisymmetric, piecewise homogeneous tubes. Int. J. of Mech. Sci., 15, pp. 651-663.

36. ALEXANDER, J.M. and HARTLEY, C.S. (1973) On the hydrostatic extrusion of copper-covered aluminium rods. Int. Conf. on Hydrostatic Extrusion. Univ. of Stirling, Scotland.

37. SADAHIKO MITSUGI et al. (1973) Properties of copper-clad aluminium bus bar. Hitachi Review, 23, (6).

38. OETSCHLÄGEL, D. et al. (1973) Some properties of copper-clad aluminium products. Hitachi Review, 23, (1).

39. SIEBEL, E. and KOBITZSCH, R. (1943) Die Erwärmung des Ziehgutes beim Drahtziehen. Stahl und Eisen, 63, p.110.

40. SINGER, A.R.E. and COAKHAM, J.M. (1960/61) Temperature changes occurring during the extrusion of aluminium, tin and lead. J. Inst. of Metals, 89, pp. 177-182.

41. SINGER, A.R.E. and AL-SAMARRAI, S.H.K. (1960/61) Temperature changes associated with speed variation during extrusion. J. Inst. of Metals, 89, pp. 225-231.

42. JOHNSON, W. and KUDO, H. (1960) The use of upper-bound solutions in fast hot-rolling and axisymmetric extrusion process. Int. J. Mech. Sci., 1, p. 175.

43. FISTER, W. (1963) Beitrag zum Strnagpressproblem. Doctoral Thesis, Aachen, West Germany.

44. BISHOP, J.F.W. (1956) An approximate method for determining the temperature reached in steady motion problems of plane plastic strain. Quart. J. of Mech. and App. Math., 9, Part 2, pp. 236-246.

45. ALTAN, T. and KOBAYASHI, S. (1968) A numerical method for estimating the temperature distribution in extrusion through conical dies. ASME, J. of Eng. for Industry, 90, pp. 107-118.

46. DUSSINBERRE, G.M. (1961) Heat transfer calculations by finite differences. International Text Books.

47. GUHA, R.M. and LENGYEL, B. (1972) Temperature distribution in hydrostatic extrusion-drawing. Annals of the CIRP., 21, (1), pp. 57-58.

48. CRANDALL, S.H. (1956) Engineering analysis. McGraw-Hill.

49. KANTOROVICH, L.V. and KRYLOV, N.M. (1958) Approximate methods of higher analysis. Netherlands, P. Noordhoff.

50. FINLAYSON, B.A. and SCRIVEN, L.E. (1966) The method of weighted residuals, a review. Appl. Mech. Rev., 19, (9), pp. 735-748.

51. FINLAYSON, B.A. (1972) The method of weighted residuals and variational principles. Academic Press.

52. STECK, E. (1969) Ein Verfahren zur näherungsweisen Berechnung des Spannungs- und Verformungsanders bei Umformvorgängen. Annals of the CIRP, XVIII, pp. 251-258.

53. STECK, E. and GEIGER, M. (1972) Plastizitätstheoretische Grundlagen. Chapter 4 of Lehrbuch der Umformtechnik, 1, Edited by Kurt Lange. Berlin, Springer Verlag.

54. STECK, E. (1971) Numerische Behandlung von Verfahren der Umformtechnik. Berichte aus dem Institut für Umformtechnik, Stuttgart University. Essen, Girardet.

55. FOUNG, Y.C. (1965) Foundations of solid mechanics. Englewood Cliffs, Prentice Hall.

56. MALVERN, L.E. (1969) Introduction to the mechanics of a continuous medium. Englewood Cliffs, Prentice Hall.

57. JAOUL, B. (1965) Étude de la plasticité et application aux métaux. Paris, Dunod.

58. KRONER, E. (1960) Allgemeine Kontinuumstheorie der Versetzungen und Eigenspannungen. Arch. Rat. Mech. Anal., 4, pp. 273-334.

59. GRADOWCZYK, M.H. (1970) A theory of dislocations dynamics. Phys. Stat. Sol., 40, pp. 397-408.

60. HARTLEY, C.S. and EISENBERG, M.A. ( ) Relationships between continuum plasticity and phenomemological dislocations theory. Copy supplied by the author. To be published later.

61. FORD, H. (1963) Advanced mechanics of materials. Longmans.

62. AVITZUR, B. (1968) Metal forming: processes and analysis. McGraw-Hill.

63. PHILLIPS, A. and KAECHELE, L. (1955) Combined stress test in plasticity. ASME Ann. Mtg., Chicago, Paper 55-A-15.

64. PHILLIPS, A. and GRAY, G. (1958) ONR Tech. Report No. 5, Contract Nonr-609 (12), Yale University.

65. IVEY, H.J. (1961) Plastic stress-strain relations and yield surfaces for aluminium alloys. J. Mech. Engg. Sci., 3, (1), pp. 15-31.

66. MIASTKOWSKI, J. (1968) Analysis of the memory effect of plastically prestrained material. Archiwum Mechaniki Stosowanej, 20,(3), pp. 261-277.

67. OLSZAK, W., MROZ, and PERZYNA, P. (1963) Recent trends in the development of the theory of plasticity. Pergamon Press.

68. NAGHDI, P.M. (1960) Proc. 2nd Symp. on Naval Structural Mechanics. Ed. Lee and Symonds. New York, Pergamon.

69. CREUS, G. and HELMAN, H. (1971) Relaciones tensión-deformación en el rango plástico. Comisión Nacional de Energía Atómica (Argentina), Programe Multinacional de Metalurgia, O.E.A.-A-88.

70. DRUCKER, D.C. (1956) On uniqueness in the theory of plasticity. Quart. App. Math., 14, pp. 35-42.

71. DRUCKER, D.C. (1951) A more fundamental approach to stress-strain relations. Proc. 1st U.S. National Congr. Appl. Mech., ASME, pp. 487-491.

72. MENDELSON, A. (1968) Plasticity: theory and application. MacMillan Co.

73. DRUCKER, D.C. (1950) Some implications of work hardening and ideal plasticity. Quart. Appl. Math., 7, pp. 411-418.

74. DUNN, P. (1971) Lubrication in hydrostatic extrusion. Ph.D. Thesis, Imperial College.

75. SADIQ, S.M.P. (1970) Hydrostatic extrusion-drawing. M.Sc. Thesis, Imperial College.

76. WHITELEY, A.J. (1972) Hydrostatic extrusion-drawing and its effect on properties of stronger materials. M.Sc. Thesis, Imperial College.

77. LOWE, B. and GOULD, D. (1967) An account of some recent experimental work on the hydrostatic extrusion of non-ferrous metals. Conf. on High Pressure Engng., Paper 10.

78. BABB, S.E. Jr. (1970) The measurement of high pressure. Chapter 3: The mechanical behaviour of materials under pressure. Elsevier.

79. HELMAN, H. and LENGYEL, B. (1973) Hydrostatic extrusion-drawing of composites materials. 11th Ann, Meeting European High Pressure Group. Imperial College, London. (A more comprehensive and detailed paper was published, see Ref. 34.)

80. ARNOLD, R.R. and WHITTON, P.W. (1959) Stress and deformation studies for sandwich rolling hard metals. Proc. Inst. Mech. Eng., 173, (8), pp. 241-256.

81. AFONJA, A.A. and SANSOME, D.H. (1972) An experimental investigation of the sandwich rolling of thin hard sheets. Proc. 13th Int. M.T.D.R. Conf., Paper 41.

82. WEINSTEIN, A.S. and PAWLESKI, O. (1967) Plane strain drawing of sandwiched metals. Proc. 8th Int. M.T.F.R. Conf., pp. 961-980. Pergamon Press.

83. JOHNSON, W. and MELLOR, P.B. (1962) Plasticity for mechanical engineers. New York, Van Nostrand, p. 251.

84. ROWE, G.W. (1965) An introduction to the principles of metalworking. E. Arnold.

85. GUHA, R. Personal communication.

86. HILL, R. (1950) Mathematical theory pf plasticity. Oxford University Press.

87. KACHANOV, L.M. (1971) Foundation of the theory of plasticity. Amsterdam, North Holland Pub. Corp.

88. ALEXANDER, J.M. and BREWER, R.C. (1963) Manufacturing properties of materials. D. van Nostrand.

89. AVITZUR, B. (1968) Metal forming: processes and analysis. New York, McGraw-Hill.

90. AVITZUR, B. (1965) Analysis of metal extrusion. Trans. ASME, Ser. B, 87.

91. KAMYAB-TEHRANI, S. (1972) On pressure distribution and frictional conditions in hydrostatic extrusion dies. Ph.D. Thesis, Mech. Eng. Dept., Imperial College.

92. FINLAYSON, B.A. and SCRIVEN, L.E. (1965) The method of weighted residuals and its relation to certain variational principles for the analysis of transport processes. Chem. Eng.Sci., 20, pp. 395-404.

93. COLLATZ, L. (1960) The numerical treatment of differential equations. Springer Verlag.

94. KAPLAN, S. (1963) On the best method for choosing the weighting functions in the methods of weighted residuals. Trans. American Nuclear Society, 6, pp. 3-4.

95. ERDOGAN, F. (1962) On the approximate solution of heat conduction problems. Trans. ASME J. Heat Transfer, Paper No. 62-HT 19.

96. FRAZER, et al. (1937) Approximations to functions and the solutions of differential equations. Aero. Res. Comm., Reports and Memos.

97. DUNCAN, W.J. (1937) Galerkin method in mechanics and differential equations. Aero. Res. Comm., Reports and memos.

98. SCHETZ, J.A. (1963) On the approximate solution of the viscous flow problems. J. Appl. Mech., 30, pp. 263-268.

99. RICHARDSON, P.D. (1968) Further results from use of transcendental profile function in conduction and convection. Int. J. Heat and Mass Transfer, 11, pp. 359-365.

100. FROBERG, C.E. (1969) Introduction to numerical analysis. Addison Wesley.

101. LANCZOS, C. (1938) Trigonometric interpolation of empirical and analytical functions. J. Math. Phys., 17, pp.123-199.

102. LANCZOS, C. (1956) Applied analysis. Englewood Cliffs, New Jersey, Prentice Hall.

103. SOUTHWELL, R.V. (1946) Relaxation methods in theoretical physics. Oxford University Press.

104. MASON, J.C. (1965) Some new approximations for the solution of differential equations. D. Phil. Thesis, Oxford.

105. MASON, J.C. (1969) Chebyshev method for separable partial differential equations - Information processing 68. Amsterdam, North Holland Co.

106. KNUDSEN, J.G. and KATZ, D.L. (1958) Fluid dynamics and heat transfer. McGraw-Hill.

107. FOX, L. and PARKER, I.B. (1968) Chebyshev polynomials in numerical analysis. Oxford University Press.

108. PICONE, M. (1937) Analisi quantitativa ed essistenziale nei problemi di propagazione. Atti dei 1° Congresso dell'Unione Mathematica Italiana.

109. FICHERA, G. (1954) Methods of functional analysis in mathematical physics. Proc. Int. Math. Congr. Amsterdam.

110. BIRD, B.R., STEWART, W.E. and LIGHTFOOT, E.N. (1960) Transport phenomena. John Wiley & Sons.

111. CARSLAW, H.S. and JAEGER, J.C. (1959) Conduction of heat in solids. Oxford University Press.

112. LOEWENSTEIN, P. and TUFFIN, W.B. Metallurgical bonding of dissimilar metals by co-extrusion. West Concord Massachussetts, Nuclear Metals Div., Textron Inc.

113. TYLECOTE, R.F. (1968) The solid phase welding of metals. New York, St. Martin's Press.

114. MILNER, D.R. and ROWE, G. (1962) Metallurgical reviews. 7, pp. 433/480.

115. SHORSHOROV, M.Kh. (1965) Physical and chemical principles of the welding of dissimilar materials. Symposium Achievements of Science and Technology - Welding.VINITI.

116. CAVE, J.A. and WILLIAMS, J.D. (1973) The mechanism of cold pressure welding by rolling. J. Inst. of Metals, 101, pp. 203-207.

117. VAIDYANATH, L.R. and MILNER, D.R. (1960) Significance of surface preparation in cold pressure welding. British Welding Journal, 7, pp. 1-6.

118. DURST, G. (1956)
J. Metals, 8, p. 328.

119. VAIDYANATH, L.R., NICHOLAS, M.G. and MILNER, D.R. (1959) Pressure welding by rolling. Brit. Welding J., 6, pp. 13-28.

120. HELMAN, H. (1966) Influencia de la humedad y tiempo en el umbral de deformación para la union de metales por colaminación. Technical Report, Department of Metallurgy, National Commission of Atomic Energy, R. Argentina.

121. HELMAN, H. and MARTINEZ VIDAL, C.A. (1968) Union de metales por indentacion. Metalurgia Moderna, Soc. Argentina de Metales, 17, p. 65.

122. SHERWOOD, W.C. and MILNER, D.R. (1969) The effect of vacuum machining on the cold welding of some metals. J. Inst. Metals, 97, pp. 1-5.

123. KELLER, D.V. and SPALVINS, T. (1964) Trans. Vacuum Metallurgy Conf. 1963, p. 149. Ed: Bunshaw, R.F., Boston, Mass.

124. CANTALEJOS, N.A. and CUSMINSKY, G. (1972) Morphology of the interface of roll-bonded aluminium. J. Inst. Metals, 100, pp. 20-23.

125. CAVE, J.A. and WILLIAMS, J.D. (1973) The mechanism of cold pressure welding by rolling. J. Inst. Metals, 101, pp. 203-207.

126. OTTO, H,E, and CARPENTER, S.H. (1973) Explosive cladding of large steel plates with lead. Metals and Materials, pp. 75-79.

127. WYLIE, H.K., WILLIAMS, P.E.G. and CROSSLAND, B. (1970). An experimental investigation of explosive welding parameters, Dept, of Mech. Eng. Report 514, Queens University, Belfast.

128. CROSSLAND, B. (1970) Explosives for welding. Physics Bull., 21, pp. 498-502.

129. CROSSLAND, B. and WILLIAMS, J.D. (1970) Welding parameters for explosive cladding. Proc. Conf. in Advances in Welding. Welding Institute.

130. McEWAN, K.J.B. and MILNER, D.R. (1962) Pressure welding of dissimilar metals. Brit. Welding J., 9, pp. 406-420.

131. WRIGHT, K. (1964) Chebyshev collocation methods for ordinary differential equations. The Computer Journal, 6, pp. 358-365.

132. CLEMENT, P.R. (1952) The Chebyshev approximation methods. Proc. I.R.E., XI, (2).

133. HELMAN, H. and ORTIZ, E.L. (1975) A new method for the numerical solution of partial differential equations based on economization in several variables. Fifth Canadian Congress of Applied Mechanics, Fredericton.